SOME CHARACTERISTICS

OF

FERRO-RESONANT PARAMETRIC MACHINES

by

BRIAN HARTLEY SMITH, B.E.

Thesis submitted for the degree of

DOCTOR OF PHILOSOPHY

at the UNIVERSITY OF ADELAIDE

Electrical Engineering Department

JANUARY 1972

CONTENTS

1.	INTRODUCTION	1.1
1.1	Background	1.1
1.2	Structure of the Report	1.4
2.	GENERAL PRINCIPLES OF OPERATION	2.1
2.1	Ferro-resonant behaviour	2.1
2.2	Variable-reluctance devices	2.3
2.3	Ferro-resonant parametric machines	2.6
3.	PROTOTYPE MACHINE AND MEASUREMENT OF ITS CHARACTERISTICS.	3.1
3.1	General	3.1
3.2	Torque measurement	3.2
3.3	Measurement of stator flux linkages	3.3
3.4	Results	3.4
4.	MATHEMATICAL MODEL AND EQUIVALENT CIRCUIT	4.1
4.1	Mathematical models for λ-i relationships	4.1
4.2	Representation of the λ-i characteristic by $\lambda=ai/(1+b\|i\|)$.	4.3
4.2.1	Curve fitting	4.4
4.2.2	Torque from $\lambda=ai/(1+b\|i\|)$.	4.5
4.3	Representation of the λ-i characteristics by power series	4.8
4.3.1	Curve fitting	4.9
4.3.2	Stored energy and torque	4.11
4.3.3	Equivalent circuit of the machine	4.13
4.3.4	System equations	4.14
4.3.5	Normalized simplified equations	4.15
4.4	Iron losses	4.18
5.	ANALOGUE COMPUTER SIMULATION	5.1
5.1	Simulation of the prototype machine	5.1

5.1.1 Results from the simulation of the prototype 5.4

5.2 Analogue computer simulation of the ideal system equations 5.9

5.2.1 Improved analogue representation 5.10
5.2.2 Torque-speed curves of idealized machines 5.10

6. NUMERICAL SOLUTION OF THE SYSTEM EQUATIONS 6.1

7. ANALYTICAL SOLUTION UNDER BLOCKED ROTOR CONDITIONS 7.1

7.1 Steady state solution by harmonic balance 7.1

7.1.1 Natural frequency of the unperturbed system 7.6

7.2 Steady state solution using $\omega L_f I_f$ curves 7.8

7.2.1 Equivalent linear inductance 7.9

7.3 Selection of approximate operating conditions 7.11

8. TRANSITION CHARACTERISTICS OF THE JUMP 8.1

8.1 Integral curves 8.1

8.1.1 Plotting integral curves 8.3
8.1.2 System behaviour as indicated by the integral curves 8.4

8.2 The nature of the singular points 8.6

8.2.1 Stability of the steady state solution 8.7
8.2.2 Boundaries between different types of singularity 8.8

9. PHASE-AMPLITUDE PLOTS 9.1

9.1 First order equations for amplitude and phase 9.1
9.2 Analogue computer solution of amplitude and phase equations 9.2

9.2.1 Results from the analogue computer 9.3
9.2.2 Results from torque-speed plots 9.6

9.3 Discussion 9.6

10. ANALYTICAL SOLUTION 10.1

10.1 Form of the solution 10.1
10.2 Possible methods of solution 10.4
10.3 Systematic solution for ψ 10.4

10.3.1 General outline of the method 10.5
10.3.2 Application of the method 10.6

10.4 Current associated with a particular sideband 10.13
10.5 Approximate natural frequency of the system 10.15
10.6 Analytical expressions for average torque 10.20

10.6.1 Calculation of average torque from the instantaneous torque 10.20

10.6.1.1 Asynchronous torque 10.21
10.6.1.2 Synchronous torque 10.22
10.6.1.3 Asynchronous torque from the Manley-Rowe relationships 10.25

10.7 Results from analysis 10.28

10.7.1 Ideal machines 10.30
10.7.2 Prototype machine 10.33

11. EFFICIENCY OF FERRO-RESONANT PARAMETRIC MACHINES 11.1

11.1 Power-frequency relationships 11.2
11.2 Torque production 11.4

11.2.1 Synchronous torque 11.6

11.3 Efficiency 11.6

11.3.1 Operating efficiency 11.7

12. STABILITY 12.1

12.1 Steady state solutions with relatively large load inertia 12.3
12.2 Solutions when the load has finite inertia 12.4
12.3 Investigation of the stability of a solution 12.5

12.3.1 Linearising the system equations 12.6
12.3.2 Investigating the transient behaviour of a solution 12.10

13. FURTHER WORK 13.1

14. CONCLUSIONS 14.1

15. REFERENCES 15.1

16. APPENDICES

I I.E.E. Paper (see back pocket)

II(a) Some details and specifications of the analogue computer A.1

II(b) Generation of $f'(\theta)$ and $f(\theta)$ A.2

II(c) Analogue computer scaling factors A.3

III(a) Average torque under sine-flux conditions A.5

III(b) Fundamental component of current under sine-flux conditions A.6

III(c) RMS component of current under sine-flux conditions A.7

III(d) Equivalent linear inductance A.9

III(e) Plots of V_L-I_R versus plots of V_L-I_f. A.11

IV Domains in the frequency damping plane in which ferro-resonant jumps can occur A.14

IV.1 Cubic approximation A.16
IV.2 Quintic approximation A.17
IV.3 Discussion A.18

V Nature of the singular points and stability A.20

V.1 Boundaries between different singularities in the B^2/r^2 plane A.22

V.1.1 Boundaries between nodes and foci A.22
V.1.2 Boundaries between nodes and saddles A.22

VI Analogue computer determination of phase-amplitude relations A.24

VII Further details of the perturbation method A.26

VIII(a)	Expansion of sideband series raised to some power	A.32
VIII(b)	Interaction of rotor and sidebands Expansion of $F(\theta)g_1^q$.	A.36
IX	Current associated with a particular sideband	A.41
X	Solution when one sideband only is present	A.44
XI	Asynchronous torque when leakage reactance and iron losses are present	A.48
XII	Parameters of prototype machine	A.50
XIII	Analytical Programme	A.53

SUMMARY

The thesis deals with a class of brushless a.c. reluctance machines, capable of operating over a wide speed range. The principle of operation depends upon the exploitation of the properties of a series RLC circuit in which the inductance (in this case, the stator winding inductance) is a function of current and of rotor position.

The system is described by non linear differential equations having periodic coefficients. Analogue and numerical methods are used to obtain theoretical results for comparison with those obtained experimentally from a prototype machine and for comparison with results obtained from an approximate analytical solution to the system equations.

Because of the strongly non linear behaviour and the consequent impossibility of extrapolating quantitative results from one set of system parameters and inputs to another and the cost in computing time of obtaining accurate analytic solutions, phase amplitude plots and the Manley-Rowe relationships are used in an attempt to provide insight into the essential physical behaviour of the machine.

It is suggested that such a machine is the electrical equivalent of a two-stroke, while the overall torque speed characteristics and theoretical maximum efficiency of an n-pole machine correspond approximately to those which would result from a composite machine comprising a number of single phase induction machines having 2n, 6n, 8n ..... poles all connected to one shaft, with the supply being automatically transferred to machines of increasing pole number as the shaft speed falls, so tending to maintain the theoretical conversion efficiency. It

is shown however, that because of practical limitations such simple machines are unlikely to operate with better than a 50% efficiency at any speed.

This is to certify that the work described in this thesis has not been submitted previously for a degree or other similar award to any other University or Institution and that to the best of my knowledge and belief, this thesis contains no material previously published or written by another person, except where due reference is made in the text of this thesis.

ACKNOWLEDGEMENTS

Financial support from the Electrical Research Board covered the majority of the experimental and computational costs associated with this project.

The author wishes to thank Mr B. Seymour for his untiring efforts in maintaining and operating the analogue computer over a period of almost two years. Professor J. L. Woodward and Dr. B.R.Davis have also provided helpful discussions.

List of Symbols

a_n	=	normalised amplitude of n^{th} sideband
A	$\equiv$	$1 + \frac{3}{4} r^2 F$ for cubic non linearity
B	=	normalised amplitude of forcing function see p.4.16
C	=	capacity
d_{o-m}	=	coefficients in $F(\theta)$
D_{o-m}	=	coefficients in $f(\theta)$
$f(\theta)$	=	function representing rotor geometry
$F(\theta)$	=	normalised rotor geometry
F	=	value of $F(\theta)$ at a fixed rotor position
G	=	coefficient of friction; N-m/rad/sec
i	=	instantaneous current
i_p	=	peak value of instantaneous current
I_f	=	rms value of fundamental component of current
I_r	=	rms value of current
J	=	moment of inertia; $kg\text{-}m^2$
K	=	saturation factor
K_p	=	peak value of K at i_p
ℓ	=	normalised leakage inductance; see p.4.16
L	=	inductance
L_o	=	small signal inductance
L_ℓ	=	leakage inductance of stator windings
L_f		
L_r	=	equivalent linear inductance
N	=	number of winding turns
P	=	number of poles in the machine
q	=	degree of single non linearity term
r	=	amplitude of ψ
R	=	resistance
R_c	=	resistance representing iron loss

S	=	Reluctance
S_i	=	Reluctance of iron path
S_a	=	Reluctance of air gap
S_n	=	$\gamma+np\Omega$
t	=	time
T	=	Torque
T_e	=	instantaneous electromagnetic torque
T_m	=	instantaneous mechanical torque
T_{ave}	=	average torque
v	=	instantaneous applied voltage
v_{c_o}	=	initial voltage across the capacitor
V	=	rms applied voltage
$x(t)$	=	real component of $\psi(t)$
$y(t)$	=	quadrature component of $\psi(t)$
β	=	phase angle of forcing function
γ	=	normalised forcing frequency; See p.4.16
γ_n	=	natural frequency of saturated system
γ_N	=	natural frequency of doubly perturbed system
δ_{o-m}	=	phase angle of terms in $f(\theta)$ and $F(\theta)$
η_n	=	phase of n*th* sideband
θ	=	rotor angular position
Ω	=	normalised rotor angular velocity; see p.4.16
τ	=	normalised time; see p.4.16
ρ_1	=	normalised series resistance; see p.4.16
ρ_2	=	normalised shunt resistance; see p.4.16
ϕ	=	instantaneous flux
ψ	=	instantaneous flux linkages
λ	=	normalised flux linkages; see p.4.16
Λ	=	peak normalised flux linkages
ω	=	angular frequency of supply voltage
ω_o	=	small signal natural frequency; see p.4.16

CHAPTER 1: INTRODUCTION

1.1 Background

Although the principles of operation of squirrel cage induction motors have been known for almost a century, and such motors have provided the majority of prime movers wherever constant speed drives are required, no such simple, rugged, brushless self contained motor, capable of economical operation over a continuous speed range has yet been developed.

A history and analysis of some previous attempts to solve this and allied problems are presented by Laithwaite in the book "Special Purpose Induction Machines" [20], where the point is well made that there are a number of criteria which may be used to judge the effectiveness of a machine, and that the relative importance of these criteria may change dramatically from one application to another.

The investigations discussed in this report represent yet another approach to the problem of developing a self contained, variable speed, brushless a.c. machine and refer to work carried out between June 1965 and June 1969. Discussion centres around the qualitative and quantitative behaviour of a class of asynchronous, brushless, a.c. reluctance machines, which depend for their operation upon the exploitation of the properties of a series RLC circuit in which the inductance (in this case the stator winding inductance) is a function of current and of rotor position. Such a circuit may have more than one stable state, and under appropriate conditions transitions from one state to another and back may be induced by relatively small changes in any one of the circuit parameters. For the class of machines under consideration, such transitions

are induced by the changes, as the rotor turns, in the reluctance associated with the stator windings.

As the principle of operation appeared to be novel, a provisional patent application was made in conjunction with the National Research Development Corporation of Great Britian in 1967 [8]. A search of previous patents revealed that an application for a patent relating to "Improvements in and relating to means for electrically producing oscillatory or reciprocatory motion" was made by the British Thomson-Houston Co. Ltd and other on March 4, 1931 and accepted on September 5, 1932. [6]. Figure 1.1 shows a copy of the drawings submitted with the application, from which it can be seen that the mechanism described is similar to that shown in Figure 2.2(d) of this report. In the latter case however, the functions of the coils marked 1 and 3 in Figure 1.1 may be combined as a result of the specially shaped armature.

The only other application of any relevance referred to a machine comprising a multi-pole stator and salient pole rotor having a lesser number of poles than the stator. It was the subject of a patent application on July 13, 1950 [7]. Operation of this machine depends upon the fact that the inductance of the stator windings on each pole is a function of the rotor position; so that by the appropriate interconnection of windings and shunt capacitors the m.m.f of the stator pole towards which the rotor pole in advancing, is greater than the m.m.f. of the stator pole from which the rotor pole is retreating. Hence continuous rotation results once motion is started. A number of refinements including an auxiliary rotor and stator were proposed.

Such a machine is similar to those under consideration in this paper but does not appear to take advantage of the

Fig 1.

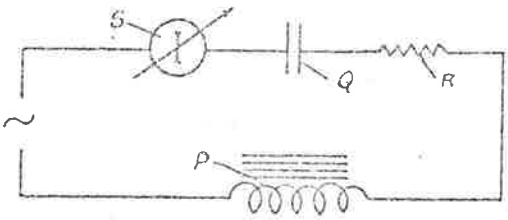

Fig 2.

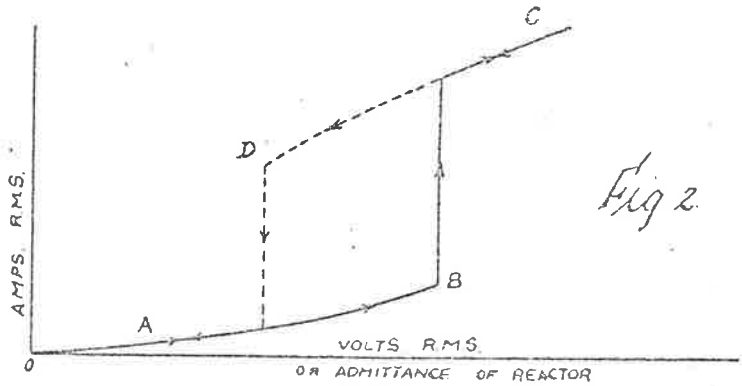

Fig 3.

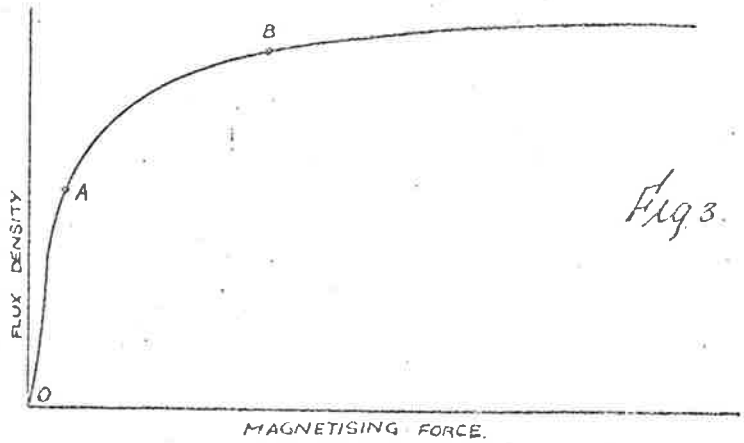

Fig 4

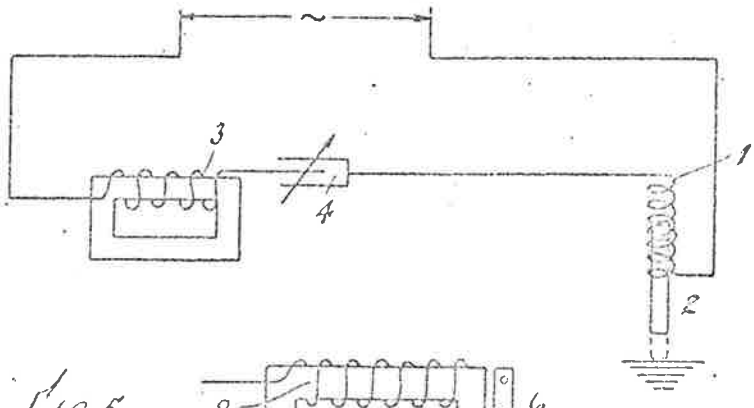

Fig 5

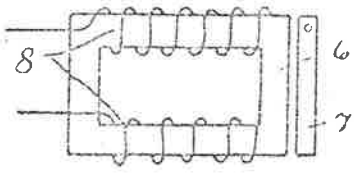

Charles & Read Ltd. Photo Litho.

ferro-resonant jump effect [29,40], a phenomenon which is utilized by the devices under consideration in this report.

Interest in electro-mechanical transducers which could exploit the latter phenomenon was stimulated by a paper on an oscillating ring motor [39], the operation of which was attributed by the authors to two effects; viz the ferro-resonant jump phenomenon together with the effect of the delayed response in a near resonant, series RLC circuit to changes in the circuit inductance. However, in view of the shape of the magnetic circuit employed it seems likely that the latter effect would predominate.

The ferro-resonant jump effect can be utilized to amplify the effect of small changes in one or more of the circuit parameters. Advantage is taken of this properly in an a.c. servo-motor described by Teodorescu [35] which otherwise has little in common with the class of machines under consideration.

Although the machines under discussion are essentially asynchronous reluctance machines, this report is concerned primarily with presenting an analysis of their behaviour in terms of a given set of input and machine parameters; so that virtually no reference has been made to the large body of literature on synchronous reluctance machines, as it is relevant neither to these machines nor to the analysis. It would almost certainly be relevant however, to any discussion directed towards the design of a machine utilizing the principles under discussion.

1.2 Structure of the report

Because the relevant electro-mechanical system representing these machines is described by strongly non-linear differential equations having periodic coefficients it is impossible to extrapolate quantitative results from one set of system parameters and inputs to another. Hence much emphasis has been placed on the gaining of insight into the essential physical behaviour of such machines.

Following Sections 2 and 3, in which the principles of operation and the measured characteristics of an experimental machine are presented, a mathematical model of the machine is proposed in Section 4. Section 4.2 may be omitted on a first reading as it represents work which, while it led to an interesting engineering approximation of use in saturated circuits, was not used subsequently in the report.

Simulation of the prototype machine on an analogue computer led to results which suggested that the proposed mathematical model may be used with reasonable confidence as a means of exploring the behaviour of this class of machine. In order to provide a check on numerical and analytical methods of solution discussed in Sections 6 and 10 respectively, analogue methods were used to obtain some results for somewhat idealized machines. These results appear in Section 5.2.

Qualitative behaviour of the system is explored firstly by investigating the behaviour under conditions of a blocked and a slowly moving rotor respectively, followed by an investigation of the transistion characteristics of the jump phenonenon which is presented in Section 8.

Phase-plane methods presented in Section 9 are shown to be qualitatively correct but quantitatively inadequate at practical rotor speeds, although valuable insight into the behaviour is

gained by their use.

Further valuable insight is obtained from the nature of an analytical solution for the instantaneous flux or current obtained in Section 10. It comprises a fundamental plus an infinite series of top and bottom sidebands based on the fundamental and its harmonics. Agreement between the torque-speed curves obtained by analytical methods on the one hand, and numerical or analogue methods on the other, improves in general with the number of sidebands included in the analysis. However the computational time required, rapidly becomes prohibitive.

Application of the Manley-Rowe relationships [21] gives further insight into the physical behaviour and provides an indication of the conversion efficiency of such machines.

Presentation of an analytical solution to a set of non-linear differential equations is not complete until the stability of such a solution is determined. This problem is discussed briefly in Section 12, but in view of the approximate nature of the solutions obtainable within a reasonable amount of computational time, the matter has not been pursued.

The latter problem together with others discussed in Section 13, provide challenging, if somewhat academic, topics for further investigation.

CHAPTER 2: GENERAL PRINCIPLES OF OPERATION

2.1 Ferro-resonant behaviour.

When conditions are such that lumped parameter analysis of electrical circuits is valid, it is convenient to represent the presence of a magnetic field by the so-called inductance of the circuit. Inductance is defined as flux linkages, with some closed electrical circuit, per ampere of current which sets up these flux linkages. In general such a concept is only useful and meaningful when there is a linear relationship between the flux linkages and the current which establishes them. The presence of ferro-magnetic material in the magnetic field normally results in a non linear relationship between flux linkages and current and hence in an 'inductance' which is dependent upon the current.

Throughout the remainder of this thesis we shall be concerned with the exploitation of some of the characteristics of circuits containing such non linear 'inductances'. For convenience, the general concept of inductance will be retained and used where no undue ambiguity exists as to its meaning, in order to avoid the use of repeated qualifying statements. However, under certain specific circuit conditions a precise meaning will be assigned when and if it is necessary.

In order to gain some simple physical insight into the manner of operation of the devices under consideration, the following explanation, after Rudenberg [29], is offered as an introduction. In later sections, further discussion will be found concerning the accuracy and utility of this approach.

Consider a series LCR circuit, fed with an alternating voltage, $v = \sqrt{2}V \sin \omega t$, where the inductance L is a function of current. An approximate solution for the magnitude of the latter may be obtained graphically by considering the fundamental component only.

In which case, we may write

$$V^2 = R^2 I_f^2 + [\omega L(i) - 1/\omega C]^2 I_f^2 \qquad \ldots\ldots (2.1)$$

or

$$\omega L(i)\, I_f = \sqrt{V^2 - I_f^2 R_f^2} + I_f/\omega C \qquad \ldots\ldots (2.2)$$

Each side of equation 2.2 may be plotted as a function of I_f, as shown in Figure 2.1, where the right hand side appears as a tilted ellipse. A solution for the current in the circuit may then be obtained from the intersection of the ellipse and the curve representing $\omega L(i) I_f$, which is merely the voltage across the inductance plotted against I_f. Inspection of Figure 2.1 shows that there are three distinct possibilities, represented by the three different $\omega L(i) I_f$ curves, respectively.

The intersections labelled 'A' represent inductive circuit conditions with relatively low flux and current amplitudes, whereas the intersections labelled 'B' represent capacitive circuit conditions with relatively large flux and current amplitudes. Point C represents an unstable solution (see sections 7. and 8.)

Further inspection of Figure 2.1 suggests that transitions from an A state to a B state may be induced, under certain conditions, by any one of the following operations:-

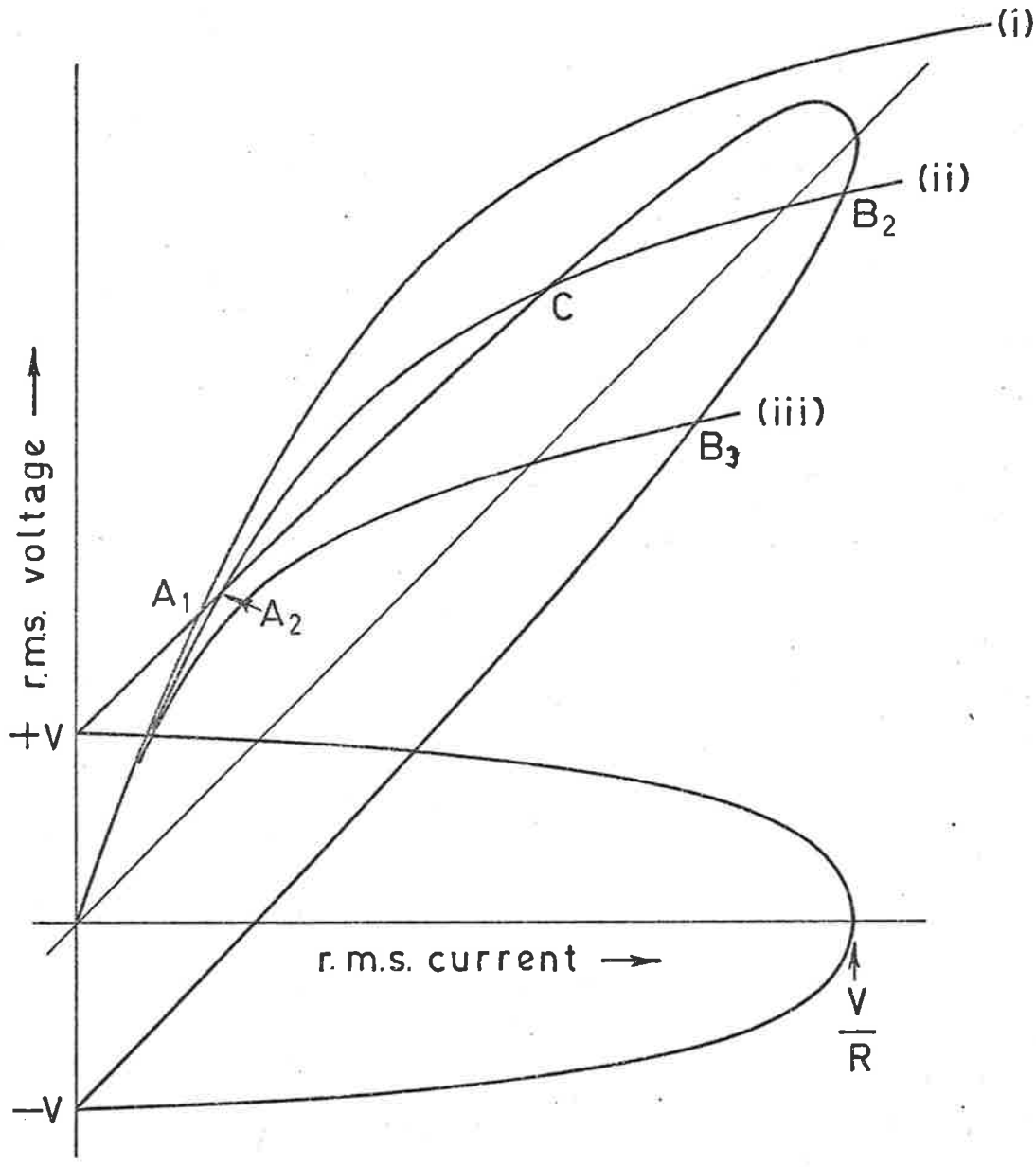

FIGURE 2.1: GRAPHICAL SOLUTION OF

$$\sqrt{(V^2 - I^2R^2)} + 1/\omega C = \omega L(i)I$$

(a) increasing the magnitude of V

(b) decreasing C

(c) decreasing R

(d) changing the $I_f \omega L(i)$ characteristic in the direction from curve (i) to curve (iii)

(e) decreasing ω.

Similarly a transition from a B state to an A state may also be induced under certain conditions by reversing any one of these operations.

Circuit behaviour during transition from one state to another is discussed in section 8, following a more rigorous analysis of the behaviour of such circuits under steady state conditions.

Other means, not obvious from Figure 2.1, also may be used to induce a change of state, but whichever method is used, any complete cycle from A to B to A, always involves hysteresis.

Thus the possibility arises of using such a circuit for energy conversion.

In particular, if the $\omega L(i) I_f$ characteristics can be varied by mechanical means then the way is open for the exploitation of this ferro-resonant jump phenomenon for the purposes of electro-mechanical energy conversion.

2.2 Variable reluctance devices.

Variation of the reluctance in the path of the flux associated with a coil can produce a family of $\omega L(i) I_f$ - I_f curves of the form shown in Figure 2.1. Some possible configurations of stator and rotor, capable

of producing such curves, are shown in Figure 2.2, where (a) and (b) are similar to conventional synchronous reluctance motors, except that the variation in reluctance is accomplished here by variation in the iron circuit reluctance, instead of by the more conventional change in airgap.

The theory of operation of reluctance motors [10] makes it clear that, for unsaturated conditions, net positive average torque can be obtained from the machine only if

$$\int_0^{\pi} -\frac{1}{2}\phi^2 \frac{\partial S}{\partial \theta}\, d\theta \equiv \int_0^{\pi} \frac{1}{2} i^2 \frac{\partial L}{\partial \theta}\, d\theta > 0 \qquad \ldots\ldots (2.3)$$

When fed from a source of alternating voltage, this inequality is satisfied at synchronous speed by the relative position of the rotor with respect to the flux cycle. At sub-synchronous speeds, net positive average torque can be obtained from such a machine, only by arranging that:-

$$\int_{S_{max}}^{S_{min}} -\frac{1}{2}\phi^2 \frac{\partial S}{\partial \theta}\, d\theta > \int_{S_{min}}^{S_{max}} \frac{1}{2}\phi^2 \frac{\partial S}{\partial \theta}\, d\theta \qquad \ldots\ldots (2.4)$$

or in terms of current and inductance

$$\int_{L_{min}}^{L_{max}} \frac{1}{2} i^2 \frac{\partial L}{\partial \theta}\, d\theta > \int_{L_{max}}^{L_{min}} \frac{1}{2} i^2 \frac{\partial L}{\partial \theta}\, d\theta \qquad \ldots\ldots (2.5)$$

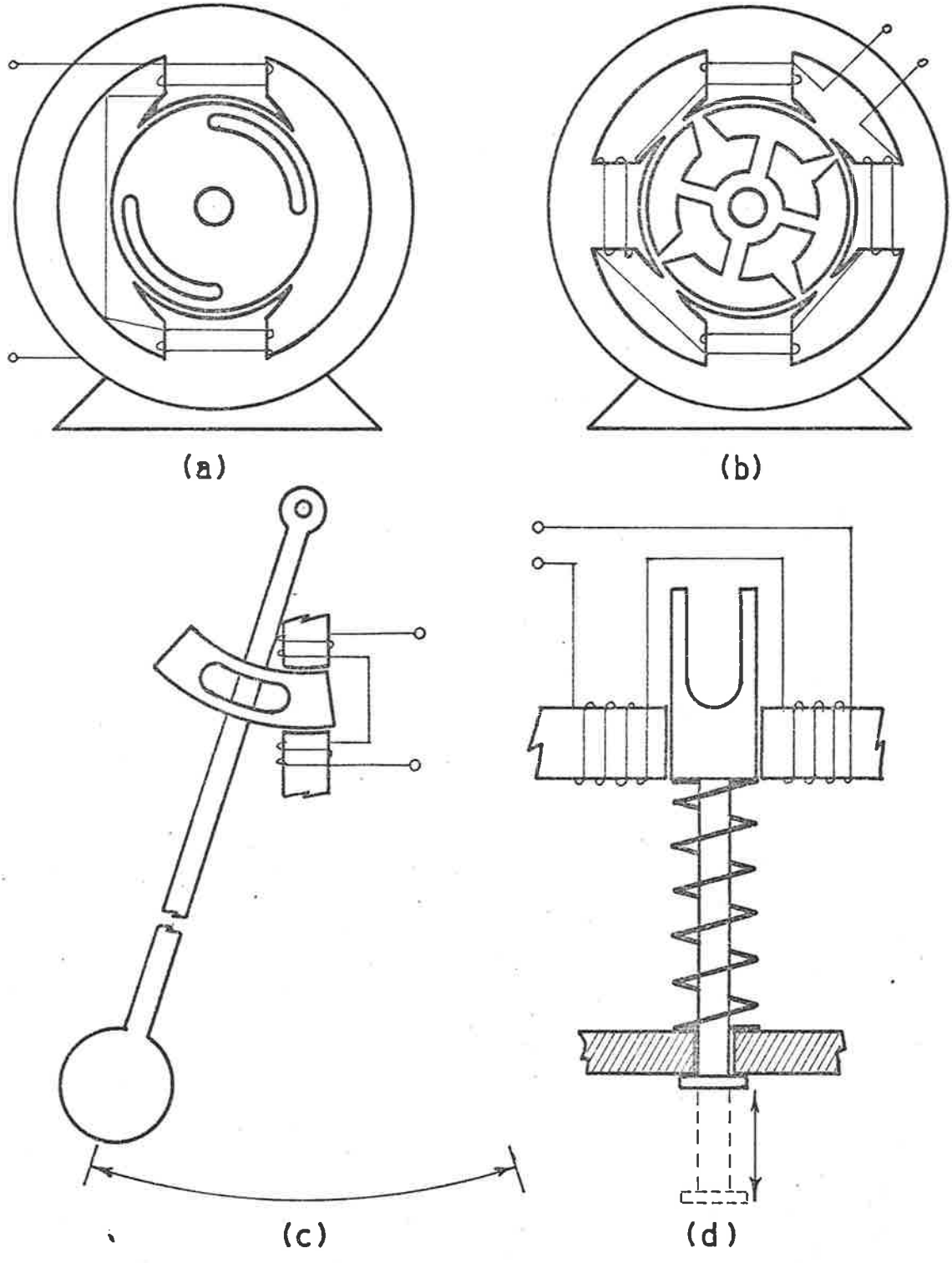

FIGURE 2.2 : SOME FERRO-RESONANCE DEVICES

But because

$$\int_{S_{max}}^{S_{min}} \frac{\partial S}{\partial \theta}\, d\theta = -\int_{S_{min}}^{S_{max}} \frac{\partial S}{\partial \theta}\, d\theta \qquad \ldots\ldots (2.6)$$

or

$$\int_{L_{min}}^{L_{max}} \frac{\partial L}{\partial \theta}\, d\theta = -\int_{L_{max}}^{L_{min}} \frac{\partial L}{\partial \theta}\, d\theta \qquad \ldots\ldots (2.7)$$

the inequalities in expressions (2.4) and (2.5) must be satisfied by increasing the average amplitude of ϕ or i during the first interval with respect to the average amplitude during the second.

Furthermore, if inequalities (2.4) and (2.5) could be satisfied for the devices sketched in Figure 2.2(c) and (d), the mechanical losses of the pendulum could be made up electrically and a negative loss spring could be obtained, i.e. more work could be obtained from the expanding spring and moving armature than would be expended in compressing it.

The circuit characteristics discussed in section 2.1 may be utilized to accomplish automatically the variations in flux and current amplitude required to satisfy the inequalities (2.4) and (2.5) and hence to produce useful work from devices of the nature depicted in Figure 2.2.

2.3 Ferro-resonant parametric machines.

In order to understand how such automatic variation in flux magnitude may be accomplished, consider an elementary reluctance motor taking the form shown in Figure 2.2 (a) or (b) and having a suitable capacitor connected in series with its stator windings. Curves (i) and (ii) of Figure 2.3 may be considered to represent the $\omega L(i)\ I_f$-I_f curves for the stator winding when the rotor is in the position of minimum and maximum reluctance respectively. Particular values of applied voltage, frequency, capacity and resistance determine the position and size of the ellipse representing the right hand side of equation (2.2).

With the rotor of the machine in the position of minimum reluctance, steady state current amplitude will correspond to point A_1. As the rotor is turned slowly into the quadrature or maximum reluctance position, the $\omega L(i)\ I_f$ characteristic will move to a position corresponding to curve (ii) of Figure 2.3. During this time, the steady state solution for the current amplitude corresponds to the intersection of the ellipse and the $\omega L(i)\ I_f$ curve, which moves from point A_1 towards the point Q. This latter point represents the maximum amplitude which the current can have in the inductive or non-resonant state. When the rotor reaches a position such that the whole of the $\omega L(i)\ I_f$ curve lies below the ellipse, the steady state solution for the current will be represented by B_2.

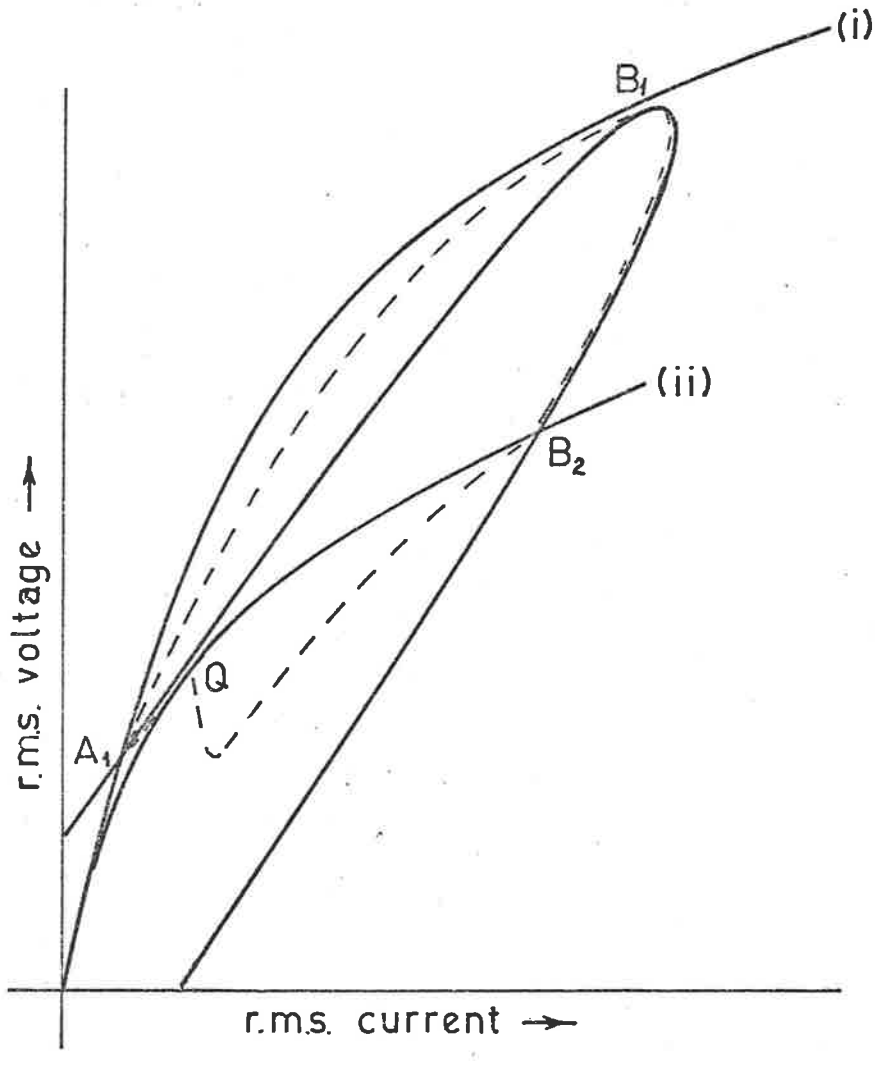

FIGURE 2.3 : FORM OF LOCUS OF R.M.S. VOLTAGE AND CURRENT ASSOCIATED WITH L(i)

Methods discussed in section 8 enable the transition time and path to be obtained within the limits of the method with reasonable accuracy. However, at this stage, some physical insight into the behaviour may be gained by noting that, in the vicinity of resonance, the current amplitude approaches its correct steady state value, from some other initial value, in an exponential fashion, whereas it tends to approach the non-resonant inductive state in an oscillatory fashion.

Thus for the purposes of the present discussion, the current may be considered to increase approximately exponentially from the magnitude at Q to that at B_2.

During the movement of the rotor from the direct to the quadrature axis position the electromagnetic torque developed in the direction of motion is negative, in accordance with equations (2.4) or (2.5).

As the rotor continues to turn into the direct axis position, the characteristic will rise again to position (i) of Figure 2.3. Provided that this curve clears the top of the ellipse, the current will, at the moment when the characteristic ceases to be tangential to the ellipse at point B_1, decay in a damped oscillatory fashion to a value corresponding to point A_1.

Positive electromagnetic torque is developed as the rotor moves from the quadrature to the direct axis position. It is shown in a later section (Appendix 1) that the area enclosed by the current and inductance-voltage locus during one complete cycle is a measure of the work done by the rotor of the machine.

Thus the variation in rotor reluctance with angular position may be used to switch the circuit from non-resonant to resonant state and back. By a suitable selection of the circuit voltage, which determines the intercept of the ellipse on the voltage axis of Figure 2.3, and of the capacitance which determines the slope of the ellipse, the rotor position at which transitions occur may be selected; so that the inequalities (2.4) and (2.5) are as large as possible, consistent with other circuit limitations such as dissipation.

From the above discussion it is clear, at least for a very slowly moving rotor, that the variation in reluctance should be obtained by saturation in the iron rather than by an increase in the airgap, as in the latter case, the position of Q will, in general, be close to B_1 and the area enclosed by the voltage-current locus will be relatively small.

The above explanation of behaviour, valid only at rotor speeds slow enough that this approximate steady state theory applies, is applicable also to the linear reciprocating devices shown in Figure 2.2 (c) and (d). As the rotor or armature speed increases current excursions will be restricted by the circuit inertia; so that a fall in torque with speed may be expected. However before any useful qualitative or quantitative information can be gained concerning the behaviour at finite rotor speeds, a far more accurate model of the machine is required.

CHAPTER 3: PROTOTYPE MACHINE AND MEASUREMENT OF ITS CHARACTERISTICS

3.1 General.

In order to test the ideas set out in the previous section a simple machine was constructed by using standard ¼ H.P. single phase induction motor frame and unpunched laminations. Constructional details, dimensions and winding data are shown in Figure 3.1 and Table 3.1.

This machine was built early in 1965, before any analysis of its operation, other than that already presented in section 2, had been carried out, so that its actual form is the result of logic and intuition rather than of design based upon the results presented in this thesis. Its characteristics have proved to be typical of such devices, and have therefore been measured as carefully as possible in order to provide an experimental check on the theory subsequently developed.

Information of interest concerning such a machine is contained in the following measured characteristics:-

(a) torque-speed)
(b) current-speed) Obtained for a range of applied voltage, series capacity and resistance.
(c) efficiency-speed))
(d) core loss-speed)

(e) current and flux waveforms.

In addition, the following relationships, measured under blocked rotor conditions with no series capacitor, provide information leading to the establishment and checking of an equivalent circuit for the machine, viz:-

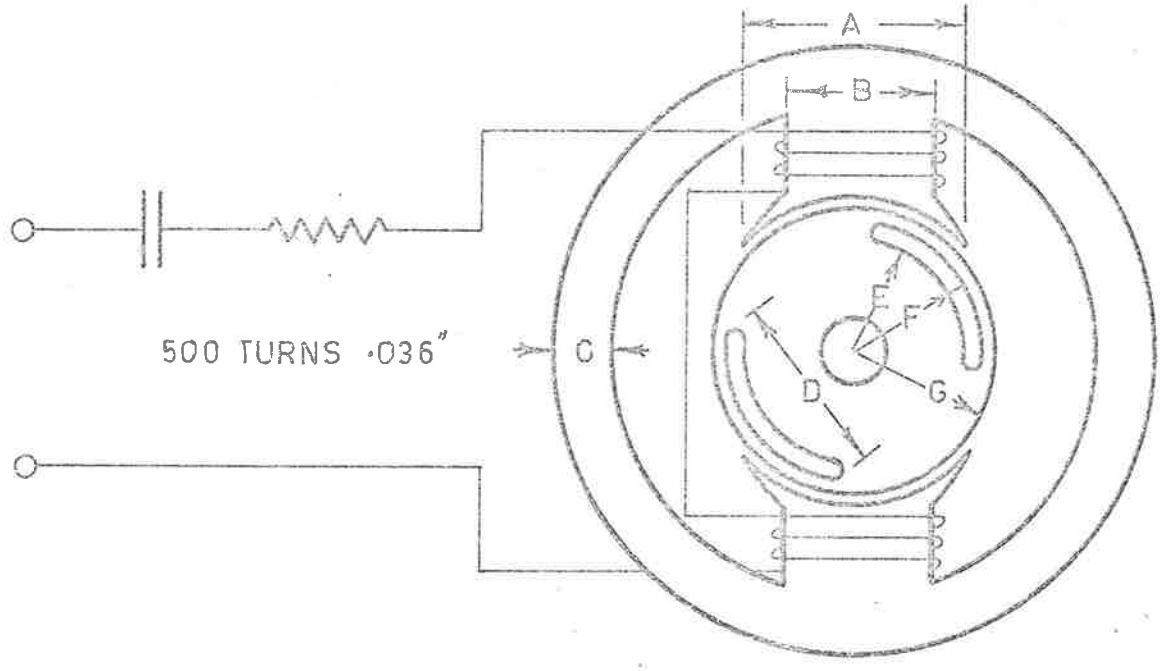

FIGURE 3.1 : DETAILS OF PROTOTYPE MACHINE

A	B	C	D	E	F	G	Air gap
2.0	1.0	0.5	2.25	1.43	1.68	1.93	.0075 ins

TABLE 3.1 : DIMENSIONS OF PROTOTYPE

R.M.S. current, input power, peak current, peak flux, and torque versus applied voltage for a range of rotor positions.

The experimental set up used to obtain the above information is discussed briefly in the following sections.

3.2 Torque measurement.

Measurement of developed electromagnetic torque may be accomplished by mounting the stator on ball bearings at each end, and restraining it with a spring steel bar as shown schematically in Figure 3.2 and in Plate 3.1. Ferranti silicon strain gauges glued to the top and bottom of the bar and connected as shown in Figure 3.3 give an output proportional to electromagnetic torque after certain corrections have been applied.

Possible errors in this measurement result from:-

(a) non-linear stress-strain relationship in the bar

(b) non-linearity in strain gauges

(c) variation in bar temperature due to heating as the machine is loaded

(d) friction and windage loss between stator and rotor

(e) friction in stator trunnion bearings.

Of these (a) and (b) can be kept to a minimum by appropriate design of the bar to match the expected torque and then eliminated entirely by calibration, while the effect of (c) can be minimised by using matched pairs of strain gauges, high stability, matched fixed R and

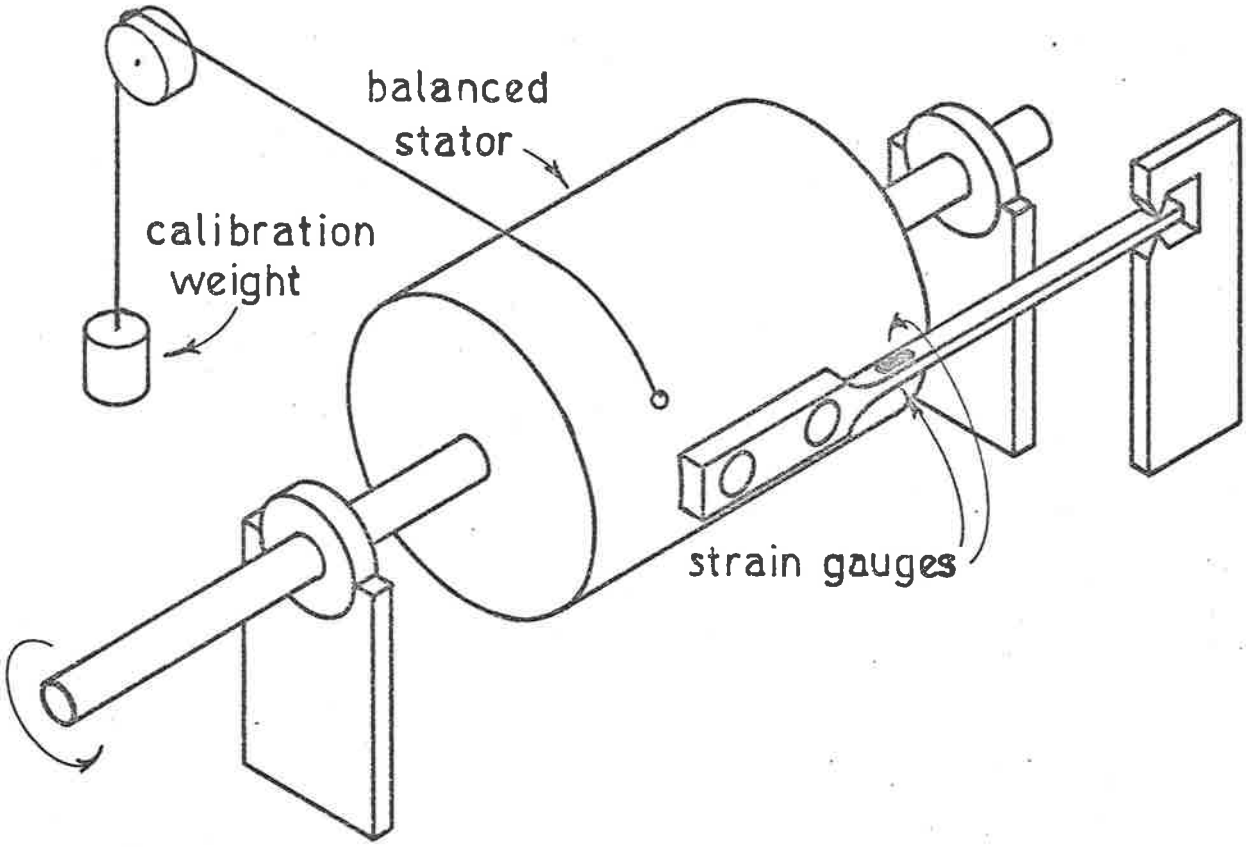

FIGURE 3.2 : SCHEMATIC OF TORQUE MEASUREMENT

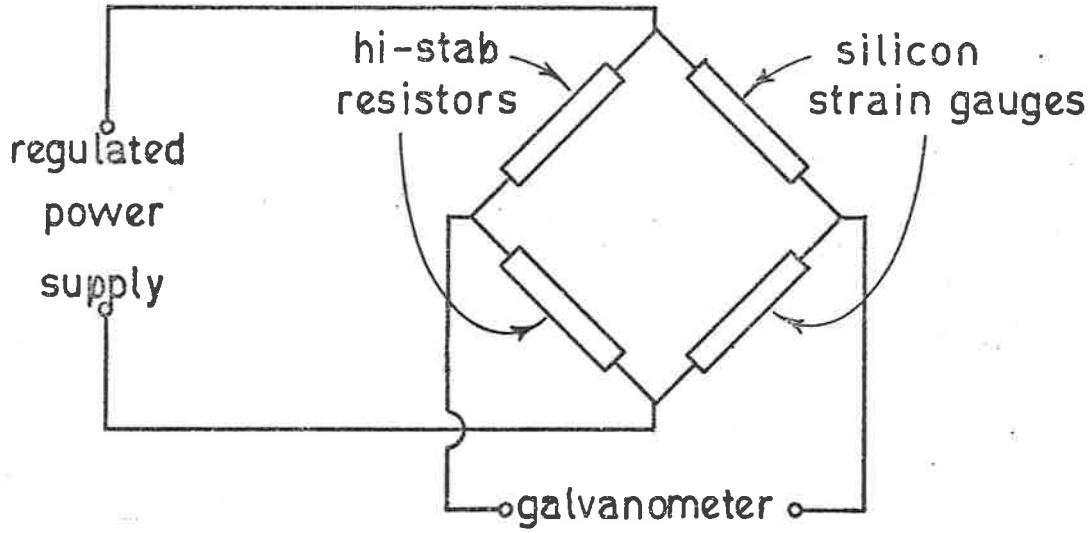

FIGURE 3.3 : STRAIN GAUGE CONNECTIONS

PLATE 3.1

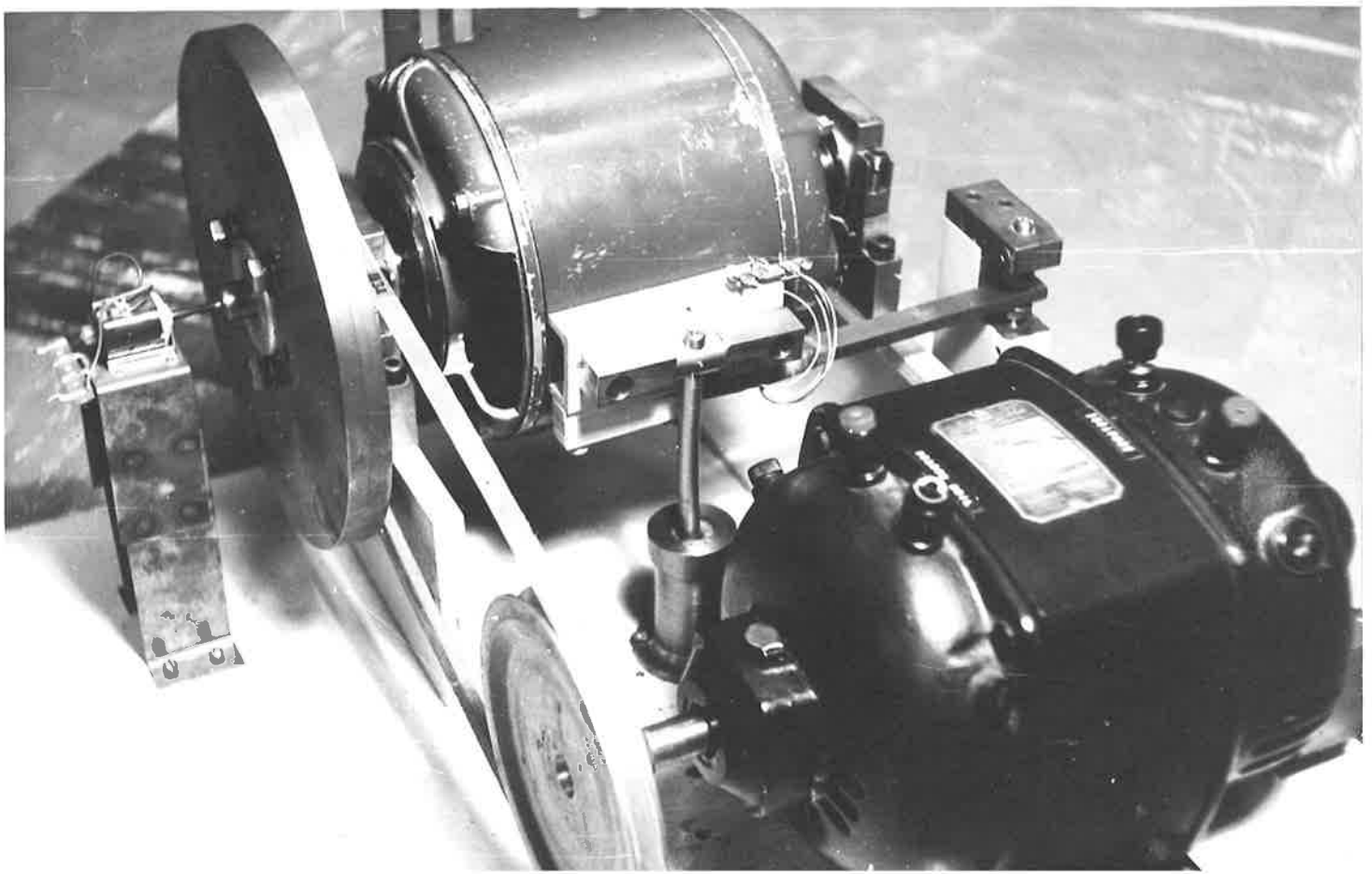

frequent bridge zero checks after allowing a suitable warm up period.

The magnitude of (d) can be measured by driving the test machine by another motor and noting the torque on the stator of the test machine with the stator windings open circuited.

Finally, (e) tends to be removed by calibration, but good design can keep it to a negligible value. Note that this error is effectively doubled by adding the friction and windage (d) to the measured torque in order to obtain the total developed electromagnetic torque.

Calibration is accomplished by the application of a series of known torques to the stator as suggested in Figure 3.2.

With this arrangement, properly calibrated, both blocked rotor and running torques may be measured; the former by locking the test machine rotor in the desired position and the latter by loading the test machine with a separately excited armature fed d.c. machine.

Accurate control of the latter was accomplished by using a solid state convertor developed by the author for the purpose. Two published papers dealing with the operation and design of such a convertor are appended to this thesis [32,33].

3.3 Measurement of stator flux linkages.

As with most electromagnetic energy conversion devices it is convenient to separate the winding flux into two distinct portions. That which does not cross the airgap contributes nothing to the actual energy conversion process, its path is largely in air, and hence its magnitude is proportional to the m.m.f. which establishes it. On the other hand,

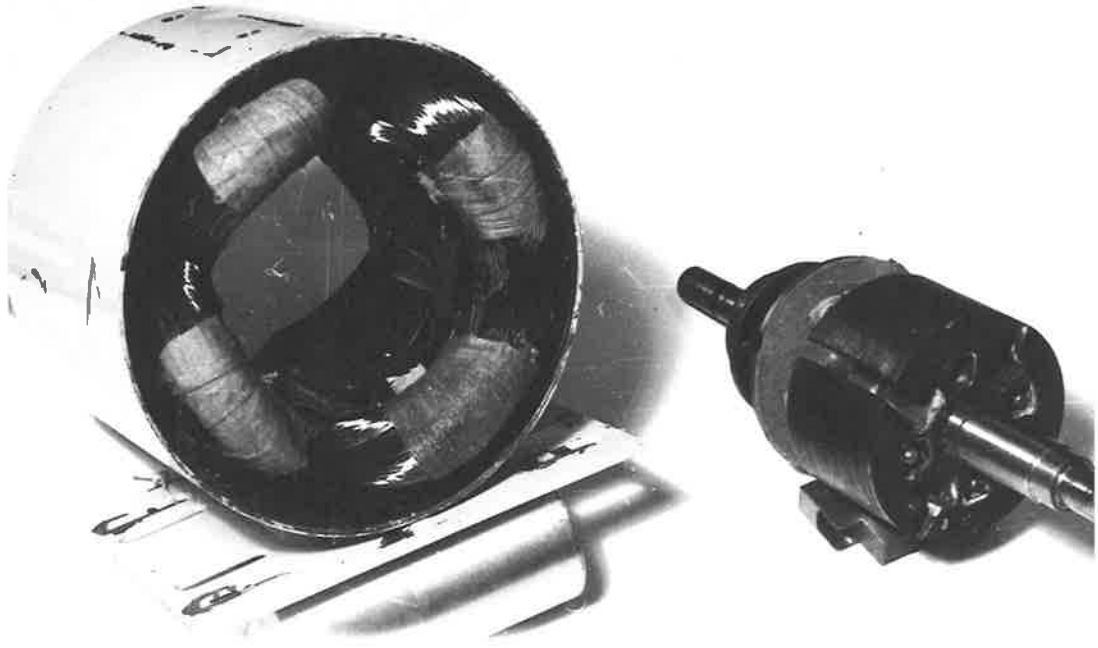

(b)

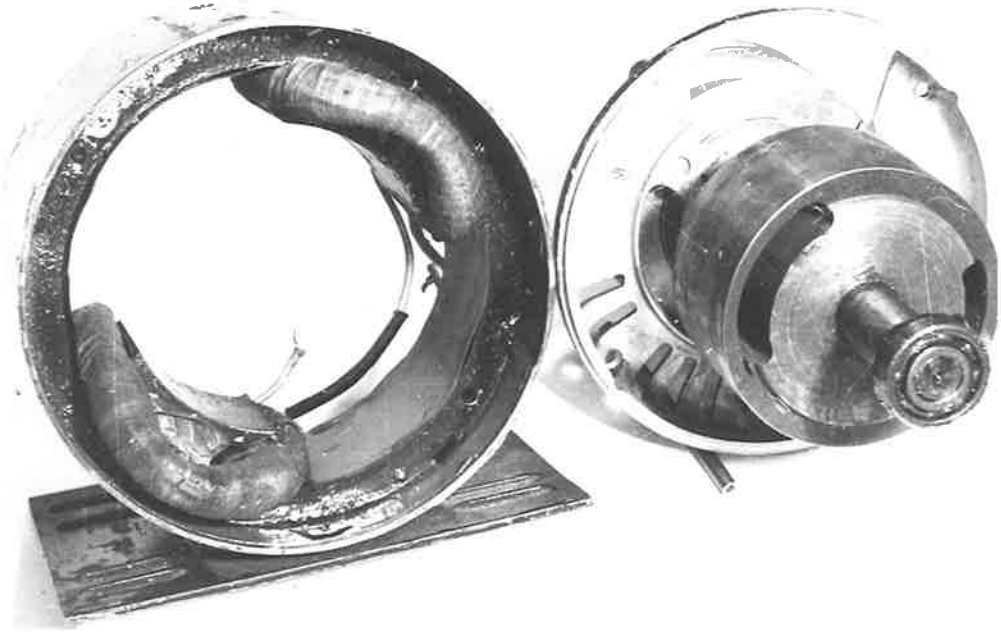

(a)

PLATE 3.2

for the particular configuration in which we are interested, flux leaving a stator pole face and crossing the airgap to the rotor, will follow a path in which ferromagnetic material predominates. This latter component of flux will not be proportional to the m.m.f.; so that direct measurement of the flux itself is required.

This is accomplished conveniently by surrounding the pole faces with search coils of N_s turns and integrating the voltage induced in the search coil with a simple RC network to give the total stator flux linkages due to airgap flux as:-

$$\lambda = \frac{N}{N_s}\int v_s dt \qquad \ldots\ldots (3.1)$$

The mean magnetization curve of the machine, expressing airgap flux linkages (λ) versus current (i) may be obtained by plotting the peak values of λ and i for a range of values of applied stator voltage.

Leakage flux linkages may be found from the difference in applied voltage and airgap voltage as measured by the search coils, after correction for turns ratio and stator winding resistance. This result represents the difference between two relatively large quantities; so providing the possibility of a large percentage error in the final result. By taking the mean value of a large number of experimental determinations greater accuracy may be obtained.

3.4 Results.

Typical results are presented in Figures 3.4, 3.5 and 3.6 which show electromagnetic torque, r.m.s. current, core loss and efficiency as

FIGURE 3.4(a) : MEASURED TORQUE & CURRENT

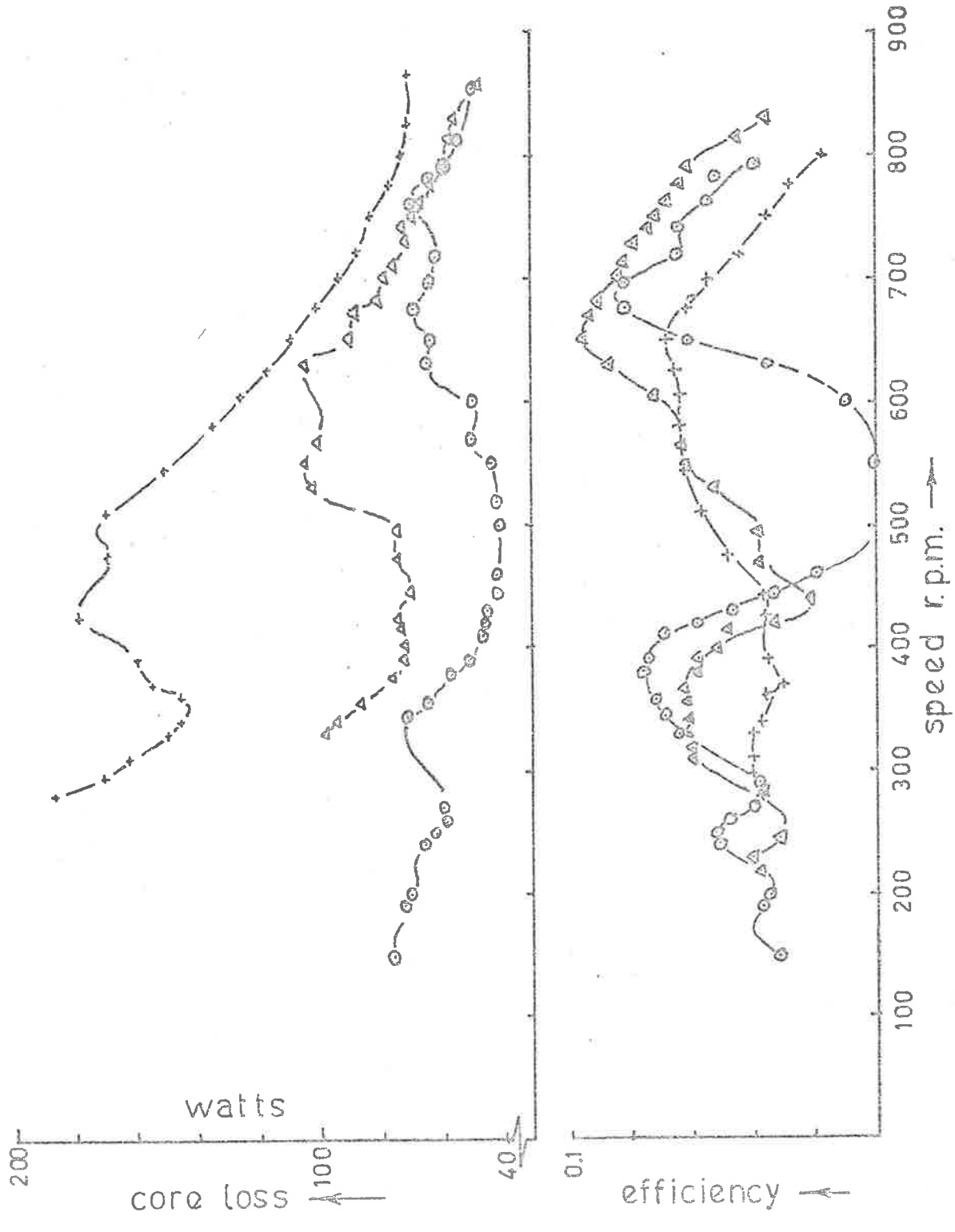

FIGURE 3.4(b): MEASURED CORELOSS & EFFICIENCY

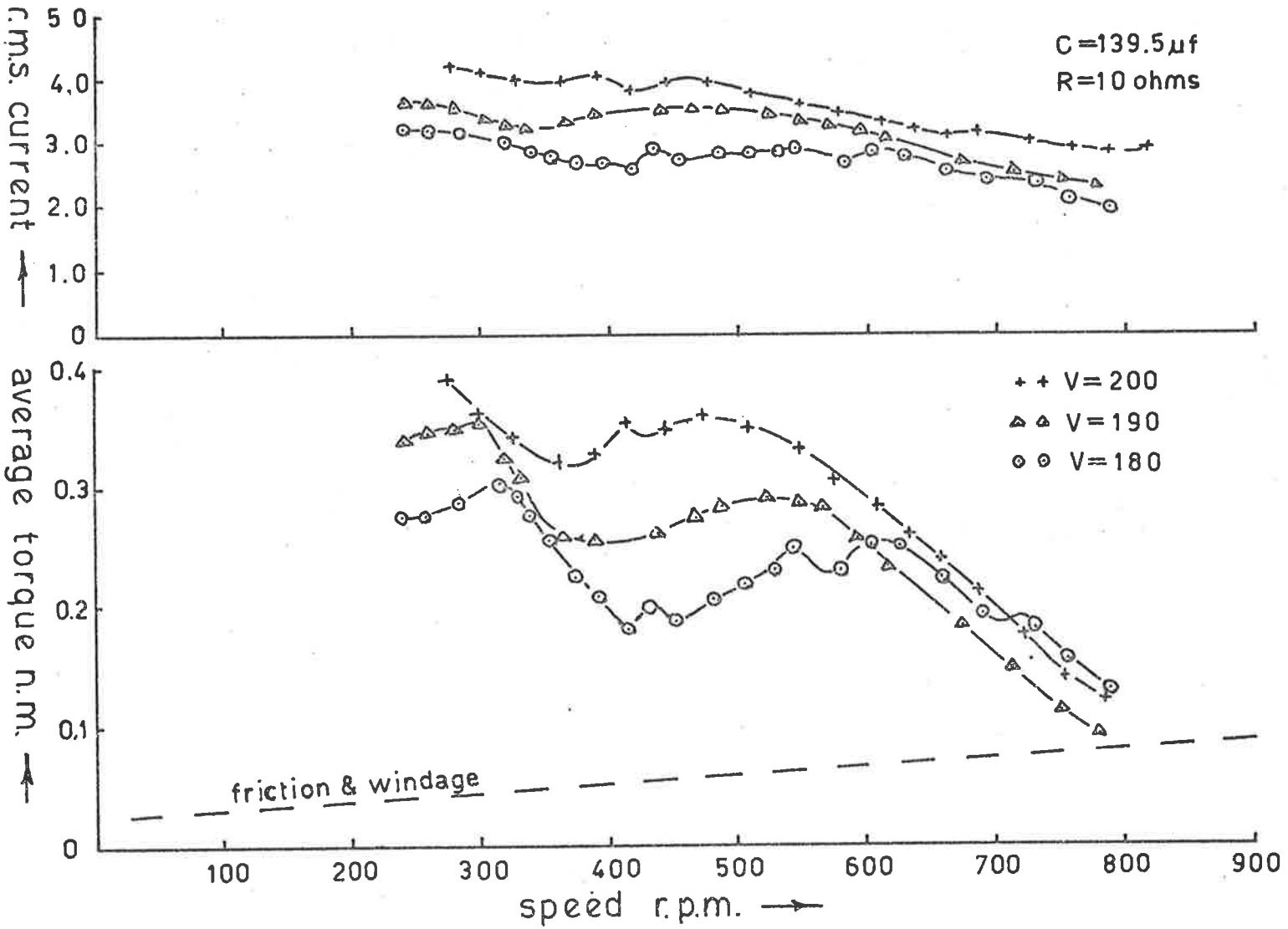

FIGURE 3.5(a): MEASURED CURRENT & TORQUE

FIGURE 3.5(b): MEASURED CORELOSS & EFFICIENCY

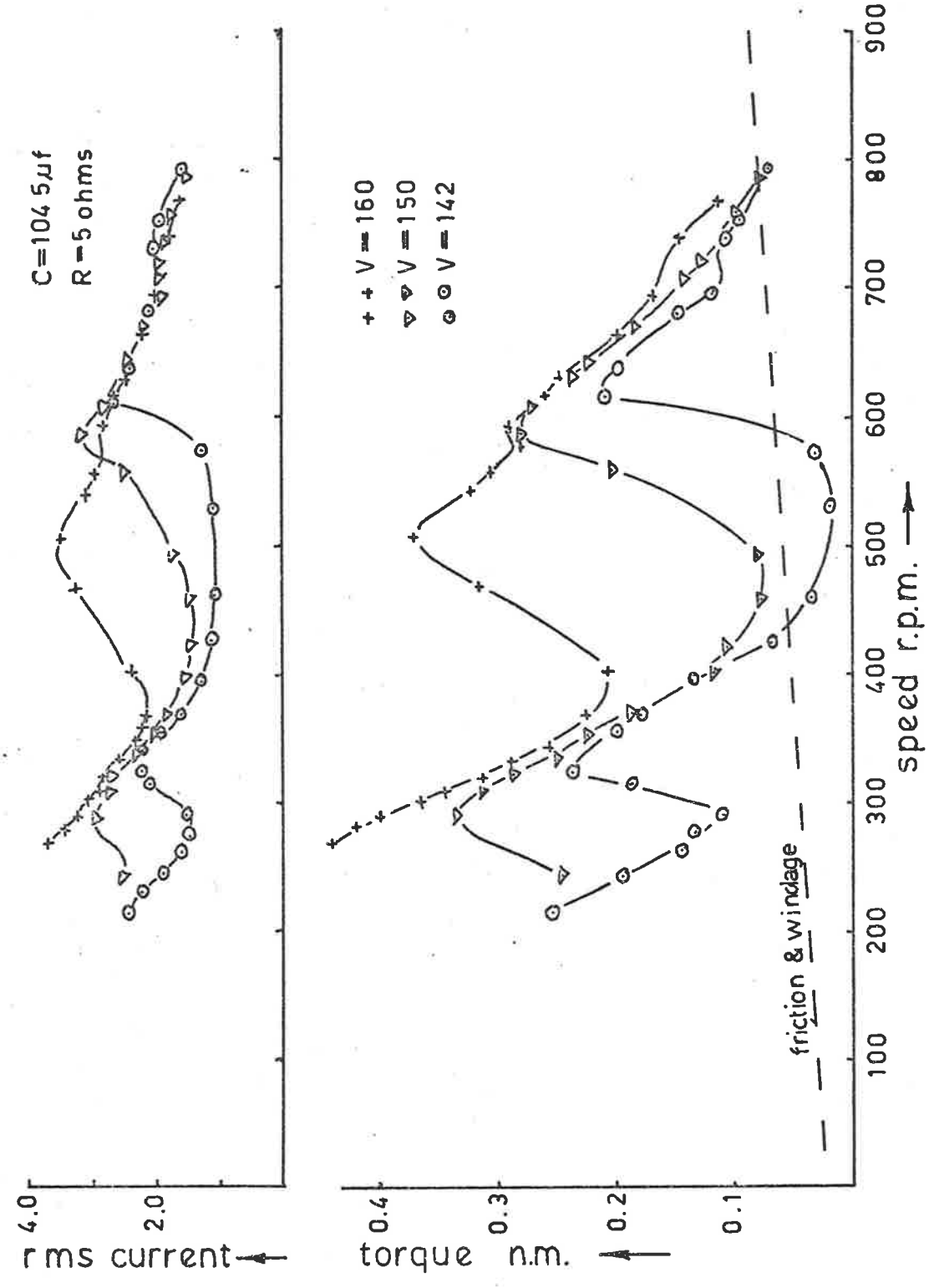

FIGURE 3.6(a): MEASURED CURRENT & TORQUE

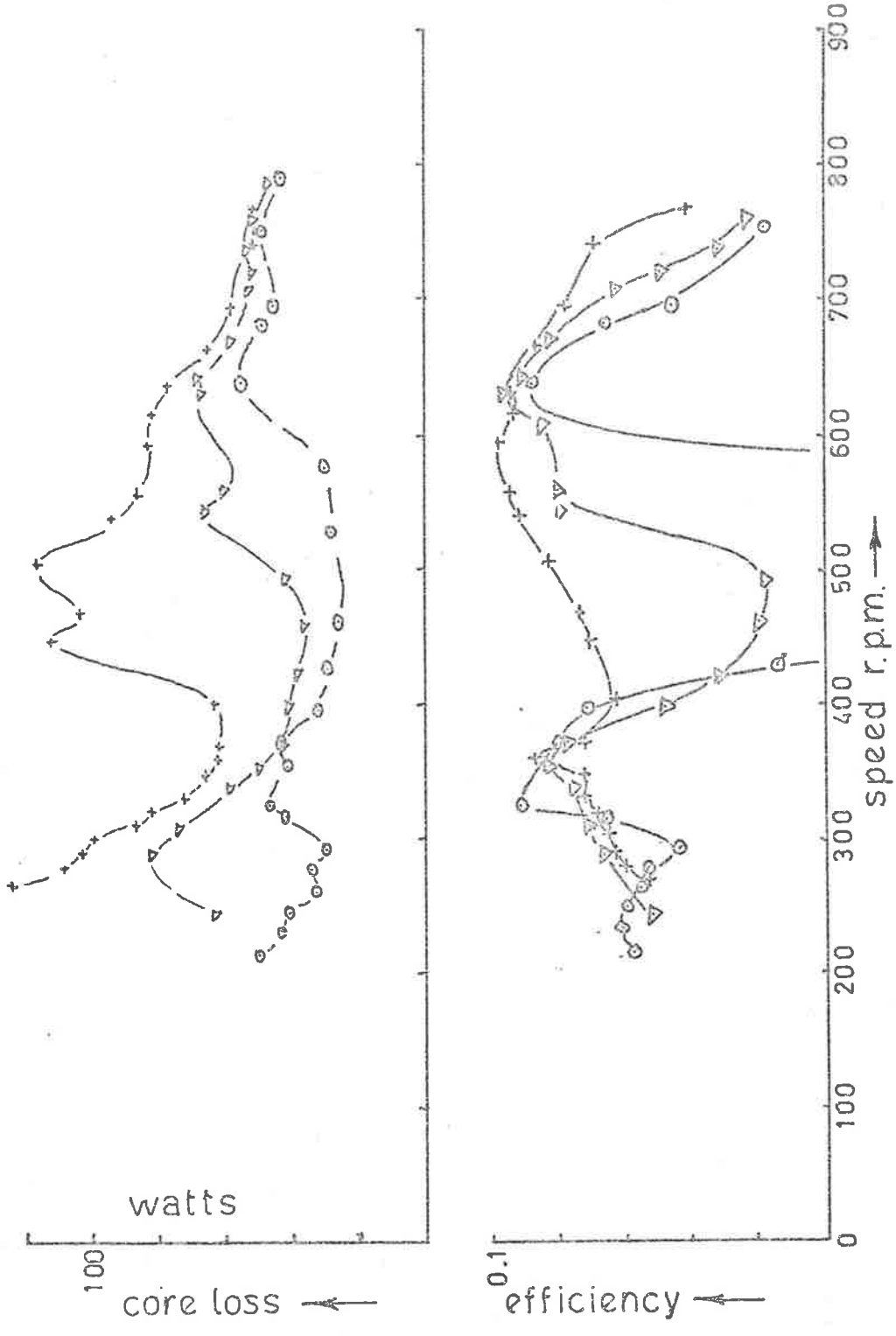

FIGURE 3.6(b): MEASURED CORELOSS & EFFICIENCY

functions of speed for a number of values of applied voltage, series capacity and series resistance.

The torque shown in these figures is essentially torque developed under asynchronous conditions. Superimposed upon these curves are a number of small synchronous spikes which occur at speeds which are integral fractions of the nominal synchronous speed of the machine.

The nature of the asynchronous torque, comprising alternate positive and negative pulses, makes accurate measurement of the small synchronous spikes difficult unless impracticably large load inertia is present.

Throughout the remainder of this thesis the emphasis will be placed upon the asynchronous torque, however expressions which determine the amplitude and location of these synchronous spikes will be presented where appropriate.

Figures 3.7 and 3.8 show the stator airgap flux linkages as functions of current and rotor position. To these must be added the leakage flux in order to obtain the total stator winding flux linkages.

Representative flux and current waveforms are shown in Figure 3.9 for two different values of speed while Figure 3.10 shows instantaneous flux versus current for the same conditions as Figure 3.9.

Additional experimental data will be presented as required.

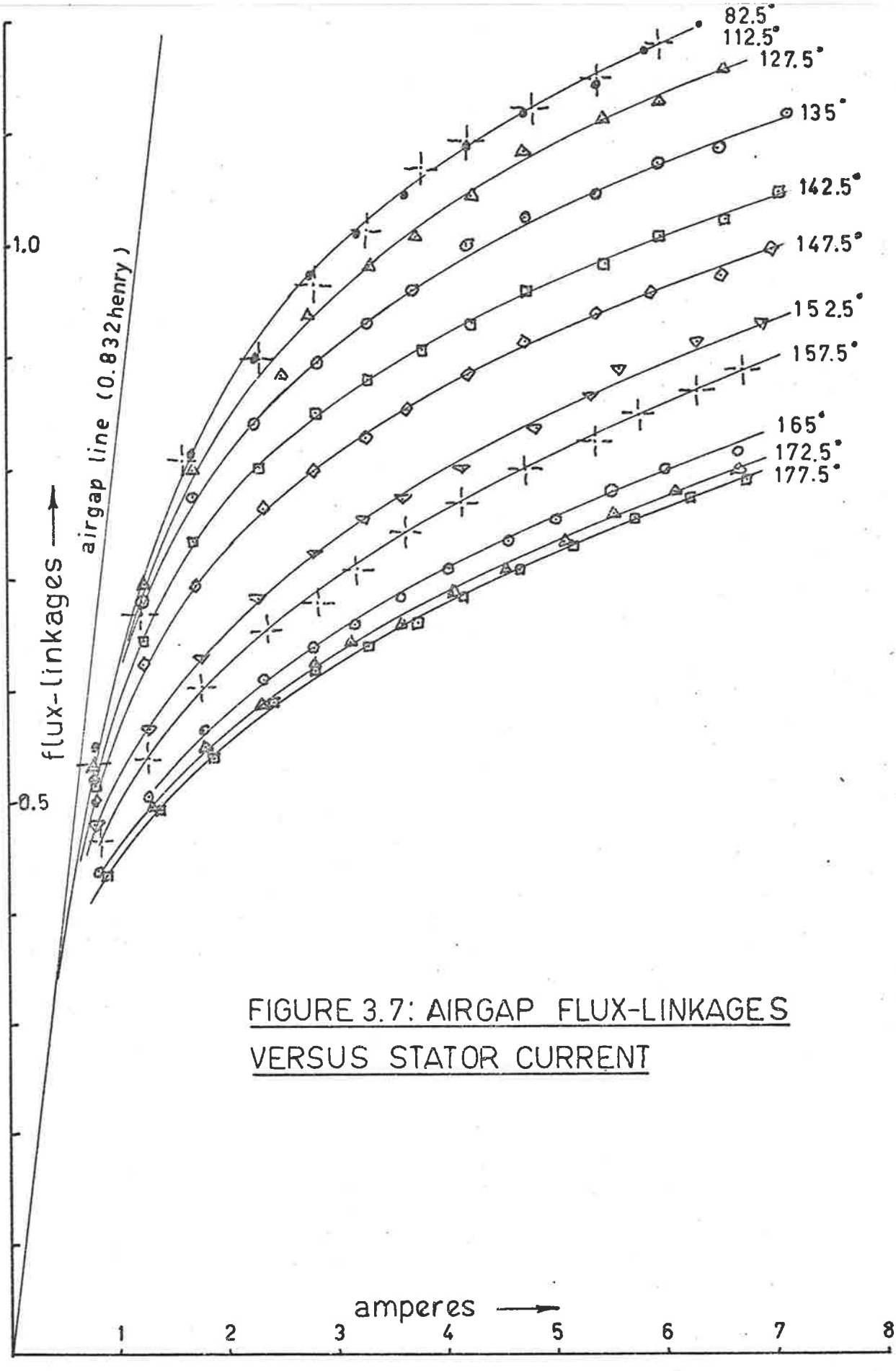

FIGURE 3.7: AIRGAP FLUX-LINKAGES VERSUS STATOR CURRENT

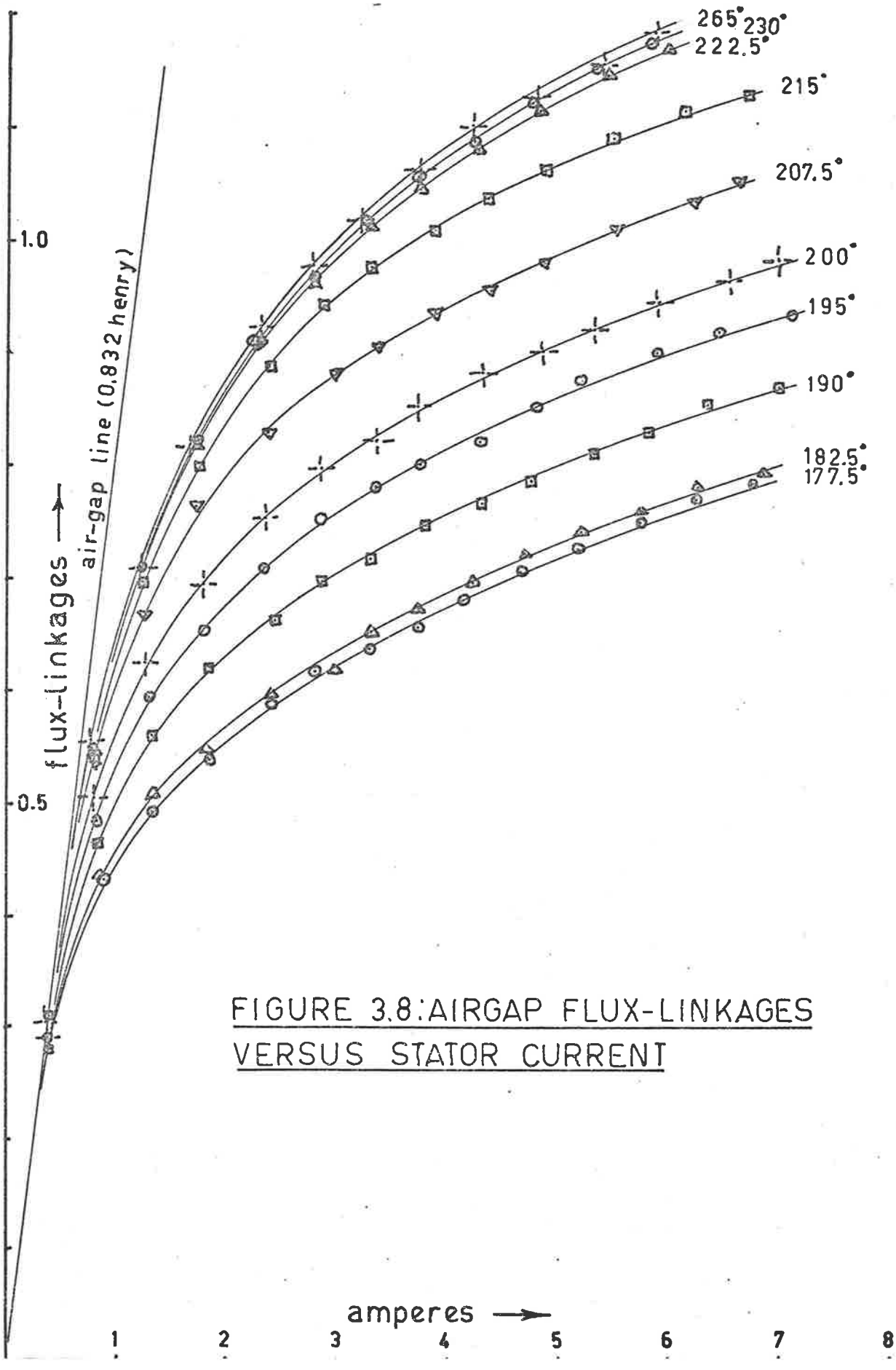

FIGURE 3.8: AIRGAP FLUX-LINKAGES VERSUS STATOR CURRENT

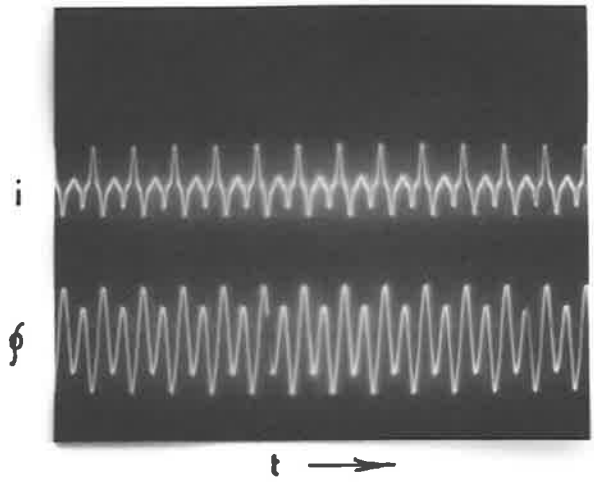

(a) 760 r p m

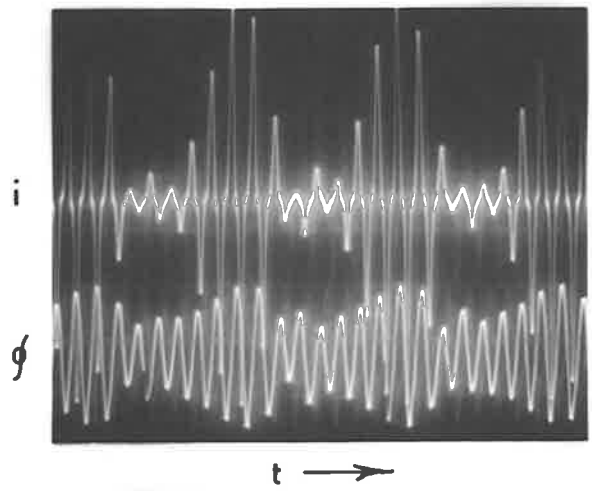

(b) 225 r p m

FIGURE 3.9

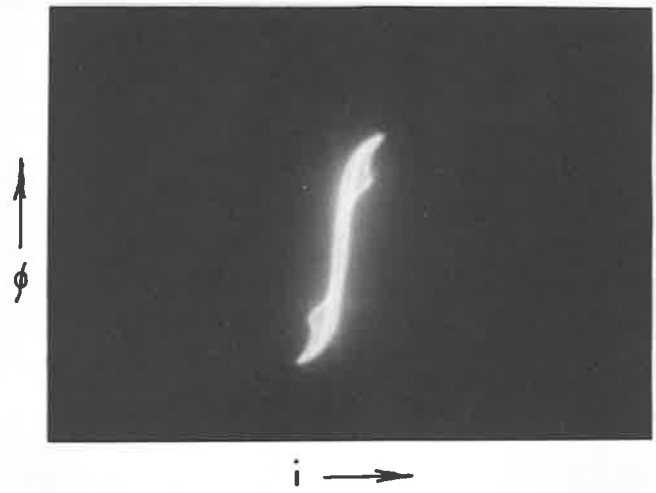

(a) 760 rpm

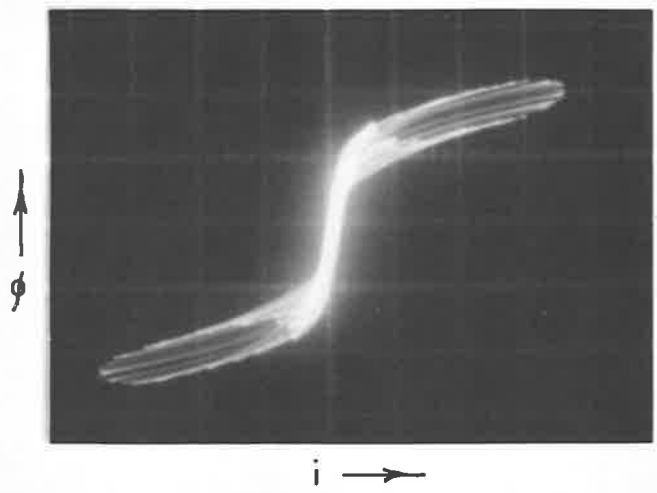

(b) 225 rpm

FIGURE 3.10

CHAPTER 4: MATHEMATICAL MODEL AND EQUIVALENT CIRCUIT

Calculation of the λ-i characteristic pertaining to a particular magnetic circuit of known geometry and material or conversely, determination of the geometry required to provide a particular λ-i characteristic, are problems which are common to all electro-magnetic devices. Although relevant, these problems are not the ones under investigation in this report. Here our interest is centred on the performance of devices which possess flux-linkage characteristics having the general form shown in Figure 4.1 or in Figures 3.7 and 3.8. These are idealized characteristics, as no allowance is made for the effects of hysteresis or eddy currents. This aspect is discussed in section 4.4.

4.1 Mathematical models for λ-i relationship.

Before the analysis of such a machine can proceed, a suitable mathematical model of the family of flux linkage-current curves must be adopted.

From the introductory and very elementary discussion on the mode of operation which was presented in section 2.3, it may be inferred that a higher average torque per unit volume and per unit average current will result if the parametric variation of the circuit inductance is accomplished by changes in the iron circuit reluctance rather than changes in the airgap. The latter would result in a family of characteristics having the general form shown in Figure 4.2. In general the form of the ω L(i) I_f-I_f characteristics is similar to the λ-i characteristics, as will be shown in Chapter 7.

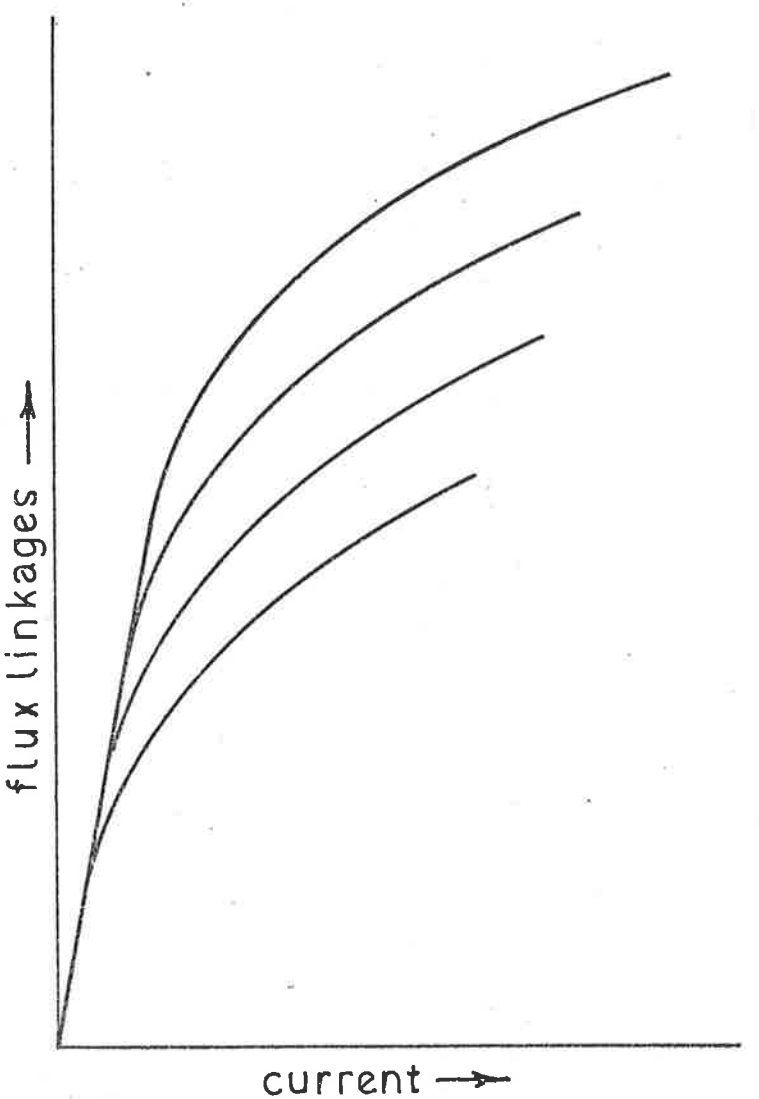

FIGURE 4.1 : VARIABLE IRON RELUCTANCE

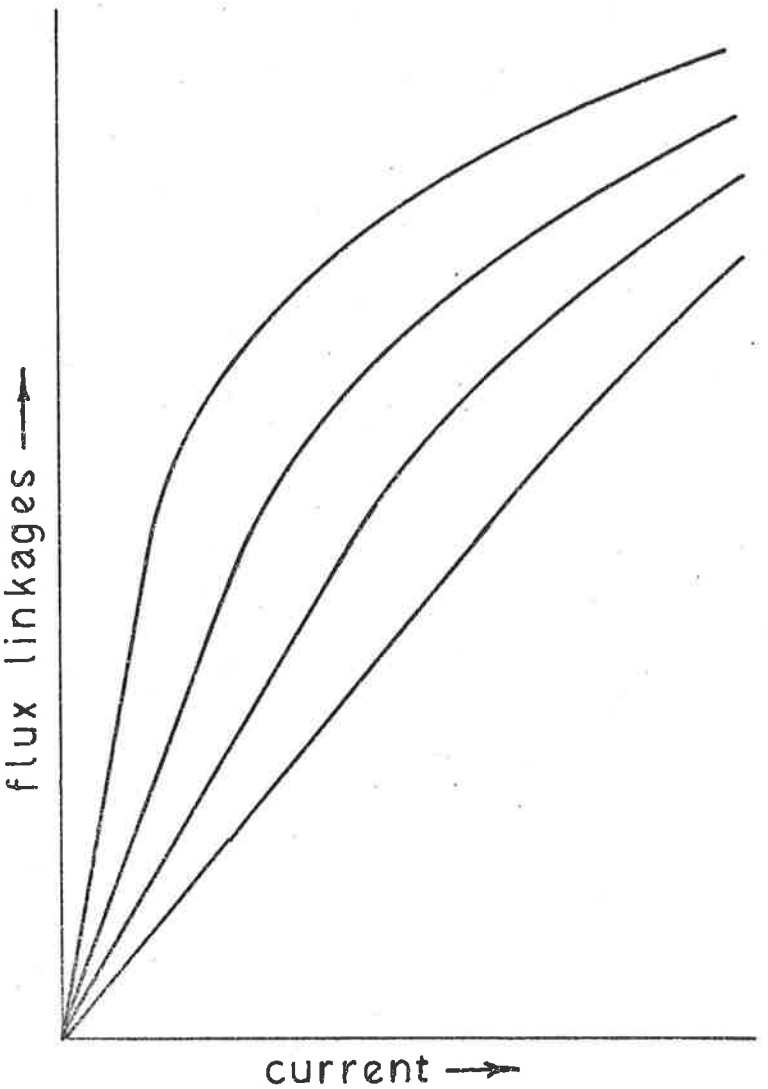

FIGURE 4.2 : VARIABLE AIRGAP

In other words it is likely that we shall want the ω L(i) I_f-I_f, and hence the λ-i characteristics to 'peel off' from the top down as shown in Figure 4.1, rather than to 'rotate' about the origin as in Figure 4.2. The former will ensure, at least at slow speeds, that the negative torque produced in moving from the minimum to the maximum reluctance position will remain as small as possible in accordance with equations (2.4) or (2.5). Thus, while a suitable model should be able to represent characteristics such as those in Figure 4.1 with a minimum of complexity, it should if necessary be able to include those of Figure 4.2. Some possible representations of the λ-i relationships are as follows [11,24,37]:-

$$i = a \sin h\,(b\lambda) \qquad \ldots\ldots (4.1)$$

$$i = a \tan (b\lambda) \qquad \ldots\ldots (4.2)$$

$$\lambda = a \tan h\,(bi) \qquad \ldots\ldots (4.3)$$

$$\lambda = ai - bi^3 \qquad \ldots\ldots (4.4)$$

$$\lambda = \frac{ai}{1 + b|i|} \qquad \ldots\ldots (4.5)$$

$$i = a\lambda(1 + b_1\lambda^2 + b_2\lambda^4 \text{ -----}) \qquad \ldots\ldots (4.6)$$

where the values taken by a and b will not necessarily be the same in each case. If the small signal inductance is to remain constant, i.e. a constant airgap, then the first three relationships will require the product ab to be constant. Thus in order to represent the curves of Figure 4.1 both a and b must be periodic functions; so that the manipulation and expansion of the RHS of each could be tedious. Expression (4.4) must be used with caution because $d\lambda/di$ becomes negative for $i^2 > a/b$, and as for all but (4.6), curve fitting can be approximate only, because of the presence of

but two parameters, a and b.

The apparent simplicity of (4.5) makes it attractive, and while its use leads to a simple and useful expression for forces or torques in electromagnetic equipment having such characteristics, it proves to be cumbersome for numerical and analogue computation; so that the majority of the analysis in this report is carried out with the use of (4.6).

However because of the engineering simplicity of some of the results obtained by using (4.5) some further discussion concerning its use follows in section 4.2.

4.2 Representation of the λ-i characteristic by $\lambda = ai/(1+b|i|)$.

Appendix I of this report comprises a copy of a publication by the author [31], portion of which publication is summarized in this section. Although much of this material, strictly is not pertinent to the main problem, it is relevant to the calculation of forces or torques in electromechanical devices subject to saturation. It is not pertinent, simply because (4.6) is used subsequently in the analysis rather than (4.5).

The form of (4.5) follows from the relationship:-

$$\text{flux linkages} = \frac{\text{turns} \times \text{m.m.f.}}{\text{total reluctance}} \qquad \ldots\ldots (4.7)$$

$$\text{i.e. } \lambda = \frac{N^2 i}{S_a + S_i} = \frac{N^2}{S_a} \frac{i}{1 + \frac{S_i}{S_a}}$$

$$= L_o i/(1 + \frac{S_i}{S_a}) \qquad \ldots\ldots (4.8)$$

Here S_a represents the total reluctance of all series airgaps in the magnetic circuit and S_i represents the current and position dependent reluctance of the iron path, which may be expressed conveniently by:-

$$S_i = \frac{N|i|}{f(\theta)} \qquad \ldots\ldots (4.9)$$

Here the iron permeability has been replaced by $1/N|i|$ and the ratio of the effective area of the iron to its effective length has been replaced by $f(\theta)$. This latter function is dependent upon the rotor geometry and has a period of one pole pitch. Thus:-

$$\lambda = \frac{L_o i}{1+\frac{N|i|}{S_a f(\theta)}} = \frac{L_o i}{1+\frac{L_o|i|}{N f(\theta)}} = \frac{L_o i}{K} \qquad \ldots\ldots (4.10)$$

where K is the saturation factor.

4.2.1 Curve fitting.

When supplied from a source of alternating voltage both λ and i become period functions of time; so that (4.10) may be written:-

$$\frac{\Lambda}{L_o i_p} + \frac{\Lambda}{N f(\theta)} = 1 \qquad \ldots\ldots (4.11)$$

where Λ and i_p correspond to the peak values of the flux and current waveforms. Thus plotting measured values of Λ/i_p against Λ should result in a straight line, which extended, intercepts the Λ/i_p axis at L_o and the Λ axis at $f(\theta)$, provided the machine characteristics can be represented by an expression of the form of (4.5). By this means values may be assigned to L_o and to $f(\theta)$ for all θ, so leading to a family of theoretical λ-i

curves for the machine. Typical results are presented in Figures 7 and 8 of Appendix I.

4.2.2 Torque from $\lambda = ai/(1 + b|i|)$.

Torque may be calculated from the partial derivative of co-energy with respect to rotor position, i.e.

$$T = \frac{\partial W'(\theta,i)}{\partial \theta} \qquad \ldots\ldots (4.12)$$

Using (4.12), Section 8.1 of Appendix I, shows that the instantaneous torque may be expressed as

$$T = L_o \frac{f'(\theta)}{f(\theta)} i^2 \frac{1}{(K-1)}^2 (K - \frac{1}{K} - 2\ln K) \qquad \ldots\ldots (4.13)$$

where K is the instantaneous value of the saturation factor defined in (4.10), which depends upon the values of the instantaneous flux or current and rotor position.

Under conditions of alternating voltage supply a knowledge of the average, rather than of the instantaneous torque is required but the average value of (4.13) clearly depends upon the current waveform.

In practical devices, where good efficiency is important, the circuit resistance is, in general, sufficiently low that sinusoidal flux conditions exist in the windings when the supply voltage itself is sinusoidal Displays of λ-$\dot{\lambda}$ for the actual machine, when fed with an alternating voltage in the absence of a capacitor, showed that an assumption of sinusoidal flux would be reasonable under these conditions even for saturation factors approaching 10.

Thus if $\lambda = \Lambda \sin \omega t$ ..... (4.14)

then $i = \frac{\Lambda}{L_o} \quad \frac{\sin \omega t}{1 - \frac{\Lambda |\sin \omega t|}{N f(\theta)}}$ ..... (4.15)

and $K = \frac{1}{1 - \frac{\Lambda |\sin \omega t|}{N f(\theta)}}$ ..... (4.16)

which, at peak values of i and λ, becomes:-

$$K_p = \frac{1}{1 - \frac{\Lambda}{N f(\theta)}} \qquad \text{..... (4.17)}$$

Substitution of (4.15) and (4.16) into (4.13), followed by integration and averaging over one half of one flux cycle leads to an expression for the average torque. This, in turn, may be expressed in terms of the peak, fundamental or R.M.S. current as derived from (4.15). Each particular expression however, contains a term which is a function of K_p. For example, it is shown in Section 8.4.1 of Appendix I, that the average torque may be expressed as

$$T_{av} = L_o \frac{f'(\theta)}{f(\theta)} I_r^2 F_4(K_p) \qquad \text{..... (4.18)}$$

where $F_4(K_p)$ is shown as curve 'd' in Figure 6 of Appendix I and I_r is the R.M.S. value of the current in the circuit after subtraction of the core loss component. The accuracy of (4.18) may be judged by reference to Figure 10 of Appendix I in which the full lines represent theoretical values for torque calculated using (4.18), while the points represent measured values.

It is apparent that the adopted model can lead to quite reasonable results in spite of the discrepancies apparent in Figure 7 of Appendix I.

However application of (4.18) requires a knowledge of Λ in order to evaluate $F_4(K_p)$.

A useful engineering simplification results if the average torque is expressed as

$$T_{av} = \frac{1}{2} \frac{\partial L_e}{\partial \theta} I_r^2 \qquad \ldots\ldots (4.19)$$

where L_e is the equivalent linear inductance expressed as a function of K_p. It is plotted in Figure 14 of Appendix I together with its approximation $L_e = L_o \left[0.55 - \frac{\ln(K_p-1)}{4.8} \right]$

which gives

$$T_{av} = \frac{L_o}{9.6} \frac{f'(\theta)}{f(\theta)} I_r^2 \qquad \ldots\ldots (4.20)$$

which corresponds to (4.18) with $F_4(K_p)$ replaced by a constant $1/9.6 = 0.104$

As the maximum difference between (4.18) and (4.20) is approximately 10% for $1.5<K_p<7$, and as (4.20) requires no knowledge of the degree of saturation associated with a particular current, it provides a useful engineering approximation applicable to any electro-mechanical device having λ-i characteristics similar to those in Figure 4.1 and which can be matched by an expression of the form of (4.10).

Some additional results, using this particular model to represent the machine λ-i characteristics, are presented in Appendix I. However for a number of reasons the power series representation given by (4.6) proves to be more convenient. No division process is necessary for analogue representation, greater accuracy may be obtained, and it is more satisfactory in its behaviour when attempting either numerical or analogue solutions.

Furthermore there is a considerable body of literature dealing with the behaviour of systems which include a relationship similar to (4.6) but in which all the coefficients are constants and not periodic as in this case.

4.3 Representation of the λ-i characteristic by a power series.

By making use of a λ-i relationship of the form given by (4.6), any desired accuracy of fit to the actual characteristics may be obtained by putting

$$i = \frac{\lambda}{L_o}\left(f_o(\theta) + f_1(\theta)\lambda^2 + f_2(\theta)\lambda^4 + f_3(\theta)\lambda^6 \ldots.\right)$$

$$= \frac{\lambda}{L_o}\sum_{n=o}^{h} f_n(\theta)\lambda^{2n} \qquad \ldots\ldots (4.21)$$

where L_o represents the mean value of the small signal airgap inductance and the various $f_n(\theta)$ are periodic functions of the rotor position θ, having a fundamental period equal to one pole pitch. These $f_n(\theta)$ are determined by the over-all geometry and magnetic characteristics of the stator and rotor iron and must have the general form

$$f(\theta) = D_o + \sum_{m=1}^{\mu} D_m \cos \overline{mp\theta + \delta_m}$$

or $$F(\theta) = f(\theta)/D_o = 1 + \sum_{m=1}^{\mu} d_m \cos \overline{mp\theta + \delta_m} \qquad \ldots\ldots (4.22)$$

where p equals the number of poles in the machine.

4.3.1 Curve fitting.

Standard techniques of curve fitting, although tedious, are straightforward and may be applied to each member of the family of λ-i curves in turn [34]; so providing sets of points for the various $f_n(\theta)$ to which fourier series may be fitted in turn. In general, it will be found that the various $f_n(\theta)$ which are obtained by this method bear no simple relationship to each other, which means that a great deal of hardware will be required for analogue simulation and much tedious algebra in any attempted analytical solution. Thus some simplification for either of these purposes is desirable.

When the family of characteristics take the form shown in Figure 4.1, $f_o(\theta)$ may be replaced by a constant equal to unity; so that the saturation factor becomes

$$K = 1 + \sum_{n=1}^{h} f_n(\theta)\lambda^{2n} \qquad \ldots\ldots (4.23)$$

Depending upon the actual slope of the characteristics certain simplifications can be made. For example if the incremental slope is constant along lines of constant K, then it is a simple matter to show that (4.21) may be written:-

$$i = \frac{\lambda}{L_o}\left(1 + \sum_{n=1}^{h} a_n \left(f_1(\theta)\,\lambda^2\right)^n\right) \qquad \ldots\ldots (4.24)$$

which is a relatively simple expression for purposes of simulation when multi-potentiometer servo-multipliers are available.

In many cases sufficient accuracy may be obtained by reducing (4.21) to one non-linear term only, usually the cubic or quintic; so leading to

$$i = \frac{\lambda}{L_o} + \frac{f(\theta)}{L_o} \lambda^q \qquad \ldots\ldots (4.25)$$

from which we obtain

$$\log (L_o i - \lambda) = \log f(\theta) + q \log \lambda \qquad \ldots\ldots (4.26)$$

Thus a plot of $(L_o i - \lambda)$ against λ on log-log paper will be a straight line of slope q, intercepting the line $\lambda = 1$ at the point corresponding to the value of $f(\theta)$, provided that the λ-i characteristic can be represented by an expression as simple as (4.25).

Figure 4.3 shows experimental data from the prototype machine, plotted as $\log(L_o i_p - \lambda_p)/\log \lambda_p$ for the rotor in the direct and quadrature axis position only, for the sake of clarity. It is clear that a simple quintic relationship provides a good approximation to the actual characteristics in this case.

By plotting (4.26) for a number of intermediate rotor positions, using experimental data, a number of values for $f(\theta)$ may be obtained as shown in Figure 4.4.

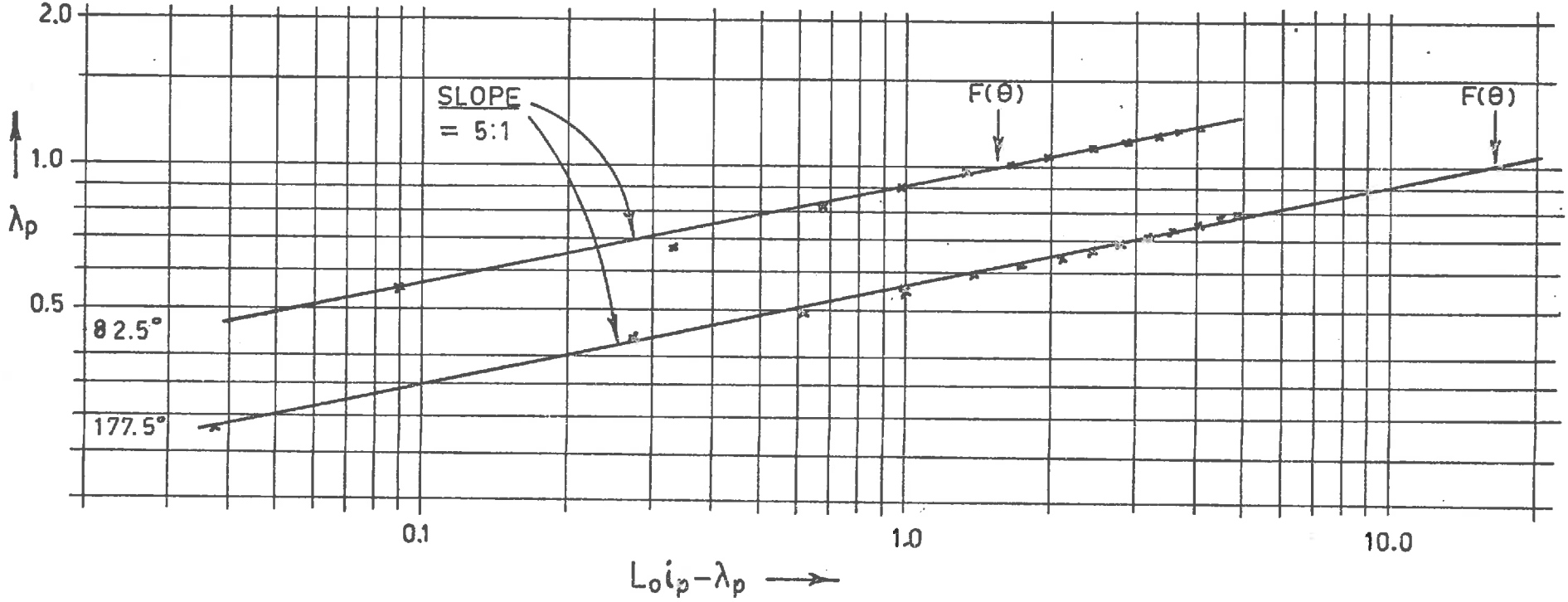

FIGURE 4.3 : DETERMINATION OF F(θ)

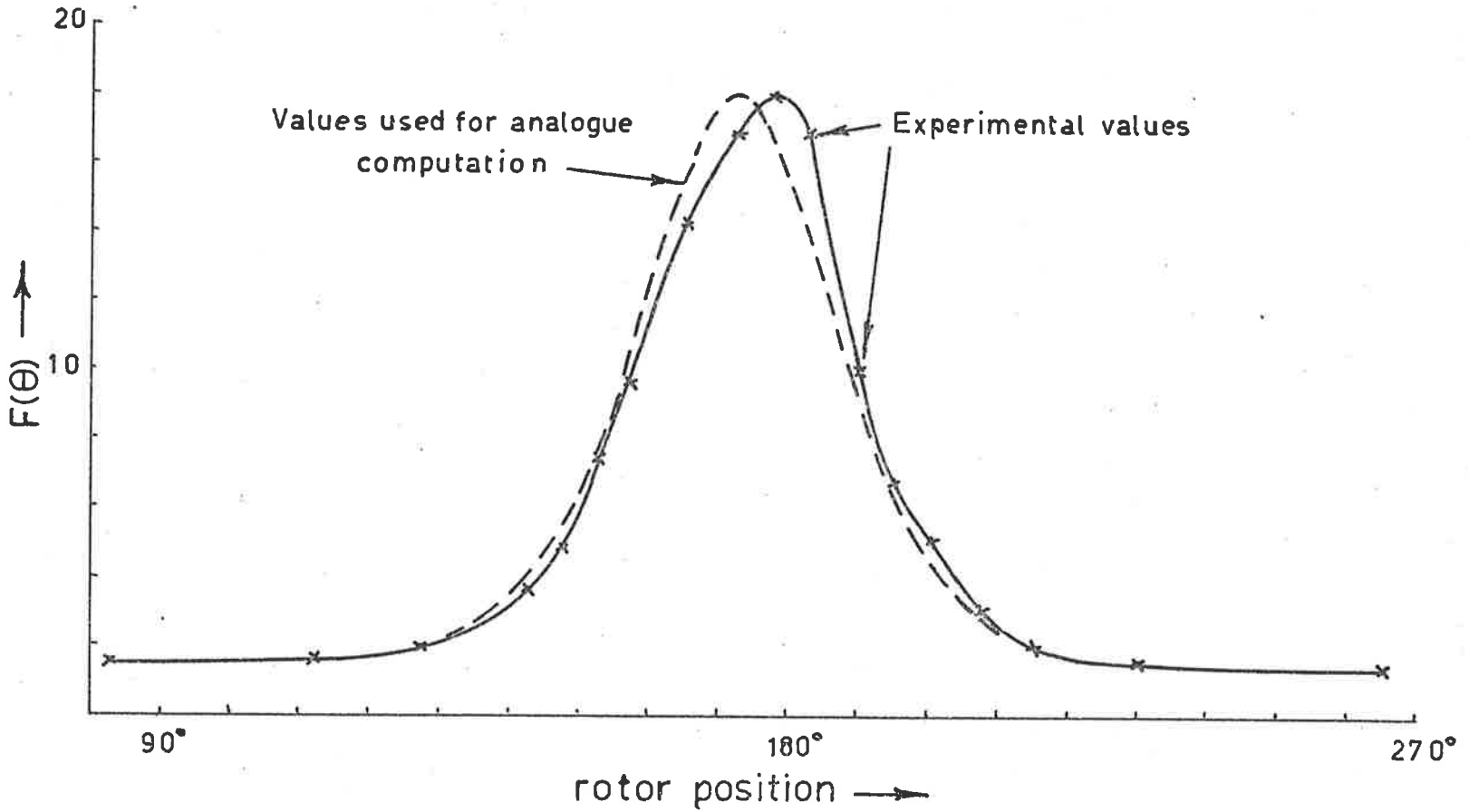

FIGURE 4.4 : F(θ) FOR QUINTIC APPROXIMATION TO λ-I RELATIONSHIPS

When these points are joined by a smooth curve, the result is a graphical representation of the function $f(\theta)$, which may be subjected to Fourier analysis, so that $f(\theta)$ may be expressed mathematically in the form of (4.22) to give a complete mathematical model of the machine λ-i characteristics. These are shown as full lines in Figures 4.5 and 4.6 for a number of particular values of rotor position, and may be compared with the experimentally obtained data shown as points in the same figures.

The agreement between the model and the observed characteristics is such that further analysis, using this model, may be undertaken with some confidence.

4.3.2 Stored energy and torque.

For a singly excited system such as the one under discussion, the stored energy in the field which crosses the airgap will be [10]:-

$$W_{fld}(\lambda,\theta) = \int_{o}^{\lambda} i \, d\varepsilon$$

which, when i is given by (4.21), becomes

$$W_{fld}(\lambda,\theta) = \int_{o}^{\lambda} \frac{\varepsilon}{L_o} \sum_{n=o}^{h} f_n(\theta) . \varepsilon^{2n} \, d\varepsilon$$

$$= \sum_{n=o}^{h} \frac{f_n(\theta) \, \lambda^{(2n+2)}}{(2n+2) \, L_o} \qquad \ldots\ldots (4.27)$$

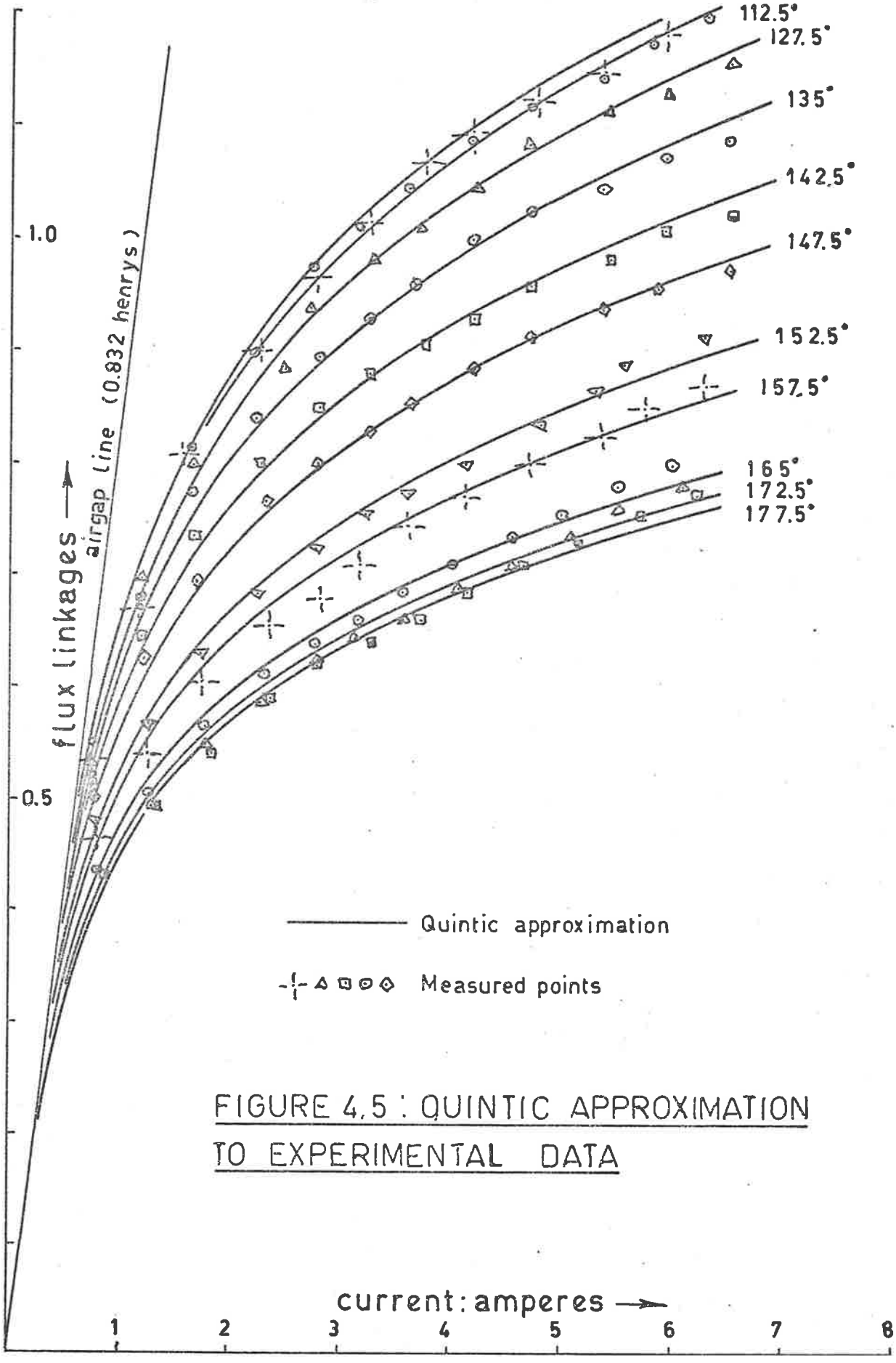

FIGURE 4.5 : QUINTIC APPROXIMATION TO EXPERIMENTAL DATA

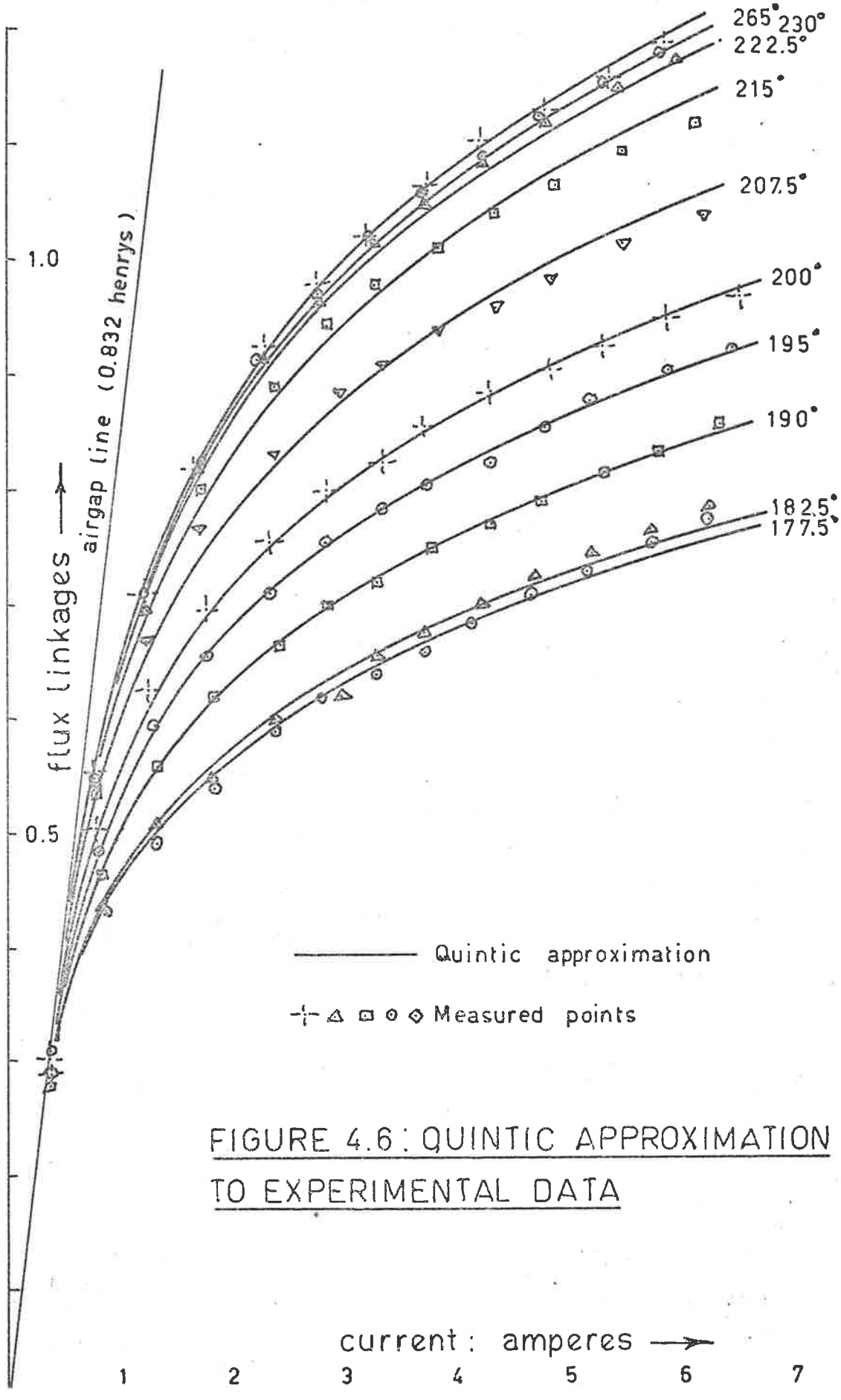

FIGURE 4.6 : QUINTIC APPROXIMATION TO EXPERIMENTAL DATA

Thus the instantaneous torque will be given by [10]:-

$$T = -\frac{\partial W_{fld}(\lambda,\theta)}{\partial\theta}$$

$$= -\sum_{n=o}^{h} \frac{f'_n(\theta)\,\lambda^{(2n+2)}}{(2n+2)\,L_o} \qquad \ldots\ldots (4.28)$$

and in particular when the flux linkages are related to the current by a simpler expression of the form given in (4.25), we have

$$T = -\frac{f'(\theta)\,\lambda^{q+1}}{(q+1)\,L_o} \qquad \ldots\ldots (4.29)$$

Leakage flux linkages, which are independent of rotor position make no contribution to the torque.

Under blocked rotor conditions, when the machine is fed from a source of alternating voltage, the flux waveform is sinusoidal and an average value for the instantaneous torque (4.28) may be calculated as shown in Appendix IIIa.

The nature of the instantaneous torque pulses, determined from (4.29), is indicated by the waveforms shown in Figure 4.7.

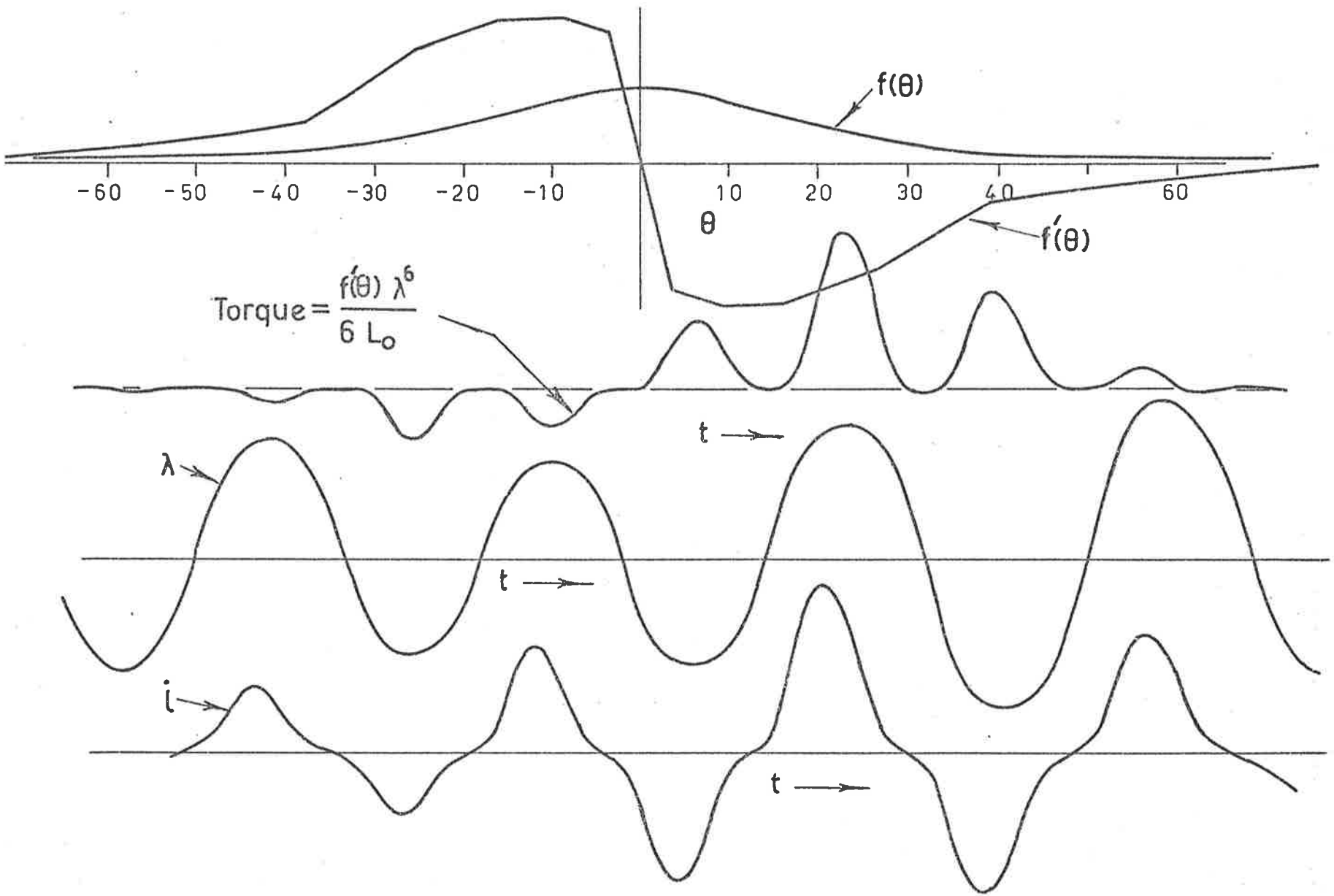

FIGURE 4.7: TYPICAL WAVEFORMS CORRESPONDING TO POINT 'A', FIG. 5.5

4.3.3 Equivalent circuit of the machine.

Details of the type of elementary machine under discussion were shown in Figure 3.1, from which it may be seen that the electrical circuit consists simply of the stator winding in series with a capacitor and a source of constant alternating voltage. In addition to the winding resistance, extra series resistance may be present. Furthermore there will be iron losses associated with the airgap flux, as distinct from the leakage flux, the path of which is substantially independent of the stator and rotor iron.

Thus the equivalent circuit of the machine will take the form shown in Figure 4.8, in which R, C and L_ℓ represent the total circuit series resistance, capacity and stator leakage inductance respectively. The time varying inductance L represents a circuit element which stores energy in a magnetic field in accordance with (4.27), whilst $R_C(\theta,\lambda)$ represents the sink for the position and flux dependent losses due to eddy currents and hysteresis in the machine iron. Further discussion on the problem of core loss representation is presented in section 4.4.

If the iron losses are sufficiently small that their effect on the operation of the machine may be neglected, then the leakage flux may be incorporated with the airgap flux; so that an expression of the form of (4.21) may include leakage flux without loss of generality. However, when iron losses are significant the circuit effectively has three independent energy storage or reactive elements instead of two, and its behaviour is fundamentally different.

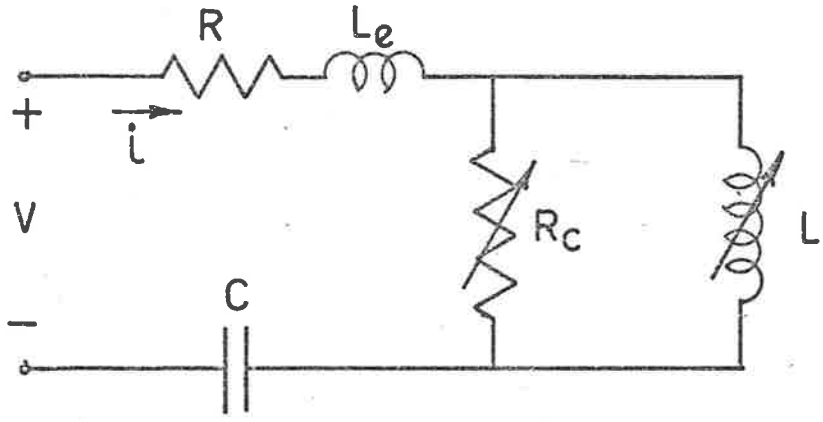

FIGURE 4.8: EQUIVALENT CIRCUIT

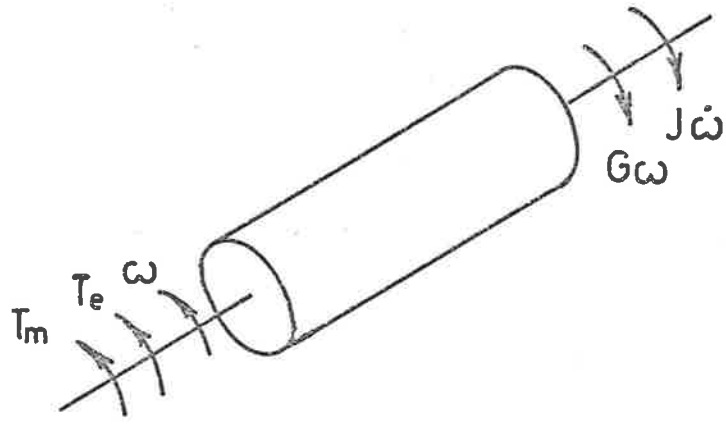

FIGURE 4.9: MECHANICAL SIGN CONVENTIONS

4.3.4 System equations.

A complete description of machine performance can be obtained only by taking into account the mechanical load associated with it. Using the notation and sign conventions shown in Figures 4.8 and 4.9 we may write:-

$$i = i_L + i_C = \frac{\lambda}{L_o} \sum_{n=o}^{h} f_n(\theta)\, \lambda^{2n} + \frac{1}{R_C(\theta,\lambda)} \frac{d\lambda}{dt} \qquad \ldots\ldots (4.30)$$

$$v = Ri + L_\ell \frac{di}{dt} + \frac{1}{C} \int idt + v_{c_o} + \frac{d\lambda}{dt} \qquad \ldots\ldots (4.31)$$

$$\text{and} \quad T_m + T_e = J\frac{d^2\theta}{dt^2} + G\frac{d\theta}{dt} \qquad \ldots\ldots (4.32)$$

where T_e is given by (4.28) and T_m represents the net mechanical input torque, other than viscous friction effects; J represents the total machine and load polar moment of inertia and G is the coefficient of viscous friction. Simultaneous solution of (4.30), (4.31) and (4.32) determines the operating point of the machine for a given set of input conditions.

Because a lumped circuit approach has been used, no account has been taken of the actual spatial distribution of flux in the airgap as a function of time, which means that any torques developed in the actual machine due to hysteresis or induction effects in the rotor iron will not be included.

Equations (4.30)→(4.32) constitute a set of simultaneous, non-linear differential equations having periodic coefficients. For a given machine under a specified set of input conditions, a particular solution to this set of equations may be found by means of analogue simulation or numerical solution. However, because of the non-linear nature of the equations, extrapolation of these particular results in order to predict the performance of a similar machine under different input conditions or of a different machine, will not be possible. By studying their behaviour over a range of machine parameters and input conditions some insight may be gained into the essential characteristics of the system.

Far greater insight may be gained from an analytical solution to the system equations. It is unlikely however, that a satisfactory solution will be found in either an explicit or a closed form. Nevertheless, even an approximate answer may provide useful information.

In sections 5→10 a number of independent approaches are presented, each of which provides further understanding of the system behaviour. They may be regarded as parallel approaches rather than as sequential, as the order in which they are taken is not particularly significant.

4.3.5 Normalized simplified equations.

If the current versus flux linkage relationship is represented by an expression containing one non-linear term only, as in (4.25), and furthermore, if the iron losses are taken into account approximately by a constant resistance R_C, then we have:-

$$pv = Rpi + L_\ell p^2 i + i/C + p^2\lambda \qquad \ldots\ldots (4.33)$$

$$i = \frac{\lambda}{L_o} + \frac{f(\theta)\lambda^q}{L_o} + \frac{1}{R_C} p\lambda \qquad \ldots\ldots (4.34)$$

$$T_m = Jp^2\theta + Gp\theta + \frac{f'(\theta)\lambda^{(q+1)}}{(q+1)L_o} \qquad \ldots\ldots (4.35)$$

where $p \equiv d/dt$.

From (4.33) and (4.34) we find

$$pv = \frac{L_\ell}{R_C} p^3\lambda + \left(\frac{R}{R_C} + 1\right)p^2\lambda + \frac{1}{R_C C} p\lambda + \frac{1}{L_o}\left(\frac{1}{C} + Rp + L_\ell p^2\right)\left(\lambda + f(\theta)\lambda^q\right) \qquad \ldots\ldots (4.36)$$

Then after making the following substitutions:-

$$\left.\begin{aligned}
v &= \sqrt{2}\, V \cos\overline{\omega t + \beta} \equiv \sqrt{2}\, V \cos\overline{\gamma\tau + \beta} \\
\omega_o &\equiv 1\Big/\sqrt{(L_o + L_\ell)\, C} \\
\tau &\equiv \omega_o t \\
\gamma &\equiv \omega/\omega_o \\
\rho_1 &\equiv R/2\omega_o\,(L_o + L_\ell) \\
\rho_2 &\equiv \omega_o L_o/2R_C \\
\ell &\equiv L_\ell/(L_o + L_\ell) \\
F(\theta) &\equiv f(\theta)/D_o \\
\psi &\equiv \lambda D_o^{\frac{1}{q-1}} \\
B &\equiv \sqrt{2}V(1-\ell)\,\gamma^2\, D_o^{\frac{1}{q-1}}\Big/\omega
\end{aligned}\right\} \qquad \ldots\ldots (4.37)$$

equations (4.35) and (4.36) may be written as:-

$$\frac{Tm}{J\omega_o^2} = \ddot{\theta} + \frac{G}{J\omega_o}\dot{\theta} + \frac{F'(\theta)\,\psi^{(q+1)}}{(q+1)L_o J\omega_o^2 D_o^{\frac{2}{q-1}}} \qquad \ldots\ldots (4.38)$$

$$-B \sin\overline{\gamma\tau+\beta} = 2\rho_2 \ell\dddot{\psi} + (1+4\rho_1\rho_2)\,\ddot{\psi} + 2(\rho_1+\rho_2)\,\dot{\psi} + \psi + \left(1 + \frac{2d}{dt} + \frac{\ell d^2}{d\tau^2}\right) F(\theta)\,\psi^q \qquad \ldots\ldots (4.39)$$

where the dot superscripts imply differentiation with respect to τ.

When iron losses may be neglected, $\rho_2 \to 0$ and the leakage flux may be incorporated with the airgap flux to give a modified L_o and $f(\theta)$; so that (4.39) simplifies to

$$-B \sin\overline{\gamma\tau+\beta} = \ddot{\psi} + \left(1+2\rho_1\frac{d}{dt}\right)\left(\psi + F(\theta)\,\psi^q\right) \qquad \ldots\ldots (4.40)$$

Both an understanding of the physical nature of the problem and an inspection of (4.38) suggest that as the load inertia J increases, so does the acceleration $\ddot{\theta}$ decrease; i.e. the excursions of θ about its mean value become smaller. The situation is entirely analagous to that of a two-stroke internal combustion engine and its fly wheel.

In theory at least, J may be increased until speed fluctuations are as small as desired; so that the machine may be considered to be running at a constant speed. I.e. $\ddot{\theta}=0$. Under these conditions a study of the system behaviour reduces to a study of (4.39) or (4.40) at the machine speed of interest. Once a solution to (4.39) or (4.40), as the case may be, has been found under these conditions it is a simple matter to calculate the instantaneous and hence the average torque.

Thus a study of (4.40) should provide much information about the essential behaviour of the machines to which it applies. Once this is understood, the investigation may be widened to allow for the effects of core loss, leakage inductance and finite inertia.

4.4. Iron losses.

For the machines under discussion, not only does the magnitude of the total airgap flux vary with time in a complex manner as indicated in Figure 3.9., but also, because of saturation, its distribution within the stator and rotor iron depends upon the total flux as well as the rotor position and speed. Thus the formulation of a model to represent iron losses under operating conditions presents a formidable problem and constitutes a major study in itself. Any serious attempt to solve it could be justified only if the operating characteristics of the machine proved to be critically dependent upon the precise nature of these time and position dependent losses.

Analogue computer, experimental and analytical studies all show that the magnitude of the torque developed by these machines is very sensitive to the circuit damping which means that any equivalent circuit of an actual machine, if it is to be at all useful, must include the core losses in such a way that the effective circuit damping is correct.

When the rotor is stationary the problem is straightforward, as it is a relatively simple matter to represent mathematically, a double valued λ-i relationship which may be fitted to the measured hysteresis loops. Under sinusoidal flux conditions, having a frequency of ω radians per second, a

possible representation would be:-

$$i = \frac{\lambda}{L_o} \sum_{n=0}^{N_1} f_n(\theta)\, \lambda^{2n}$$

$$+ \frac{K_n}{\omega} \frac{d\lambda}{dt} \sum_{n=0}^{N_2} h_n(\theta)\, \lambda^{2n}$$

$$+ K_e \frac{d\lambda}{dt} \sum_{n=0}^{N_3} g_n(\theta)\, \lambda^{2n} \qquad \ldots\ldots (4.41)$$

where the first term gives the mean magnetization curve as before, the second gives the current component required to form the static hysteresis loop which is made independent of frequency by means of the ω in the denominator, and the third term represents the current component due to eddy currents in the iron. The use of $d\lambda/dt$ as a coefficient in the second term is simply a convenient means of obtaining the correct sign and magnitude for the current increment whereas in the third term it expresses the fundamental nature of the eddy current component. Normally the third term could be expressed as $K_e \frac{d\lambda}{dt}$ with sufficient accuracy, but where high saturation factors are present, together with somewhat complex iron geometrics, the full expression in (4.41) may be required. Instead of using (4.30), expression (4.41) may be substituted into (4.31) to give the complete electrical circuit equations for the motor under stationary rotor conditions.

Figure 4.10 shows iron losses measured in the prototype machine, for a range of applied voltages and for a number of fixed rotor positions. By repeating these for a range of supply frequencies sufficient information would be available to enable (4.41) to be expressed as:-

$$i = \frac{\lambda}{L_o} \sum_{n=0}^{N} f_n(\theta)\, \lambda^{2n} + \left[\frac{1}{\omega R_h(\theta,\lambda)} + \frac{1}{R_c(\theta,\lambda)}\right] \frac{d\lambda}{dt} \qquad \ldots\ldots (4.42)$$

or at one fixed supply frequency ω, it may be simplified to (4.30), and the particular function $\frac{1}{R_c(\theta,\lambda)}$ found from curves such as those in Figure 4.11 by methods similar to those used in establishing a model for the λ-i characteristics.

Such a model is necessarily valid only while the rotor is stationary. At finite rotor speeds much more information is required concerning the flux distribution in the rotor before an adequate model can be developed. As we are primarily concerned in this report with the behaviour of devices incorporating periodic non-linear inductances no attempt has been made to establish an accurate model of the core. Nevertheless, the core losses contribute to the circuit damping and so affect its behaviour; so some attempt must be made to include them in the equivalent circuit.

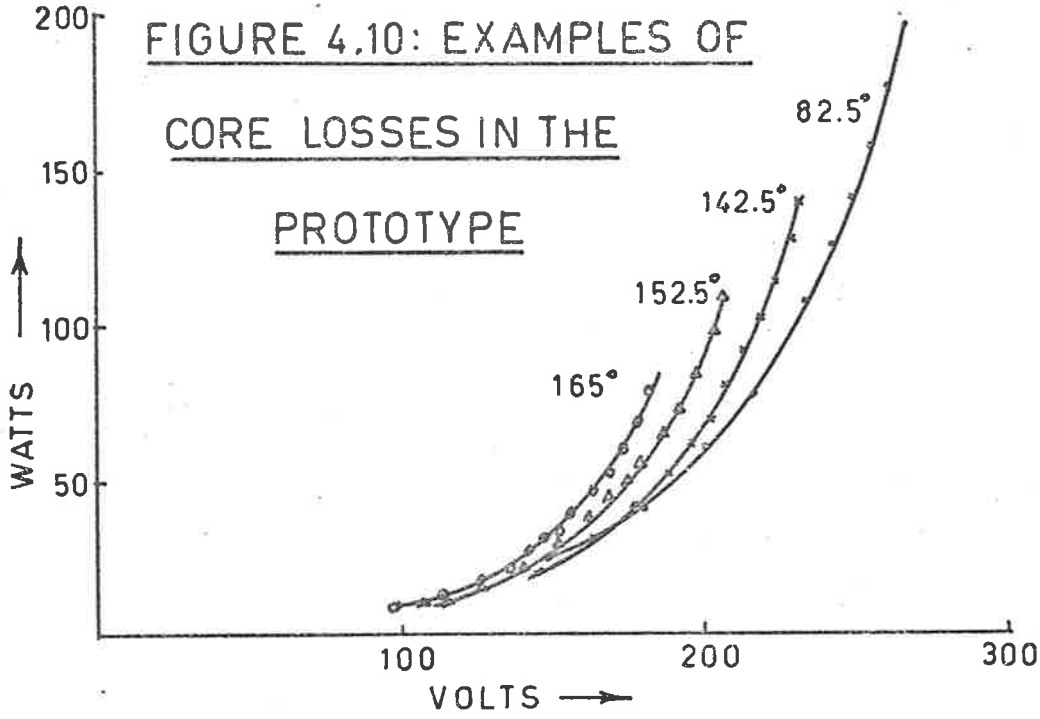

FIGURE 4.10: EXAMPLES OF CORE LOSSES IN THE PROTOTYPE

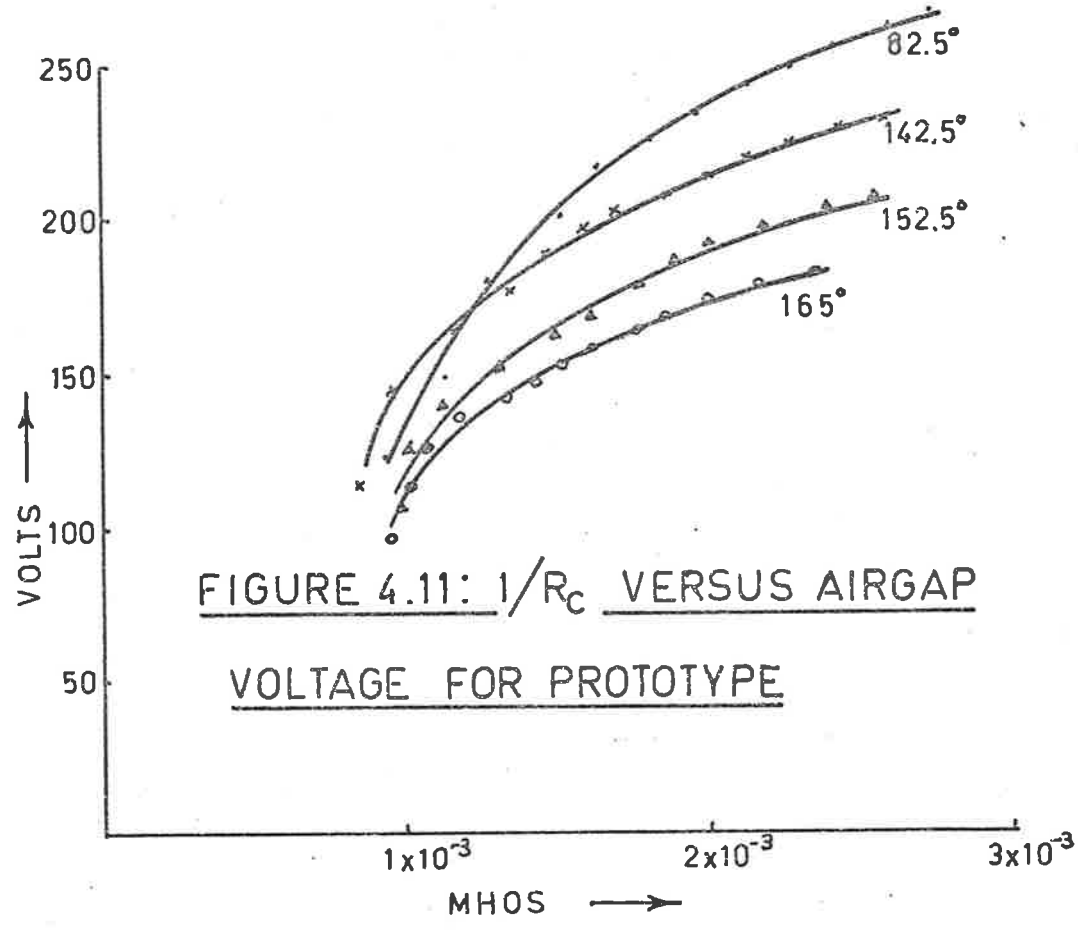

FIGURE 4.11: $1/R_C$ VERSUS AIRGAP VOLTAGE FOR PROTOTYPE

Three practical possibilities exist in the absence of a complete model. The first would be to use the model of $1/R_C(\theta,\lambda)$, found from curves such as those in Figure 4.11, at all rotor speeds.

Alternatively an average value for R_C could be found from the experimental data, for a particular applied voltage over the speed range of interest.

Thirdly, the parallel combination of R_C and the average value of the airgap inductance of the stator windings could be replaced with its equivalent series representation at the supply frequency in accordance with

$$R_S = R_C/(1+Q^2) \qquad \ldots\ldots (4.43)$$

$$L_S = L_e/(1+1/Q^2) \qquad \ldots\ldots (4.44)$$

where $Q = R_C/\omega L_e$

Equations 4.43 and 4.44 are valid only for the replacement of a parallel combination of constant linear inductance L_e and resistance R_C with a series combination R_S and L_S under steady state sinusoidal excitation at frequency ω. Justification for the use of these equations cannot be found analytically but possibly may be from a comparison of theoretical and practical results.

Throughout the remainder of this report wherever solutions to the system equations are sought, whether it be by analogue, numerical or analytical methods, fixed values for either R_c or R_s, as the case may be, are used.

Using the data presented in figures 4.10, 4.11 and A III 1, it is a relatively simple matter to calculate the circui Q for the prototype machine stator, by calculating the ratio of the voltamperes in the winding inductance to the total watts

loss in the core and series resistance. Figure 4.12 shows some representative values under blocked rotor conditions, for three different winding voltages at the two extremes of rotor position. These indicate, as one would expect, that the circuit Q falls as the applied voltage increases, but that for this particular machine the circuit Q increases as the rotor reluctance increases.

Approximate representation of the iron losses by means of a fixed shunt resistance R_c will result in a similar but much exaggerated variation in circuit Q with rotor position. On the other hand, representation by additional series resistance R_s will result in a decrease in circuit Q with increasing reluctance. A combination of both might provide an acceptable model under conditions of a slowly varying rotor position. Under normal running conditions however it is likely that the above discussion is irrelevant.

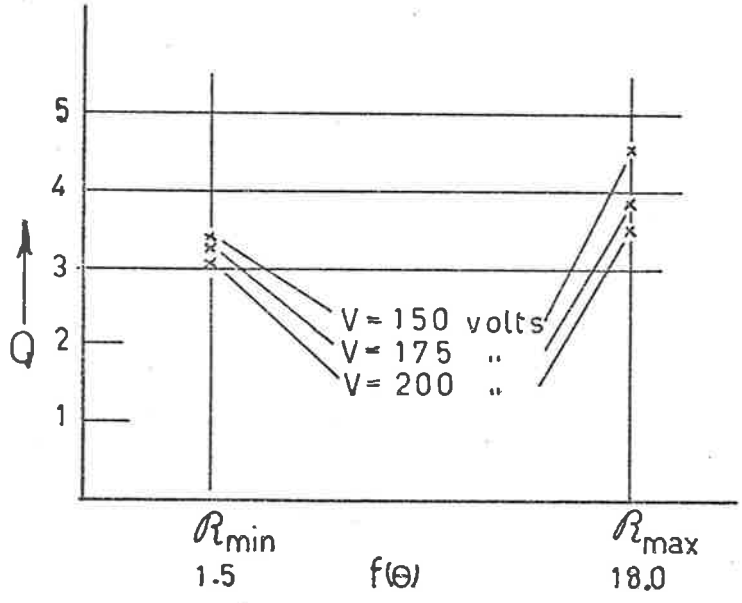

FIGURE 4.12 : VARIATION OF CIRCUIT 'Q' WITH ROTOR POSITION AND WINDING VOLTAGE

CHAPTER 5: ANALOGUE COMPUTER SIMULATION.

The contents of this section may be divided conveniently into two distinct portions. Firstly the results obtained from an attempt to simulate the prototype machine will be presented and discussed. Secondly, an improved computer set up provides information on the behaviour of a system described by equations (4.38) and (4.40), using a cubic approximation for the λ-i characteristics. These latter results may then be compared with the results from numerical and analytical solutions of these equations.

Restriction of the investigation, at this stage, to a cubic approximation, simply facilitates comparison between the three approaches. It will be shown in a later section that the computational time involved in obtaining an approximate analytical solution to these equations is about two orders higher when using a quintic instead of a cubic representation. As the behaviour of the systems described by either of these representations differs only in details but not in essentials, the author has chosen to work with the cubic.

5.1. Simulation of the prototype machine.

From the experimental results presented in section 3, values for the various fixed parameters in the system equations (4.22), (4.30), (4.31) and (4.32) may be calculated.

While any desired accuracy of fit to the λ-i characteristics may be obtained by means of the power series representation in equation (4.30), hardware limitations on the computer and the reasonable agreement between

model curves and measured points shown in Figures 4.5 and 4.6 suggest that a simple quintic approximation should be adopted.

Fourier analysis of the points depicting $f(\theta)$ in Figure 4.4 enables the various D_m and δ_m of (4.22) to be found. However for purposes of simulation it is more convenient to generate $f'(\theta)$ from the variable θ by means of a diode function generator [2,17], and from $f'(\theta)$, to form $f(\theta)$ as discussed subsequently in this section.

Using a quintic approximation and neglecting core losses, the system equations become:-

$$i = \frac{\lambda}{L_o}\left(1 + f(\theta)\lambda^4\right) \qquad \ldots\ldots (5.1)$$

$$v = Ri + \frac{1}{C}\int idt + \frac{d\lambda}{dt} + L_\ell \frac{di}{dt} + v_{c_o} \qquad \ldots\ldots (5.2)$$

$$T_m = J\frac{d^2\theta}{dt^2} + G\frac{d\theta}{dt} + \frac{f'(\theta)\,\lambda^6}{6L_o} \qquad \ldots\ldots (5.3)$$

$$f(\theta) = D_o + \sum_{m=1}^{\mu} D_m \cos \overline{m\,p\,\theta + \delta_m} \qquad \ldots\ldots (5.4)$$

These represent the complete behaviour of the machine, with the following reservations:-

(i) the effect of core loss has not been specifically included.

(ii) (5.1) will normally only approximate the true family of λ-i characteristics.

(iii) the only electrical torque considered is that due to reluctance effects.

Some details and specifications of the analogue computer will be found in Appendix II(a). This equipment (Plate 5.1) was designed and constructed in the Electrical Engineering Department, University of Adelaide, during the years 1952-56 as a series of postgraduate projects.

The manner in which (5.1)→(5.4) were implemented on the computer in order to simulate the prototype machine, is shown in Figures 5.1 and 5.2, while the details of the manner of generation of $f(\theta)\lambda^5$ and $f'(\theta)\lambda^6$ by means of multipotentiometer servo-multipliers are shown schematically in Figure 5.3. The block diagram representing (5.1) and (5.2) is quite straightforward and follows conventional practice, however that shown in Figure 5.2 requires some explanation.

Problems arise because one of the independent variables, viz. rotor position represented by θ, increases indefinitely with time, but which nevertheless must be represented by a voltage which does not exceed 100. As the ultimate requirement is not θ but $\dot{\theta}$, $f(\theta)$ and $f'(\theta)$, and as the latter two are periodic with respect to θ, the possibility arises of restricting the range of θ.

We may form $f(\theta)$ as follows:-

$$f(\theta) = \int df(\theta) = \int \frac{df(\theta)}{d\theta}\frac{d\theta}{dt}\,dt = \int f'(\theta)\,\dot{\theta}\,dt \qquad \ldots\ldots (5.5)$$

PLATE 5.1

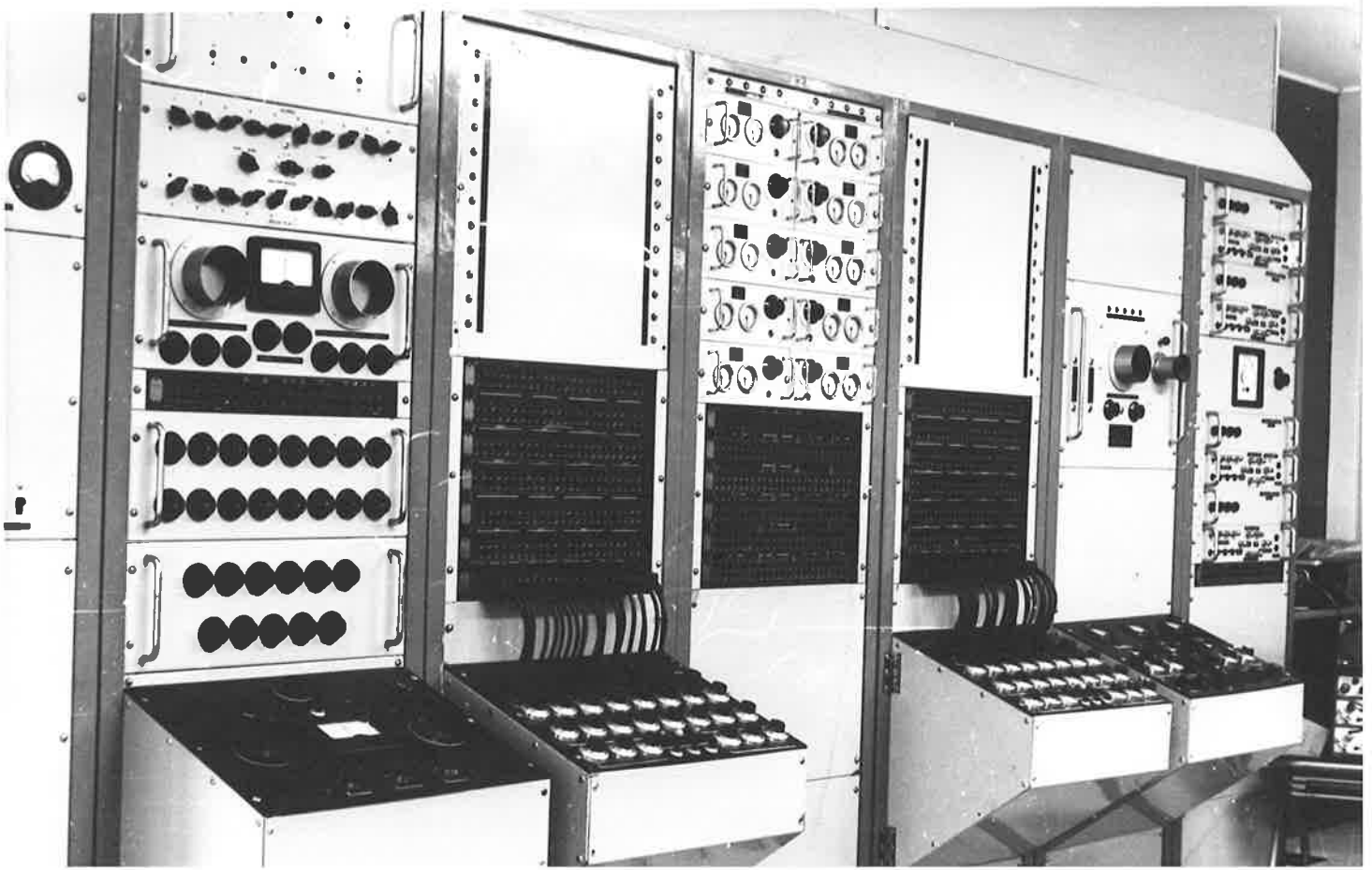

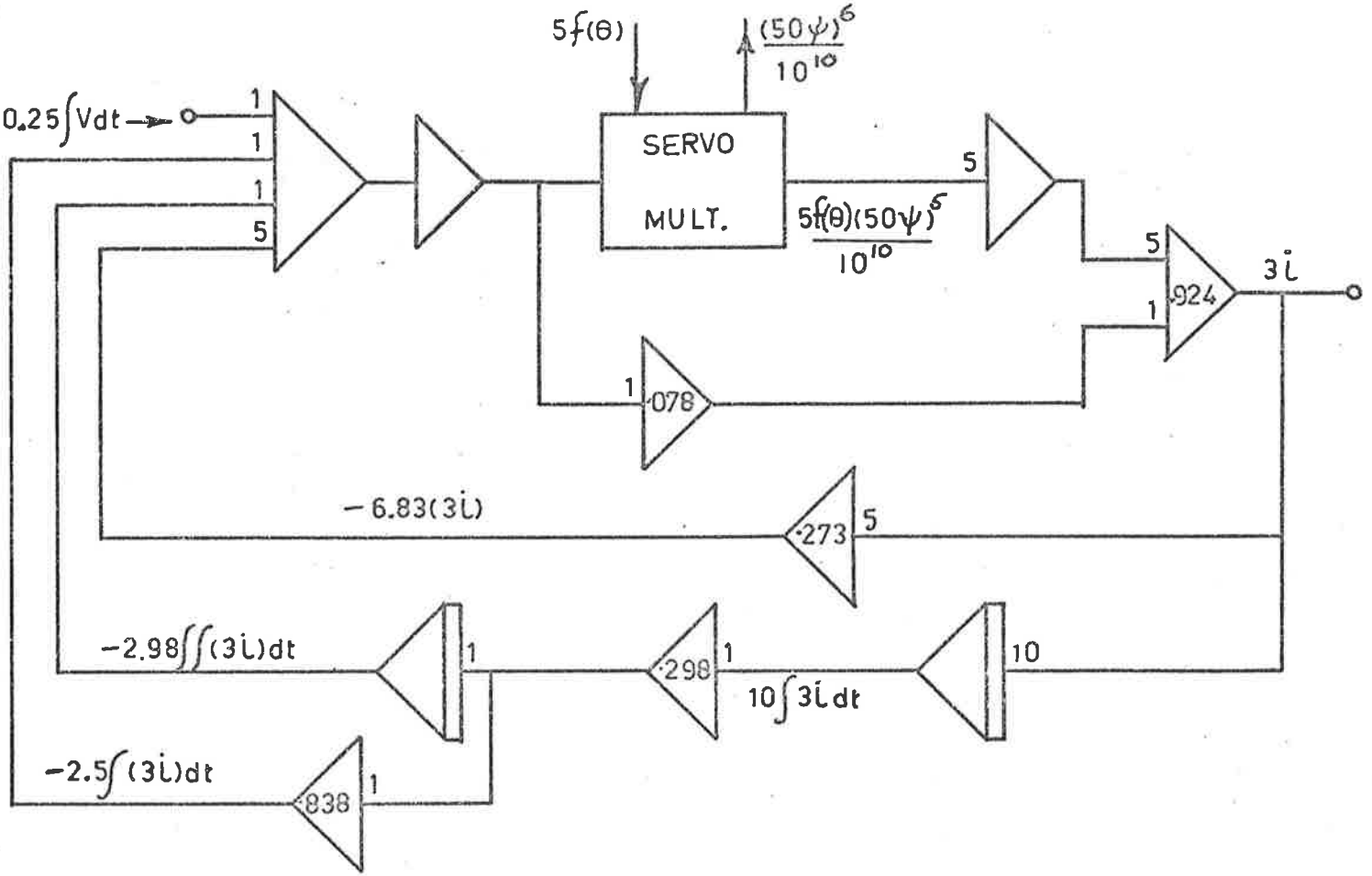

FIGURE 5.1: COMPUTER SIMULATION OF EQUATIONS II.2 & II.3 FOR THE PROTOTYPE WITH C = 139.5μf

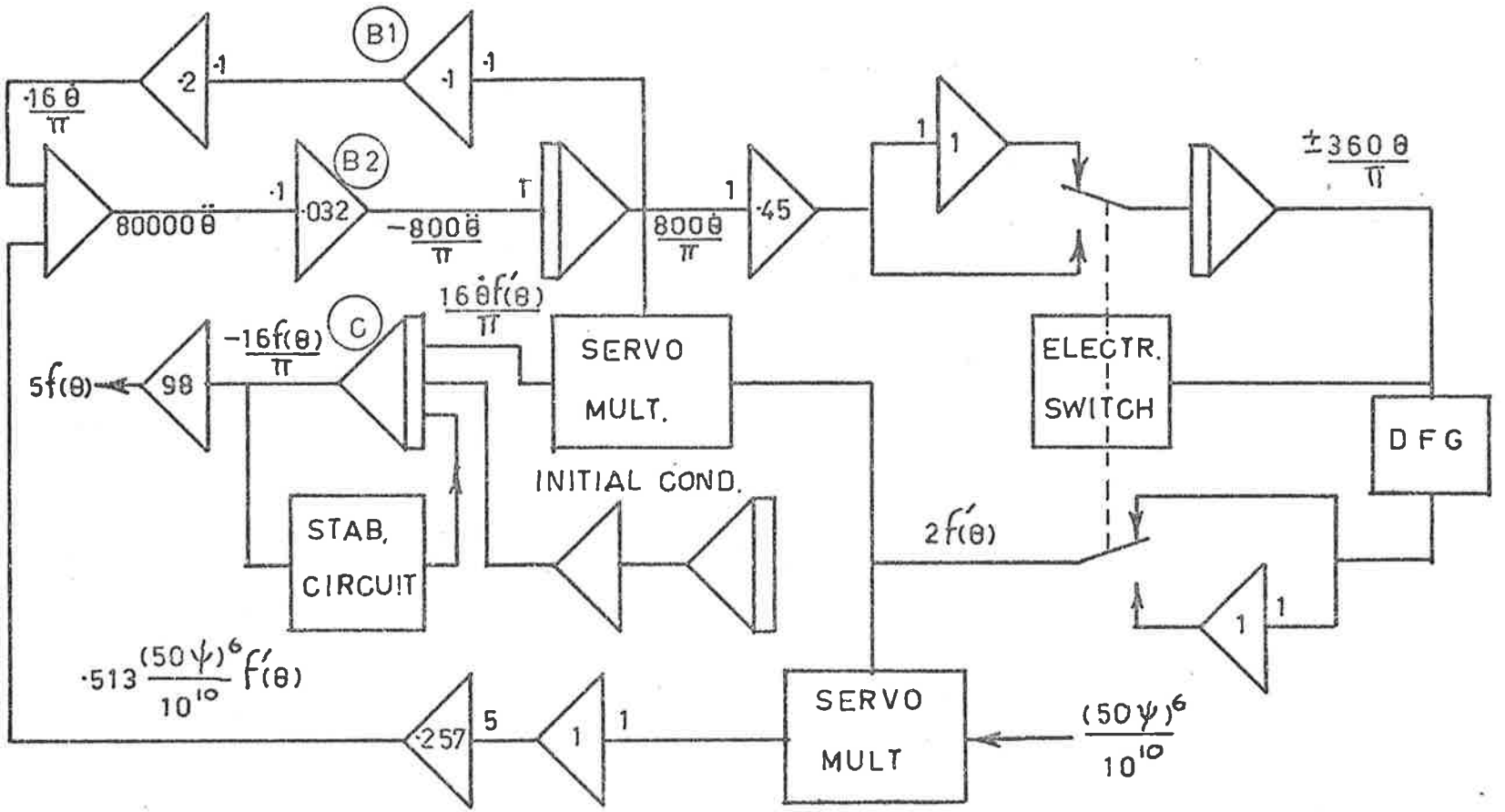

FIGURE 5.2: COMPUTER SIMULATION OF EQUATION II.4 FOR THE PROTOTYPE

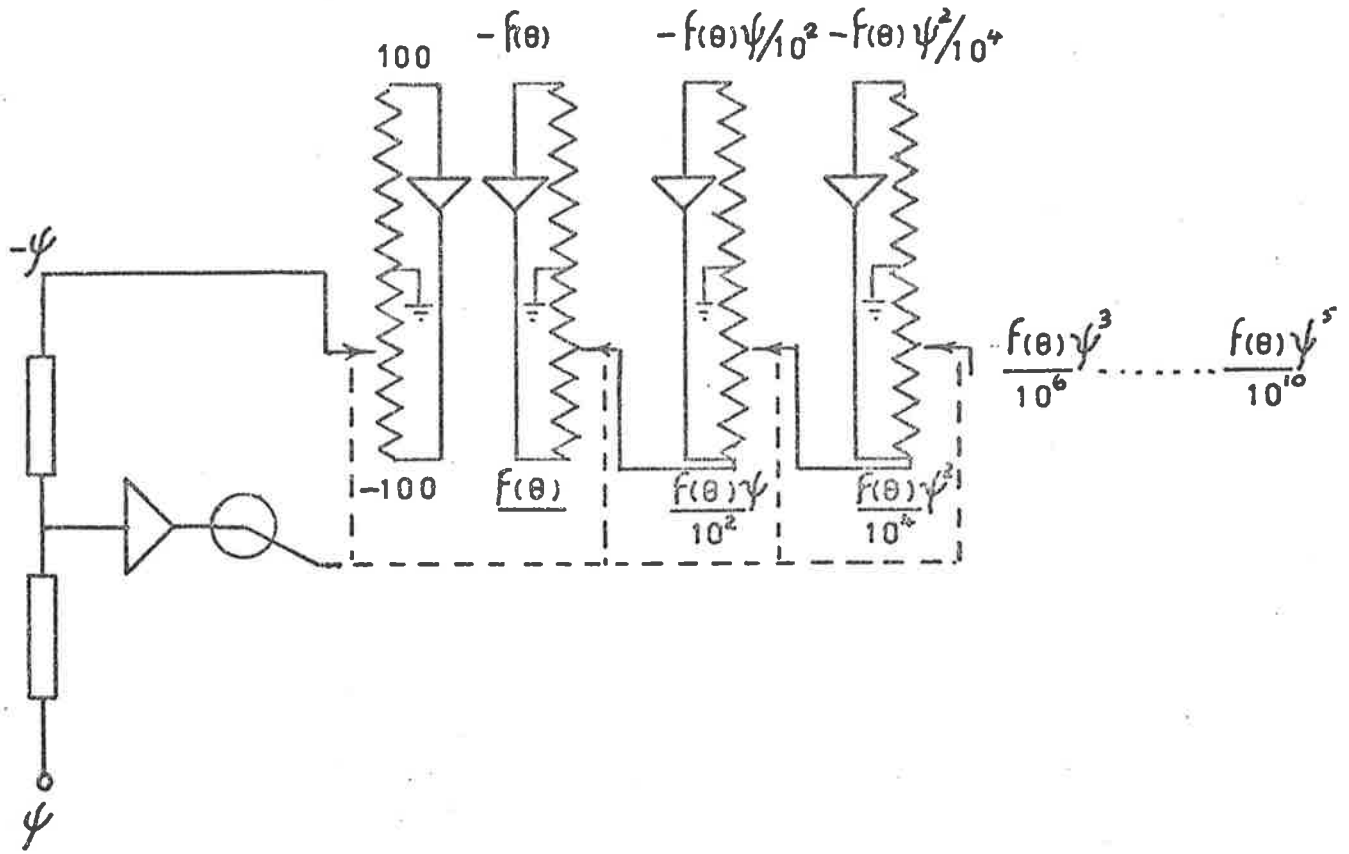

FIGURE 5.3: SERVO MULTIPLIER IMPLEMENTATION OF $f(\theta)\psi^5$

after forming $f'(\theta)$ by means of a diode function generator. When $f(\theta)$ is a symmetrical function, economy in the use of diode function generator segments may be obtained while at the same time restricting the range of θ. See Figure 5.4. The method requires that the rotor direction be reversed each time θ reaches a value of 0 or $\pi/2$, and, simultaneously with the reversal in direction, the sign of the output from the function generator forming $f'(\theta)$ must also be changed; so generating successive positive and negative half cycles of $f'(\theta)$. Details of the electronic switch and the stabilizing circuit required in the generation of $f(\theta)$ are given in Appendix II(b). This latter circuit proved to be necessary in order to counteract the effect of the finite operating time of the changeover relay. Additional points of interest including the scaling of the independent and dependent variable are also included in Appendix II.

5.1.1. Results from the simulation of the prototype machine.

Computer hardware limitations precluded the incorporation of either a fixed or variable shunt resistance for the representation of core losses. Instead, mean values of R_C and ωL were estimated, from the results shown in Figures 3.4, 3.5 and 3.6, as $\simeq 600\Omega$ and 60Ω respectively, which, when inserted in (4.43) and (4.44) suggest an increase in series resistance of $\simeq 6\Omega$ and a decrease in inductive reactance of $\simeq 0.6\Omega$.

A check on these may be obtained by adjusting the series resistance in the analogue computer model until ferro-resonant jumps occur in both the model and the actual machine, at precisely the same value of applied voltage and current for a given series capacitance and blocked

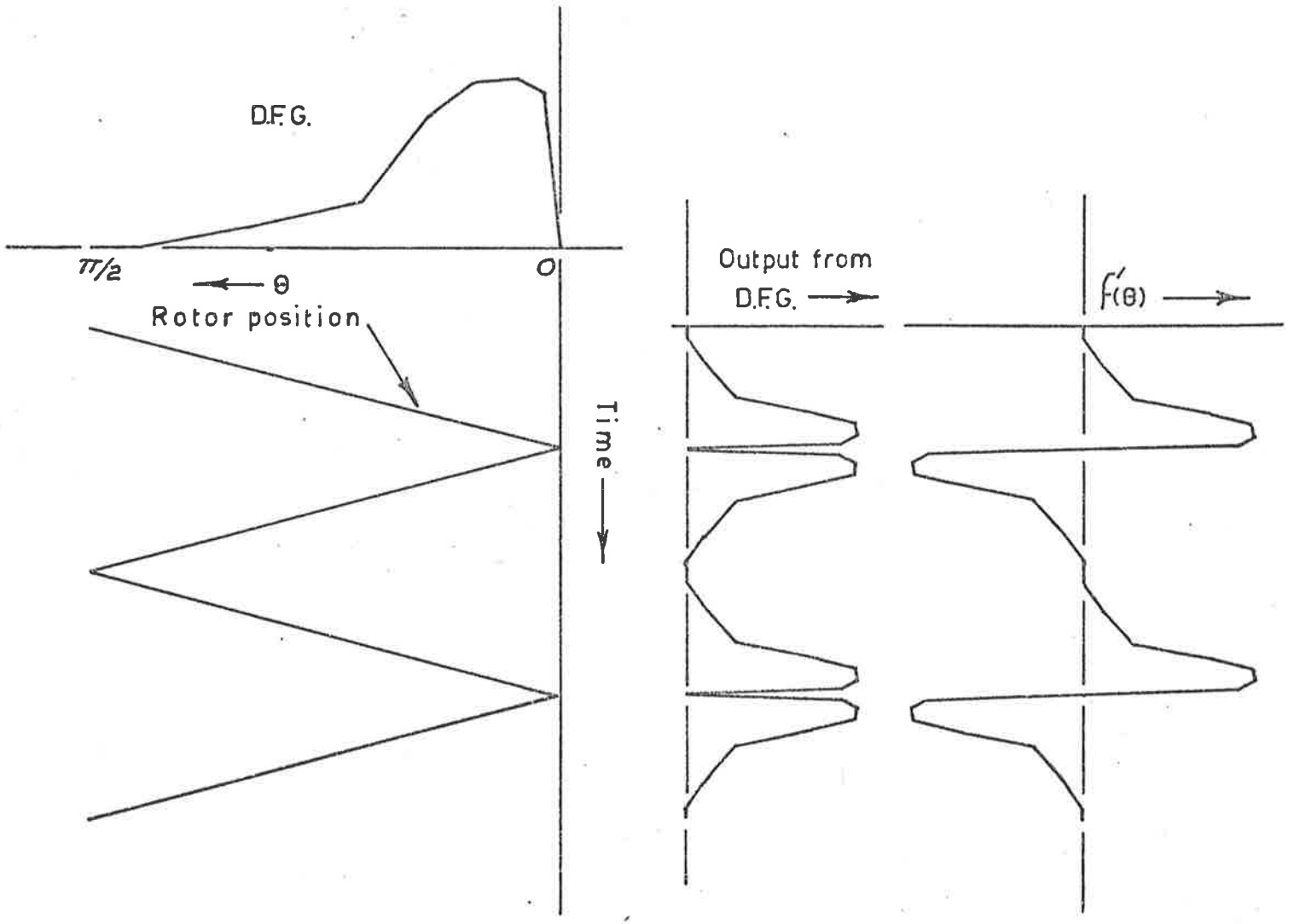

FIGURE 5.4: GENERATION OF $f'(\theta)$ FROM θ

rotor position.

By this means, virtually identical results were obtained in the model and the prototype when the model series resistance was increased by 5Ω up to 10Ω while at the same time leaving the leakage reactances unchanged at ≃ 26Ω.

Thus in the simulation, core losses were taken into account approximately, by an increase of 5Ω in the circuit series resistance.

A symmetrical $f(\theta)$ results from the method of generation in the model, whereas the actual $f(\theta)$ of the prototype machine is slightly asymmetrical as shown by the full line in Figure 4.4.

Using the computer set-up shown in Figures 5.1 and 5.2, with appropriate values corresponding to the particular circuit conditions, the results depicted in Figures 5.5 and 5.7 were obtained, which may be compared with the experimental torque speed curves from the actual machine, reproduced in Figures 5.6 and 5.8.

Comparison of these results from simulation and direct measurement prompts the following comments:-

(i) The model reproduces the major characteristics of the prototype, however some minor characteristics are absent.

(ii) Quantitative agreement is far from perfect.

(iii) The simple representation of circuit damping is apparently inadequate because, while the greater steepness in the model of the positive slope portion of the torque speed curves suggests that the damping is too low, the increased voltage

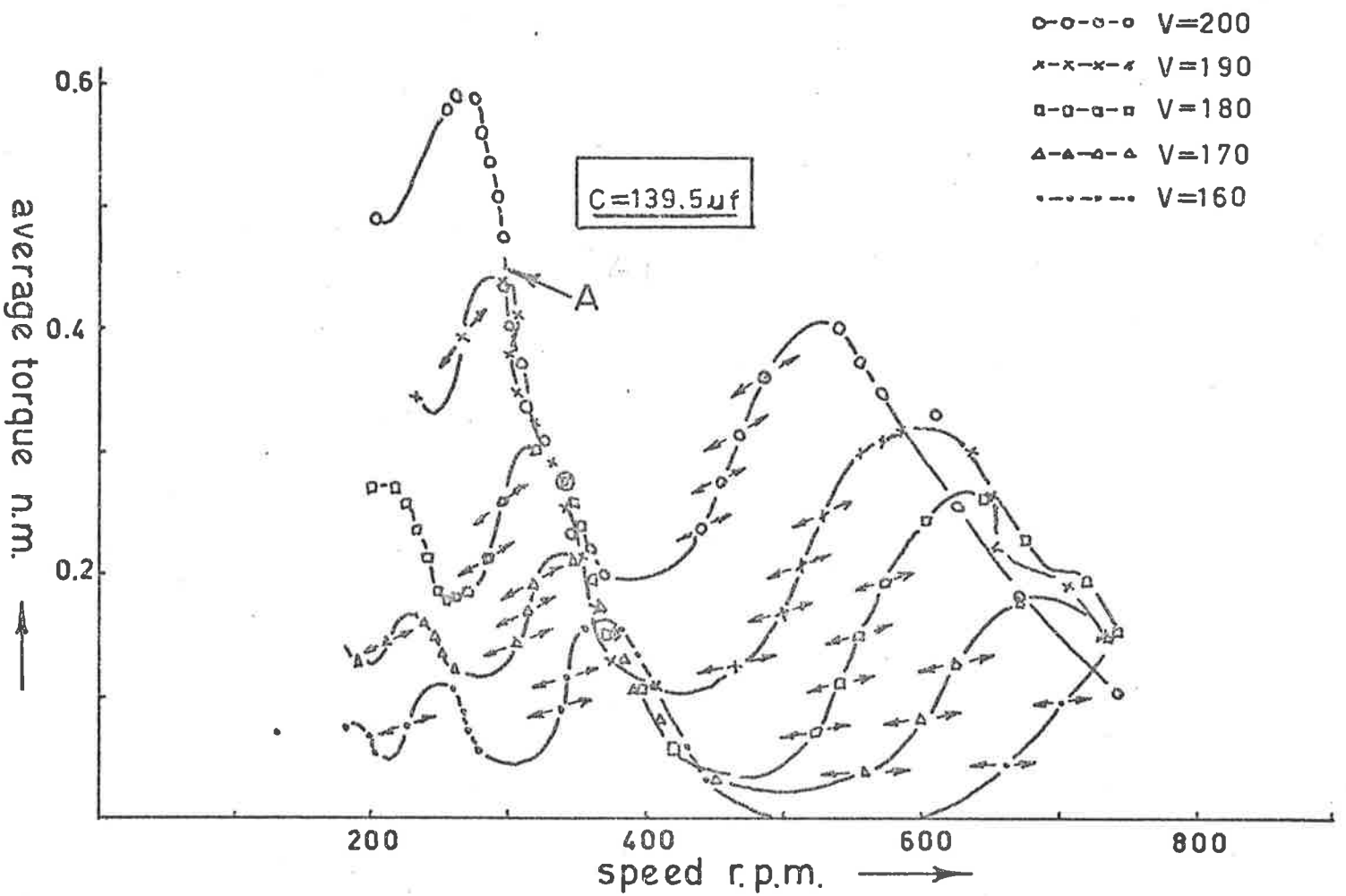

FIGURE 5.5: ANALOGUE COMPUTER SIMULATION OF PROTOTYPE

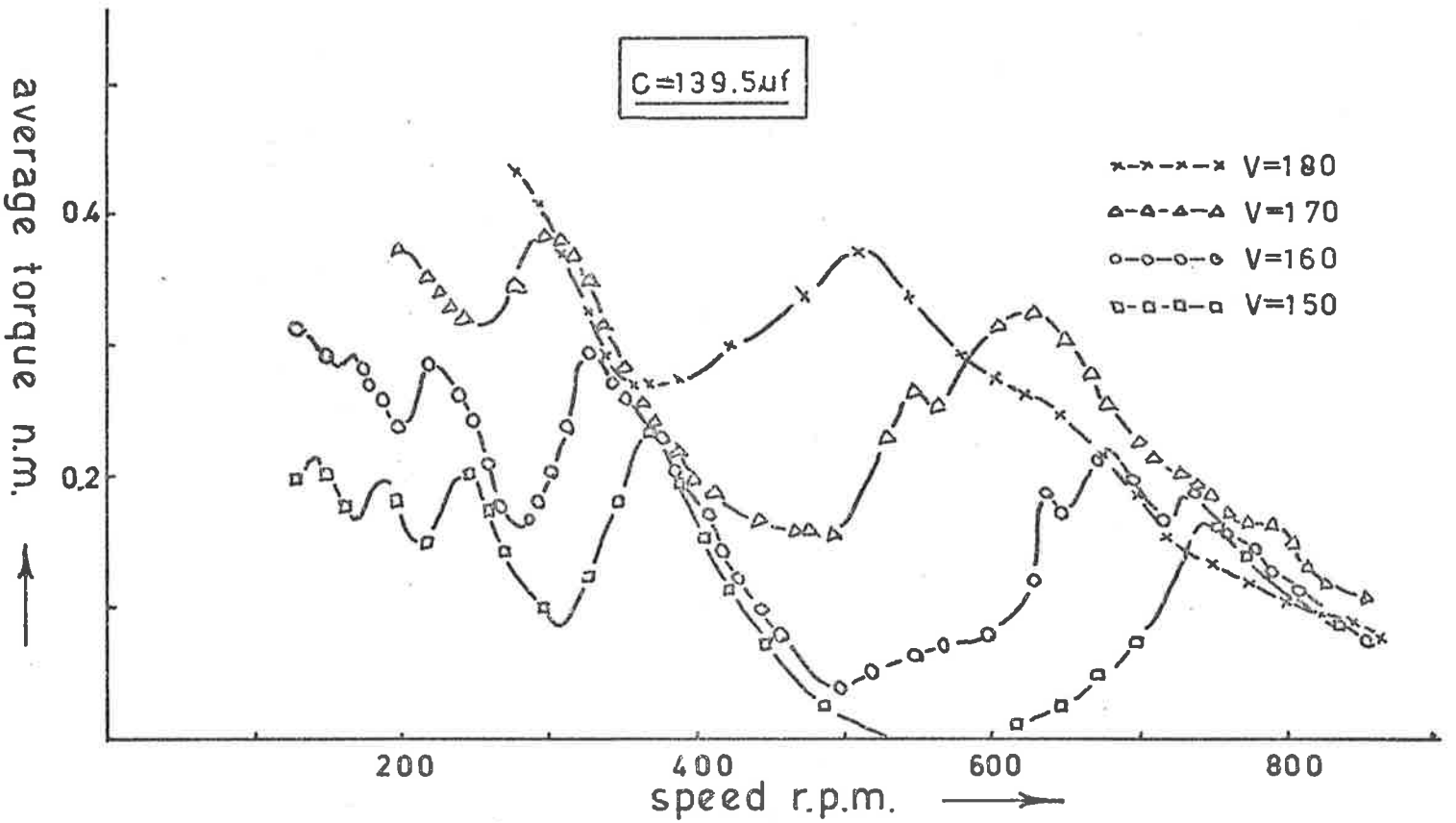

FIGURE 5.6: EXPERIMENTAL RESULTS FROM PROTOTYPE

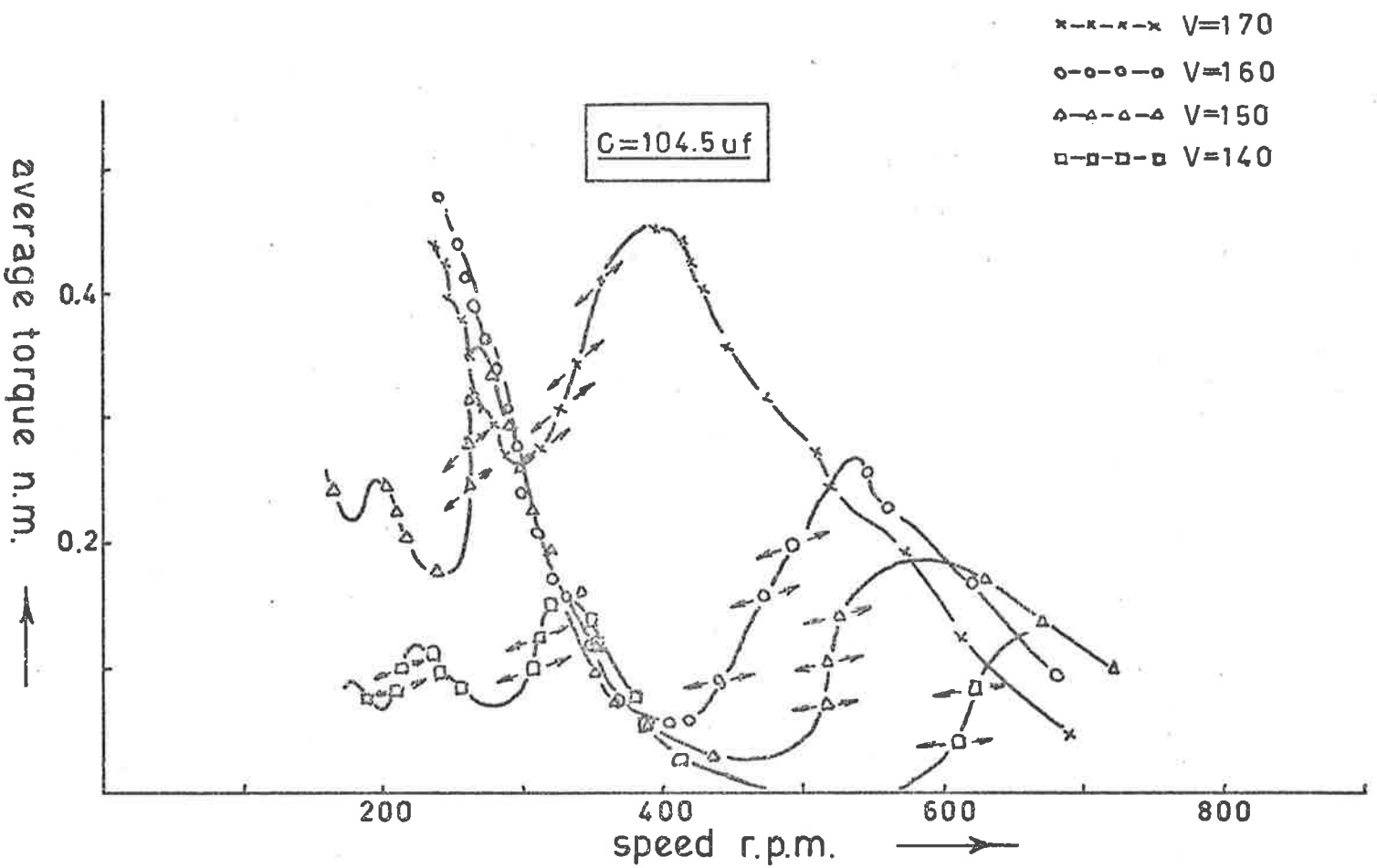

FIGURE 5.7: ANALOGUE COMPUTER SIMULATION OF PROTOTYPE

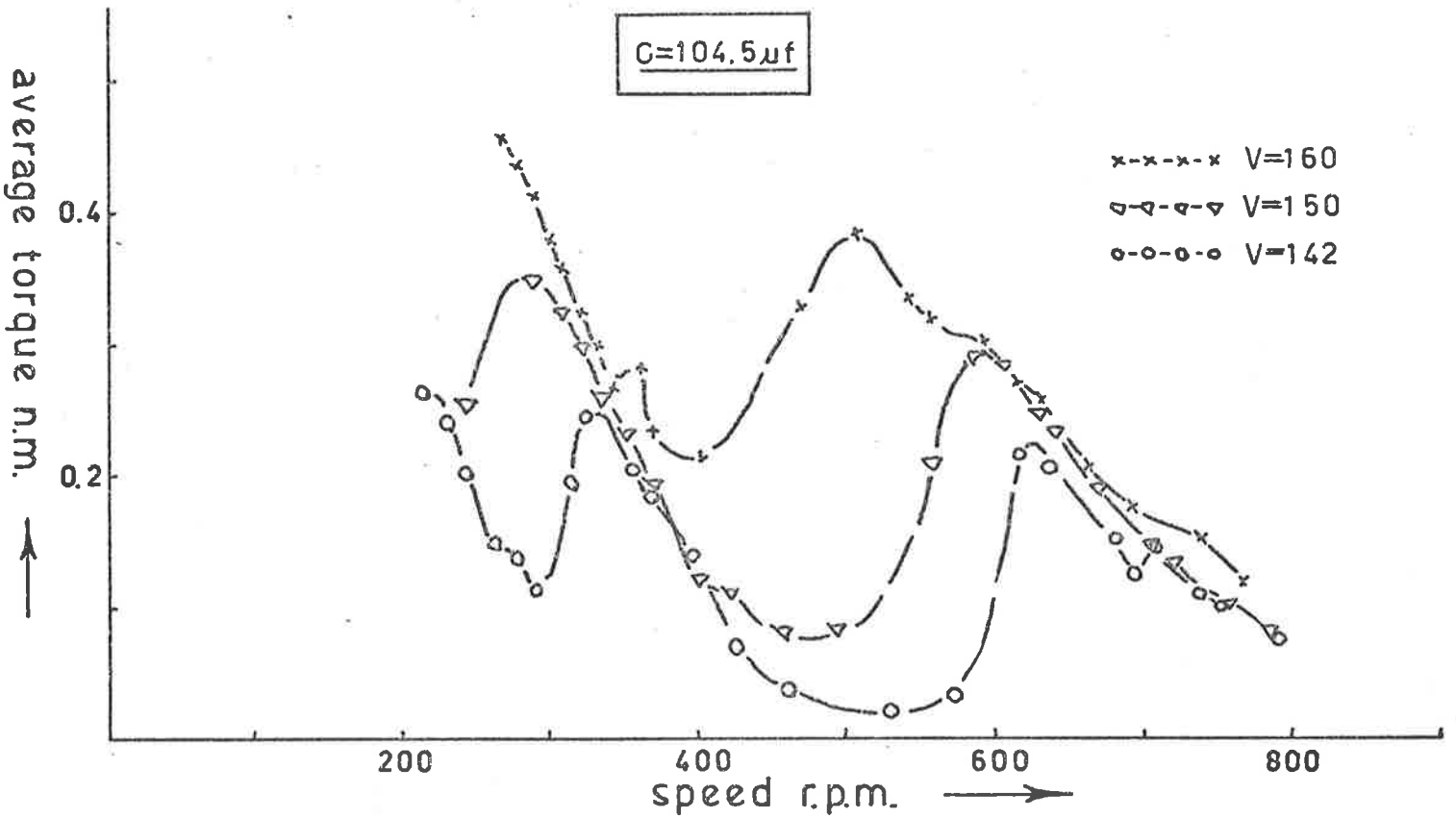

FIGURE 5.8: EXPERIMENTAL RESULTS FROM PROTOTYPE

required in the model to produce a given peak torque suggests that it is too high.

The ferro-resonant jump effect is a threshold phenomenon which may be induced under appropriate conditions, by small changes in any of the circuit parameters; so that it is not surprising that a threshold effect appears in the behaviour of these machines. Thus the voltage range leading to satisfactory operation for the conditions shown in Figure 5.6 is given approximately by $150 < V < 180$. Below 150 volts the developed torque is too small to be of much practical use whilst above 180 volts the circuit may take up permanently the high flux and current state. In other words the practical range of applied voltage in this particular case is given by $V \simeq (165 \pm 15)$ volts. This represents a variation of about ± 10%. A similar degree of sensitivity to changes in other circuit parameters also may be demonstrated.

Such sensitivity means that small variations in the gain of any of the computer elements used to simulate the machine, may lead to serious errors. Only after the introduction of a number of stringent checks, frequently repeated, was it possible to reproduce simulated results from one day to the next.

In order to obtain a point on the negative slope portion of the speed torque curve, initial values for speed, rotor position, applied voltage and phase, current and capacitor voltage, together with the load torque were set and the computer released. Instantaneous speed versus time was plotted on an x-y recorder. If and when the average speed

became constant, it could be inferred that the average electromagnetic torque was equal to the average mechanical torque at that speed. The value of the electromagnetic torque follows from (5.3) as:

$$T_{ave} = G[\dot{\theta}]_{ave} - T_m \qquad \ldots\ldots (5.6)$$

In fact it proved most convenient to put $T_m = 0$ and to vary G by changing buffer B1 in Figure 5.2. By this means the settling time is kept to a minimum.

Because of the nature of the machine, even although the average speed over a sufficiently long time may be constant, the instantaneous speed, due to the effect of the alternate negative and positive torque pulses and to beat phenomena, in general exhibits cyclic variations about its mean value.

Increasing the mechanical inertia by decreasing the gain of buffer B2 in Figure 5.2 restricts the amplitude of these variations but increases the time taken to reach a steady state and hence the time required to determine whether or not a steady state has in fact been reached. On the other hand, for a given block diagram configuration, inherent amplifier drift sets a limit on the total time for which the computer may run before the errors become significant.

There is thus a serious conflict in requirements. Decreasing the inertia in order to shorten the settling time results in larger speed fluctuations which mask the average value and, as will be seen in a later section, may even preclude the attainment of a steady state.

When using multi-potentiometer servo-multipliers to generate $f(\theta)\lambda^5$ and $f'(\theta)\lambda^6$, the wiper arm of the multiplier must follow λ, which means that the time scaling employed must place the frequency of λ within the bandwidth of the servo-multiplier in order to avoid amplitude and phase errors. See Appendix II. The results presented in Figures 5.5 and 5.7 represent a compromise between these conflicting requirements. Better resolution of the points on the torque speed curve can be obtained only by shortening the time scale which means replacement of the servo-multiplier.

Determination of the position of that portion of the speed torque curve which has a positive slope, can be carried out by searching for the boundary between rising and falling speed for a particular value of G.

After comparison of the results in Figures 5.5→5.8, bearing in mind the limitation of this particular computer implementation and the method of approximating core losses, it seems reasonable to suppose that if an accurate model were available for the latter, then the system equations (5.1)→(5.4), would provide an acceptable model of the actual machine.

It should be noted that core loss in the prototype machine is exceedingly large because of the method of machining the rotor slots. In subsequent machines great care was taken to eliminate any short circuits between laminations, with the result that losses have been substantially reduced; so that their contribution to the circuit damping and hence their effect on the machine operation has been much less significant.

5.2. Analogue computer solution of the ideal system equations.

From the discussion and results presented in Section 5.1, it seems reasonable to conclude that the essential behaviour of ferromagnetic parametric machines may be described by equations (5.1) to (5.4), provided core loss is negligible. A criterion for establishing whether or not core loss may be considered to be negligible, has not been and will not be established in this report. As discussed in Section 4.4, the determination of an accurate model is a major problem in itself. Here we are primarily concerned to investigate the particular characteristics of electromechanical devices which have position and current dependent winding inductances. Once the characteristics of such devices are known and understood further investigation can be undertaken to find out what modifications result from the presence of position dependent core losses.

In later sections, approximate analytical solutions to equations (5.1)→(5.4) are developed. From these solutions, torque speed curves for the machines may be calculated and compared with those obtained from analogue or digital computer solutions.

It will be shown that the ratio of the time taken to obtain analytical solutions in the case of cubic or quintic approximations to the λ-i characteristics is of the order of 1 : 100. The actual ratio being dependent upon the desired accuracy of the solution. Thus in order to save digital computer time, the majority of the analogue computer investigations

have been carried out using the cubic approximation.

5.2.1. Improved analogue representation.

The implementation of equations (5.1)→(5.4) shown in Figures 5.1 and 5.2 and used to simulate the prototype machine, suffered from the serious disadvantage that errors due to amplifier drift often become significant before it was possible to decide whether or not a steady state had been reached. As a consequence, uncertainty concerning the precise location of points on the torque speed curves was high.

In Figures 5.9 and 5.10 an improved implementation is shown in which diode function generators form the requisite powers of λ, and in which some of the servo-multipliers have been replaced by electronic multipliers. Design and construction of the latter was such that the maintenance of errors within specification was extremely difficult, which was the reason for avoiding the use of these particular units of the Analogue Computer when simulating the prototype. Because of this problem one servo-multiplier was retained in the main loop. This then set the upper limit on the time scale.

No provision need be made for leakage inductance when core losses are neglected, as it may be included with the airgap inductance, unless it is specifically desired to investigate the effects of external inductance on the machine performance.

5.2.2. Torque speed curves of idealized machines.

In order to facilitate comparison with later work and to bring out just what are the fundamental parameters affecting performance, results

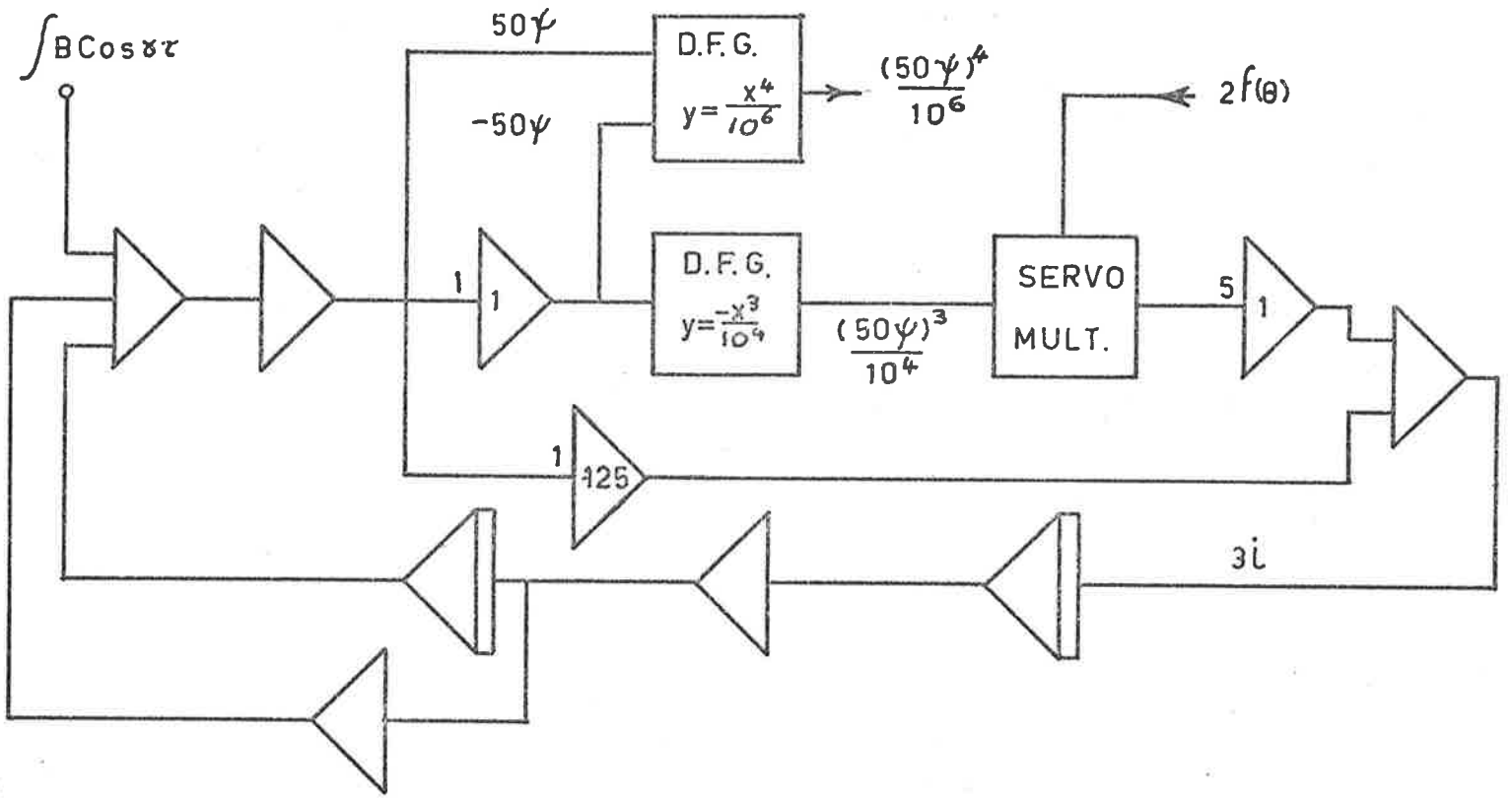

FIGURE 5.9: SIMULATION OF IDEALISED MACHINES: EQU. 5.7

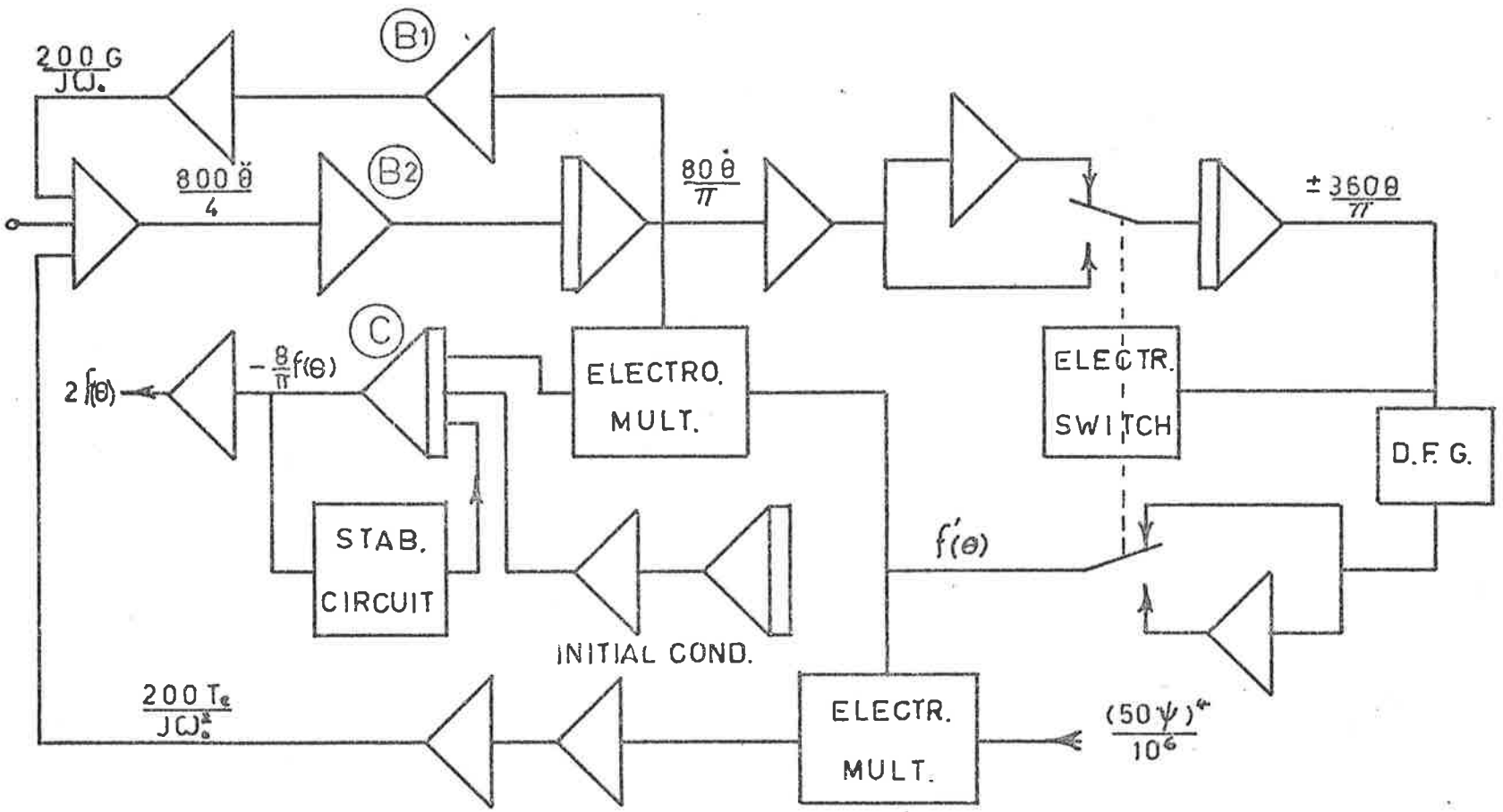

FIGURE 5.10: SIMULATION OF IDEALISED MACHINES: EQU. 5.8

are presented in terms of the normalized parameters listed in (4.37).

Thus figures 5.11 to 5.17 present some representative speed torque curves in which normalized torque T_N is plotted against the per unit speed Ω/γ, where $T_N = D_o L_o T_e$ for a cubic approximation and $\Omega/\gamma = (\omega_r/\omega_o)/(\omega/\omega_o) = \omega_r/\omega$. These results represent the performance of (4.38) and (4.40) reproduced here for convenience as

$$\ddot{\theta} + \frac{G}{J\omega_o}\dot{\theta} - \frac{T_N}{D_o L_o J\omega_o^2} - \frac{T_m}{J\omega_o^2} = 0 \qquad \ldots\ldots (5.7)$$

and

$$- B \sin \gamma\tau = \ddot{\psi} + (1+2\rho\frac{d}{dt})(\psi + F(\theta)\,\psi^3) \qquad \ldots\ldots (5.8)$$

Three different values of series capacity give three different values of natural frequency and hence three values of γ, viz. 2.5, 3 and 4. In addition two different rotor geometries are considered together with a small range of series resistance. When using a cubic approximation and no leakage reactance the normalized excitation magnitude is represented by $B = \sqrt{2}V\,\gamma^2\,D_o^{\frac{1}{2}}/\omega$. In practice there is an upper limit to B, above which the circuit adopts the high current and flux state and remains there for all rotor positions, and also a lower limit, below which torque production is negligible.

Identical parameters were used with the original computer set-up shown in Figures 5.1 and 5.2. Except for the lack of discrimination mentioned previously the results obtained from the two different computer implementations agreed well on the negative slope portions of the torque speed curves. However, there was some discrepancy between the two sets of

results for the positive slope portions of the curves and consequently on the location of the peaks.

Inspection of Figures 5.11 to 5.16 shows the extreme sensitivity of the positive slope portions to relatively small percentage changes in B or ρ, and hence to small changes in V, D_o, R or C. Results from the higher speed implementation shown in Figures 5.9 and 5.10, easily repeatable from day to day, must be considered as the most reliable of the two different sets, but the author feels that the precise location of all positive slope portions of these curves is still in some doubt. Firstly because the points represent unstable solutions and must be found by searching for such a position and secondly, as will be discussed in a later section, the mechanical inertia of the system can have a marked influence on behaviour.

Note that Figure 5.15 shows results from the original computer set-up using servo-multipliers, as these particular conditions were not repeated with the improved implementation.

Detailed discussion on the significant characteristics of these curves and of the flux and current waveforms is deferred until deeper insight into the physical nature of the system behaviour has been gained.

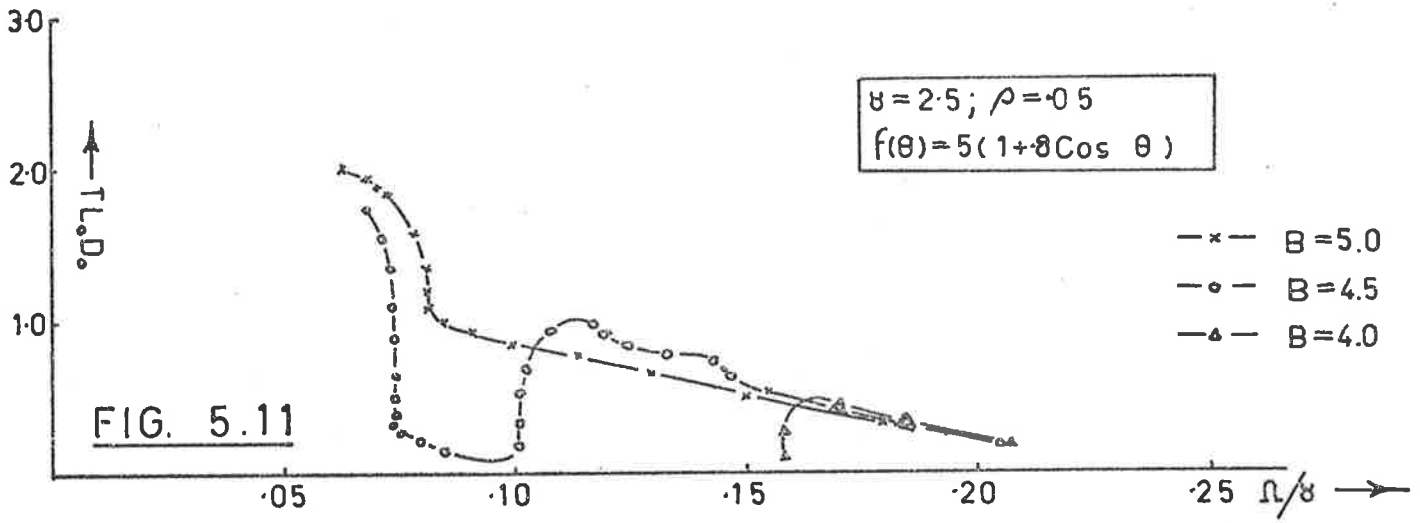

FIG. 5.11

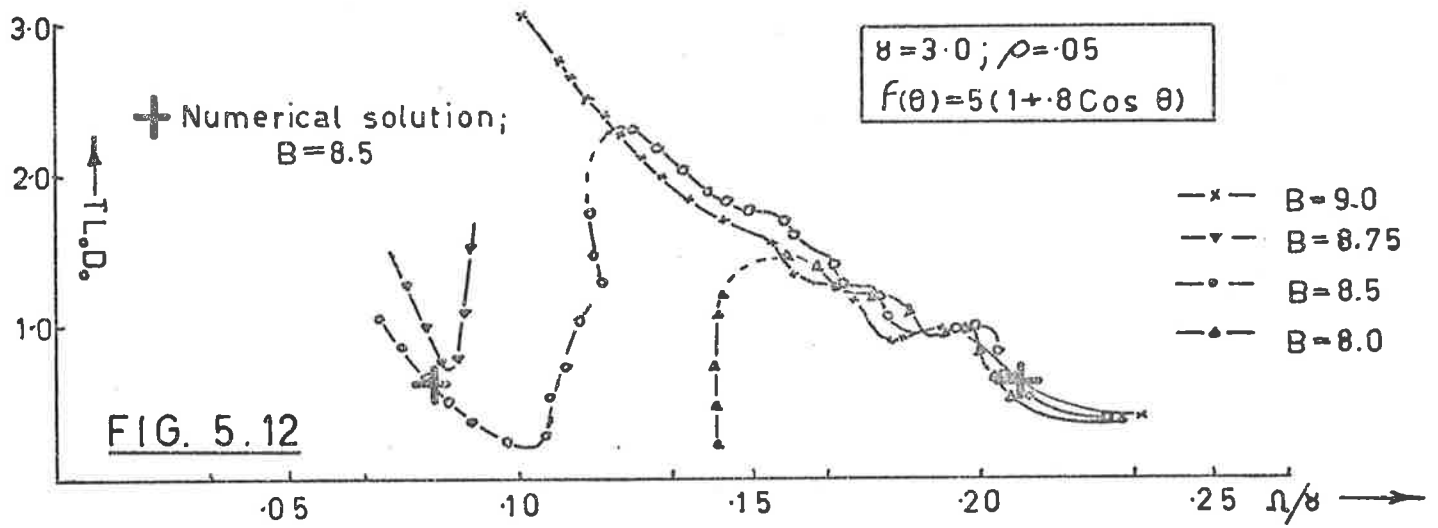

FIG. 5.12

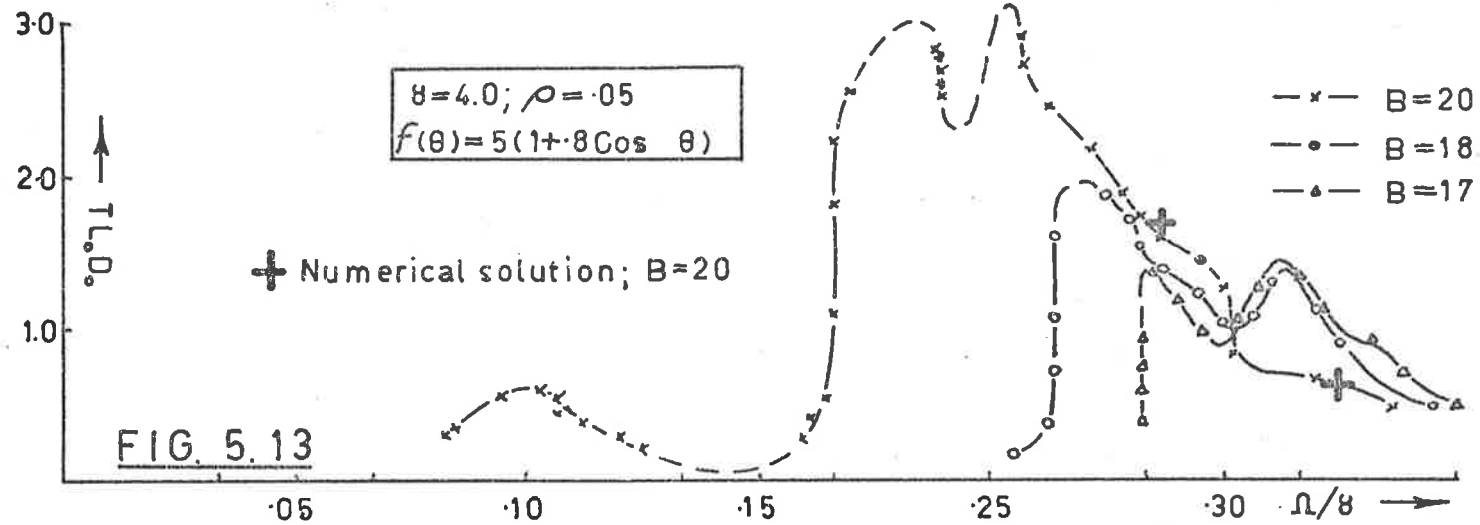

FIG. 5.13

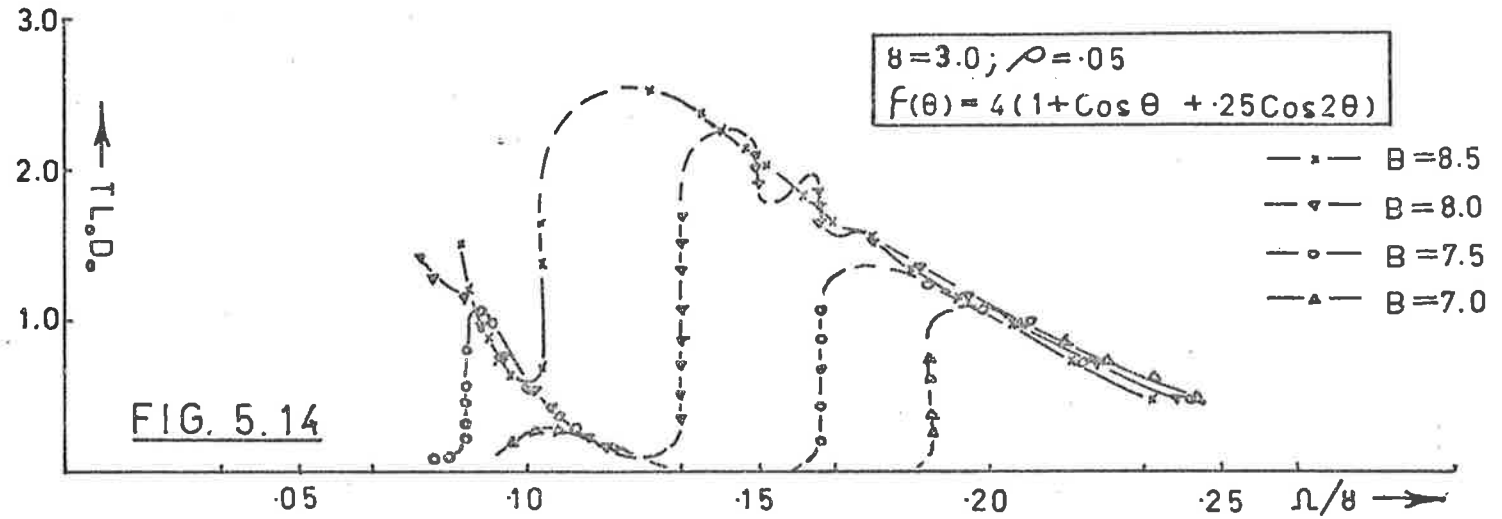

FIG. 5.14

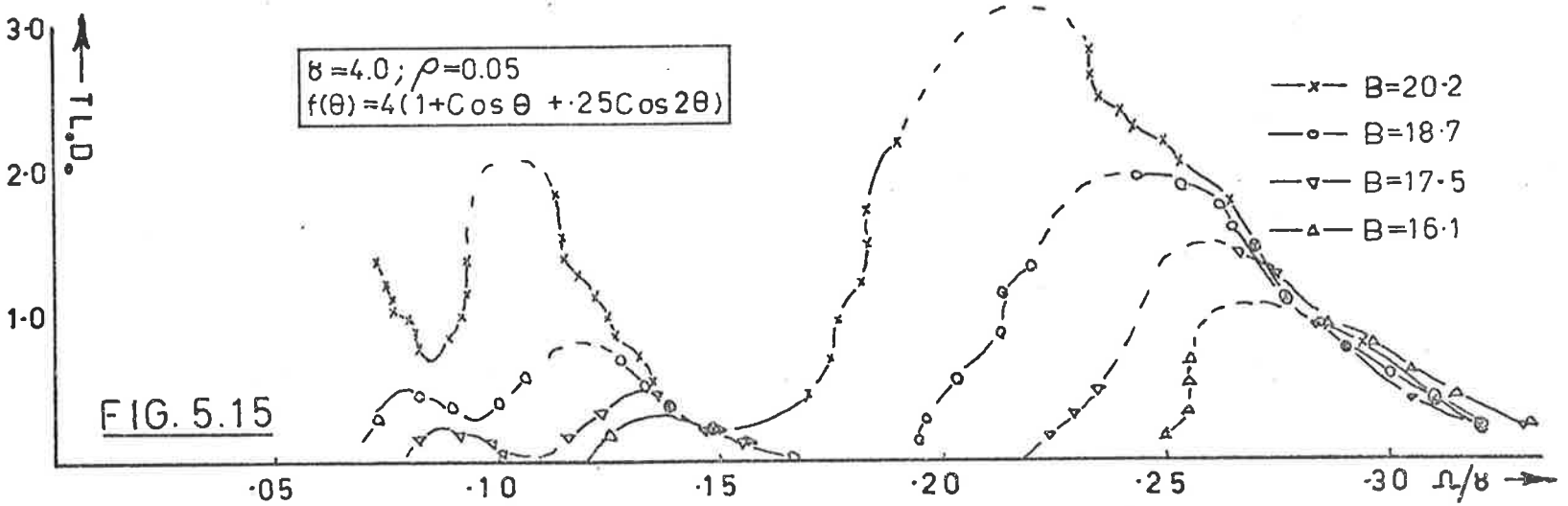

FIG. 5.15

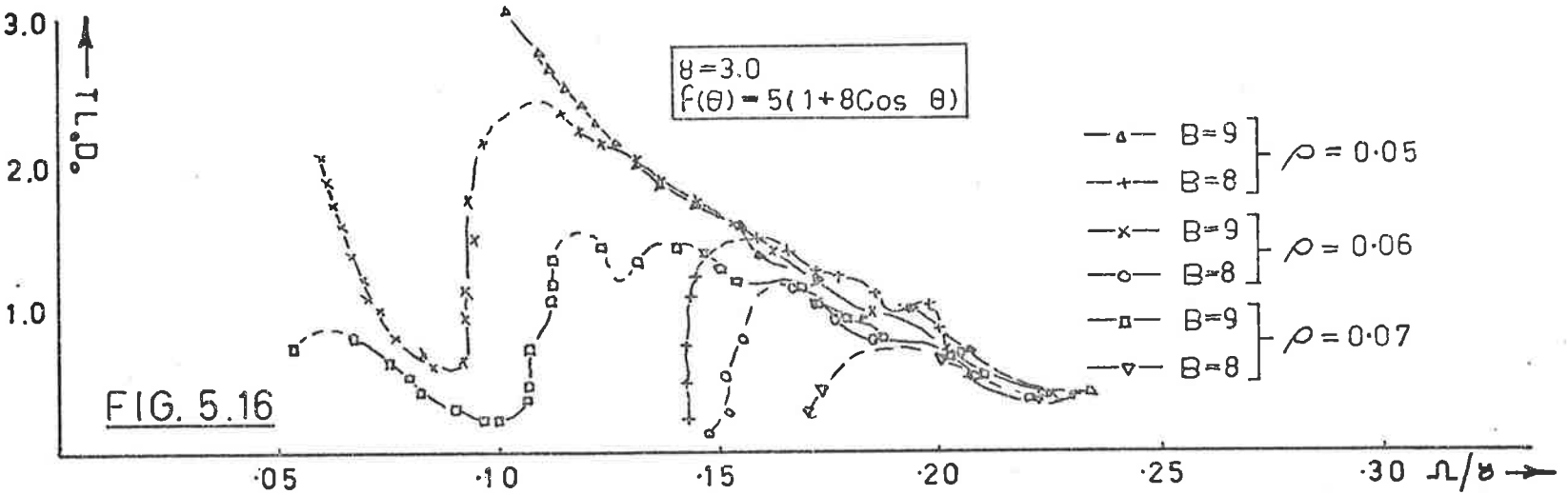

FIG. 5.16

CHAPTER 6: NUMERICAL SOLUTION OF THE SYSTEM EQUATIONS.

Instead of using an analogue computer, the system differential equations may be solved by numerical methods on a digital computer. Just as for the analogue computer, all initial conditions are set and the computation continued until the average speed becomes constant. However, unless a console is available with graphical display facilities the method is unsatisfactory and time consuming, particularly when searching for the unstable solutions on the positive slope portions of the speed torque curves.

Programmes were written, using a Runge Kutta fourth order method, to solve equations (4.33) to (4.35) which require re-arrangement for solutio Thus when both core loss and leakage reactance are included the equations become:-

$$\ddot{\psi} = \frac{1}{2\rho_2}\left[\dot{\vartheta}(1-\ell)-(1+q\,F(\theta)\,\psi^{q-1})\,\dot{\psi}-\psi^{q}\,F'(\theta)\,\dot{\theta}\right] \qquad \ldots\ldots (6.1)$$

$$\ddot{\vartheta} = -\frac{1}{\ell}\left[B\sin\overline{\gamma\tau+\beta} + \ddot{\psi} + 2\rho_1\dot{\vartheta} + \vartheta\right] \qquad \ldots\ldots (6.2)$$

$$\ddot{\theta} = \frac{\gamma^2 Tm}{J\omega^2} - \frac{F\gamma\dot{\theta}}{J\omega} - \frac{\psi^{q+1}\,\gamma^2\,F'(\theta)}{L_o J(q+1)\omega^2 D_o^{2/(q-1)}} \qquad \ldots\ldots (6.3)$$

where $\vartheta = (L_o+L_\ell)\,D_o^{\frac{1}{q-1}}i$

However when core loss can be neglected, or is treated approximately by adding extra series resistance, the leakage flux may be incorporated with the airgap flux; so that equations (6.1) and (6.2) reduce to:-

$$\ddot{\psi} = -B\sin\overline{\gamma\tau+\beta} - (1+2\rho_1\frac{d}{d\tau})\ (\psi+F(\theta)\psi^q) \qquad .....(6.4)$$

Solutions to (6.3) and (6.4) obtained by digital computer are marked on some of the curves in Figures 5.11 to 5.16, 10.9 and 10.11, while some instantaneous speed versus time plots obtained by numerical solution of (6.3) and (6.4) are shown in Figure 10.13. This latter Figure is referred to in section 10.7.1, in which a comparison is made of the results obtained by different methods.

CHAPTER 7:

Analytical Solution under Blocked Rotor Conditions

The computational methods outlined in Chapters 5 and 6 enable solutions to be found for the system equations. These solutions provide information concerning the instantaneous flux and current in the machine as well average torque versus speed characteristics. Furthermore, the results of Chapter 5 suggest that, provided an adequate model is available with which to represent the instantaneous iron losses, these equations may be used to predict the performance of practical machines.

However, these methods of solution provide little physical insight into the essential behaviour of such machines; so this and the two following Chapters will be given over to the investigation of this particular aspect of the problem.

We begin by exploring the nature and the stability of the steady state solutions which arise in the electrical circuit of such a machine when the rotor is locked in some particular position.

7.1 Steady state solution by harmonic balance.

As our immediate aim is physical understanding, core loss and leakage inductance may be disregarded at this

stage; so the relevant normalized circuit equation may be written:

$$B \cos(\gamma\tau+\beta) = \ddot{\psi}+(1+2\rho\frac{d}{d\tau})(\psi+\Sigma F_n\psi^{2n+1}) \qquad .....(7.1)$$

where the various

$$F_n = F_n(\theta)]_{\theta=\alpha}$$

Further simplification is possible when the λ-i relationship can be represented by one non-linear term only. In this case, when n=1, (7.1) assumes a particular form of Duffing's Equation, the solution of which is treated extensively in the literature, of which there is a very large body dealing with non-linear second order differential equations with constant coefficients. Perhaps the most satisfactory, from an engineering point of view, is that due to Hayashi [13], while two papers by West and Jayawant [40,16], following the approach of Hayashi, deal specifically with some aspects of the steady state and transient performance of (7.1).

It may be shown [13,23]that the solution to (7.1) contains not only a fundamental component having a period $2\pi/\gamma$, but also a series of harmonics of the fundamental, the relative magnitudes of which depend upon the degree of non-linearity, the amplitude of the driving function and the initial conditions. However in practical RLC circuits

where good efficiency is of some consequence, circuit parameters are such that the flux waveform is virtually sinusoidal; so that harmonics of the fundamental flux waveform usually may be neglected. This is not the case with the corresponding current waveform.

Under these circumstances the periodic solution of (7.1) may take the form [13]:-

$$\psi = x \sin \gamma\tau + y \cos \gamma\tau = r \sin \overline{\gamma\tau+\eta} \qquad \ldots\ldots (7.2)$$

Substituting (7.2) into (7.1) and equating the coefficients of cos $\gamma\tau$ and sin $\gamma\tau$ separately yields:-

$$B \cos \beta = (A-\gamma^2)y + 2\rho\gamma Ax \qquad \ldots\ldots (7.3)$$

$$B \sin \beta = 2\rho\gamma Ay - (A-\gamma^2)x \qquad \ldots\ldots (7.4)$$

where $A = \sum_{o}^{\infty} r^{2n} P_n$

$$r^{2n} = (x^2+y^2)^n$$

and $$P_n = F_n \frac{1}{2^{2n}} \frac{(2n+1)!}{(n+1)!n!}$$

Eliminating x and y from (7.3) and (7.4) yields

$$B^2 = [(A-\gamma^2)^2 + 4\rho^2\gamma^2A^2]r^2 \qquad \ldots\ldots (7.5)$$

$$\left.\begin{aligned} &\text{and} \quad \eta = \xi+\beta \\ &\text{where} \quad \tan\xi = \frac{A-\gamma^2}{2\rho\gamma A} \end{aligned}\right\} \qquad \ldots\ldots(7.6)$$

Thus when n = 1,

$$A = 1 + \frac{3}{4} r^2F; \text{ so that}$$

$$B^2 = [(1+\tfrac{3}{4} r^2F-\gamma^2)^2 + 4\rho^2\gamma^2(1+\tfrac{3}{4}r^2F)^2]r^2 \qquad \ldots\ldots(7.7)$$

$$\text{or } B^2F = [(1+\tfrac{3}{4}r^2F-\gamma^2)^2 + 4\rho^2\gamma^2(1+\tfrac{3}{4}r^2F)^2]r^2F \qquad \ldots\ldots(7.8)$$

Figures 7.1 to 7.3 show plots of r^2F versus B^2F for γ=2.5, 3 and 4 respectively for a range of values of ρ.

Now for a given machine with particular stator windings and fixed supply frequency, variations in γ are determined simply by changes in the series capacitance in the stator circuit; so that under these conditions Figures 7.1 to 7.3 represent the circuit behaviour for three different values of series capacity. These curves illustrate a number of the important characteristics of systems described by equation (7.1)

e.g:-

(i) for a particular value of ρ less than some critical value, there is a range of values of B^2F within which

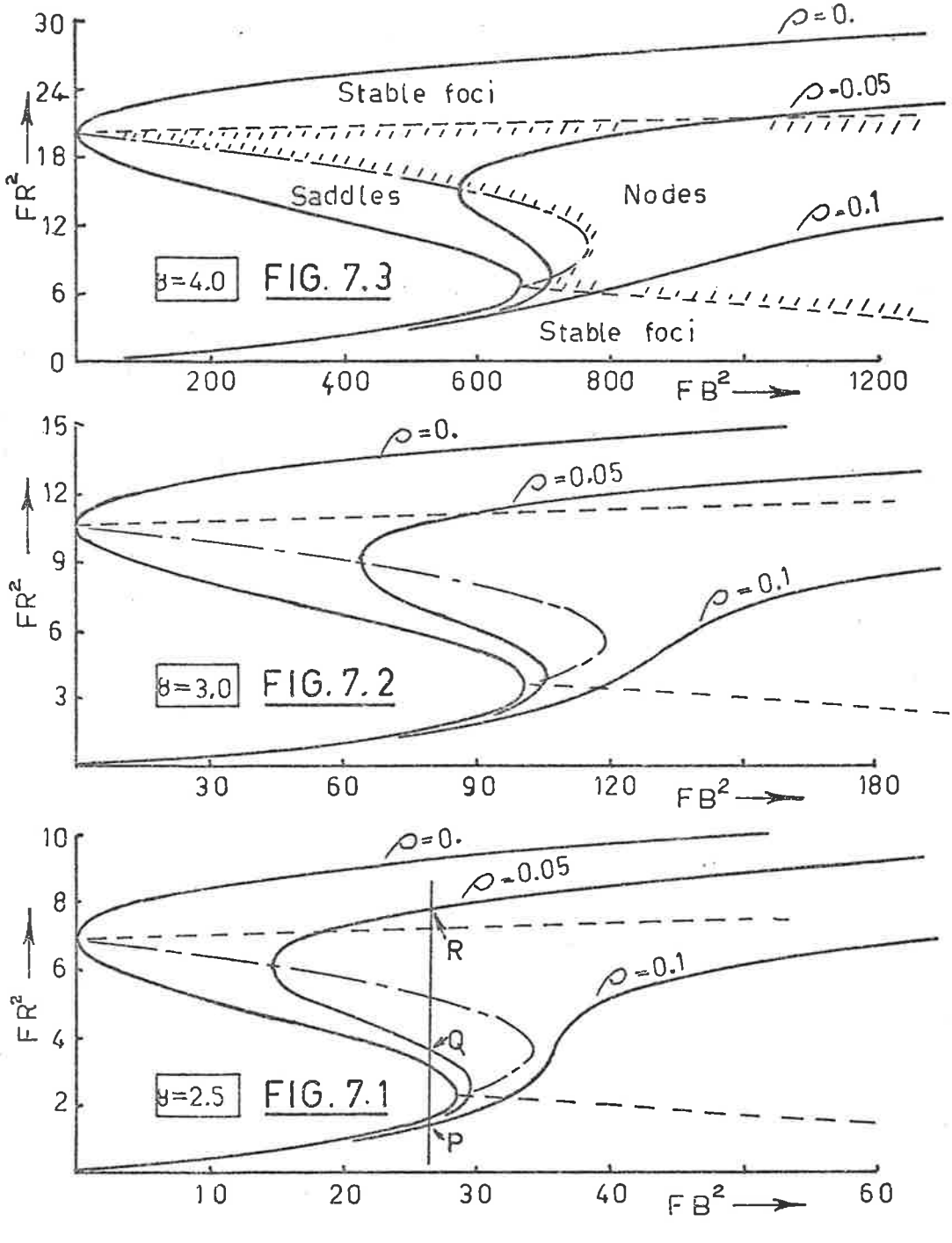
30
24
18
12
6
0
FR^2
ρ=0.
Stable foci
ρ=0.05
Saddles
Nodes
ρ=0.1
β=4.0
FIG. 7.3
Stable foci
200
400
600
800
FB^2
1200
15
12
9
6
3
FR^2
ρ=0.
ρ=0.05
ρ=0.1
β=3.0
FIG. 7.2
30
60
90
120
FB^2
180
10
8
6
4
2
FR^2
ρ=0.
ρ=0.05
R
ρ=0.1
Q
β=2.5
FIG. 7.1
P
10
20
30
40
FB^2
60
SOLUTIONS TO EQUATION 7.8 : FR^2/FB^2
Boundaries between nodes and foci
(Equation V.3)
Boundaries between nodes and saddles
(Equation V.4)

three different values of r^2F may be found which satisfy (7.8), for a particular value of B^2F within this range. e.g. at P,Q and R in Figure 7.1

(ii) for a particular value of γ, there is an upper limit to the value of ρ, above which only one solution exists for any value of B^2F.

(iii) discussion in Chapter 8 shows that the solution which corresponds to the point on the negative slope portion of the characteristic is unstable and does not exist in practice.

(iv) changes from a high state to a low state and vice versa may be induced under appropriate conditions by changes in B,F,ρ or γ.

A domain in the frequency-damping plane, within which two stable states may occur, may be derived [40]

Figure 7.4 shows these domains for different degrees of non-linearity, namely for n=1,2 and 3. When leakage reactance and iron losses are present these two parameters will affect the size of these domains, leading to results as presented in Figure 7.5 following an analysis in Appendix IV. The physical significance and relevance of these results will be discussed in sections 7.2 and 7.3.

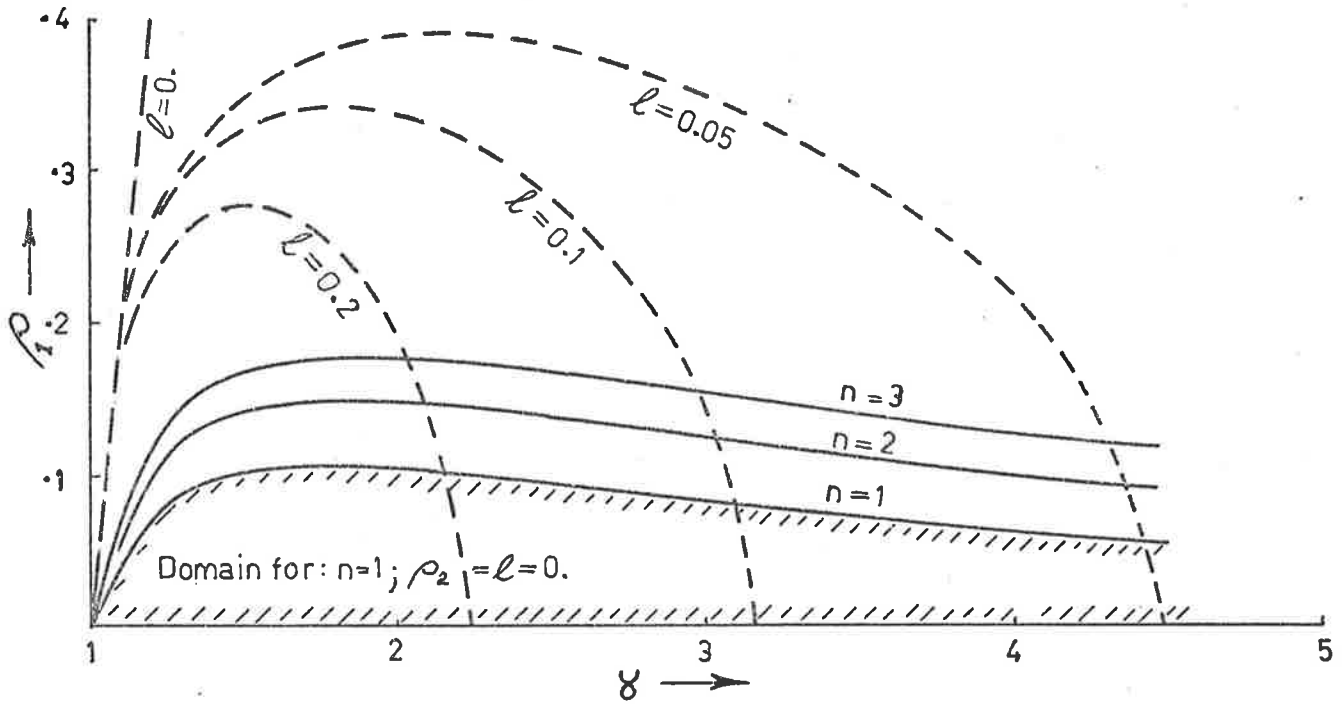

——— Boundaries for real roots when $\ell=\rho_2=0$ and n=1, 2, etc. (Equations (IV.13), (IV.20) etc)

– – – – Boundaries for positive roots for range of values of leakage inductance ℓ.

(Equation (IV.14))

FIGURE 7.4 : DOMAINS WITHIN WHICH MULTIPLE SOLUTIONS TO (IV.5) EXIST

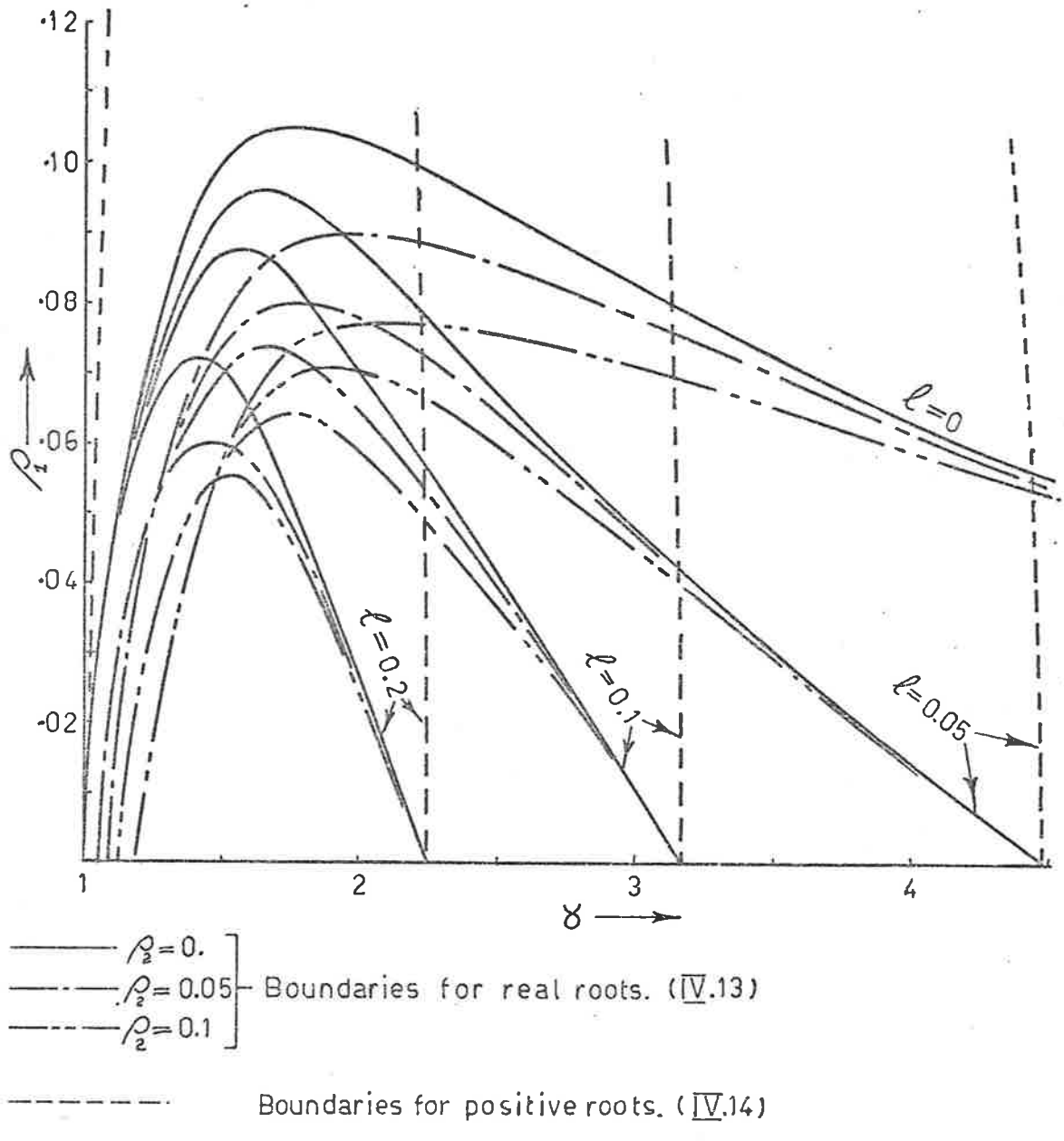

FIGURE 7.5(a): DOMAINS WITHIN WHICH MULTIPLE SOLUTIONS TO (IV.5) EXIST WHEN n=1. (CUBIC)

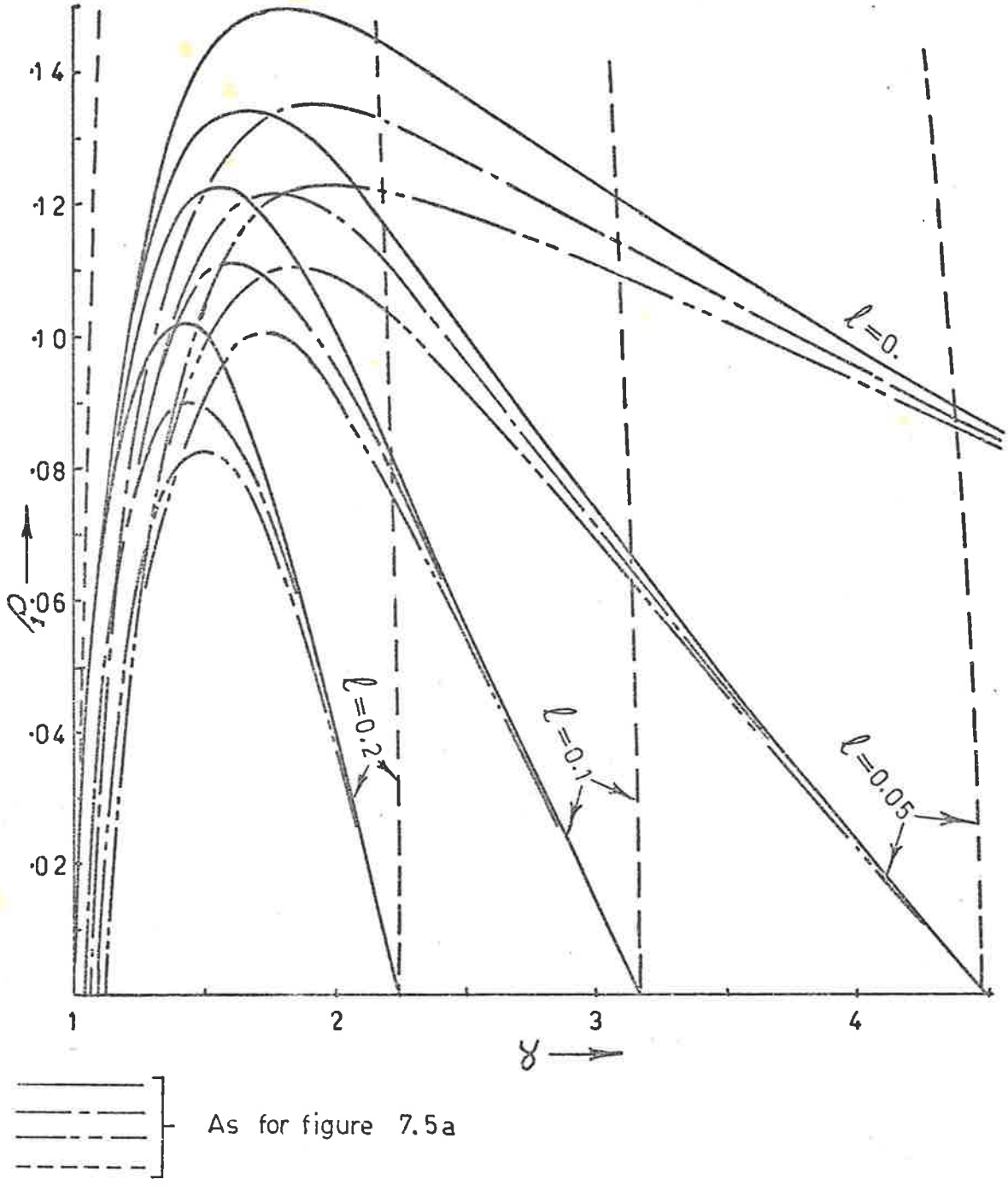

FIGURE 7.5(b): DOMAINS WITHIN WHICH MULTIPLE SOLUTIONS TO (IV.5) EXIST WHEN n=2. (QUINTIC)

7.1.1 Natural frequency of the unperturbed system

Systems described by equations taking the form of (7.1), exhibit skewed resonance curves, examples of which are shown in Figure 7.6, where the amplitude r^2F is plotted as a function of γ for a number of different values of B^2F/γ^2. This Figure 7.6 shows plots of

$$r^2F = \frac{(B^2F/\gamma^2)\gamma^2}{(A-\gamma^2)^2+4\rho^2\gamma^2A^2} \qquad .....(7.9)$$

as γ is varied, whilst keeping B^2F/γ^2 constant, i.e. whilst keeping $2V^2F/\omega_o^2$ constant. Clearly the natural frequency of the system increases as the amplitude of response increases. This is in accordance with our physical understanding because as the current and flux amplitudes increase in the windings the effective inductance falls due to saturation of the iron core; so raising the natural frequency.

An expression for the effective natural frequency, in terms of amplitude, may be found by studying the undamped autonomous form of Duffing's Equation:-

$$\ddot{\psi}+\psi+F\psi^3 = 0 \qquad .....(7.10)$$

This leads to the following expression for the undamped natural frequency [9,23].

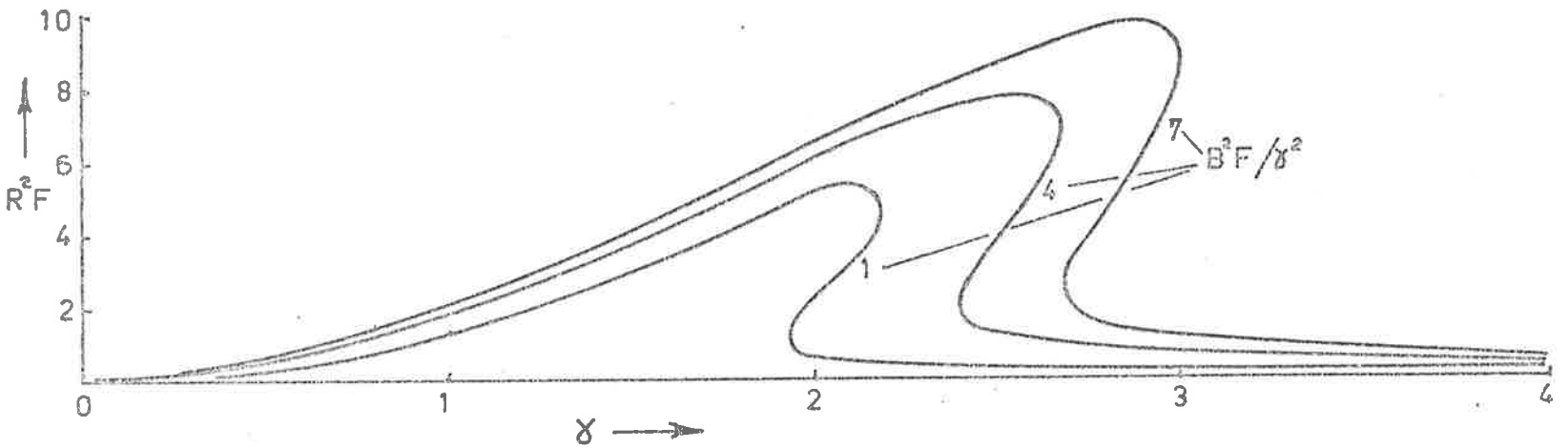

FIGURE 7.6: RESONANCE CURVES

$$\gamma_n^2 = 1+\frac{3}{4}Fr^2+\frac{3}{128}F^2r^4-\frac{57}{4096}F^3r^6+\ldots \quad .....(7.11)$$

$$\text{or } \gamma_n^2 \simeq 1+\frac{3}{4}Fr^2 \quad .....(7.12)$$

which is identical with the expression A, above. Thus (7.8) may be written as:-

$$B^2F = [(\gamma_n^2-\gamma^2)^2+4\rho^2\gamma^2\gamma_n^4]r^2F \quad .....(7.13)$$

Subsequently it will be found convenient to be able to relate the effective natural frequency to B^2F, γ and ρ; so (7.13) may be re-written as:-

$$\frac{3}{4}\frac{B^2F}{\gamma^4} = (\gamma_n^2-1)[(\frac{\gamma_n^2}{\gamma^2}-1)^2 + 4\rho^2(\frac{\gamma_n^2}{\gamma^2})^2] \quad .....(7.14)$$

and plotted as $\frac{3}{4}\frac{B^2F}{\gamma^4}$ versus γ_n^2/γ^2 for a range of γ and ρ, as shown in Figure 7.7.

Before we discuss the implications of the above results as far as parametric ferro-resonant machines are concerned, it is of interest to return to the graphical approach to obtaining the steady state solution which was discussed in the introductory sections.

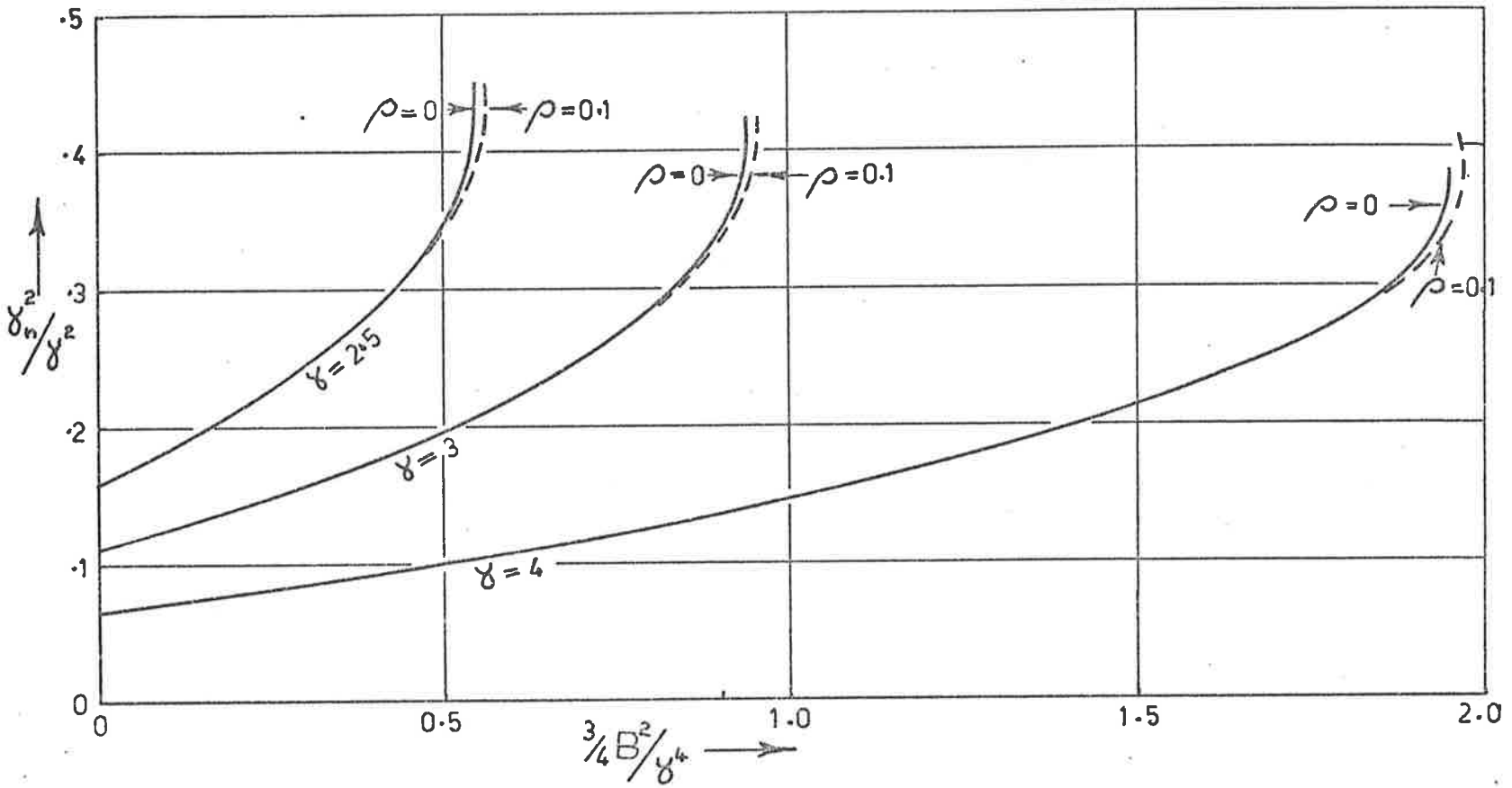

FIGURE 7.7: NATURAL FREQUENCY OF SYSTEMS DESCRIBED BY EQUATION 7.8

7.2 Steady state solution using $\omega L_f I_f$ curves

It was suggested in Section 2.1 that if the effects of harmonics in the current wave form could be neglected then a graphical solution for the steady state rms fundamental current in a series RLC circuit could be obtained by plotting both sides of equation (2.2), reproduced here for convenience as (7.15):-

$$\omega L_f I_f = \sqrt{V^2 - I_f^2 R^2} + I_f/\omega C \qquad \ldots\ldots(7.15)$$

Points of intersection of the two resultant curves would then correspond to possible steady state solutions.

When L_f is a constant, independent of current and time, the accuracy of the solution obtained from (7.15) is limited only by the method of solution. However, when L_f is some function of current, (7.15) becomes an approximation only to the circuit conditions and its practical usefulness will depend upon the closeness of the approximation.

The term $\omega L_f I_f$ represents the r.m.s. fundamental voltage across the winding inductance which must be measured, for any particular machine under consideration, as a function of I_f before the left hand side of (7.15) can be plotted. For practical machines, fed with sinusoidal periodic voltages in which good efficiency is important; so that ρ is relatively small, experimental evidence shows that, even for saturation factors as high as 10, the voltage and flux waveforms are essentially sinusoidal. Thus the measurement of $\omega L_f I_f$ is straight forward.

On the other hand, measurement of the fundamental component of the current waveform requires a dynamometer

type instrument and some care. Assuming that such a measurement can be made, the question arises concerning the relationship between the steady state solutions obtained by this graphical method and the solutions found by the method outlined in 7.1.

7.2.1 Equivalent linear inductance

Such a comparision becomes possible if we define what is meant by L_f.

When dealing with currents which are periodic functions of time, in a circuit element which has a known but non-linear λ-i relationship, an equivalent linear inductance may be found from the following relationship [22]

$$\tfrac{1}{2}L_f I_f^2 = \frac{1}{2\pi}\int_0^{\pi} \lambda i \, d(\omega t) \qquad \ldots\ldots(7.16)$$

Thus for i given by (4.24) and $\lambda=\Lambda\sin\omega t$, Appendix III(d) shows that

$$L_f = \frac{1}{\sum_{n=0}^{h} f_n(\theta)\frac{\Lambda^{2n}}{L_o}\,\frac{(2n+1)!}{2^{2n}(n+1)!n!}} \qquad \ldots\ldots(7.17)$$

Furthermore, Appendix III(b) shows that

$$I_f = \sum_{n=0}^{h} \sqrt{2}\,\frac{f_n(\theta)\Lambda^{2n+1}}{L_o}\,\frac{(2n+1)!}{2^{2n+1}(n+1)!n!} \qquad \ldots\ldots(7.18)$$

$$\left.\begin{aligned} &\text{so that } L_f = \frac{\Lambda}{\sqrt{2}I_f} \\ &\text{or } \omega L_f I_f = \frac{\omega\Lambda}{\sqrt{2}} = 4.44\Lambda f = 4.44N\Phi f \end{aligned}\right\} \quad \ldots\ldots(7.19)$$

which is the familiar expression for voltage across a coil of N turns, linked by a sinusoidal flux of frequency f and a peak value of Φ. Thus it is possible to define a suitable equivalent linear inductance which, when multiplied by the fundamental component of current and by the radian frequency, gives the correct reactive voltage across the winding. Conversely, plotting the measured coil voltage against the r.m.s. fundamental component of current I_f, and noting the intercepts with the right hand side of (7.15) leads to solutions identical with those found in 7.1. This follows, because when the relationship

$$V^2 = R^2 I_f^2 + (\omega L_f - 1/\omega C)^2 I_f^2$$

is converted to normalised parameters, with, for example, $f_o(\theta)=1$ and $f_1(\theta)=F$, it becomes:-

$$B^2F = \Lambda^2F[(1+\tfrac{3}{4}\Lambda^2F-\gamma^2)^2+4\rho^2\gamma^2(1+\tfrac{3}{4}\Lambda^2F)^2]$$

or $$B^2F = \Lambda^2F[(\gamma_n^2-\gamma^2)^2+4\rho^2\gamma^2\gamma_n^4]$$

which is identical with (7.13).

Although, for convenience, the comparison has been made for the case of a simple cubic non-linearity, it holds for non-linearities of any degree and complexity as may be seen from a study of Appendix III. Thus this graphical approach provides a practical and convenient means of investigating the blocked rotor behaviour of such a machine, based on the measured voltage-current characteristics of the stator windings.

Measurement of the total r.m.s. current I_R is far more convenient than measuring I_f, the r.m.s. fundamental component. Discussion presented in Appendix III(e) shows that any errors which result from plotting V_L against I_R instead of V_L against I_f are of little consequence as far as the problem of selecting appropriate operating conditions is concerned.

7.3 Selection of approximate operating conditions

So far, the discussion in Chapter 7 has been concerned with finding analytical solutions for the flux, current and torque under blocked rotor conditions. Although in later Chapters appropriate analytical methods are presented for the determination of these three quantities under running conditions, explicit solutions cannot be found. As a consequence, very few satisfactory design criteria can be established from such an analysis.

Nevertheless some of the practical limitations on the various circuit parameter values can be inferred from a study of the behaviour of the machine under blocked rotor or very slowly moving rotor conditions.

For any particular machine of the type under discussion, having associated with it a particular family of λ-i characteristics, there exists a restricted range for the values of V,R,ω and C within which satisfactory operation may take place as an energy conversion device.

It is shown in Appendix I that the area contained within the loop traversed by the V_L/I_f locus as discussed in Section 2.3, while the rotor slowly makes one complete revolution, is a measure of the work output; so that under these conditions changes in V,C or R leading to an increased loop area also lead to increased output, but not necessarily to increased efficiency. Unless ferro resonant jumps occur, the loop area and hence the output must be zero. The possibility of these occuring exists only if at least two stable solutions exist. Appendix IV analyses the conditions which ensure the latter situation, whilst Figures 7.4 and 7.5 present typical results showing the domains in the frequency damping plane within which such jumps are possible.

It may be seen that no jump can occur unless $\gamma>1$ for all values of ρ, a fact which may be deduced from Figure 7.9, because the relative slope of the $I_f\omega L_o$ line and the $I_f/\omega C$ line is $\omega^2 L_o C = \omega^2/\omega_o^2 = \gamma^2$. Clearly, unless this is greater than one, all of the $I_f\omega L_f$ curves must lie below the $I_f/\omega C$ line and no jump is possible. In general an upper limit to γ exists because of the presence of leakage inductance which sets a limit to the mimimum slope of the $I_f\omega L_f$ curve and hence to the slope of the $I_f/\omega C$ curve. A practical upper limit in the vicinity of $\gamma=4$ is suggested by the curves of Figure 7.5.

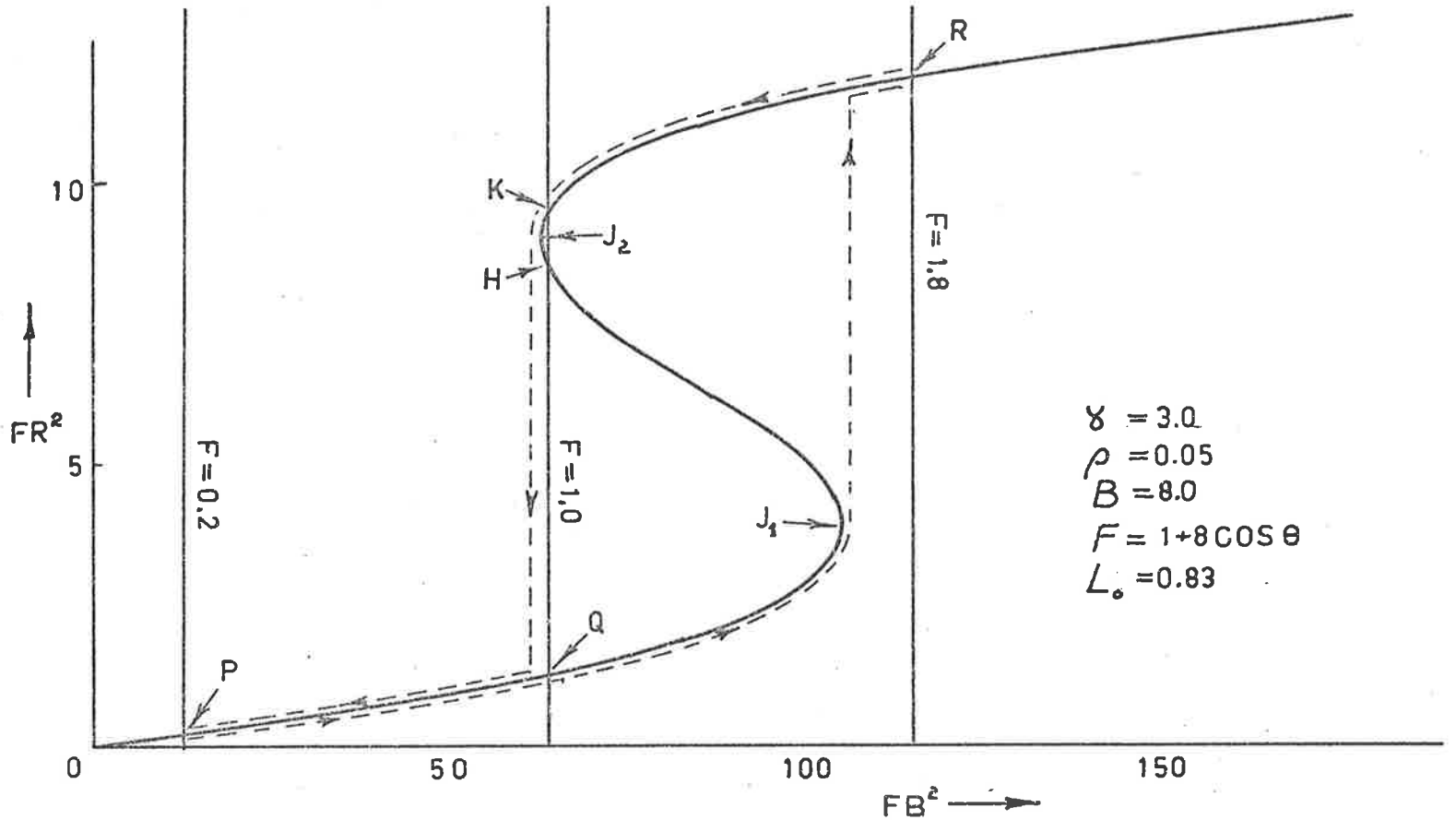

FIGURE 7.8 : LOCUS OF SOLUTION TO (7.20) AS θ SLOWLY CHANGES;

c.f. FIG. 7.9

The families of torque-speed curves presented in Figures 5.5 to 5.8 and Figures 5.11 to 5.16 suggest the presence of a threshold to the voltage magnitude, below which negligible torque is developed at any speed. Some indication of the magnitude of this voltage is given by the minimum voltage necessary to induce a jump from the low state to the high state when the rotor is clamped in the maximum reluctance position.

By way of example, consider a machine identical with one previously simulated on the analogue computer, as discussed in Chapter 5.2, for which:-

$$\gamma = \omega/\omega_o \equiv 3.0$$
$$\rho \equiv 0.05 \quad ; R \equiv 8.7\Omega$$
$$B \equiv 8.0 \quad ; V = 88.4 \text{ Volts}$$
$$f(\theta) \equiv 5(1+0.8 \cos\theta)$$
$$L_o \equiv 0.83$$

Typical torque speed curves of such a machine are shown in Figure 5.12, while the B^2F/r^2F characteristics obtained by the methods outlined in 7.1 and representing the solution of:-

$$B \cos\overline{\gamma\tau+\beta} = \ddot{\psi}+(1+2\rho\frac{d}{d\tau})(\psi+F\psi^3) \qquad .....(7.20)$$

are shown in Figure 7.8. In this particular case B=8.0 and F=1+0.8 cos θ, while $r^2 \equiv \psi^2 \equiv D_o\lambda^2 = 5\lambda^2$; so that $12.8 < B^2F < 115.2$. In other words, the above equation has been so normalised that the mean value of the coefficient of ψ^3 equals unity.

By way of comparison, Figure 7.9 shows curves of $I_f\omega L_f = \omega\Lambda/\sqrt{2} = V_L$ and $\sqrt{V^2-I_f^2R^2}+I_f/\omega C$ plotted against I_f,

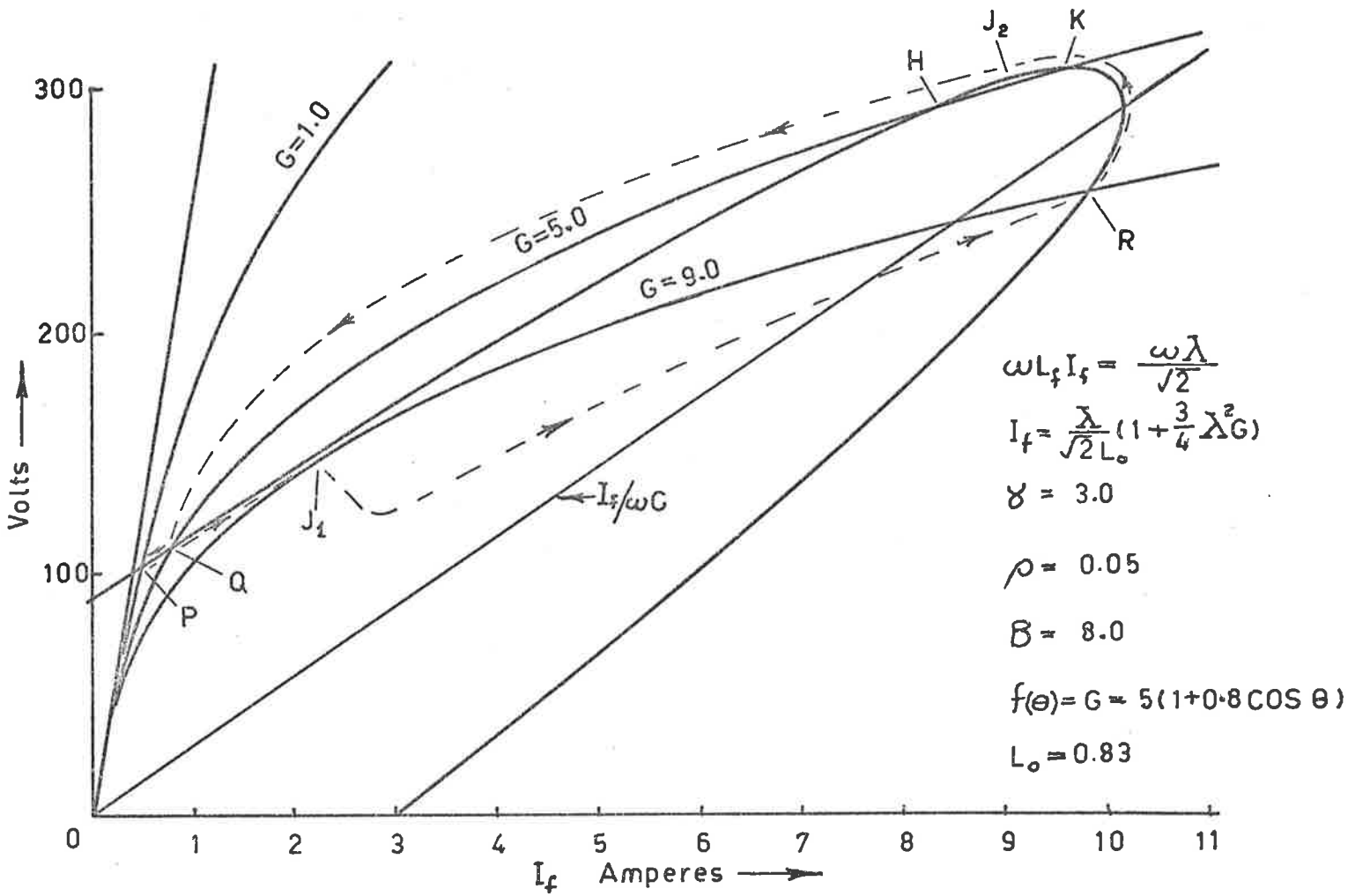

FIGURE 7.9: LOCUS OF SOLUTION TO (7.15) USING (7.21) & (7.22) AS θ SLOWLY VARIES; c.f. FIG 7.8

where Λ is the peak value of the actual flux linkages. Thus from (7.17) and (7.18) we have:-

$$L_f = \frac{L_o}{1+\frac{3}{4}\Lambda^2 G} \qquad \ldots\ldots(7.21)$$

and

$$I_f = \frac{\Lambda}{\sqrt{2}L_o}\ (1+\tfrac{3}{4}\ \Lambda^2 G) \qquad \ldots\ldots(7.22)$$

where G takes the value of $5(1+0.8 \cos \theta)$ and hence

$$1.0 < G < 9.0$$

The points marked P, Q R H and K correspond to identical machine conditions are represented in each of Figures 7.8 and 7.9 whilst the broken lines indicate the locus of the point representing coil voltage V_L and coil current I_f as the rotor slowly moves through one complete pole pitch.

It is clear that unless a jump from J_1 to R can occur before the rotor reaches the position of maximum reluctance, the area of the loop enclosed by the above locus will be zero provided the rotor is allowed to move only very slowly. As the rotor speed is increased under these conditions, the response of the electrical circuit will lag the rotor position; so that the possibility arises of having a finite loop area at finite rotor speeds, even although the conditions for a ferro-resonant jump are not satisfied. Such behaviour is discussed in sections 8 and 9.

Thus although we might expect to find some correspondence between the threshold voltage below which ferro-resonant jumps cannot occur with a stationary rotor, and the threshold voltage

below which negligible torque is developed at any speed, this correspondence is likely to decrease as γ increases because the speed at which maximum torque occurs, increases with increasing γ.

Thus for this particular case when ρ = .05 and F = 1.8, Figure 7.1 and 5.11 to 5.13 provide the following information:-

γ	2.2	3.0	4.0
B threshold for Jump	4.05	7.6	19.8
B threshold for torque (approximate only)	4.0	7.5	16.5

A similar rough correspondence occurred for other measured torque speed characteristics but no such simple upper practical limit for applied voltage can be found from this approach via the steady state -stationary rotor behaviour; because excessive current densities are likely to be the limiting factor.

The methods outlined in sections 7.1, 7.2 and 7.3 enable accurate solutions to be found for current, flux and torque in terms of the various network parameters for any fixed rotor position. Furthermore they enable some estimate to be made of the practical range for a number of these parameters such as C, R and V.

However, these methods tell us nothing about behaviour under moving rotor conditions, but before attempting to find an adequate analytical solution, applicable when the rotor is moving at finite speeds, it is of interest to study the nature of the transitions from one state to the other and back.

CHAPTER 8:

Transition Characteristics of the Jump

Discussion in Chapter 7 has shown that a system described by an equation of the form of (7.1), may have more than one stable state for a given set of input conditions and furthermore, that changes in any one of a number of parameters may induce a change from one stable state to another.

It is of interest to investigate the nature of the transient and the behaviour in the vicinity of a particular solution. Hayashi [13] treats this type of problem most comprehensively for similar but not identical systems, while West and Jayawant [40,16] have dealt with some aspects of the behaviour of circuits described specifically by equation (7.1). As the analysis which follows in 8.1 is similar to that used by these authors, only the bare essentials have been included.

8.1 Integral Curves

As in section 7.1, if harmonics of the fundamental component of the solution of (7.1) are negligible with respect to the fundamental itself, then the solution to (7.1) during transient states may be approximated by [13,40]:-

$$\left.\begin{aligned}\psi(\tau) &= x(\tau)\sin\gamma\tau + y(\tau)\cos\gamma\tau \\ &= r(\tau)\sin(\gamma\tau+\phi(\tau))\end{aligned}\right\} \qquad \ldots\ldots(8.1)$$

in which both the amplitudes $x(\tau)$ and $y(\tau)$ are functions of τ which finally become constants after completion of the transient.

Substituting (8.1) into (7.1) and equating coefficients of cos $\gamma\tau$ and sin $\gamma\tau$ separately, yields:-

$$2\gamma\frac{dx}{d\tau} = B\cos\beta-(A-\gamma^2)y-2\rho\gamma Ax \qquad .....(8.2)$$

$$2\gamma\frac{dy}{d\tau} = B\sin\beta-2\rho\gamma Ay+(A-\gamma^2)x \qquad .....(8.3)$$

where $A = \sum_{o}^{\infty} r^{2n}p_n$

$$r^{2n} = (x^2+y^2)^n$$

$$P_n = F_n\frac{1}{2^{2n}}\frac{(2n+1)!}{(n+1)!n!}$$

under the assumption that the amplitudes $x(\tau)$ and $y(\tau)$ are such slowly varying functions of τ that $d^2x/d\tau^2$ and $d^2y/d\tau^2$ may be neglected and that ρ is sufficiently small that products of ρ and the first derivatives may also be neglected.

Steady state solutions arise whenever both $dx/d\tau$ and $dy/d\tau$ are zero. Under these conditions (8.2) and (8.3) revert to (7.3) and (7.4) respectively to give results identical with those in (7.5) to (7.8).

When the rotor is stationary, (8.2) and (8.3) represent a pair of simultaneous, first order non linear equations in two quadrature components of the amplitude of the fundamental component of the solution of (7.1). Except for the case of a conservative system with $\rho=0$, when direct integration is possible, finding an analytical solution to (8.2) and (8.3) is a tedious exercise. However elimination of τ from (8.2) and (8.3) gives

$$\frac{dy}{dx} = \frac{B \sin \beta - 2\rho\gamma Ay + (A-\gamma^2)x}{B \cos \beta - (A-\gamma^2)y - 2\rho\gamma Ax} \qquad \ldots\ldots(8.4)$$

As τ does not appear explicitly in the RHS of (8.4), it is possible to draw, in the x-y plane, the integral curves of this equation by using one of a number of accepted graphical techniques [9, 40].

Beginning with some initial condition $x(o), y(o)$ in the x,y plane the representative point $x(\tau), y(\tau)$ moves, with increase of τ, along the particular integral curve passing through the point $x(o), y(o)$, until it reaches a stable singular point of (8.4) corresponding to $dy/d\tau = dx/d\tau = o$. Thus transient solutions of (7.1) may be correlated with passage along integral curves of (8.4), whilst steady state solutions may be correlated with the singular points of (8.4).

8.1.1 Plotting integral curves

When the λ-i curves are represented by a simple cubic approximation, the analogue computer implementation of (8.2) and (8.3) takes the form shown in Figure 8.1. By setting initial values for both x and y, releasing the computer whilst recording the instantaneous values on an x-y plotter, families of integral curves corresponding to particular values of γ, ρ, B and β may be drawn.

Taking $\gamma=3$, $\rho=.05$, $\beta=0$, $B=8.0$ and $F=F(\gamma)=[1+0.8\cos\theta]_{\theta=\gamma}$

i.e. $0.2 \leqslant F \leqslant 1.8$, we get the families of curves shown in Figures 8.2(a)-8.2(h) for a number of different values of F corresponding to different fixed rotor positions.

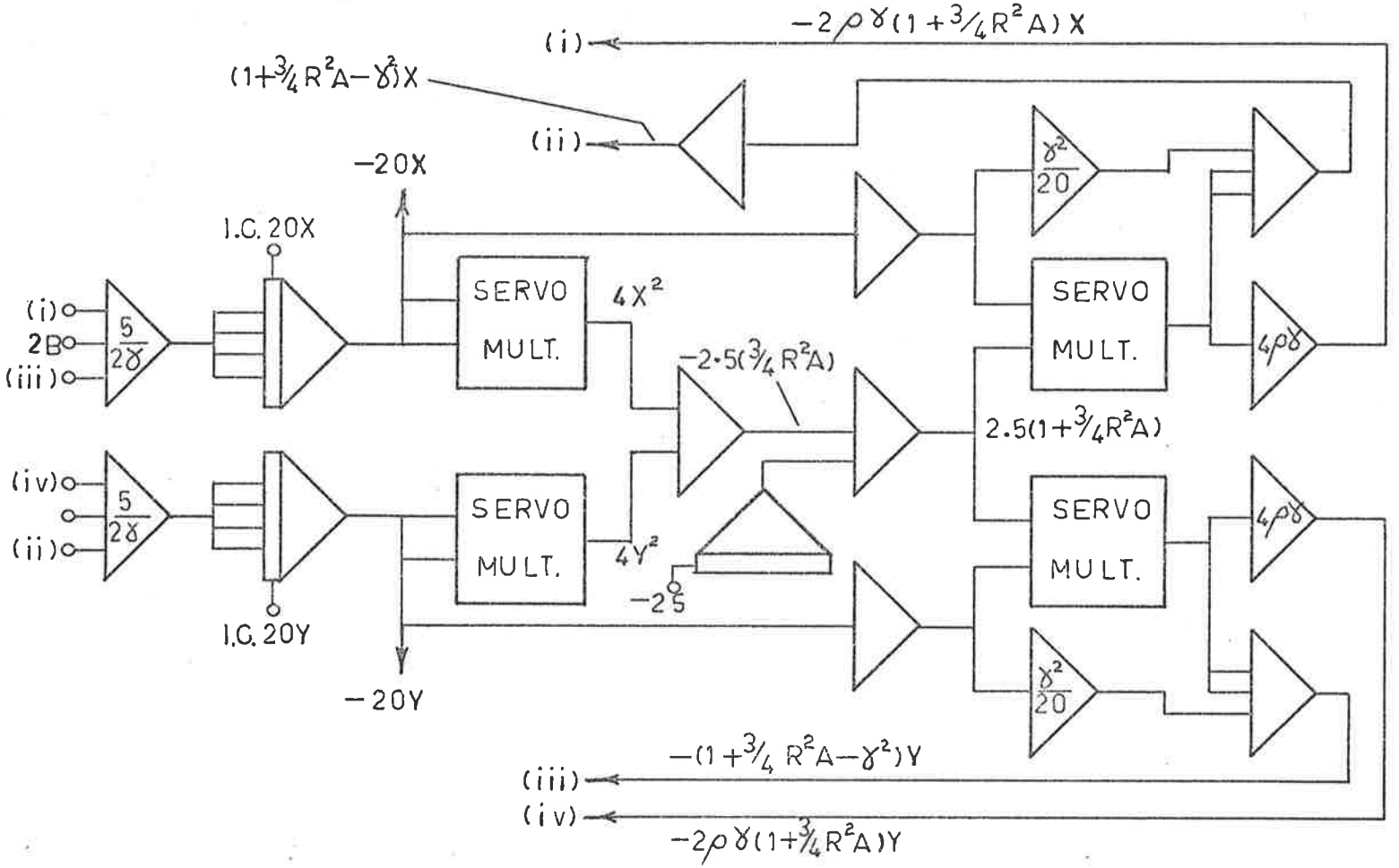

FIGURE 8.1 : A/C REPRESENTATION OF INTEGRAL EQUATIONS

From the derivation of equations (7.1), (8.2) and (8.3) it can be seen that the phase angle of the flux and hence of the fundamental component of the current with respect to the applied voltage, must be $\phi(\tau)-\beta$. Thus when $\beta=0$ the reference axis for the applied voltage corresponds to the positive x axis in Figure 8.2.

Points marked P,Q,R,H and K in Figure 8.2 represent possible steady state solutions in amplitude and phase, for three special values of F, equal to o.2, 1.0 and 1.8, corresponding to $F = F(\theta)_{min}$, $F(\theta)_{mean}$ and $F(\theta)_{maximum}$ respectively. Furthermore these lettered points correspond with the points similarly marked in Figures 7.8 and 7.9.

8.1.2 System behaviour as indicated by the integral curves

From an inspection of the integral curves in Figure 8.2, the following observations may be made concerning the physical performance of the circuit:-

(i) Behaviour in the vicinity of solutions corresponding to the low or anti-resonant state is strongly oscillatory, as indicated by the fact that the singularity comprises a lightly damped spiral focus. Furthermore the steady state solution represents conditions in a highly inductive circuit as indicated by the fact that the phase of the flux and hence current lags the voltage by almost 90°. Figure 8.2(h)

(ii) On the other hand, behaviour in the vicinity of a high or resonant state suggests an over damped response where the solution smoothly approaches the final solution with little overshoot and no oscillatory behaviour.
i.e. the singularity is a stable node or a heavily damped

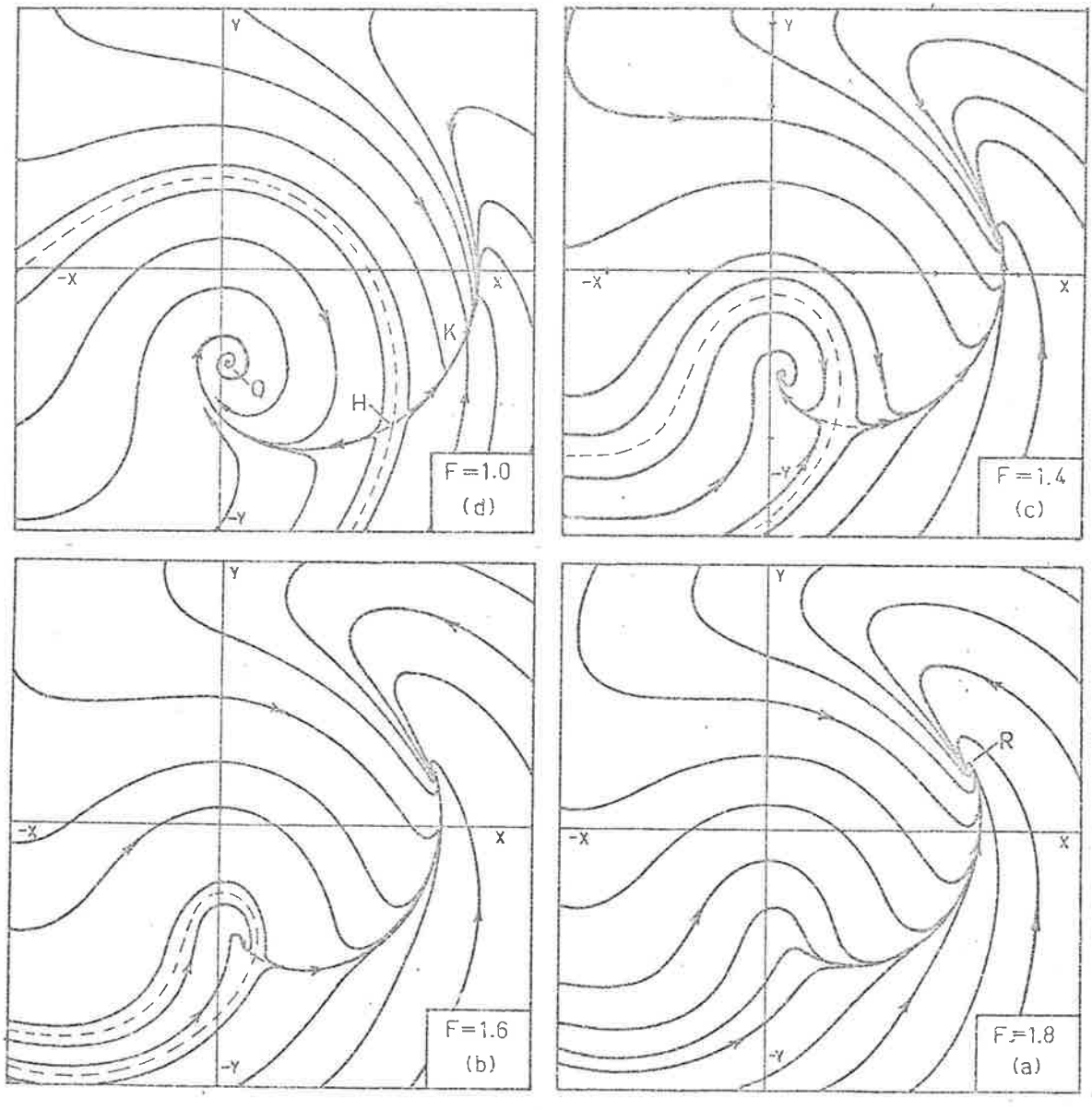

FIGURE 8.2a-d : INTEGRAL CURVES FROM (7.1)

FOR CUBIC NON LINEARITY

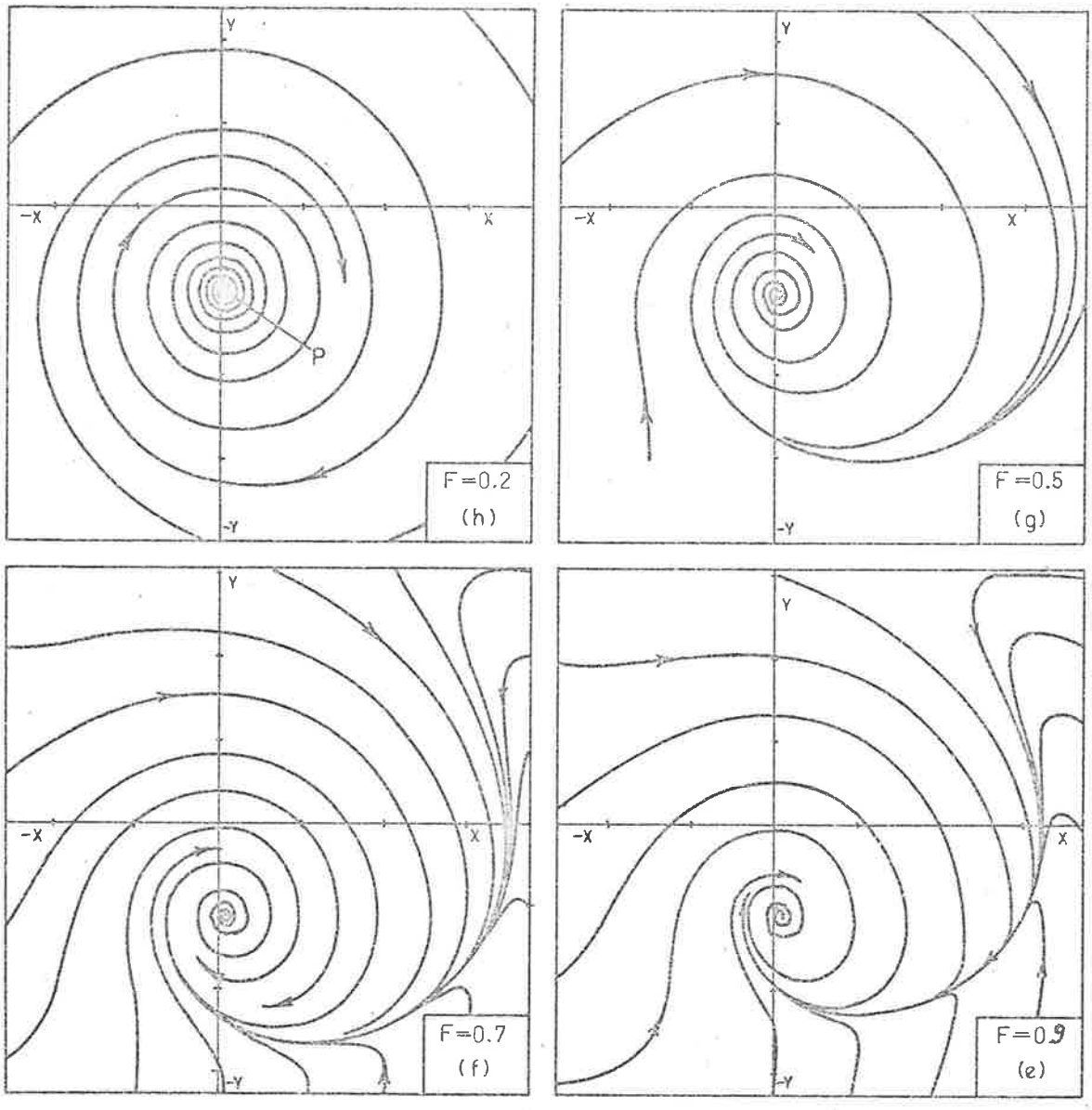

FIGURE 8.2e-h

stable focus in this case. In general such solutions correspond to capacitive circuit conditions as indicated by the fact that the singularity lies in the first quadrant.

(iii) When the circuit parameters are such that three possible steady state solutions exist, as at Q,H and K in Figures 7.8, 7.9 and 8.2(d), the singularity corresponding to the intermediate solution H is a saddle point. Associated with any saddle is the so called sepatrix which divides the x-y plane into two separate portions. Any initial condition x(o),y(o) must then lead to whichever stable solution lies on the same side of the sepatrix as the initial point x(o),y(o) which in turn has a unique correspondence with a given set of initial circuit conditions [40].

(iv) Beginning with the circuit in the anti-resonant state corresponding to point P in Figures 7.8, 7.9 and 8.2 and slowly turning the rotor, results in the points Q and H merging at J_1 in Figure 7.9 or the focus and the saddle merge, as is about to occur in Figure 8.2(b). This particular value of the steady state solution then becomes the initial value of the transient solution which corresponds to the integral curve through this point and which terminates at the node corresponding to the point R in Figures 7.8, 7.9 and 8.2(a).

Continued motion of the rotor leads to the initiation of the downward jump at the instant when H and K coincide at J_2. This transient, which is strongly oscillatory, corresponds to the integral curve which passes through the point on the x-y plane at which the node and saddle merge.

Time does not appear explicitly on the integral plots but may be evaluated along any path by means of the following expression [13]:-

$$T = \oint \frac{ds}{\sqrt{\left(\frac{dx}{d\tau}\right)^2 + \left(\frac{dy}{d\tau}\right)^2}} \qquad \ldots\ldots(8.5)$$

where $ds = \sqrt{(dx)^2+(dy)^2}$

The above analysis enables steady state and transient behaviour of the circuit under blocked rotor conditions to be evaluated within the limitation of the method.

For our purposes the most important observation to be made is that concerning the markedly different behaviour in the vicinity of the anti-resonant and resonant states respectively. Definite boundaries may be found which separate the different types of behaviour.

8.2 The Nature of the singular points

The behaviour of equation (7.1) in the vicinity of a particular steady state solution may be directly related to the nature of the corresponding singularity of equation (8.4). In turn, the nature of the singularity is related to the nature of the roots of the characteristic equation of the perturbed system [9].

Thus if $dy/d\tau = Y(x,y) = dx/d\tau = X(x,y) = 0$ when $y=y_o$ and $x=x_o$, then (x_o,y_o) is a singular point of (8.4). Transforming the origin of co-ordinates to this point we have:-

$$\left.\begin{aligned} x &= x_o+u \\ y &= y_o+v \end{aligned}\right\} \qquad \ldots\ldots(8.6)$$

Then if u and v are small excursions in the vicinity of (x_o, y_o); so that higher order terms in u and v may be neglected, then

$$\left.\begin{aligned} \frac{du}{d\tau} &= au+bv \\ \frac{dv}{d\tau} &= cu+dv \end{aligned}\right\} \qquad \ldots\ldots(8.7)$$

and $$\frac{dv}{du} = \frac{cu+dv}{au+bv} \qquad \ldots\ldots(8.8)$$

where a,b,c and d are defined in Appendix V.

The characteristic equation of the system defined by (8.7) is given by

$$\begin{vmatrix} a-\lambda & b \\ c & d-\lambda \end{vmatrix} = 0$$

or $$\lambda^2-(a+d)\lambda+ad-bc=0 \qquad (8.9)$$

and depending on the nature of the roots of (8.9), the singularity may be classified according to the criteria set out in Appendix V

8.2.1 Stability of the steady state solution

Provided any small disturbances u and v, away from a singular point x_o, y_o, approach zero with increasing time, then the point (x_o, y_o) represents a stable solution. This will be the case if the real part of λ is -ve. This stability condition corresponds to the Routh-Hurwitz criterion which requires that

$$-(a+d)>0 \text{ and } ad-bc>0 \qquad \ldots\ldots(8.10)$$

for stability [9]. It may be shown [13,40] that the stability

condition for a system described by (7.1) is that

$$\frac{dB^2}{dr^2} > 0 \qquad \ldots\ldots(8.11)$$

i.e. stable solutions exist only on the positive slope portions of Figures 7.1, 7.2, 7.3 and 7.8, for example.

The boundary of the unstable region is given by:

$$\frac{dB^2}{dr^2} = 0 \qquad \ldots\ldots(8.12)$$

and the criteria in Appendix V establish that the singularities in this region are saddles; a conclusion which agrees with the results shown in Figure 8.2.

8.2.2. Boundaries between different types of singularity

Expressions for the boundaries between regions of stable nodes and stable foci are established in Appendix V and some representative results are shown plotted in Figures 7.1 to 7.3. These suggest that for practical ranges of both γ and ρ, approaches to anti-resonant or low states will be more or less oscillatory whereas approaches to resonant or high states will be well damped.

CHAPTER 9
Phase amplitude plots

In the previous section we were concerned with the behaviour of the system when the machine rotor is fixed in one position or is allowed to move so slowly that steady state solutions still apply. In this section we shall use the methods of Chapter 8 to investigate the nature of the system behaviour as the rotor speed is slowly increased.

9.1 First order equations for amplitude and phase

Beginning once again with equation (7.1) in which the various fixed F_n are replaced with the various $F_n(\theta)$ which describe the rotor geometry, assuming a solution of the form given by (8.1) and using the methods of section 8.1, we obtain the following alternative pairs of first order equations:-

$$2\gamma\frac{dx}{d\tau} = B\cos\beta-(A-\gamma^2-2\rho\Omega\frac{\partial A}{\partial\theta})y-2\rho\gamma Ax \qquad .....(9.1)$$

$$2\gamma\frac{dy}{d\tau} = B\sin\beta-2\rho\gamma Ay+(A-\gamma^2-2\rho\Omega\frac{\partial A}{\partial\theta})x \qquad .....(9.2)$$

or:-

$$2\gamma\frac{dr}{d\tau} = B\cos\overline{\beta-\phi}-2\rho\gamma Ar \qquad .....(9.3)$$

$$2\gamma r\frac{d\phi}{d\tau} = B\sin\overline{\beta-\phi}+(A-\gamma^2-2\rho\Omega\frac{\partial A}{\partial\theta})r \qquad .....(9.4)$$

where A is given by the expressions following (7.4).

Similar equations may be obtained by the method [9] of variation of parameters but in either case, the approximations made in obtaining (9.1)→(9.4) are valid only

provided:

$$\dot{\phi} << 1 \text{ and } \left|\frac{\dot{r}}{r}\right| \frac{2\pi}{\gamma} << 1 \qquad \ldots\ldots(9.5)$$

Identical provisions apply to equations (8.2) and (8.3) so that in general, they may be used with confidence, only in the vicinity of a singular point.

However, in the results which follow, these inequalities are far from satisfied, except at low rotor speeds, but nevertheless, the qualitative behaviour of (9.1) and (9.2) agrees well with the actual system and provides valuable insight into its behaviour.

9.2 Analogue computer solution of amplitude and phase equations

The method of implementing equations (9.1) and (9.2) on the analogue computer is shown in Figures 9.1 and 9.2 while further details may be found in Appendix VI.

These equations were derived on the assumption that the electrical circuit is subjected to a driving function $v = \sqrt{2}V\sin\overline{wt+\beta}$, the amplitude and phase of which is retained in the terms $B\cos\beta$ and $B\sin\beta$ of equations 9.1 and 9.2 respectively. Furthermore the rotor geometry in normalised form is expressed as

$$F(\theta) = 1+\sum_{m=1}^{\mu} d_m \cos\overline{mp\theta+\delta_m} \qquad \ldots\ldots(9.6)$$

where p is the number of poles in the machine; so that in equations (9.1) and (9.2) a definite phase relationship is implied between the electrical and mechanical forcing functions. However the frequencies of these two functions are, in general, incommensurate; so that this relative phase is relevant and meaningful only in that it specifies

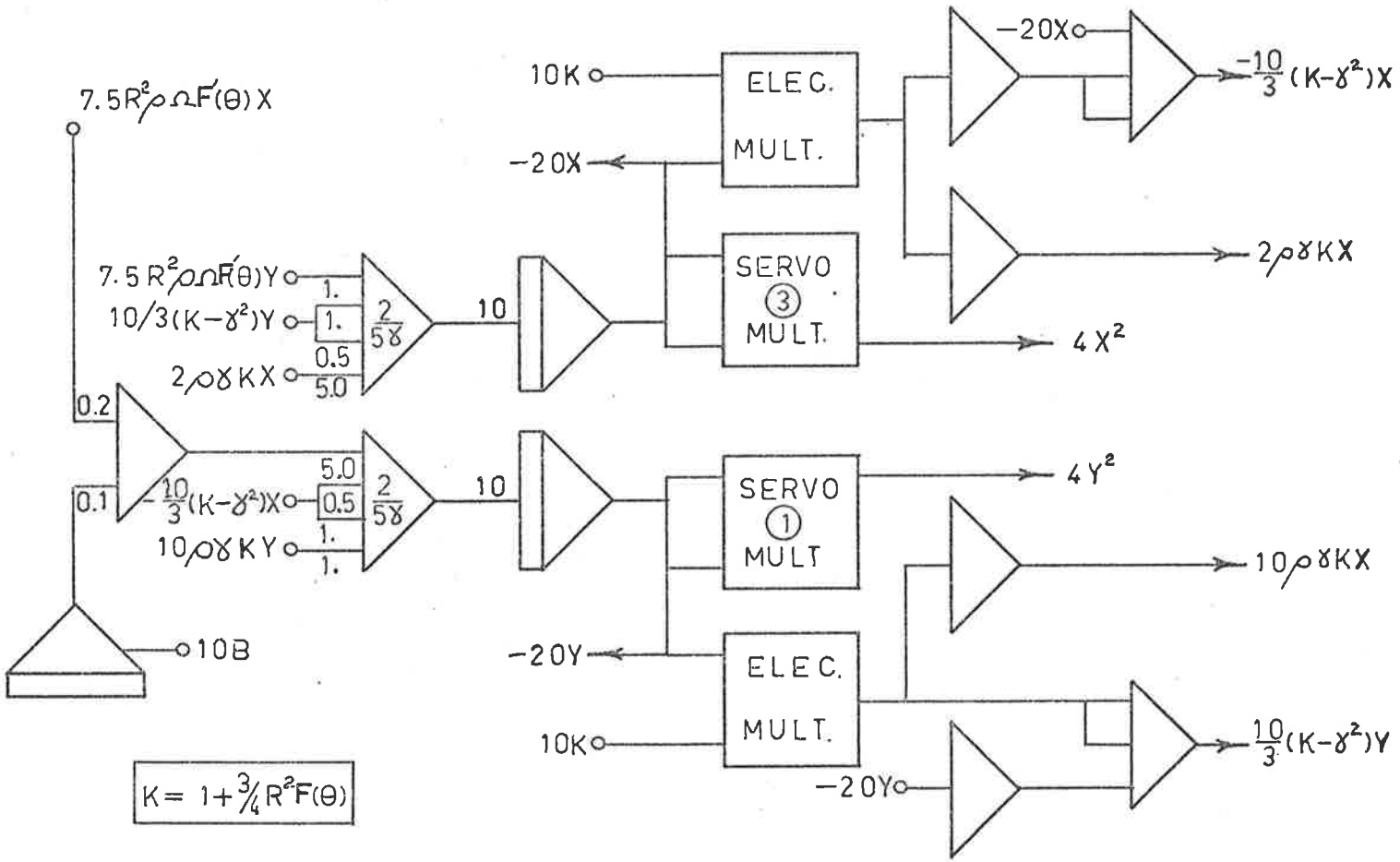

FIGURE 9.1: A/C DETERMINATION OF PHASE-AMPLITUDE PLOTS

(see also figure 9.2)

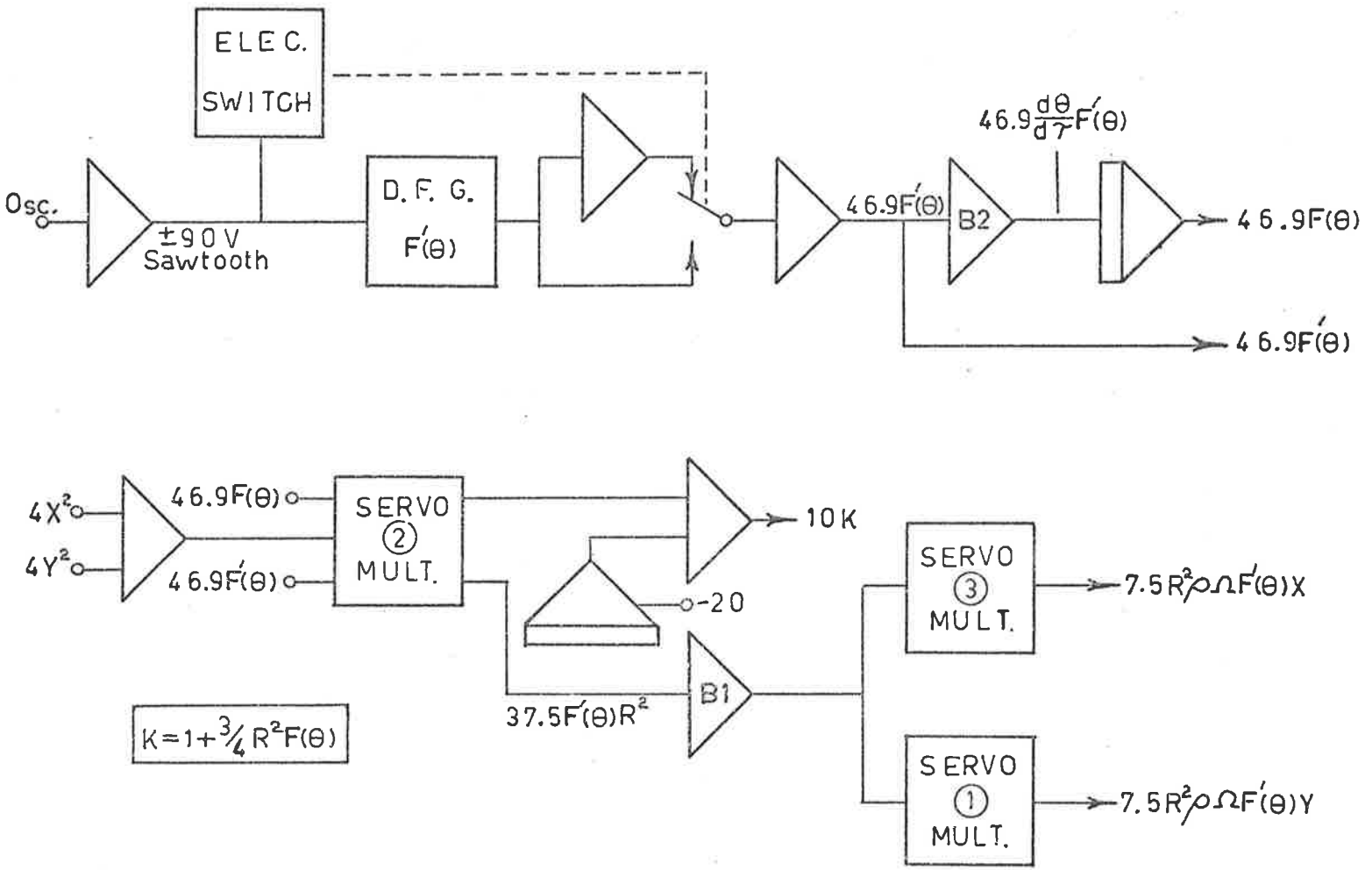

FIGURE 9.2: A/C DETERMINATION OF PHASE-AMPLITUDE PLOTS

(see also figure 9.1)

definite initial conditions.

In the actual practical system having finite inertia in which speed variations occur, the effect of the initial conditions may be lost very quickly, but in setting up equations (9.1) and (9.2) on the computer, the speed Ω is treated as a constant. Thus, under these conditions, equations (9.1) to (9.4) can be taken to represent a practical system having infinite inertia, and running at a constant speed Ω.

As a result, the initial relative phase angle between the two forcing functions may be significant, and care must be taken to have it under control if consistent results are to be obtained.

9.2.1 Results from the analogue computer

Typical examples of the results obtained are shown in Figures 9.3(a)-(e) which give the performance of equations (9.1) and (9.2) or (9.3) and (9.4) when $\gamma=3$, $\rho=.05$, $F(\theta)=1+\cos 2\Omega\tau+0.25\cos 4\Omega\tau$ for two different values of $B=8.0$ and 7.0.

By putting $\Omega=0$ in equations (9.1)→(9.4) they revert to equations (8.2) and (8.3) discussed in section 8.1. Thus the steady state solution in amplitude and phase, for any fixed rotor position may be found readily. Points P,Q and R in Figures 9.3 and 9.4 represent the steady state solutions when the rotor is in positions such that $F(\theta)$ takes its minimum, mean and maximum values respectively. Such solutions may be represented by fixed phasors, drawn from the origin to the point in question, as in Figure 9.5(a).

On the otherhand, solutions to (9.1) and (9.2) are trajectories in the x,y plane traced out by the tip of a moving phasor. At relatively high speeds these trajectories

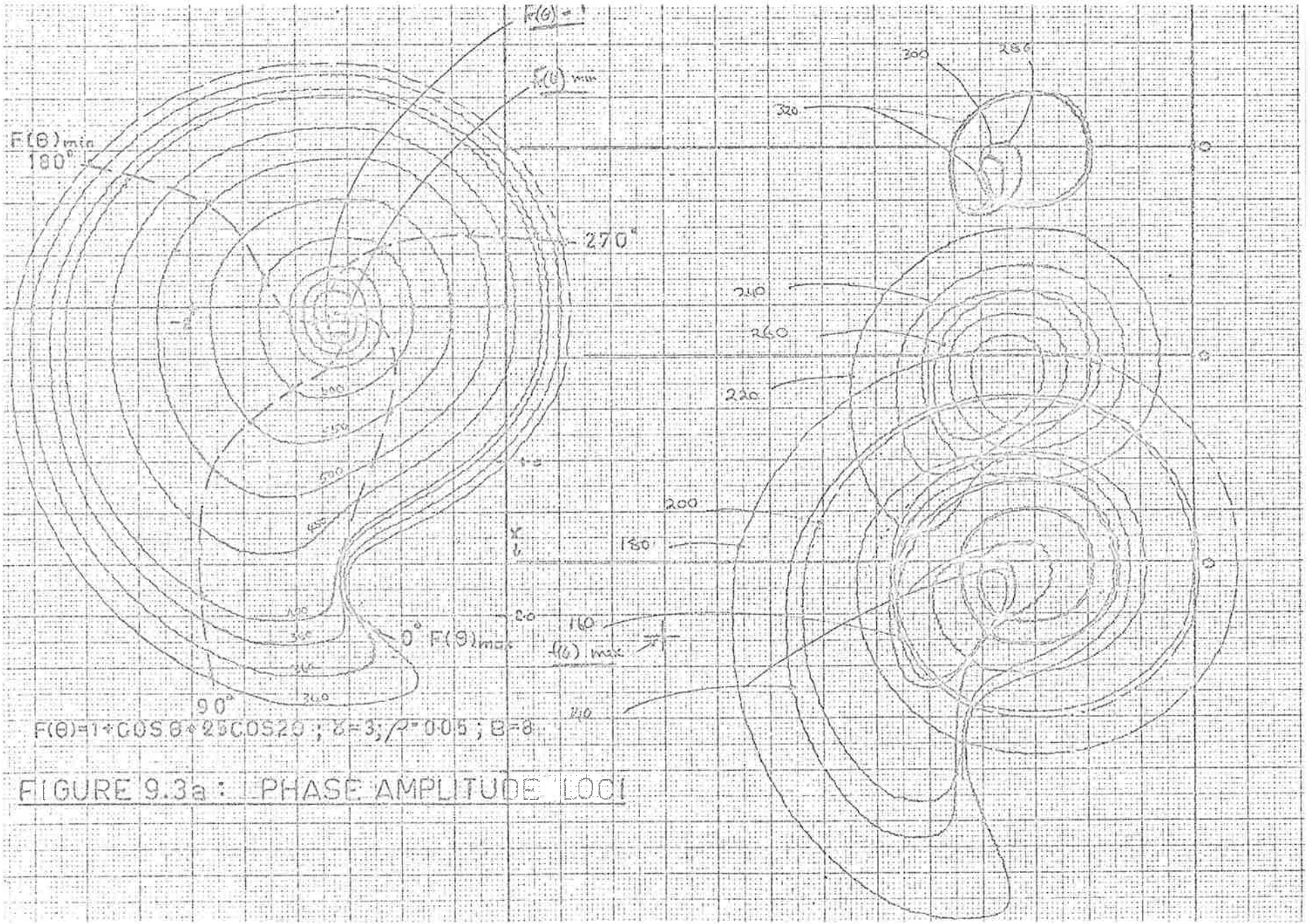

FIGURE 9.3a : PHASE AMPLITUDE LOCI

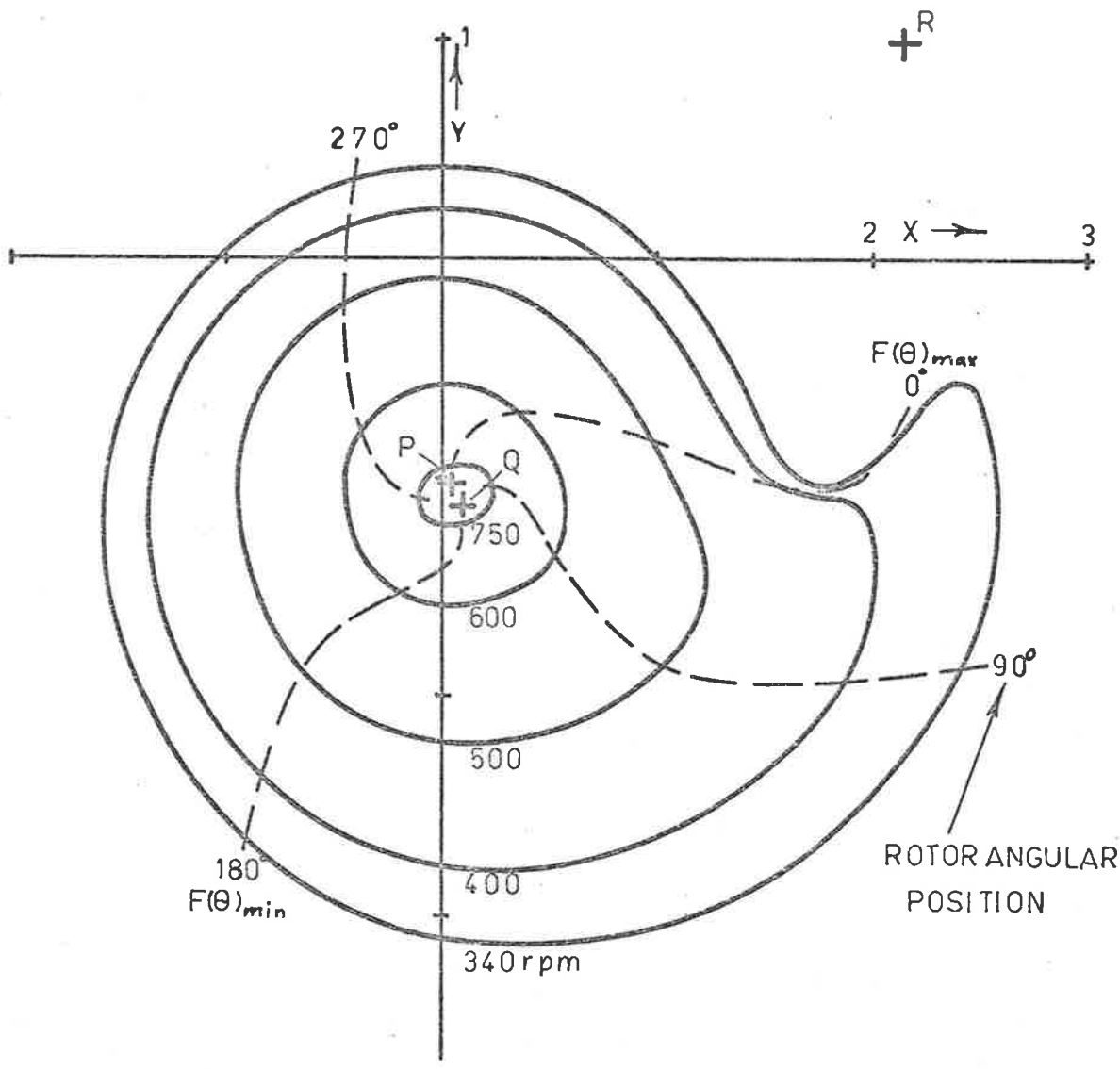

$F(\theta) = 1 + \cos\theta + .25\cos 2\theta$; $\gamma = 3$; $\rho = 0.05$; $B = 8$

FIGURE 9.3b : FIRST RESONANCE

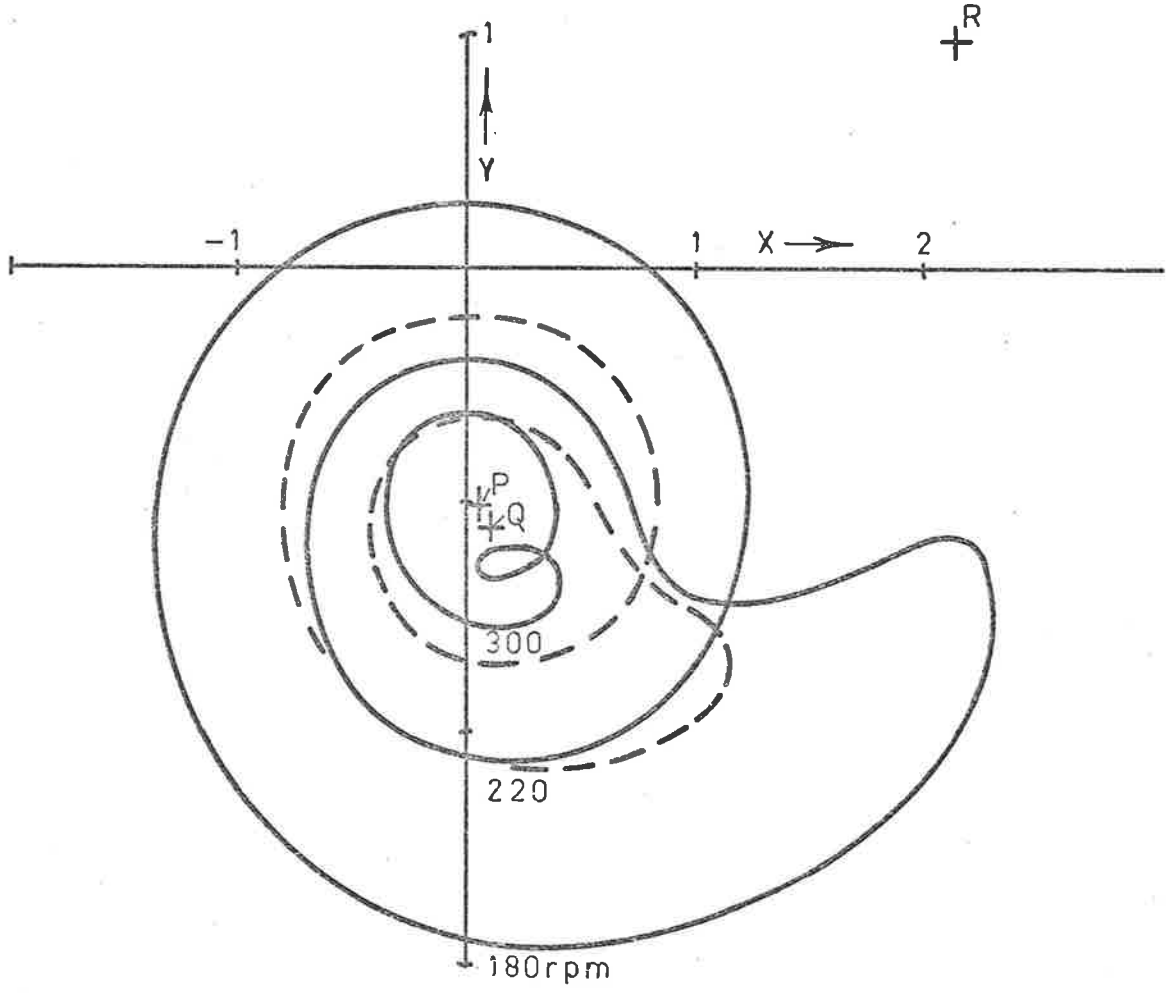

FIGURE 9.3c : SECOND RESONANCE

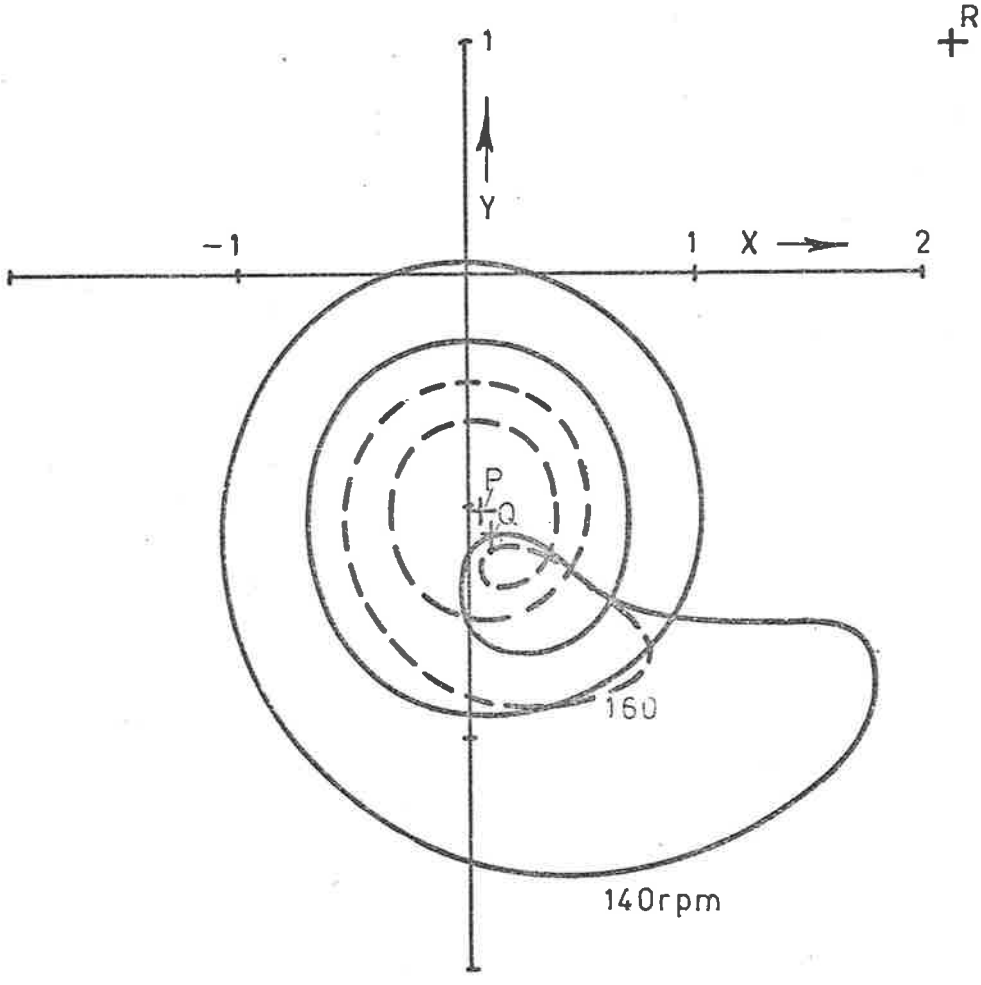

FIGURE 9.3d : THIRD RESONANCE

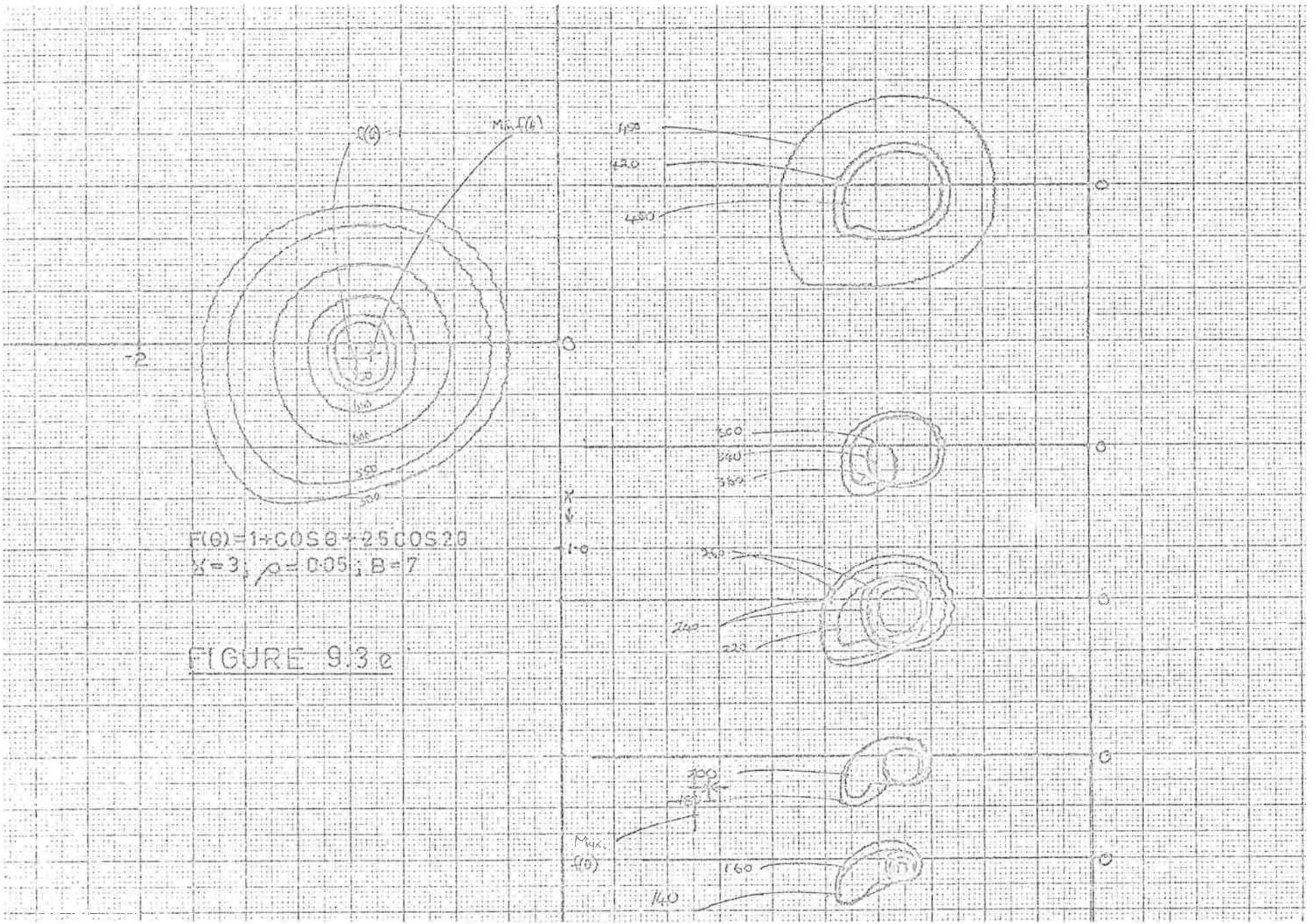
F(θ)=1+COS θ+.25COS 2θ
α=3; ρ=0.05; B=7
FIGURE 9.3e

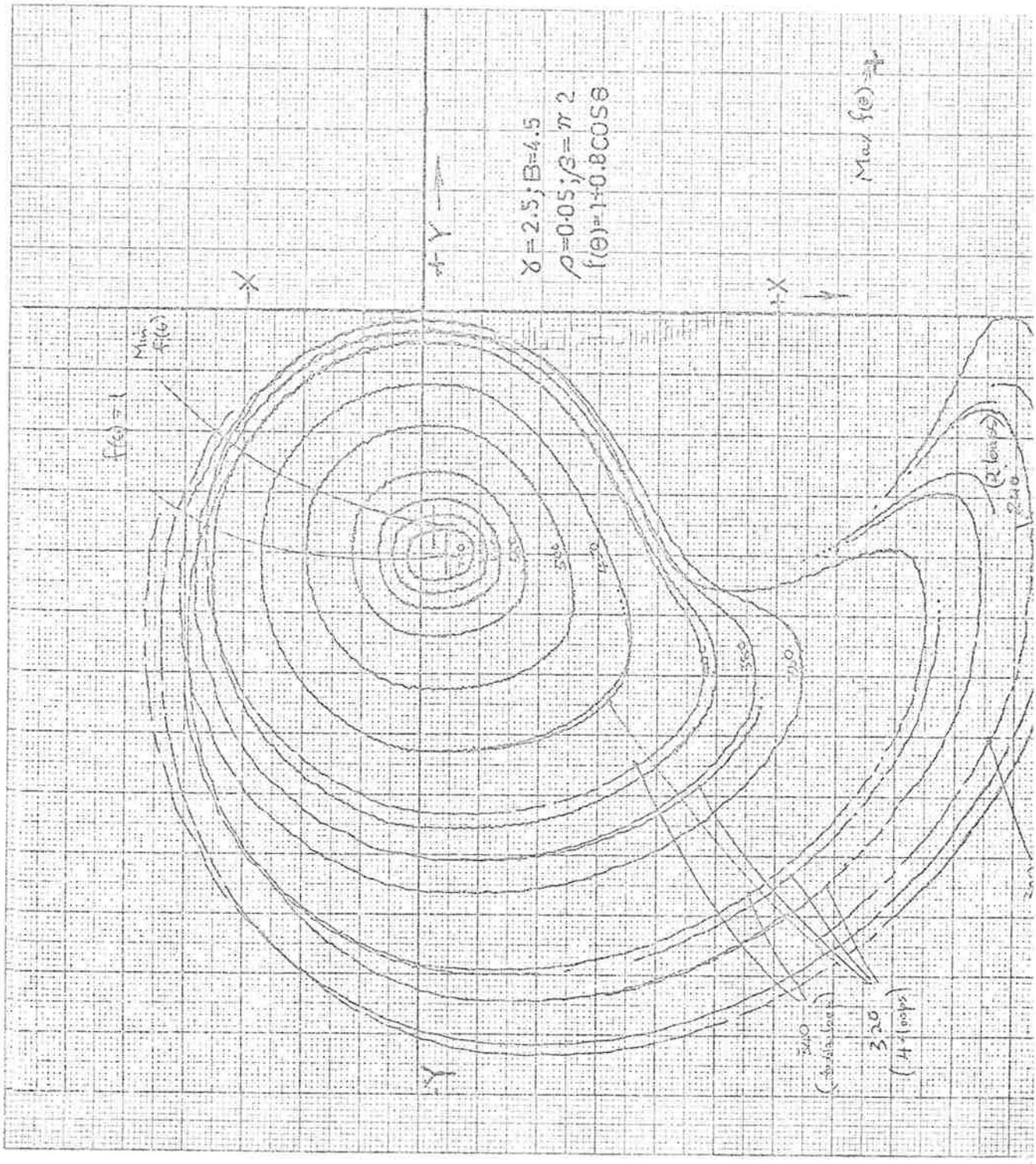

FIGURE 9.4a : PHASE AMPLITUDE LOCI

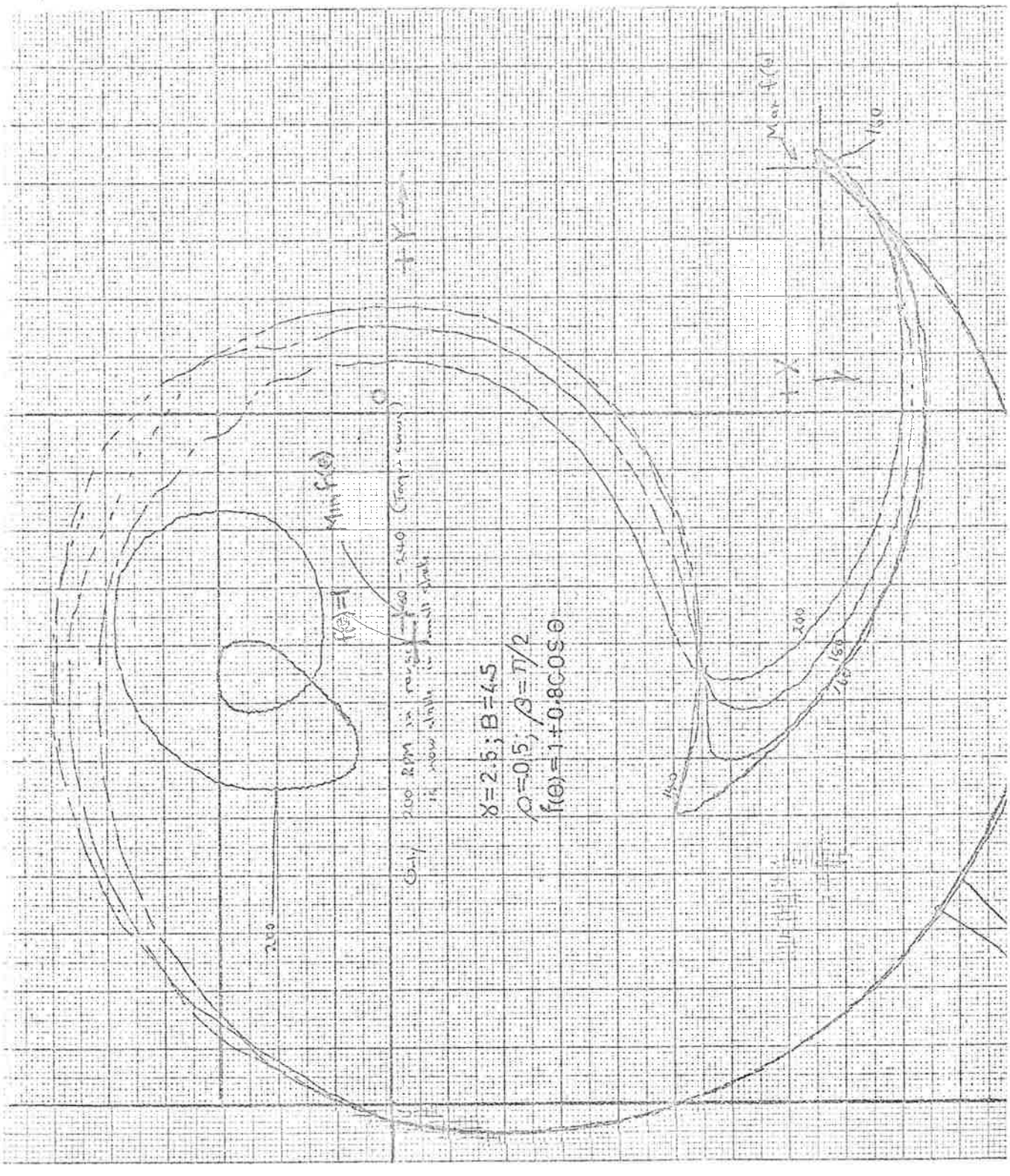

FIGURE 9.4 b: PHASE AMPLITUDE LOCI

approximate circles about point Q. Perfect circles would imply the presence of the fundamental steady state solution, represented by phasor OQ plus a single lower sideband of frequency γ-mpΩ, represented by a phasor rotating clockwise about Q at an angular frequency of mpΩ; so that it makes 'm' complete revolutions about Q for one cycle of $F(\theta)$, i.e. whilst the rotor moves one pole pitch. This situation is sketched in Figure 9.5(b).

Departures from a circular trajectory imply the presence of other side bands but in this particular problem upper side bands play an insignificant part, as will be shown in Chapter 10; so that the shapes of the trajectories shown in Figures 9.3 and 9.4 are determined principally by the magnitude and phase of the lower side bands present. Bearing this in mind, it can be seen by inspection of Figures 9.3 and 9.4, that as the speed decreases from a value in the vicinity of 750 rpm (in this particular case), the first lower side band steadily increases in amplitude and advances in phase until some critical point is reached at which it falls to a relatively small amplitude. For B=8.0 this point is reached at about 340 rpm. Further decrease in speed results in the build up of a trajectory which encircles the point Q twice for one cycle of $F(\theta)$ i.e. the second lower sideband now dominates the solution. This pattern is repeated as the speed is lowered, with successive lower side bands building up in turn. Thus the 'm'th lower sideband apparently goes through a resonance as the trajectory has time to encircle the mean point Q, 'm' times. This behaviour may be seen more clearly in Figure 9.6.

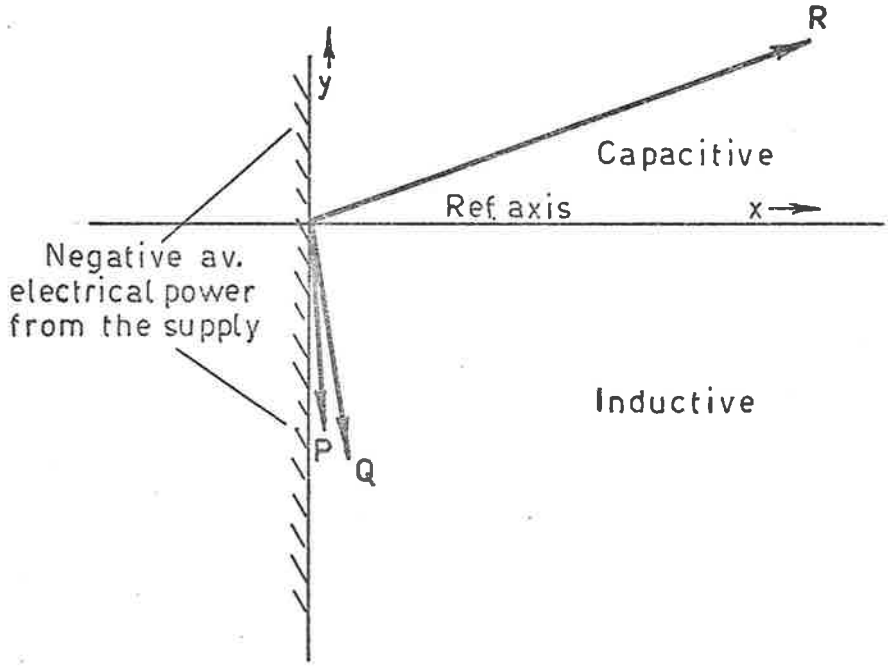

FIGURE 9.5a

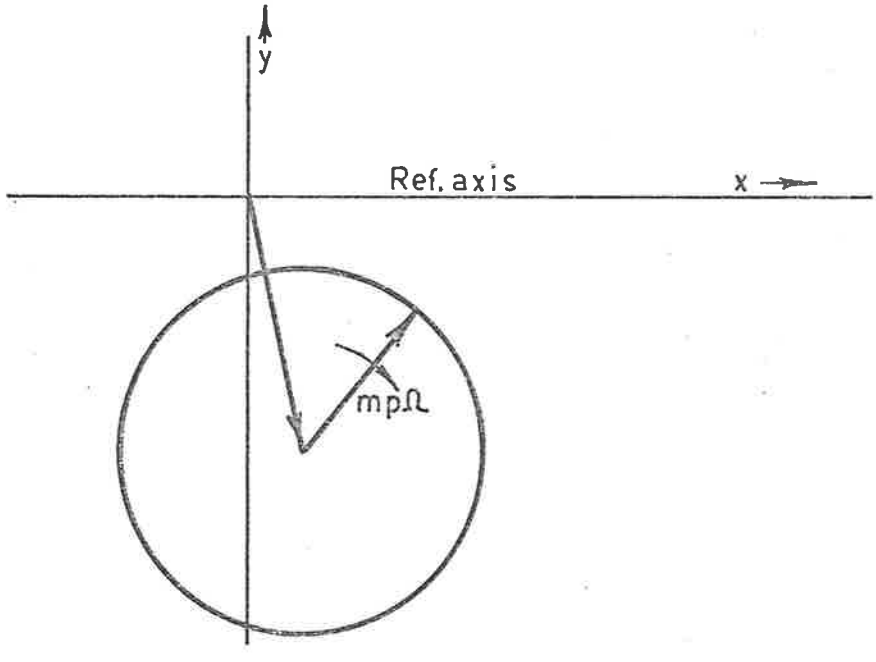

FIGURE 9.5b

The general shape of these trajectories may be understood by reference to the curves in Figure 8.2. At any instant, for a given rotor position there will be a family of integral curves similar to those in Figure 8.2, on one of which the instantaneous value of the solution lies, and along which the solution tends to move towards the instantaneous position of a stable singular point. The latter moves as the rotor position changes and so in turn the trajectory changes. It is clear however that the large circular sweeps of the trajectories in Figures 9.3 and 9.4 correspond to the approach to the low state stable focus in Figure 8.2(b), whereas the 'beak' on the trajectories represents an approach to the high state node or heavily damped focus in the first quadrant. Under certain conditions with large B and low speed the trajectory may actually reach the point R, as in Figure 9.4(b).

Also under certain conditions it was found that more than one stable trajectory could exist. Such a situation is shown in Figure 9.6 for speeds between 300 and 260 rpm. The actual trajectory assumed depended upon the initial conditions but no serious attempt was made to establish the boundaries on the initial conditions leading to a particular state because equations (9.1)→(9.4) represent true system behaviour only approximately.

Using the analytical solution developed in Chapter 10 phase-amplitude trajectories were calculated and the results plotted in Figure 9.7, for conditions identical to those used to produce the results shown in Figure 9.3. Comparison and discussion of the two sets is deferred until section 9.3.

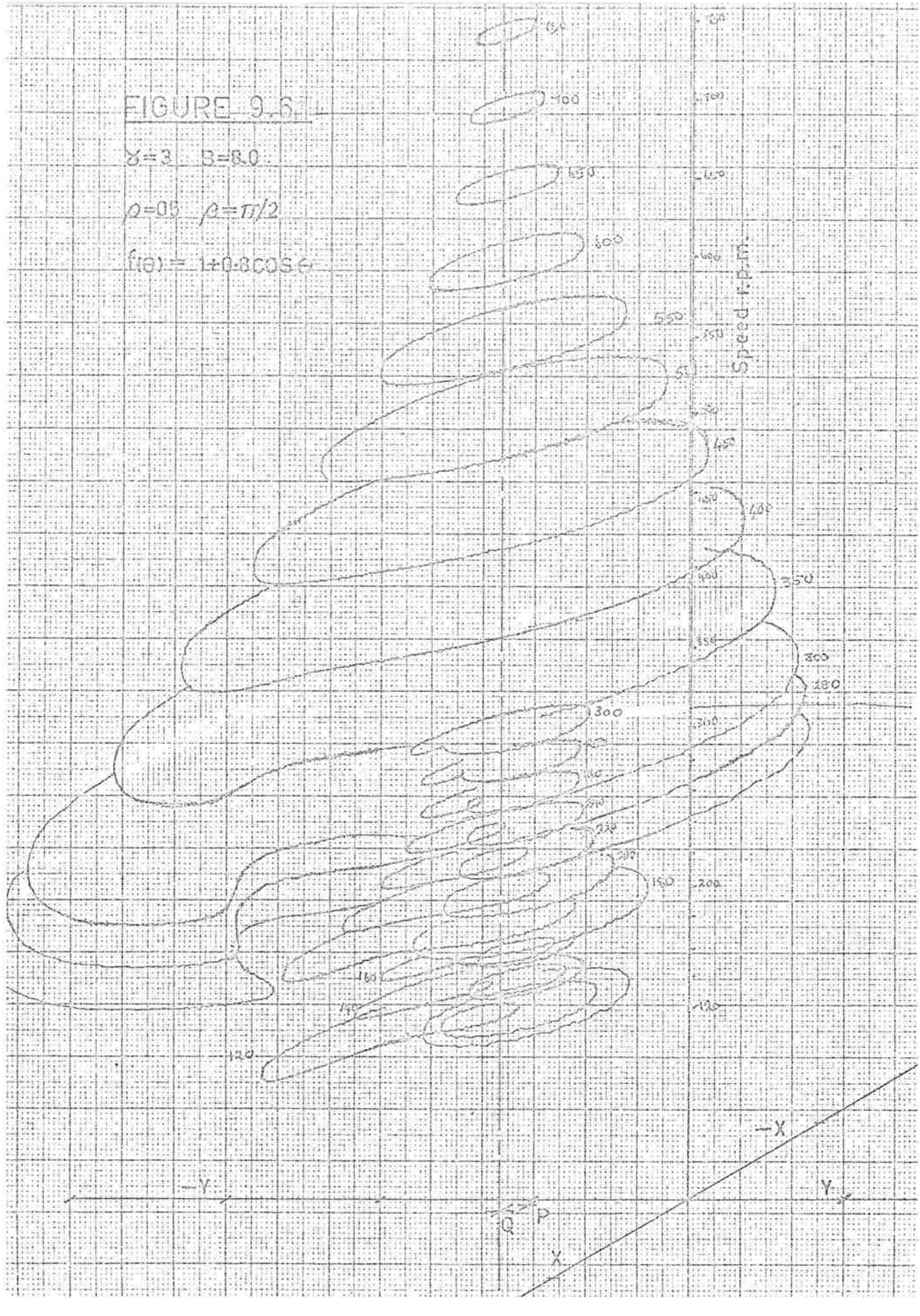
FIGURE 9.6
$\gamma=3$ $B=8.0$
$\rho=0.5$ $\beta=\pi/2$
$f(\theta) = 1+0.8\cos\theta$
Speed in rpm
650
600
550
500
450
400
350
300
250
200
150
100
-Y
Y
-X
X
Q
P

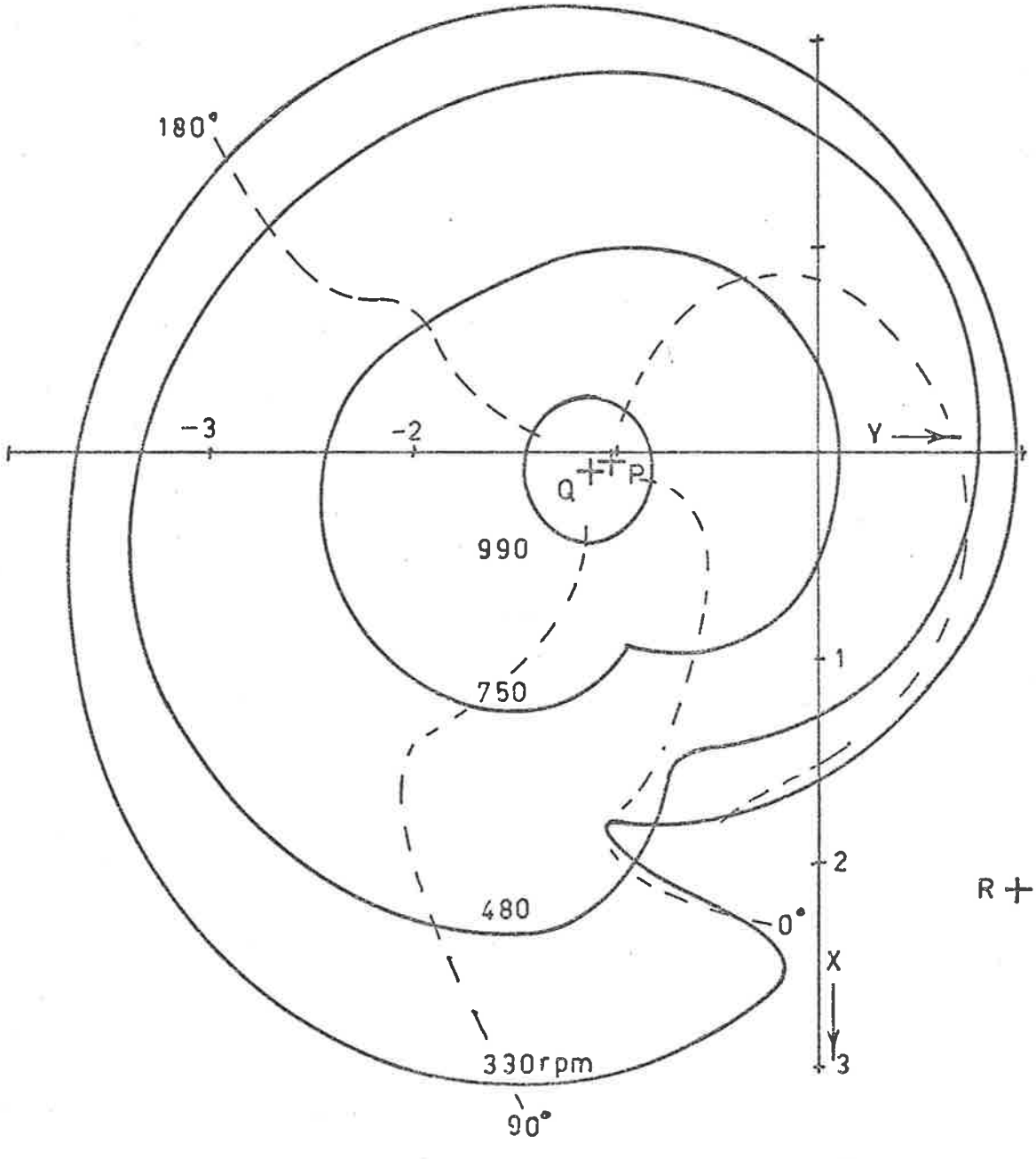

$F(\theta) = 1 + \cos\theta + .25\cos 2\theta$; $\gamma = 3$; $\rho = 0.05$; $B = 8$

FIGURE 9.7a: PHASE AMPLITUDE LOCI FROM ANALYTICAL SOLUTION (c.f. 9.3 b)

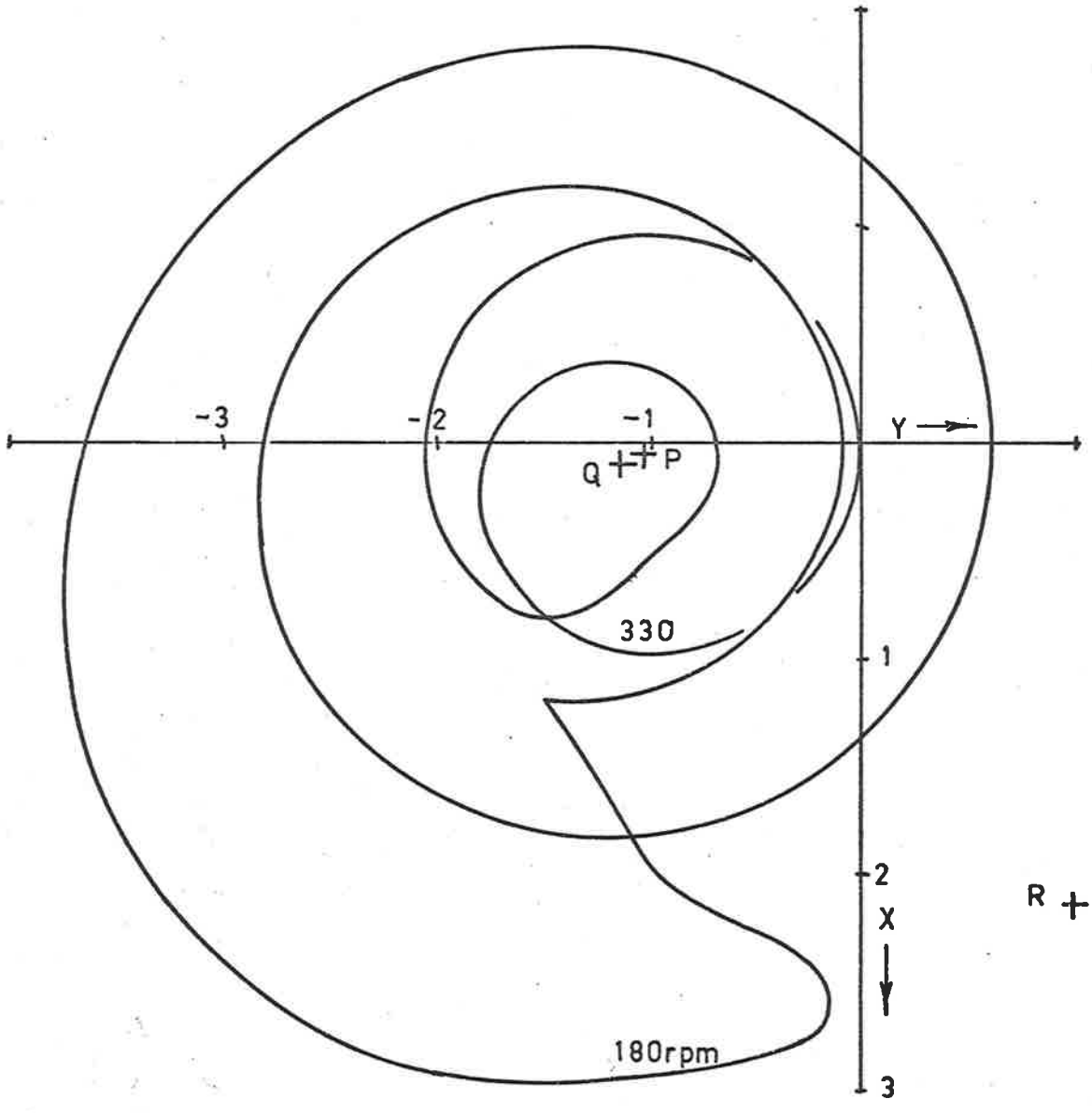

FIGURE 9.7b : SECOND RESONANCE

9.2.2. Results from torque speed plots

By making use of the expression developed in Appendix III(a), for the average torque in terms of the r.m.s. value of a sinusoidal flux waveform, the average torque during one complete revolution of the rotor in terms of the flux envelope will be given approximately by:-

$$T_{ave} = -\frac{1}{2\pi}\int_{o}^{2\pi}\frac{3}{32}\frac{F'(\theta)r^4}{D_o L_o}\,d\theta \qquad .....(9.7)$$

for a cubic approximation to the λ-i curves.

Some representative torque/speed curves, obtained from (9.1),(9.2) and (9.7) by using the analogue computer, are shown in Figures 9.8 → 9.11. The circuit parameters cover the same range as those used to obtain the results presented in 5.12 → 5.15; so that a direct comparision may be made.

9.3 Discussion

Comparision of Figures 5.12 → 5.15 with Figures 9.8 → 9.11 suggests that while equations (9.1) and (9.2) are inadequate, at other than very slow rotor speeds, to provide quantitative information about the true system behaviour, they can give useful qualitative information. The two groups of speed torque curves exhibit the same characteristics, suggestive of a series of skewed resonance curves, which for given circuit parameters, have similar thresholds and operating ranges for B in each system.

Similar conclusions are prompted by comparison of Figures 9.3 and 9.7.

Thus it seems reasonable to conclude that the characteristics of a system represented by equations (9.1)

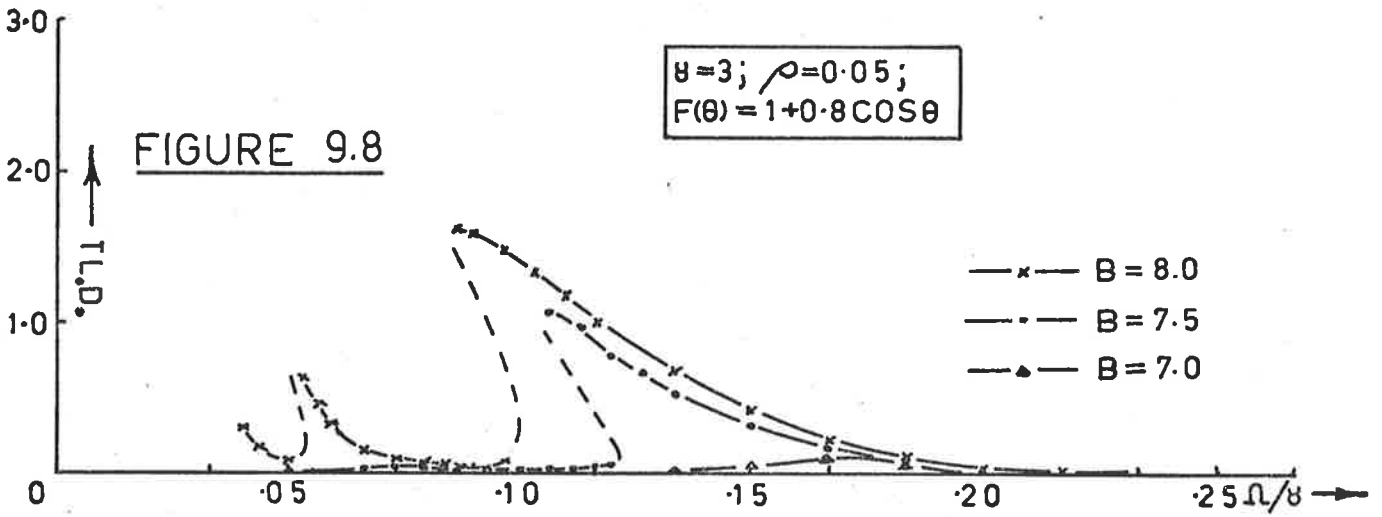

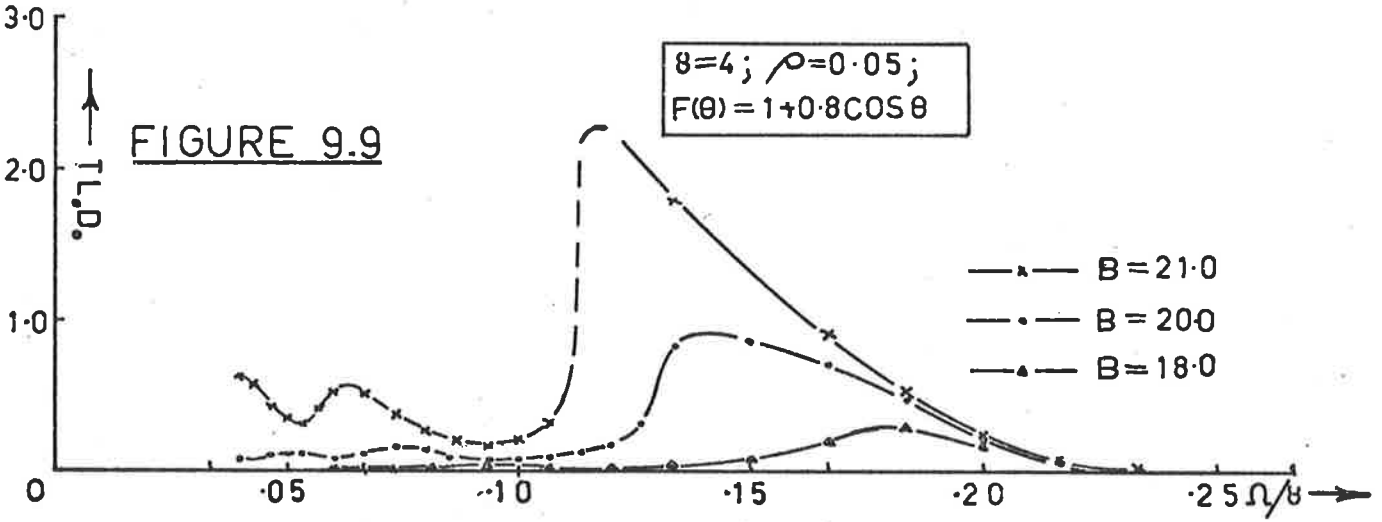

Torque derived from the analogue computer solution for the phase and amplitude.

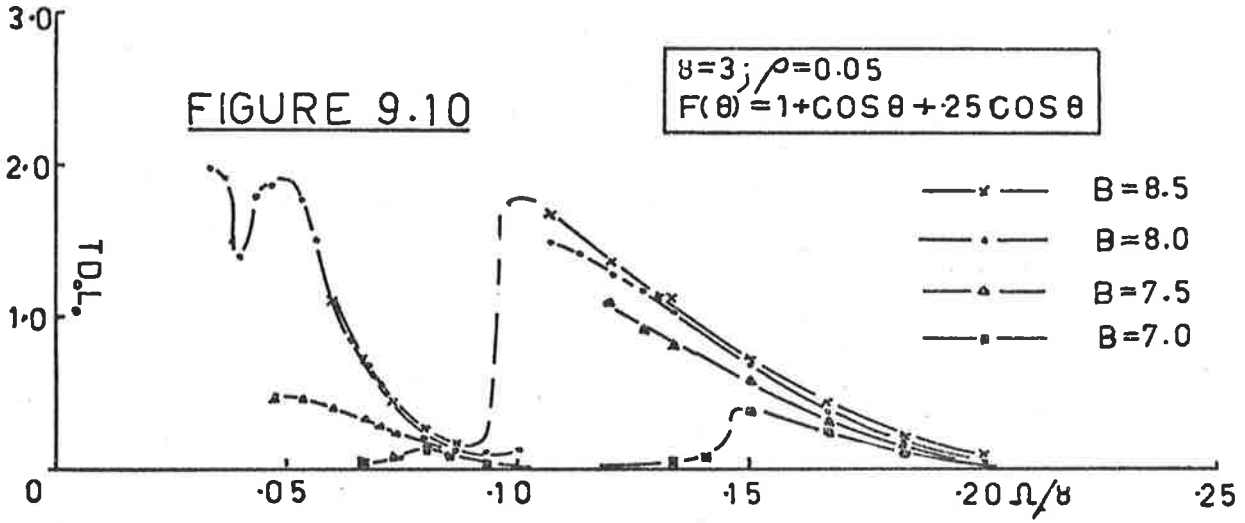

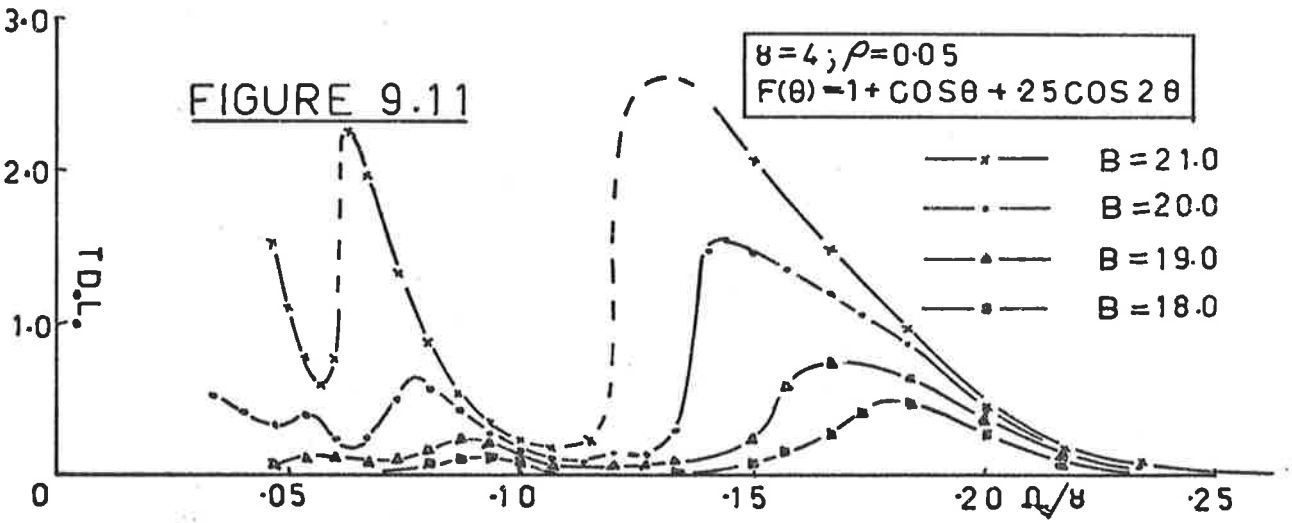

As for figures 9.8 & 9.9

and (9.2) will also be representative of a system described by equation (7.1) when the speed is an independent variable, taken as a constant.

CHAPTER 10

Analytical Solution

Analogue computer and numerical methods, outlined in Chapters 5 and 6 respectively, enable a solution to the system equations to be found for a given set of system parameters and input conditions, but enable few general statements to be made concerning system behaviour, except by exploring the complete input and system parameter space.

The investigation into phase-amplitude behaviour discussed in Chapter 9 enables greater insight to be obtained, but because terms containing second derivatives etc., have been discarded in finding equations 9.1 and 9.2, in order to reduce their complexity, the results are quantitatively useless at practical rotor speeds.

On the other hand an analytical solution to the system equations, giving the dependent variables in terms of the independent variables and the system parameters, can lead to complete understanding of the system behaviour and to the establishment of design criteria.

10.1 Form of the solution

Experience shows that explicit solutions to non linear differential equations rarely exist. Usually, attainment of an adequate approximate solution is facilitated by prior knowledge of the form of the solution.

We are concerned with the solution of equations (4.38) and (4.39) repeated here for convenience:-

$$-B\sin\overline{\gamma\tau+\beta} = 2\rho_2 \ell\ddot{\psi}+(1+4\rho_1\rho_2)\ddot{\psi}+2(\rho_1+\rho_2)\dot{\psi}+\psi$$
$$+(1+2\rho_1\frac{d}{d\tau}+\ell\frac{d^2}{d\tau^2})F(\theta)\psi^q \qquad \ldots\ldots(10.1)$$

$$\frac{T_m}{J\omega_o^2} = \ddot{\theta} + \frac{G}{J\omega_o}\dot{\theta} + \frac{F'(\theta)\psi^{(q+1)}}{(q+1)L_o J\omega_o^2 D_o^{q-1}} \qquad \ldots\ldots(10.2)$$

some of the characteristics of which follow from the results of investigations discussed in previous sections. Thus:-

(i) Equation (10.1) consists of a third order, non-linear differential equation, forced externally at a frequency γ, having periodic coefficients of fundamental frequency $p\Omega$. As such, we may expect, because of the behaviour of linear, non autonomous differential equations having periodic coefficients [38,5], that the solution for the flux linkages will consist of a series of sidebands of frequency $\gamma+np\Omega$ where n is an integer and $-\infty<n<\infty$.

(ii) Because of the non linear nature of the equation, sidebands will be present having frequencies $m\gamma+np\Omega$, where m = 1,2,3 etc.

(iii) The system described by (10.1) has three energy storage elements, one capacitive and two inductive with the two latter partially isolated by the effect of the iron losses. Resonant response will result whenever a particular sideband frequency, $m\gamma+np\Omega$, corresponds to a natural frequency of the system.

(iv) Natural frequencies of the system involving the capacitive element and the non-linear inductive element, under conditions of internal and external forcing will be dependent upon the amplitude of response which in turn will be dependent upon the amplitude of both the external and internal forcing functions.

(v) The relative amplitudes of the various sidebands in the complete solution will be related closely to the nearness or otherwise of their frequency to a natural resonant frequency of the system. It was shown earlier that $\gamma>1$ for a jump to occur and furthermore that the practical range for γ, determined empirically and suggested by Figure 7.5 and the results of Chapter 11, lies in the range $2.5<\gamma<4$. Thus it is unlikely that the frequency of any upper sidebands will approach the main system natural frequency. They may however coincide with the natural frequency determined primarily by the loop comprising the capacitive element, the leakage reactance and the shunt resistance representing the iron losses. This loop is relatively heavily damped, hence the amplitudes of all upper sidebands may be expected to be relatively small, with the consequent possibility of neglecting them in a first approximation.

(vi) With finite mechanical inertia in the machine, the alternate positive and negative electromagnetic torque pulses cause fluctuations in the rotor speed about the mean value determined by the average values of the electromagnetic load and friction torques. Thus the solution to equation (10.2) under steady state conditions, i.e. the load speed Ω, will consist of a constant $\overline{\Omega}$ plus periodic terms of frequency $nk\overline{\Omega}$. Under these conditions, the periodic coefficients of (10.1) become quite complex functions of time, although they may be very simple functions of rotor position.

(vii) Consequently any analytical solution to (10.1) and (10.2) will, in general, incorporate phase and amplitude information concerning all significant frequency components

of both the flux linkages and the instantaneous speed. However if the inertia is sufficiently large that speed fluctuations become very small, solution of (10.1), on the assumption that both γ and Ω are independent variables, involves much less work and may provide an adequate description of the system behaviour.

10.2 Possible methods of Solution

For the machines under discussion both the non-linear and periodic coefficients of the differential equation are large; so that methods of analysis based on assumptions that these are small, will fail.

Furthermore the approach taken in the previous Chapter, which gives results idientical to those obtained using the method of variation of parameters [9], is inadequate except at very low rotor speeds.

Taylor-Cauchy Transforms [18,19] which, although straight forward, lead to solutions in the form of Taylor series expansions in the independent variable and as a result do not contribute greatly to an understanding of the system bheaviour

Harmonic balance or perturbation techniques require a prior knowledge of the form of the expected solution and are often tedious to apply. However for this particular problem, a systematic perturbation technique due to Nicholson [23] provides a satisfactory method of finding a possible solution.

10.3 Systematic solution for ψ

For convenience a very brief outline only of the method [23] is presented below in Section 10.3.1. Further details may be found in Appendix VII.

10.3.1 General outline of the method

We write the non linear equation in the form

$$G(\dddot{\psi},\ddot{\psi},\dot{\psi},\psi) = 0 \qquad \ldots\ldots(10.3)$$

and assume that both the function G and the required solution ψ, may be expressed as a power series in an amplitude parameter μ, as follows:-

$$\psi = \mu g_1(\tau)+\frac{\mu^2}{2!} g_2(\tau) + \ldots \qquad \ldots\ldots(10.4)$$

$$G = G_{\mu=0}+\mu\left(\frac{dg}{d\mu}\right)_{\mu=0}+\frac{\mu^2}{2!}\left(\frac{d^2G}{d\mu^2}\right)_{\mu=0}+ \ldots$$

$$\equiv H_o+\mu H_1+\frac{\mu^2}{2!} H_2+ \ldots \qquad \ldots\ldots(10.5)$$

$$\text{ie} \quad H_i = \left.\frac{d^iG}{d\mu^i}\right|_{\mu=0} \qquad \ldots\ldots(10.6)$$

Here the complete derivative is to be used, not the partial, as implied in Nicholson's paper. Thus for a given funtion G, the various H_i may be expressed as explicit functions of the values, when $\mu=0$, of the partial derivatives of G with respect to $\dddot{\psi},\ddot{\psi},\dot{\psi}$ and ψ, which are all known once G is specified, as well as of the various $g_n(\tau)$ and their time derivatives which are unknown to begin with. The various H_i are conveniently expressed as:-

$$\begin{aligned} H_1 &= L_1(g_1) \\ H_2 &= L_1(g_2)+L_2(g_1,g_1) \\ H_3 &= L_1(g_3)+3L_2(g_1,g_2)+L_3(g_1,g_1,g_1) \\ H_4 &= L_1(g_4)+3L_2(g_2,g_2)+4L_2(g_3,g_1)+6L_3(g_2,g_1,g_1) \\ &\quad +L_4(g_1,g_1,g_1,g_1) \end{aligned} \qquad \ldots\ldots(10.7)$$

etc ...

as shown in reference 23 and repeated in Appendix VII for

convenience.

The original equation (10.3) now becomes

$$\sum_{i=0}^{\infty} \frac{\mu^i}{i!} H_i = 0 \qquad \ldots\ldots(10.8)$$

and because $|H_i|_{i=r}$ contains none of the g_i above g_r, it is often possible to satisfy (10.8) by means of systematic relationships among smaller goups of the H_i, such that the individual equations (10.6) can be solved in turn for a satisfactory sequence of functions g_1, g_2, etc.

Obviously the more quickly that (10.4) and (10.5) converge the better, and ideally, $\mu g_1(\tau)$ should provide a close approximation to the true solution; with the various $\frac{\mu^i}{i!} g_i(\tau)$ providing *ith* order corrections to ψ and the $\frac{\mu^i}{i!} H_i$ causing *ith* order corrections to μ.

If (10.8) is to be solved progressively for improved values of μ, the various H_i should be of similar form. Furthermore, $H_1 = \frac{dg}{d\mu}\big|_{\mu=0}$ is given by the substitution of $g_1(\tau)$ into the linear portion of G (see Appendix VII); so that any terms which appear in $g_1(\tau)$ must appear in H_1.

10.3.2 Application of the method

Consider now, the particular equation for which we require a solution. With core loss and leakage reactance present, it may be written, using one non-linear term only for simplicity, as:-

$$G = B\sin(\gamma\tau+\beta) + 2\rho_2 \ell \dddot{\psi} + (1+4\rho_1\rho_2)\ddot{\psi} + 2(\rho_1+\rho_2)\dot{\psi} + \psi$$

$$+ (1+2\rho_1 \frac{d}{d\tau} + \ell \frac{d^2}{d\tau^2}) F(\theta) \psi^q \qquad \ldots\ldots(10.9)$$

Thus $H_o = G\Big|_{\mu=0} = G\Big|_{\ddot{\psi}=\ddot{\psi}=\dot{\psi}=\psi=0}$ [from (10.4)]

$$= B\sin\overline{\gamma\tau+\beta} \qquad \ldots\ldots(10.10)$$

We find that

$$L_1(g) = 2\rho_2\ell\dddot{g}+(1+4\rho_1\rho_2)\ddot{g}+2(\rho_1+\rho_2)\dot{g}+g \qquad \ldots\ldots(10.11)$$

and furthermore that when the λ-i characteristics are represented by a function having but one non-linear term ψ^q, then only L_1 and L_q exist, with all other $L_m=0$. Hence it is consistent to choose $H_2 = 0$, leading to $L_1(g_2) = L_2(g_1,g_1) = 0$; so that again it is consistent to take $g_2 = 0$, and in turn we find from (10.7) that we may take

$$H_{2n} = g_{2n} = 0 \qquad \ldots\ldots(10.12)$$

At this stage a decision must be taken concerning the form of the remaining H_i. In fact it turns out that the decision follows almost automatically from the way in which the solution develops, after first taking the simplest and most obvious choice for $g_1(\tau)$.

Our interest lies in finding particular periodic solutions rather than initial transients; so in accordance with the discussion in Section 10.1 we may expect such solutions to contain periodic components having frequencies $S_{m,n} = m\gamma+np\Omega$, in which case the simplest choice would be for $g_1(\tau)$ to take the form $\cos\overline{\gamma\tau+\eta}$, and hence the various $H_i = A_i\cos\overline{\gamma\tau+\alpha_i}$. However if a solution is pursued from this beginning it will be found that terms of the form

$$\frac{C_{m,n}\cos\overline{S_{m,n}\tau+\varepsilon_{m,n}}}{\Delta_{m,n}}$$

appear in the various $g_i(\tau)$ other than $g_1(\tau)$.

Here $\Delta_{m,n} = \sqrt{(1-S_{m,n}^2)^2+4\rho^2 S_{m,n}^2}$; so that whenever the rotor speed Ω is such that $S_{m,n} \simeq 1$ these terms lend to diverge, and as a result they can no longer be regarded as *nth* order corrections terms, with the practical result that the series (10.4) does not converge.

Their presence in the higher $g_i(\tau)$ indicates that they should have been incorporated in $g_1(\tau)$ and hence in the H_i, when any tendency to diverge is immediately reflected in the amplitude of μ, determined from (10.8).

The next possibility might be to try

$$\left.\begin{aligned} \mu g_1(\tau) &= \sum_{n=-r}^{+r} a_n \cos(\overline{\gamma+np\Omega)\tau+\eta_n} \\ &\equiv \sum_{n=-r}^{+r} a_n \cos\overline{S_n\tau+\eta_n} \end{aligned}\right\} \qquad \ldots\ldots(10.13)$$

which represents a series of top and bottom side bands based on the fundamental frequency γ; so giving

$$\mu H_1 = \sum_{n=-r}^{r} [(1-(1+4\rho_1\rho_2)S_n^2)a_n \mathrm{Cos}\overline{S_n\tau+\eta_n} - 2\{(\rho_1+\rho_2)S_n-\rho_2 \ell S_n^3\}a_n \mathrm{Sin}\overline{S_n\tau+\eta_n}] \qquad \ldots\ldots(10.14)$$

In equations (10.13) and (10.14) above it has been assumed that the amplitude parameter μ has been absorbed in the various a_n on the right hand side of each. Taking $\mu \equiv 1$ results in simplified algebra throughout with (10.4) and (10.5) becoming power series in the various a_n.

For cubic approximation to the λ-i curves we have $g_2=H_2=0$ and

$$H_3 = L_1(g_3)+L_3(g_1,g_1,g_1) \qquad \ldots\ldots(10.15)$$

which, as shown in Appendix VII, becomes

$$H_3 = L_1(g_3)+6(1+2\rho_1\frac{d}{d\tau}+\ell\frac{d2}{d\tau^2})(F(\theta)g_1^{\,3}) \qquad .....(10.16)$$

The second term on the right hand side of (10.16) may be evaluated in terms of the components of $g_1(\tau)$ and the independent function $F(\theta)$. Then by putting H_3 equal to the sum of all those terms in $L_3(g_1,g_1,g_1)$ which have frequencies of the form $\gamma+np\Omega$, we have that
$-L_1(g_3)$ = Sum of all remaining terms in $L_3(g_1,g_1,g_1)$ whose frequencies are not of the form $\gamma+np\Omega$.

i.e. $L_1(g_3)$+remainder terms = 0 .....(10.17)

Equation (10.17) is a standard linear differential equation which may be solved for g_3 by using conventional transform techniques. Thus an explicit expression may be found for g_3 in terms of the, as yet unknown, a_n and η_n.

Proceeding in this manner, with $H_4 = g_4 = 0$, we find that for a cubic approximation

$$H_5 = L_1(g_5)+10L_3(g_1,g_1,g_3) \qquad .....(10.18)$$

from which H_5 and g_5 may be found in terms of the various a_n and η_n in a manner similar to that in which H_3 and g_3 were found, so enabling the power series (10.4) and (10.5) to be built up systematically.

Returning now to the particular problem in which $g_1(\tau)$ is assumed to be given by (10.13), we see from Appendix VIII that

$$(g_1(\tau))^3 = \sum_{j=-r}^{+r}\sum_{\ell=-r}^{+r}\sum_{m=-r}^{+r} a_j a_\ell a_m [\tfrac{3}{4}\cos(\overline{\gamma+p(j+\ell-m)\Omega)\tau+\eta_j+\eta_\ell-\eta_m}$$

$$+\tfrac{1}{4}\cos(\overline{3\gamma+p(j+\ell+m)\Omega)\tau+\eta_j+\eta_\ell+\eta_m}] \quad .....(10.19)$$

$$\equiv \sum_{n=-3r}^{+3r} [\tfrac{3}{4}A_n\cos(\overline{\gamma+np\Omega)\tau+\alpha_n}$$

$$+\tfrac{1}{4}C_n\cos(\overline{3\gamma+np\Omega)\tau+\xi_n}] \quad .....(10.20)$$

When the rotor geometry is expressed as

$$F(\theta) = \sum_{k=o}^{\mu} d_k\cos\overline{kp\Omega\tau+\delta_k} \quad .....(10.21)$$

where $d_o\cos\delta_o \equiv 1$, we see from Appendix VIII(b) that the n*th* side band terms in $F(\theta)g_1^3$ are given by:-

$$\sum_{k=o}^{\mu}\frac{d_k}{2}[\tfrac{3}{4}A_{n+k}\cos(\overline{\gamma+pn\Omega)\tau+\alpha_{n+k}-\delta_k}$$

$$+\tfrac{3}{4}A_{n-k}\cos(\overline{\gamma+pn\Omega)\tau+\alpha_{n-k}+\delta_k}$$

$$+\tfrac{1}{4}C_{n+k}\cos(\overline{3\gamma+pn\Omega)\tau+\xi_{n+k}-\delta_k}$$

$$+\tfrac{1}{4}C_{n-k}\cos(\overline{3\gamma+pn\Omega)\tau+\xi_{n-k}+\delta_k}] \quad .....(10.22)$$

Thus the n*th* side band terms in H_3 are fixed by the first two terms in (10.22), whilst the third and fourth terms determine the n*th* side band remainder terms in (10.17), from which $g_3(\tau)$ may be found and in turn in similar fashion, the various H_{2i+1} and g_{2i+1}

The power series expansion (10.8), of the original non linear function in terms of the various H_{2i+1}, now consists of a power series expansion in terms of the amplitude and phase of the principal components of the solution.

By invoking the principle of harmonic balance [9] we see that (10.8) must be satisfied by the coefficients of the sine and cosine components of each sideband individually, so that (10.8) may be expressed as a set of 2m simultaneous non linear algebraic equations, where 'm' is equal to the number of terms in $g_1(\tau)$. For example, in the case of a cubic approximation to the λ-i characteristics, we have for the n*th* sideband (from (10.10), (10.14) and (10.22)):-

$$0 = B_n \sin\beta_n + (1-(1+4\rho_1\rho_2)S_n^2)a_n\cos\eta_n$$
$$-2[(\rho_1+\rho_2)S_n - \rho_2 \ell S_n^3]a_n \sin\eta_n$$
$$+\frac{3}{4}\Delta_n \sum_{k=0}^{\mu} \frac{d_k}{2}\left[A_{n+k}\cos\overline{\alpha_{n+k}-\delta_k+\varepsilon_n} + A_{n-k}\cos\overline{\alpha_{n-k}+\delta_k+\varepsilon_n}\right]$$
$$+ \ldots\ldots\ldots \qquad \ldots\ldots (10.23)$$

$$0 = B_n \cos\beta_n - (1-(1+4\rho_1\rho_2)S_n^2)a_n\sin\eta_n$$
$$-2[(\rho_1+\rho_2)S_n - \rho_2 \ell S_n^3]a_n \cos\eta_n$$
$$-\frac{3}{4}\Delta_n \sum_{k=o}^{\mu} \frac{d_k}{2}\left[A_{n+k}\sin\overline{\alpha_{n+k}-\delta_k+\varepsilon_n} + A_{n-k}\sin\overline{\alpha_{n-k}+\delta_k+\varepsilon_n}\right]$$
$$+ \ldots\ldots\ldots \qquad \ldots\ldots (10.24)$$

where all $B_n = 0]_{n\neq o}$, $\tan\varepsilon_n = 2\rho_1 S_n/(1-\ell S_n^2)$

and $\Delta_n = \sqrt{(1-\ell S_n^2)^2 + 4\rho_1^2 S_n^2}$

Simultaneous solution of these equations gives values for the various a_n and η_n which may then be substituted into the various $g_i(\tau)$ to give a solution ψ with an accuracy increasing with the number of terms in (10.4) and (10.5) provided that these series converge.

In general, for this particular problem, sidebands based on all odd integral multiples of γ ultimately appear in the various $g_i(\tau)$. The greater the degree of non linearity, the earlier they occur in the solution and these terms tend to diverge whenever the rotor speed is such that $k\gamma+np\Omega\simeq\pm1$, i.e. whenever

$$\frac{\Omega}{\gamma} = \frac{-k\pm1/\gamma}{np} \qquad \ldots\ldots(10.25)$$

However, as may be seen from Appendix VIII or (10.19) and (10.20), the amplitude of such terms depends upon the amplitude of the terms from which they have been produced by the cross modulation effect of the non linearity. If these latter terms are in themselves inherently small in the vicinity of the speed at which (10.25) is satisfied, little error may result. However if the divergent terms are large, there is no alternative but to include them in the original generating solution $g_1(\tau)$; so that they appear in the various H_i and consequently influence the calculated magnitudes of all the a_n and η_n.

Under such conditions the analysis may rapidly get out of hand because the numerical solution of a large set of equations such as (10.23) and (10.24), becomes very time consuming. In this respect it is of interest to note that this particular solution calls for the evaluation of terms such as $F(\theta)(g_1(\tau))^q$. Where q is the degree of non linearity in the λ-i characteristics. Thus if there are 2r+1 terms in $g_1(\tau)$ and $\mu+1$ in $F(\theta)$, the number of operations involved in evaluating $F(\theta)(g_1(\tau))^q$ must be proportional to $(\mu+1)\ (2r+1)^{q+1}$; so that a change from a cubic to a quintic when r = 5 means an $(11^2=121)$ fold increase in the number of operations.

Because of the complexity of the solution and the cost of computing time involved calculations have been restricted to the evaluation of H_3 and $g_1(\tau)$ only; so that the various a_n and η_n are determined from the solution of

$$0 = H_o + H_1 + \frac{H_3}{3!} \qquad .....(10.26)$$

after which we can calculate

$$\psi = g_1(\tau) \qquad .....(10.27)$$

It should be noted that the results so obtained are identical with those which would be obtained by means of a straight forward harmonic balance carried out by the direct substitution into the differential equation, of an assumed solution taking the form of (10.13). Then by collecting and equating coefficients of like terms a set of simultaneous non linear algebraic equations, identical to the first three terms of (10.23) and (10.24) may be obtained.

10.4 Current associated with a particular sideband

For the simplified situation when one non linear term only is present, the instantaneous current is given by:-

$$\left.\begin{aligned} i &= \frac{\lambda}{L_o}\ (1+f(\theta)\lambda^{2N}) \\ &= \frac{\psi}{D_o^{\frac{1}{2N}} L_o}\ (1+F(\theta)\psi^{2N}) \end{aligned}\right\} \qquad .....(10.28)$$

Appendix IX shows that (10.22), (10.23) and (10.24) may be used to obtain:-

$$D_o^{\frac{1}{N}} L_o^{\,2} i_n^{\,2} = \frac{a_n^{\,2}}{\Delta_n^{\,2}} \left[(1+4\rho_1\rho_2-\ell)^2 S_n^{\,4} + 4\rho_2^{\,2} S_n^{\,2} (1-\ell S_n^{\,2})^2\right] \quad ..(10.29)$$

which demonstrates that the *nth* sideband current component is determined solely by the *nth* sideband flux linkage component a_n.

Expressing (10.29) in the usual circuit parameters leads to

$$I_n^2 = \frac{\Lambda_n^2 \omega_n^2}{R_c^2 (R^2 + (\omega_n L_\ell - \frac{1}{\omega_n C})^2)} [(R_c+R)^2 + (L_\ell \omega_n - \frac{1}{\omega_n C})^2] \quad ..(10.30)$$

where I_n and Λ_n represent rms values and ω_n is the particular sideband angular frequency. Referring now to the equivalent circuit, reproduced in Figure 10.1 for convenience, it is a simple matter to show that if the variable inductance is replaced by a voltage source given by $\sum_{n=-r}^{+r} \Lambda_n \omega_n$, the resultant current components delivered by this source will have magnitudes as given by (10.30). In other words the time varying inductance with its associated flux linkages may be regarded as a voltage source

$v = \frac{d\psi}{d\tau}$ where ψ comprises the various terms in $g_1(\tau)$. Because the remainder of the circuit is linear, the currents which result from each component of v may be treated independently. The effective or rms value of any particular voltage component follows from the flux linkage component. Thus:-

$$\psi_n = a_n \cos\overline{S_n \tau + \eta_n}$$

$$\text{i.e. } \lambda_n = \frac{a_n}{D_o^{\frac{1}{2}N}} \cos\overline{\omega_n t + \eta_n} \quad .....(10.31)$$

$$\text{giving } \frac{d\lambda_n}{dt} = -\frac{a_n}{D_o^{\frac{1}{2}N}} \omega_n \sin\omega_n t + \eta_n \quad .....(10.32)$$

$$\text{i.e. } v_n = -\lambda_n(\text{peak}) \omega_n \sin\overline{\omega_n t + \eta_n} \quad .....(10.33)$$

$$\text{and } V_n = \Lambda_n \omega_n \quad .....(10.34)$$

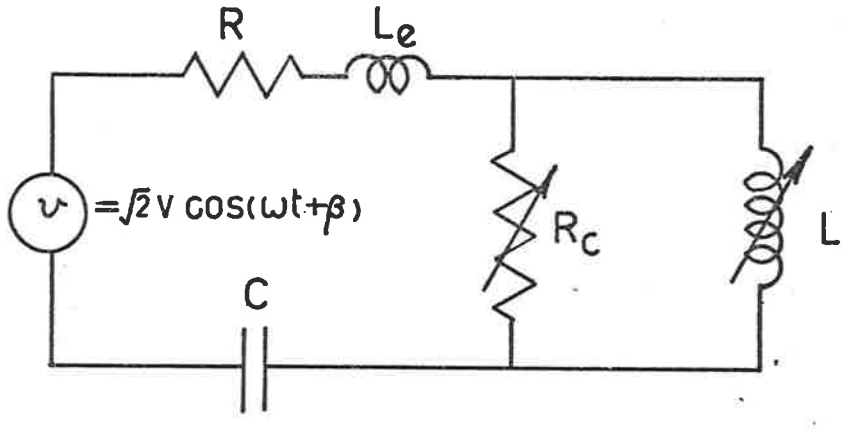

(a)

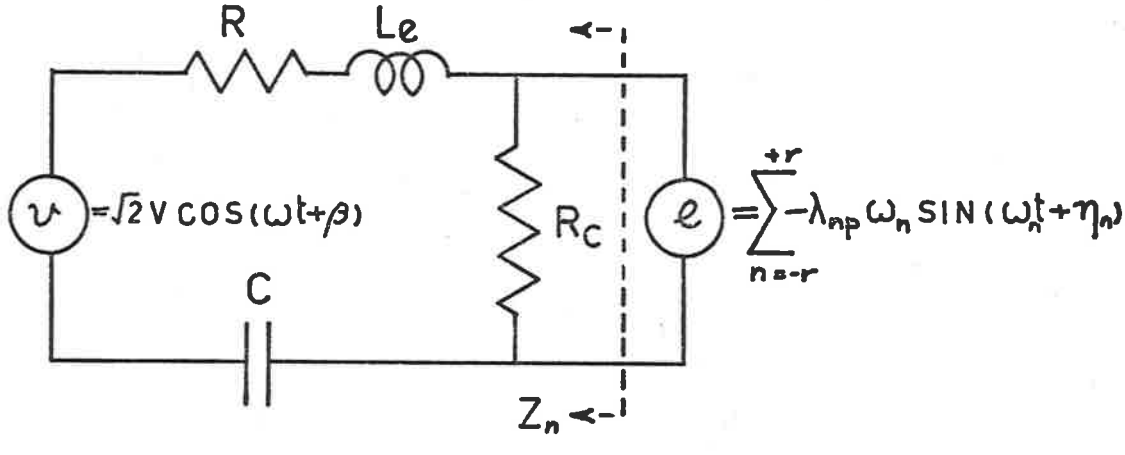

(b)

FIGURE 10.1 : EQUIVALENT CIRCUITS

Such a relationship between the flux linkages and the current at a particular frequency is not only intuitively satisfactory but also leads on to a simple expression for the average torque produced by each particular component. However the major problem of finding the various flux linkage components still remains tedious.

10.5 Approximate natural frequency of the system

For a particular value of applied voltage, the results obtained from the phase amplitude plots, as well as from analytical solutions, show that, while the amplitude of the fundamental component of ψ at frequency γ remains sensibly constant over the practical range of rotor speed, each of the various lower sideband components of ψ exhibits, in turn, a resonant response. Furthermore, the dominant, but certainly not the only components of the solution ψ, comprise the fundamental and the sideband in question.

It is possible to determine approximately the rotor speed at which a particular sideband resonates by considering only the above two components of the solution.
Thus:-

$$\psi = a_o \cos\overline{\gamma\tau+\eta_o} + a_n \cos\overline{S_n\tau+\eta_n} \qquad .....(10.35)$$

which leads to the following relationships, as shown in Appendix X

$$a_n^2 = \frac{\frac{9}{64} d_n^2 (a_o^2+3a_n^2)^2 \Delta_n^2 - \frac{4a_n^4(a_o^2+2a_n^2)4\rho^2 S_n^6}{(a_o^2+a_n^2)^2\Delta_n^2}}{(\gamma_N^2-S_n^2)^2+4\rho^2 S_n^2 \gamma_N^4} \qquad ..(10.36)$$

$$\sin(\eta_n-\eta_o-\delta_n) = \frac{8a_n.2\rho S_n^{\,3}}{3d_n a_o(a_o^{\,2}+a_n^{\,2})\Delta_n^{\,2}} \qquad .....(10.37)$$

$$\cos(\eta_n-\eta_o-\delta_n) = \frac{8a_n(\gamma_N^{\,2}-S_n^{\,2}+4\rho^2 S_n^{\,2}\gamma_N^{\,2})}{3d_n a_o(a_o^{\,2}+3a_n^{\,2})\Delta_n^{\,2}} \qquad .....(10.38)$$

$$T_{ave} = \frac{-n\frac{3}{8}a_o a_n d_n(a_o^{\,2}+a_n^{\,2})}{D_o L_o}\,\overline{\mathrm{Sin}\eta_n-\delta_n} \qquad .....(10.39)$$

$$= \frac{-na_n^{\,2}.2\rho S_n^{\,3}}{L_o D_o \Delta_n^{\,2}}$$

where $\Delta_n^{\,2} = 1+4\rho^2 S_n^{\,2}$

and $\gamma_N^{\,2} = 1 + \frac{3}{4}(2a_o^{\,2}+a_n^{\,2})$ .....(10.40)

Equations (10.36)-(10.40) are true only to the extent that (10.35) is true. Nevertheless, they provide a clear indication of some of the essential properties of the solution. Some of the most important may be summarised thus:-

(i) Although (10.36) is an involved implicit function for a_n it has, except for the second term in the numerator, the essential form of the response of a second order system of natural frequency γ_N, subjected to a forcing function of frequency S_n and amplitude d_n.

(ii) When, in addition to the condition that (10.35) is true, we have the values of B or d_n or both small enough that a_n is small, then the natural frequency approaches

$$\gamma_{N_o}{}^2 = 1+\frac{3}{2}a_o{}^2 = 2\gamma_n{}^2-1 \qquad .....(10.41)$$

where γ_n is given by (7.12).

(iii) To the extent that a_o is independent of S_n, d_n and a_n, it may be considered to depend upon B alone, assuming a value corresponding to the mean rotor position and given by (7.13).

(iv) Thus we might expect the n*th* lower side band to approach resonance when the rotor speed is such that

$$S_n = \gamma+np\Omega\simeq\sqrt{1+\frac{3}{2}a_o{}^2} = \sqrt{2\gamma_n{}^2-1} \qquad .....(10.42)$$

where n will be a negative integer for the lower side bands.

(v) As the magnitude of a_n increases, so does γ_N (see (10.40), which means that the response will be skewed in the direction of increasing S_n, i.e. in the direction of decreasing speed.

(vi) Equation (10.39), giving the average torque shows that the torque/speed curve will be skewed even more than the a_n curve because of the factor $S_n{}^3$ in the numerator.

(vii) Finally, equation (10.42) shows that increasing B (which from 7.12) and Figure 7.7 means increasing γ_n and hence increasing γ_N), results in shifting the spine of the response curves of a_n and T_{ave} in the direction of increasing

S_n.

Some of the above observations may be tested by replotting the various torque-speed curves, obtained from the analogue computer, against a normalized speed scale given by $S_n/(2\gamma_n^2-1)^{\frac{1}{2}}$. See Figures 10.2 to 10.7. In each case γ_n is taken from Figure 7.7 for the appropriate value of B, after the equations have been normalized with respect to the mean value of $f(\theta)$.

To the extent that (10.35) and (10.40) are correct we can expect the amplitude a_n, to peak when the speed is such that

$$S_n^2 \simeq 2\gamma_n^2 - 1 + \frac{3}{4} a_n^2 \equiv \gamma_{N_o}^2 + \frac{3}{4} a_n^2$$

i.e. $$\frac{S_n^2}{(2\gamma_n^2-1)} \equiv \frac{S_n^2}{\gamma_{N_o}^2} = 1 + \frac{3}{4}\frac{a_n^2}{\gamma_{N_o}^2} \qquad \ldots\ldots(10.42a)$$

At which stage

$$D_o L_o T_{ave} = \frac{2\rho n S_n^3 a_n^2}{\Delta_n^2} \qquad \text{(Using (10.42a))}$$

$$= \frac{2\rho n S_n^3}{\Delta_n^2}\left(\frac{S_n^2}{\gamma_{N_o}^2} - 1\right)\frac{4}{3}\gamma_{N_o}^2$$

$$= n\frac{8}{3}\rho\gamma_{N_o}^5 \frac{S_n^3}{\gamma_{N_o}^3}\left(\frac{S_n^2}{\gamma_{N_o}^2} - 1\right) \qquad \ldots\ldots(10.42b)$$

Torque-speed curves of idealised machines as obtained by analogue computer (figures 5.11-5.16), plotted to scales of S_n/γ_N.

$S_n = \gamma - 2n\Omega$ $\qquad$ $\gamma_N = (2\gamma_n^2 - 1)$

FIGURE 10.2

FIGURE 10.3

As for figures 10.2 & 10.3

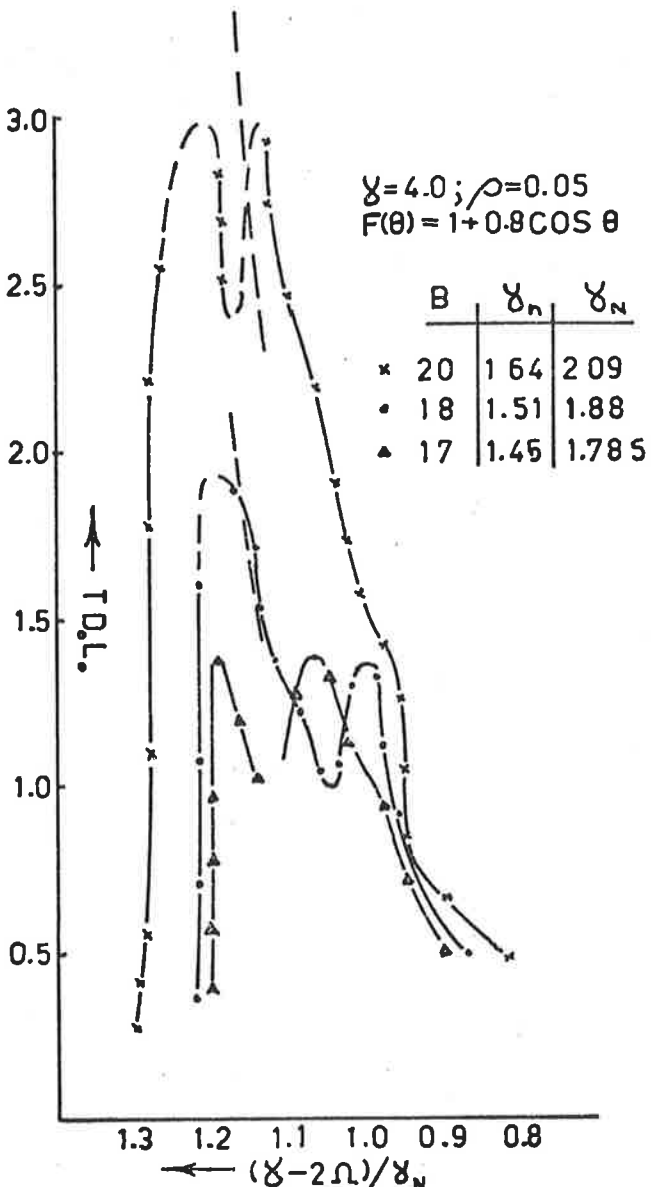

FIGURE 10.4

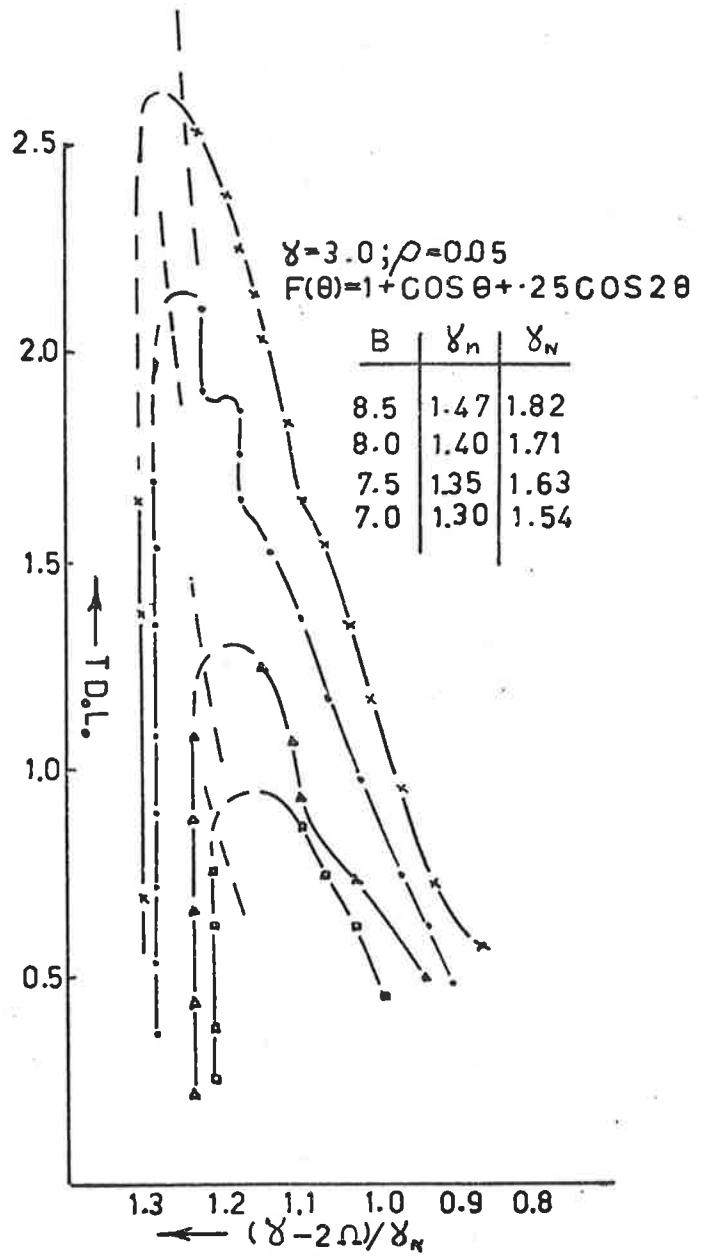

FIGURE 10.5

As for figures 10.2 & 10.3

Figure 10.6 shows second resonance plotted against S_2/γ_N

" 10.7 " first " " " S_1/γ_N

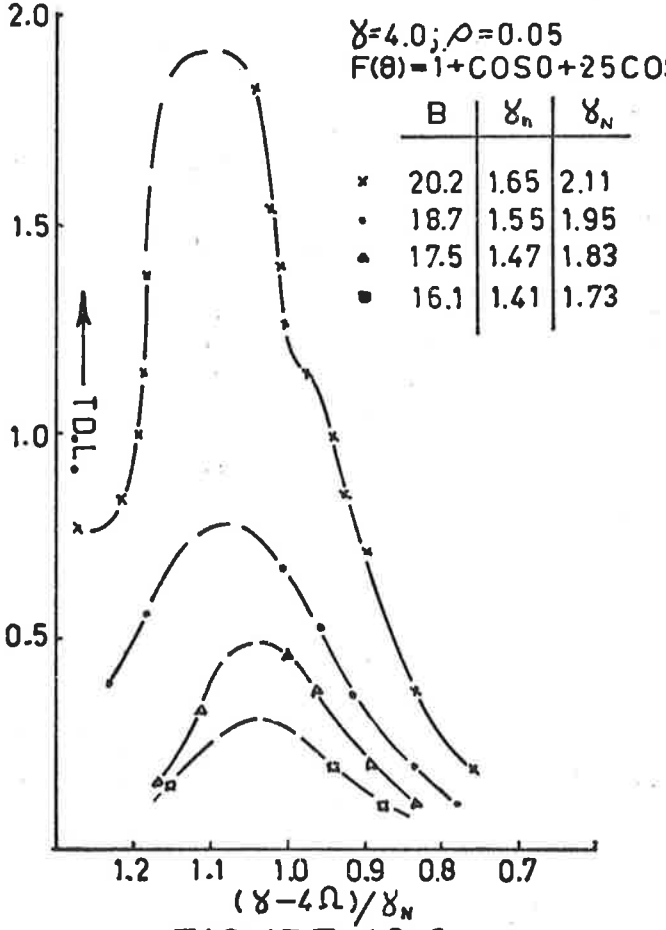

FIGURE 10.6

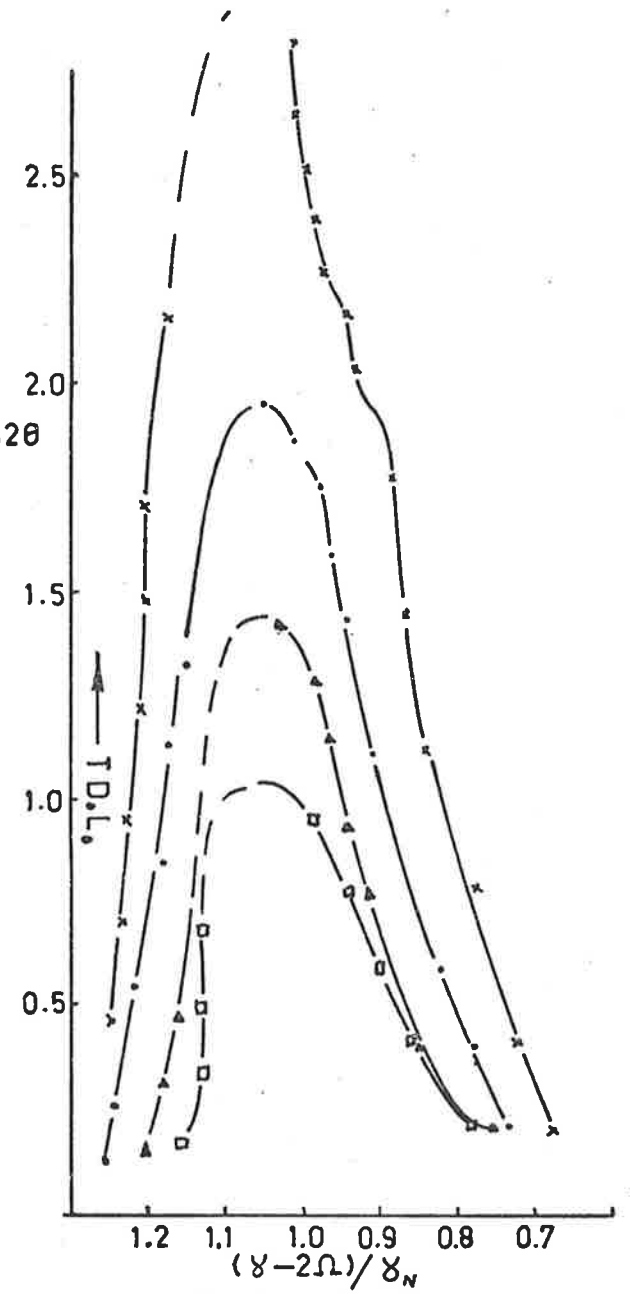

FIGURE 10.7

To the extent that (iii) above is true, γ_{N_o} must be a function of B alone. Thus equation (10.42b) provides a relationship between the peak torque and the normalized speed S_n/γ_{N_o} at which it is likely to occur for a given value of B.

This relationship is shown by the dashed lines in the vicinity of the individual torque peaks in Figures 10.2 to 10.5. It seems reasonable to conclude from a study of these Figures that (iv) - (vii) above are broadly true.

10.6 Analytical expressions for average torque

There are two possible approaches to the evaluation of torque. The first, although tedious, enables both asynchronous and synchronous torque to be evaluated. The second approach follows from the discussion in Section 11, and while it takes no account of synchronous torques, it is extremely economical on computing time and provides a simple but elegant description of the machine behaviour.

10.6.1 Calculation of average torque from the instantaneous torque

When the λ-i characteristics are represented by one non linear term only, it follows from (4.29) and (4.37) that

$$T_{inst} = -\frac{F'(\theta)\psi^{q+1}}{D_o\left(\frac{q-1}{2}\right)L_o(q+1)} \qquad \ldots\ldots(10.43)$$

and when

$$\psi = \sum_{n=-r}^{+r} a_n \cos\overline{S_n\tau+\eta_n}$$

Appendix VIII shows that ψ^{q+1} comprises a series of terms whose frequencies are given by the sums and differences of integral multiples of the supply frequency γ and the rotor speed Ω, and that the coefficient of a term of a particular frequency is readily obtained from Chebychev Polynomials.

In general ψ^{q+1} may be expressed as

$$\psi^{q+1} = \sum_{m=o}^{\frac{(q+1)}{2}} \sum_{n=-(q+1)r}^{(q+1)r} C_{2m,n} \overline{\text{Cos}(2m\gamma+np\Omega)\tau+\varepsilon_{2m,n}} \quad \ldots\ldots(10.44)$$

Also

$$F'(\theta) = -\sum_{k=1}^{\mu} kpd_k \overline{\sin kp\Omega\tau+\delta_k} \quad \ldots\ldots(10.45)$$

Using these expressions one may evaluate

$$T_{average} = \frac{1}{2\Pi} \int_o^{2\pi} T_{inst.} d\theta$$

$$= \frac{1}{2\pi} \int_o^{2\pi} -\frac{F'(\theta)\psi^{q+1}}{L_o(q+1)D_o^{\frac{2}{q-1}}} d\theta \quad \ldots\ldots(10.46)$$

or more accurately, because in general, γ and Ω are incommensurate

$$T_{ave} = \frac{1}{\tau} \int_o^{\tau\to\infty} T_{inst} d\tau \quad \ldots\ldots(10.47)$$

Only those terms which have identical frequencies in both (10.44) and (10.45) can make any contribution to the integrals in (10.46) or (10.47)

10.6.1.1 Asynchronous torque

Those terms in (10.44) for which m=0, contribute to the average torque whenever n in (10.44) equals k in (10.45). Whether or not such a contribution occurs is independent of rotor speed Ω, and dependent only on the presence of a harmonic in ψ^{q+1} of the same order as one of the harmonics of the rotor geometry.

Such torque contributions may be called asynchronous because their presence, but not their amplitude, is independent of rotor speed. Thus as far as asynchronous torque production is concerned the terms of interest in ψ^{q+1} are

$$Q_{(q+1)} \sum_{n_1=-r}^{+r} \ldots\ldots \sum_{n_{q+1}=-r}^{+r} a_{n_1} \ldots a_{n_{q+1}} \cos[p\{(n_1+\ldots n_{\frac{q+1}{2}}) - (n_{\frac{q+3}{2}}+\ldots n_{q+1})\}\Omega\tau + (n_1+\ldots n_{\frac{q+1}{2}}) - (n_{\frac{q+3}{2}}+\ldots n_{q+1})] \quad \ldots\ldots(10.48)$$

(where $Q_{(q+1)}$ is defined in Appendix VIIIa). This may be expressed more simply as

$$\sum_{n=1}^{(q+1)r} C_n \cos \overline{np\Omega\tau+\varepsilon_n} \quad \ldots\ldots(10.49)$$

Hence the average value of the asynchronous torque becomes

$$T_{ave} = \sum_{k=1}^{\mu} \frac{kpd_k C_k}{2L_o(q+1)D_o \frac{2}{q-1}} \operatorname{Sin}(\delta_k - \varepsilon_k) \quad \ldots\ldots(10.50)$$

10.6.1.2 Synchronous torque

At certain rotor speeds the possibility arises that $2m\gamma+np\Omega$ from (10.44) equals $kp\Omega$ from (10.45)

i.e. $2m\gamma+np\Omega = kp\Omega$ $\quad \ldots\ldots(10.51)$

where m, n and k are integers having the ranges specified in (10.44) and (10.45). At such rotor speeds a contribution to the torque will result from the interaction of these particular terms in (10.44) and (10.45) respectively. The particular terms involved may be expressed by a series similar to (10.48) taken over q+1 summations, except that in this case the angular frequency will be given by:-

$$2m\gamma+p\{(n_1+\ldots\frac{n_{q+2m+1}}{2}) - (\frac{n_{q+2m+3}}{2})+\ldots n_{q+1})\}\Omega \qquad \ldots\ldots(10.52)$$

and the phase by:-

$$(\eta n_1 \ldots \eta n_{\frac{q+2m+1}{2}}) - (\eta n_{\frac{q+2m+3}{2}} + \ldots \eta n_{q+1}) \qquad \ldots\ldots(10.53)$$

so that synchronous torques occur whenever the value of (10.52) = kpΩ. i.e. whenever

$$\frac{P}{2}\frac{\Omega}{\gamma} = \frac{m}{k+(n_{\frac{q+2m+3}{2}} + \ldots n_{q+1}) - (n_1+\ldots n_{\frac{q+2m+1}{2}})} \qquad \ldots\ldots(10.54)$$

As the various n_i are simply running integers which have the range $-r<n_i<r$, and as both k and m are integers, (10.54) shows that synchronous torques occur whenever the per unit speed $\frac{P}{2}\frac{\Omega}{\gamma}$ is equal to an integral fraction.

Those values of the n_i which combine to give a particular integral fraction, then determine the various side band amplitudes a_{n_i}, the product of which, in turn, determines the maximum value which the synchronous torque may take.

For example when q=3, m may take the values 1 or 2. When m=1, synchronous torque contributions at a rotor speed such that $\frac{P}{2}\frac{\Omega}{\gamma} = \frac{1}{2}$ will result from side band combinations which make

$$k+n_4 - (n_1+n_2+n_3) = 2$$

One such combination would be

$k=1$, $n_4=1$, and $n_1=n_2=n_3=0$; so that the torque contribution would be proportional to the value of $a_1 a_o^3$ when $\frac{P}{2}\frac{\Omega}{\gamma} = \frac{1}{2}$.

Shifting the rotor in time by $\Delta\tau$ may be accomplished mathematically by shifting the phase angle δ_k of each term in $F(\theta)$ by $k\Delta\theta = kp\Omega\Delta\tau$. It is a simple matter to show that if this occurs, then the *nth* side band is also shifted in phase by $n\Delta\theta$. Thus, delaying the rotor by $\Delta\theta$ delays all upper sidebands (for which n is positive) and advances all lower side bands; so that if the various n_i in (10.52) sum to j, then the total phase delay in the *jth* side band based on $2m\gamma$, as given by (10.53), will be $j\Delta\theta$.

Using the notation of (10.44), the *jth* side band term may be written as

$$C_{2m,j}\cos(\overline{2m\gamma+jp\Omega)\tau+\varepsilon_{2m,j}}$$

which, after the rotor has been delayed $\Delta\theta$ radians, becomes

$$C_{2m,j}\cos(\overline{2m\gamma+jp\Omega)\tau+\varepsilon_{2m,j}-j\Delta\theta} \qquad .....(10.55)$$

This term interacts with the delayed rotor harmonic

$$kpd_k \sin\overline{kp\Omega\tau+\delta_k-k\Delta\theta} \qquad .....(10.56)$$

to produce a synchronous torque given by

$$\frac{kp.d_k C_{2m,j}}{2L_o(q+1)D_o\left(\frac{2}{q-1}\right)} \sin \overline{\delta_k - \varepsilon_{2m,j} - (k-j)\Delta\theta} \qquad .....(10.57)$$

Because $2m\gamma+jp\Omega = kp\Omega$ and $\Delta\theta = p\Omega\Delta\tau$ we find

$(k-j)\Delta\theta = 2m\gamma\Delta\tau = \frac{2m\gamma\Delta\theta}{p\Omega}$. Thus the synchronous torque component is proportional to

$$kpd_k C_{2m,j} Sin(\delta_k - \varepsilon_{2m,j} - \frac{2m\gamma}{p\Omega}\Delta\theta) \qquad .....(10.58)$$

indicating that it behaves as a $2m\gamma/p\Omega$ pole machine as far as this component is concerned. Such torques will be significant only if at the particular value of Ω/γ in question, the amplitudes of all of the side bands which combine to produce $C_{2m,j}$ are themselves significant.

10.6.1.3 Asynchronous torque from the Manley-Rowe relationships

It is shown in Chapter 11 that the mechancial torque produced by a particular side band component of the flux waveform may be determined from the following relationship

$$T_n = -\frac{npP_{sn}}{\omega_o S_n} \qquad .....(10.59)$$

where P_{sn} is the power dissipated in the stator circuit resistance due to circulating currents of actual angular frequency $\omega_n = \omega_o S_n$; $S_n = \gamma+np\Omega$; ω_o is the small signal natural frequency and n is the order of the side band.

For the case of a simple equivalent circuit in which core loss is either neglected or taken into account by means of extra series resistance, we have:-

$$P_{sn} = I_n^2 R \qquad \ldots\ldots(10.60)$$

so that

$$T_n = -\frac{npI_n^2 R}{\omega_n} \qquad \ldots\ldots(10.61)$$

From equation (10.30) we have

$$I_n^2 = \frac{\Lambda_n^2 \omega_n^2}{R^2 + (\omega_n L_\ell - \frac{1}{\omega_n c})^2} \qquad \ldots\ldots(10.62)$$

so giving

$$\left.\begin{aligned} T_n &= -\frac{np\Lambda_n^2 \omega_n R}{R^2 + (\omega_n L_\ell - \frac{1}{\omega_n c})^2} \\ &= -\frac{npV_n^2 R}{\omega_n [R^2 + (\omega_n L_\ell - \frac{1}{\omega_n c})^2]} \end{aligned}\right\} \qquad \ldots\ldots(10.63)$$

or in normalised parameters

$$T_n = -\frac{np\rho_1 S_n^3 a_n^2}{(L_o + L_\ell)[(1-\ell S_n^2)^2 + 4\rho_1^2 S_n^2] D_o^{\frac{2}{q-1}}} \qquad \ldots\ldots(10.64)$$

so that the total asynchronous torque in the machine must be

$$T = \sum_{n=-r}^{+r} -\frac{np\rho_1 S_n^3 a_n^2}{(L_o + L_\ell)[(1-\ell S_n^2)^2 + 4\rho_1 S_n^2] D_o^{\frac{2}{q-1}}} \qquad \ldots\ldots(10.65)$$

A study of (10.64) or (10.65) shows that:-

(i) the sign of the torque is dependent only on the sign of n and of S_n (= $\gamma+np\Omega$). The latter is always positive for positive n, i.e. for upper side bands. Thus upper side bands always produce negative torque at all rotor speeds.

(ii) For lower sidebands, for which n is negative, the sign of the torque must be the same as the sign of S_n. The latter changes sign when $\gamma+np\Omega=0$, i.e. when $\Omega = -\frac{\gamma}{np}$. At lower speeds than this S_n is positive so leading to positive torque whilst for $\Omega > -\frac{\gamma}{np}$ negative torque results.

(iii) The magnitude of the torque produced by a particular side band is proportional to the square of the amplitude of that side band multiplied by the factor

$$\frac{S_n^{\,3}}{(1-\ell S_n^{\,2})^2+4\rho^2 S_n^{\,2}}$$

The latter is shown plotted in Figure 10.8 where two curves appear, one for $\ell=0$ and one for $\ell=0.046$ representing the value for the prototype machine. The very significant difference between these two curves apparently belies the statement made earlier that, in the absence of core loss, leakage reactance may be incorporated with the air gap inductance. If the latter course is taken, $f(\theta)$ and the value of a_n so obtained will be modified accordingly and correct results will still ensue.

(iv) Further discussion concerning torque production in such machines occurs in Chapter 11. At this stage it may be stated that the behaviour of one ferro-resonant machine is qualitatively similar to that of a number of single phase

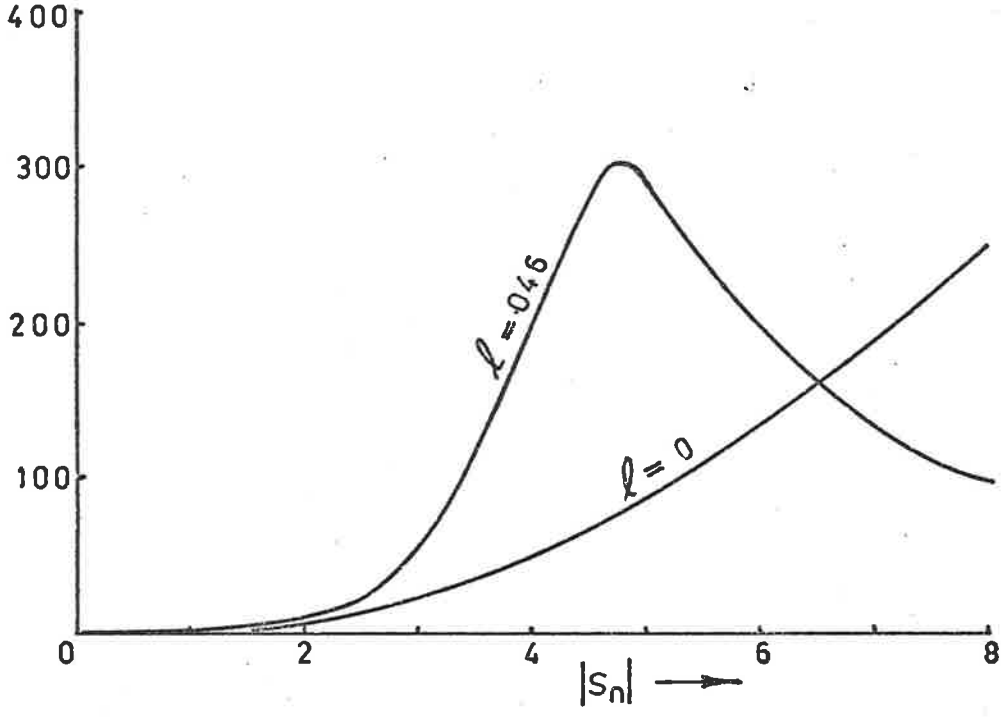

$\dfrac{|S_n^3|}{(1-\ell S_n^2)^2 + 4\rho^2 S_n^2}$ versus $|S_n|$ for $\rho = .063$; $\ell = .046$

Peak when $S_n = 4.83$; i.e. when $\Omega/\gamma = -\dfrac{1.20}{n}$ or $\dfrac{0.20}{n}$

FIGURE 10.8

induction motors, having pole pair numbers p, 2p, 3p... respectively, all connected to one shaft. The rotor is subjected to rotating mmf's of frequencies $\omega_1 - kp\omega_r$ and $-\omega_1 - kp\omega_r$. The latter produces negative torque at all positive rotor speeds while the former produces positive torque for $\omega_r < \omega_1/kp$ and negative torque in the induction generator region when $\omega_r > \omega_1/kp$.

When core loss is present, the torque produced by a particular sideband is proportional to the total power dissipated at that frequency in the resistance of (R, L_ℓ and C) in parallel with R_c. Under these conditions it is shown in Appendix XI that the torque becomes:-

$$T = \sum_{n=-r}^{+r} - \frac{npa_n^2 S_n}{L_o D_o \frac{2}{q-1}} \left[\rho_2 + \rho_1 (1-\ell) \frac{S_n^2}{\Delta_n^2}\right] \qquad .....(10.66)$$

where Δ_n is defined after (10.24)

10.7 Results from Analysis

Numerical solutions to the set of simultaneous, non linear algebraic equations (10.23) and (10.24) were sought using a minimisation programme [28]. The above sets of equations must be expressed in the form

$$F_k(a_1, a_2, \ldots a_n, \eta_1, \eta_2, \ldots \eta_n) = 0 \qquad .....(10.67)$$

after which the programme seeks numerical values for the various a_n and η_n which make

$$\sum_{k=1}^{2n} F_k^2 \leqslant \varepsilon \qquad .....(10.68)$$

A value of $\varepsilon=10^{-6}$ was used in obtaining the results published in this report, which means that absolute accuracy decreases as 'n' increases, with the smaller values of a_n and η_n being the least reliable. This approach was necessary in order to keep the cost of computing time within reasonable bounds.

Estimated initial values for all a_n and η_n, are systematically modified by the programme until (10.68) is satisfied or one of a number of designated terminating situations is reached; so resulting in an error signal. It proved convenient to calculate the various a_n, η_n and average asynchronous torque at a particular value of rotor speed, then once (10.68) had been satisfied the final values of these variables were printed out and also used as initial values for the next solution at an incremented value of rotor speed. Proceeding in this way a torque speed curve could be found.

In general, for a set of non linear equations such as (10.23) and (10.24), there will be more than one set of values for the a_n and η_n which will constitude a solution, although it is unlikely that all of such possible sets of values for the a_n and η_n would represent stable solutions.

A check on the relevance and accuracy of the approximate analytical results presented in this section may be obtained by comparing results given by analogue computer and numerical solution of the system equations with answers from (10.23), (10.24) and (10.65).

10.7.1 Ideal machines

Typical results are shown in Figure 10.9, in which the full line represents analytical results obtained from the solution of (10.23) and (10.24) followed by the use of (10.65). A total of five upper and three lower sidebands were used in the calculation, the amplitudes and phase of which appear in Figure 10.10 as a function of rotor speed. Also shown in Figure 10.9 are the results obtained from analogue solution of the system equations. These are a reproduction of those in Figure 5.13 for B =20. In addition a number of isolated points are marked to indicate results obtained by the numerical solution of the system equations as discussed in Chapter 6.

It has been suggested in previous sections that, because of the practical limitations on a number of the system parameters, the upper side bands play an almost insignificant part in the solution. This is illustrated by the dashed lines in Figure 10.10a, which indicate the results obtained when a solution is sought in terms of five lower and one upper side band in addition to the fundamental. It can be seen that there is little significant difference in the final result, compared to that obtained when three upper side bands are incorporated.

On the other hand, if a solution is sought in terms of three upper and three lower side bands the results displayed in Figures 10.11 and 10.12 are obtained.
Comparison of Figures 10.9 and 10.11 suggests that five lower side bands lead to results closer to the analogue solution than do three. It is reasonable to suppose that the more lower side bands incorporated in the solution the

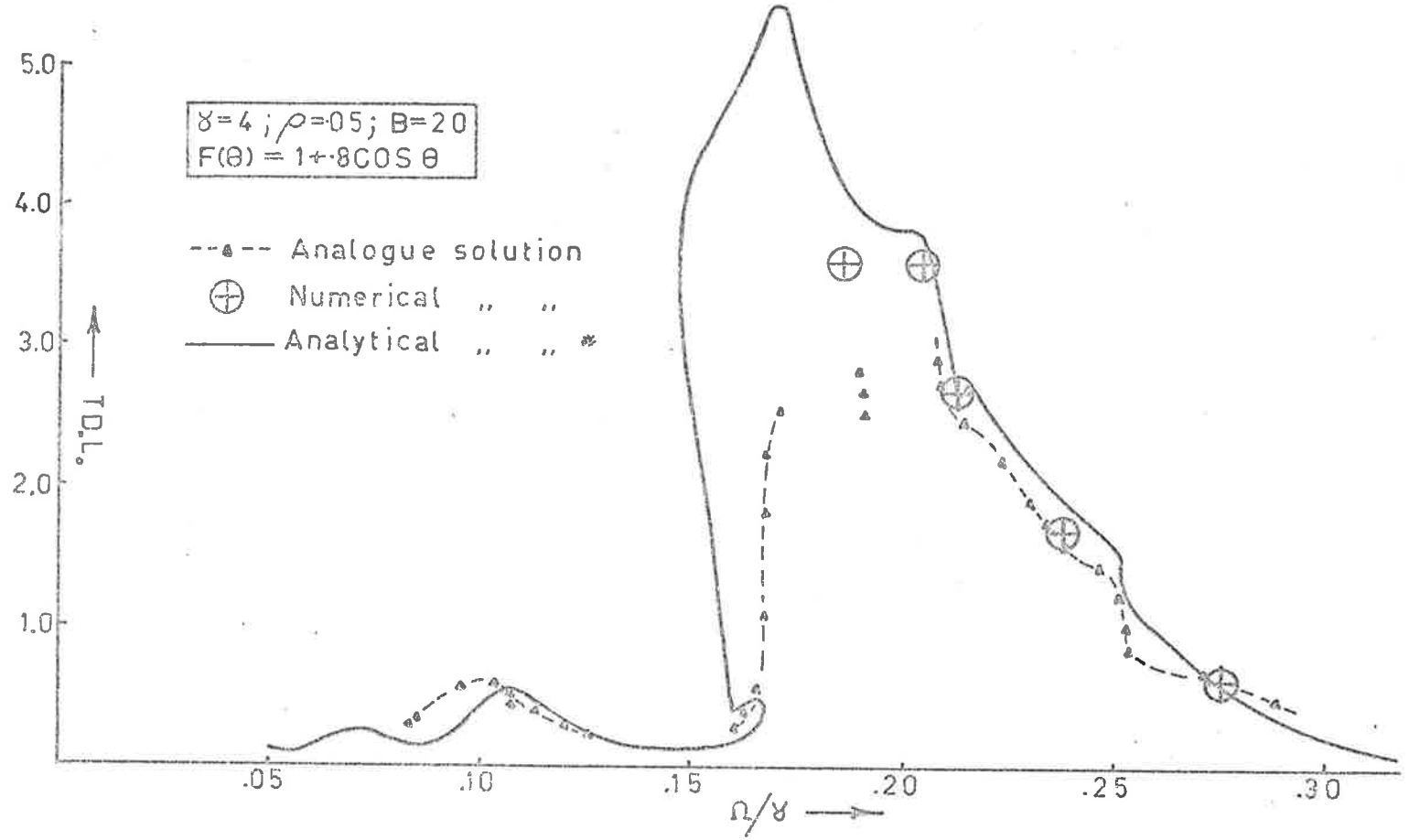

*Analytical solution for five lower, three upper sidebands and fundamental with speed as an independent variable.

FIGURE 10.9 : COMPARISON OF THREE METHODS OF SOLUTION

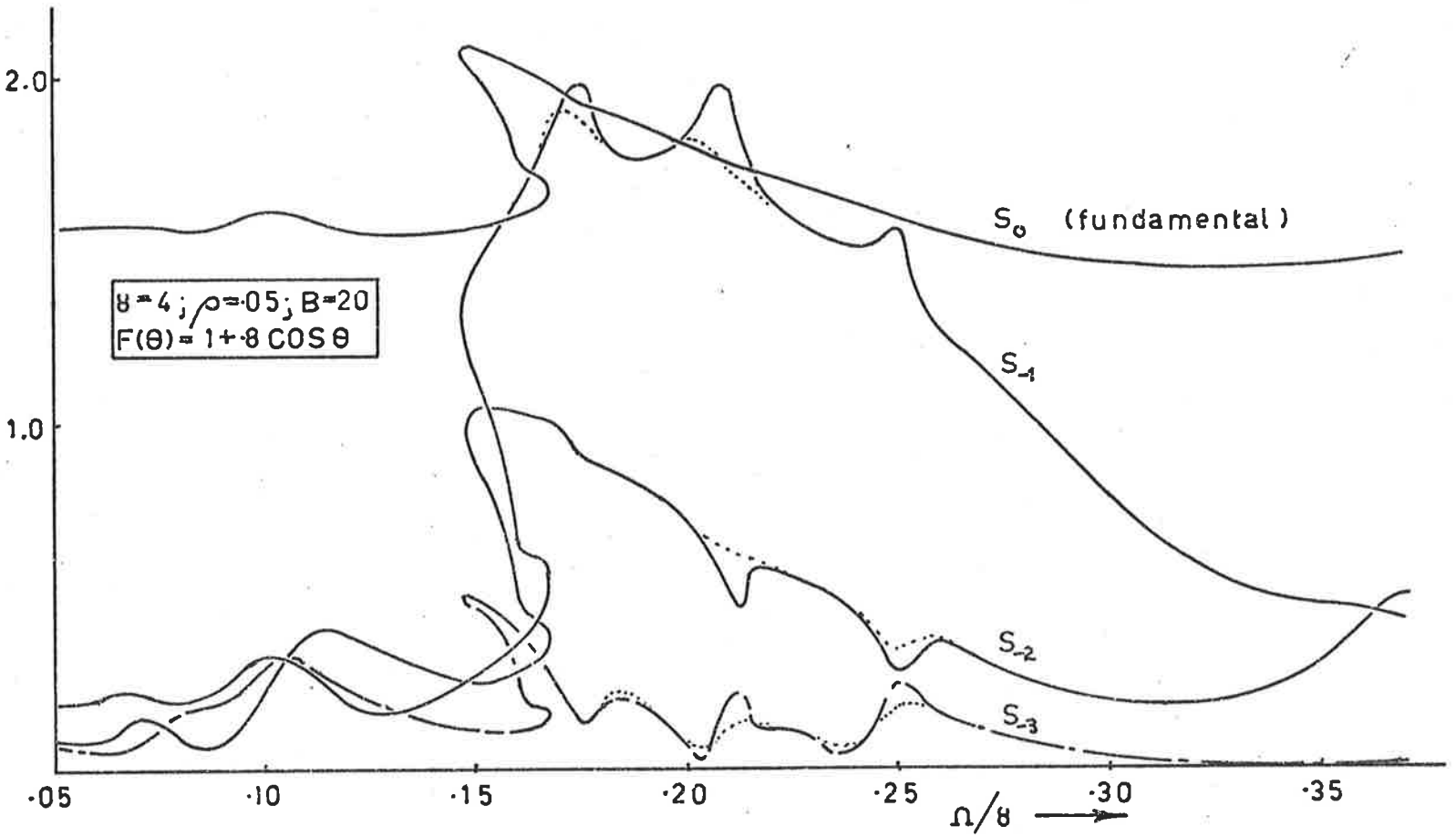

FIGURE 10.10 a : AMPLITUDES OF THE SIDEBANDS

(continued next page)

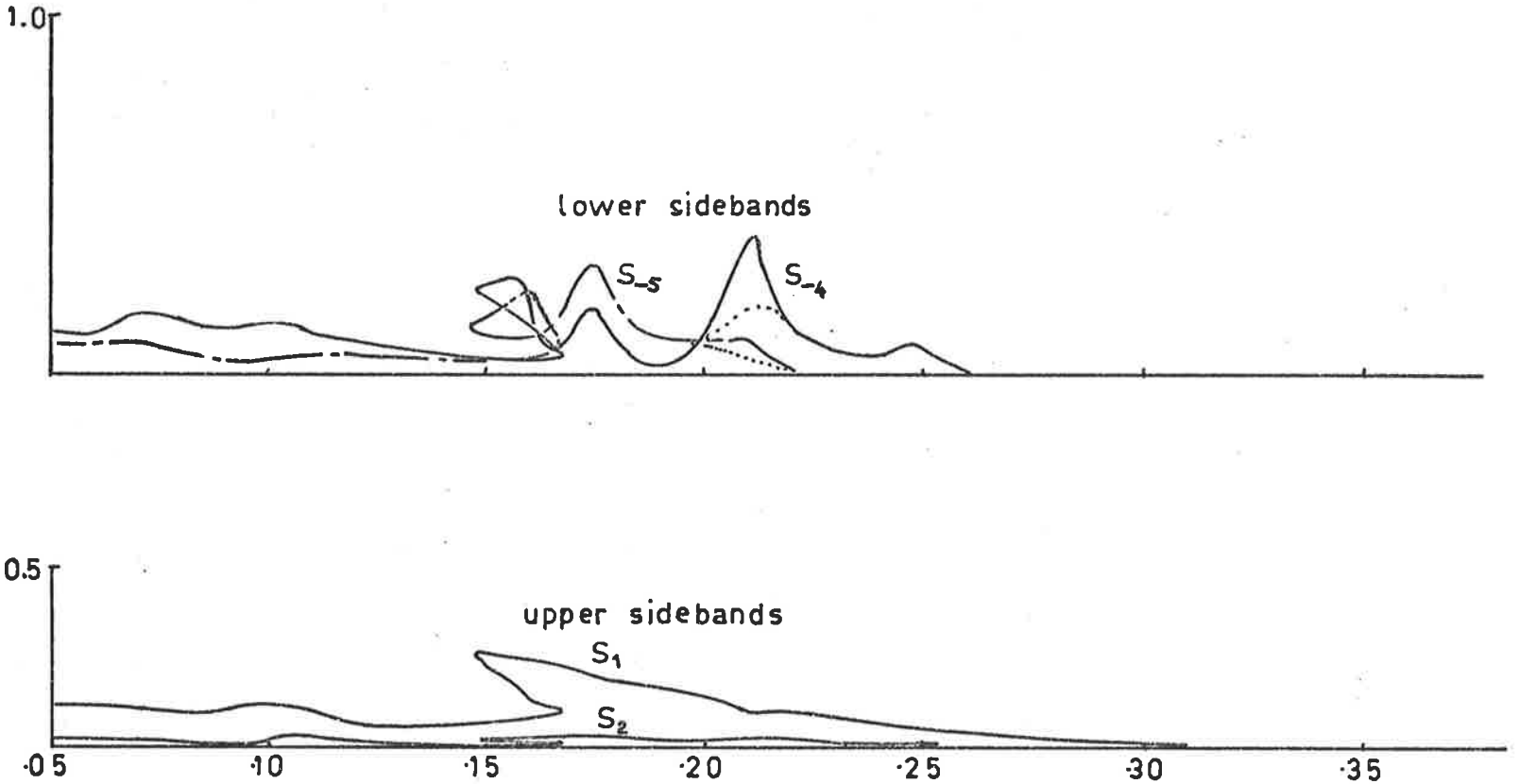

FIGURE 10.10a (continued)

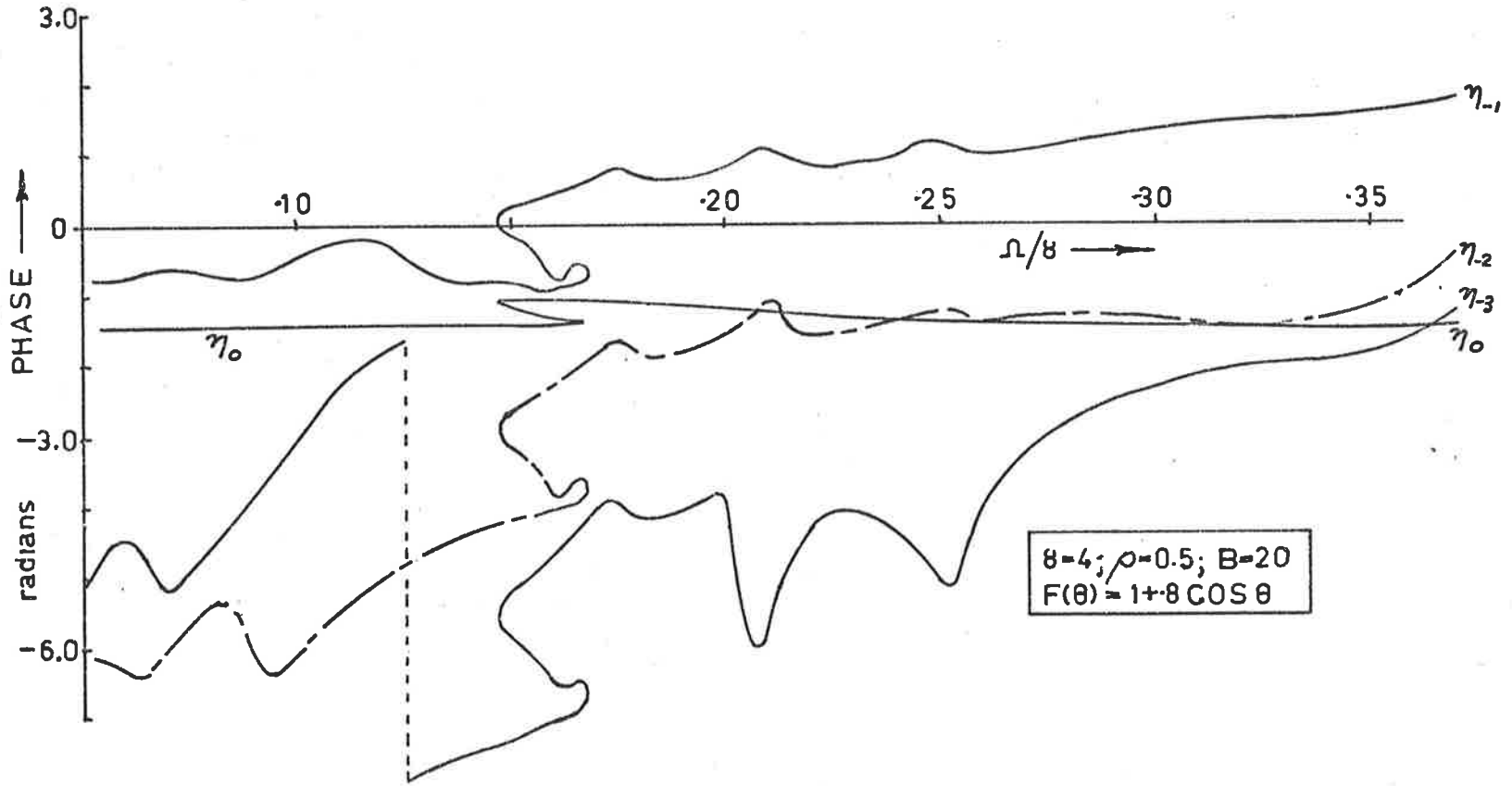

FIGURE 10.10 b : RELATIVE PHASE OF THE SIDEBANDS

(continued next page)

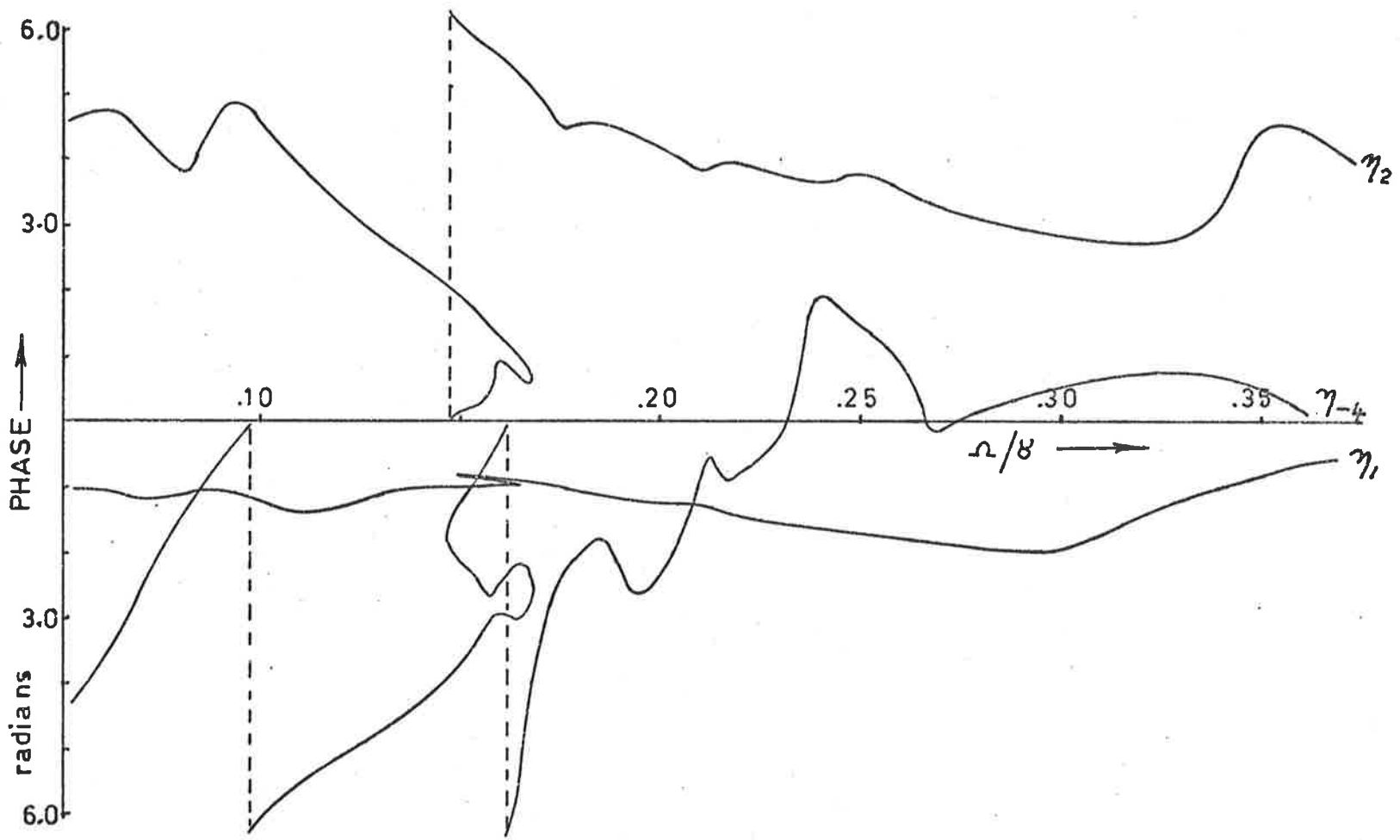

FIGURE .10.10 b (continued)

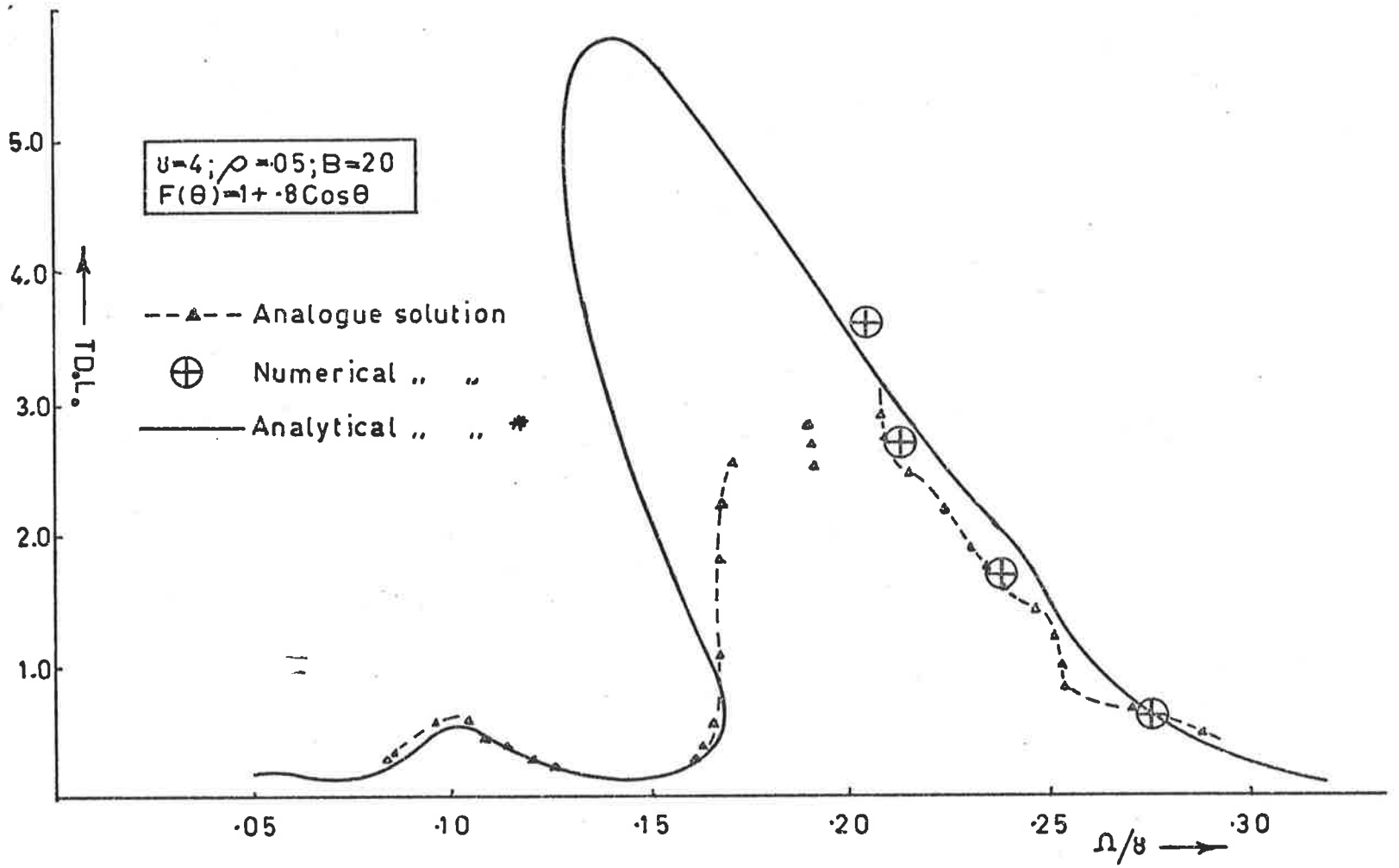

* Using three lower and three upper sidebands and fundumental.

FIGURE 10.11 : COMPARISON OF THREE METHODS OF SOLUTION

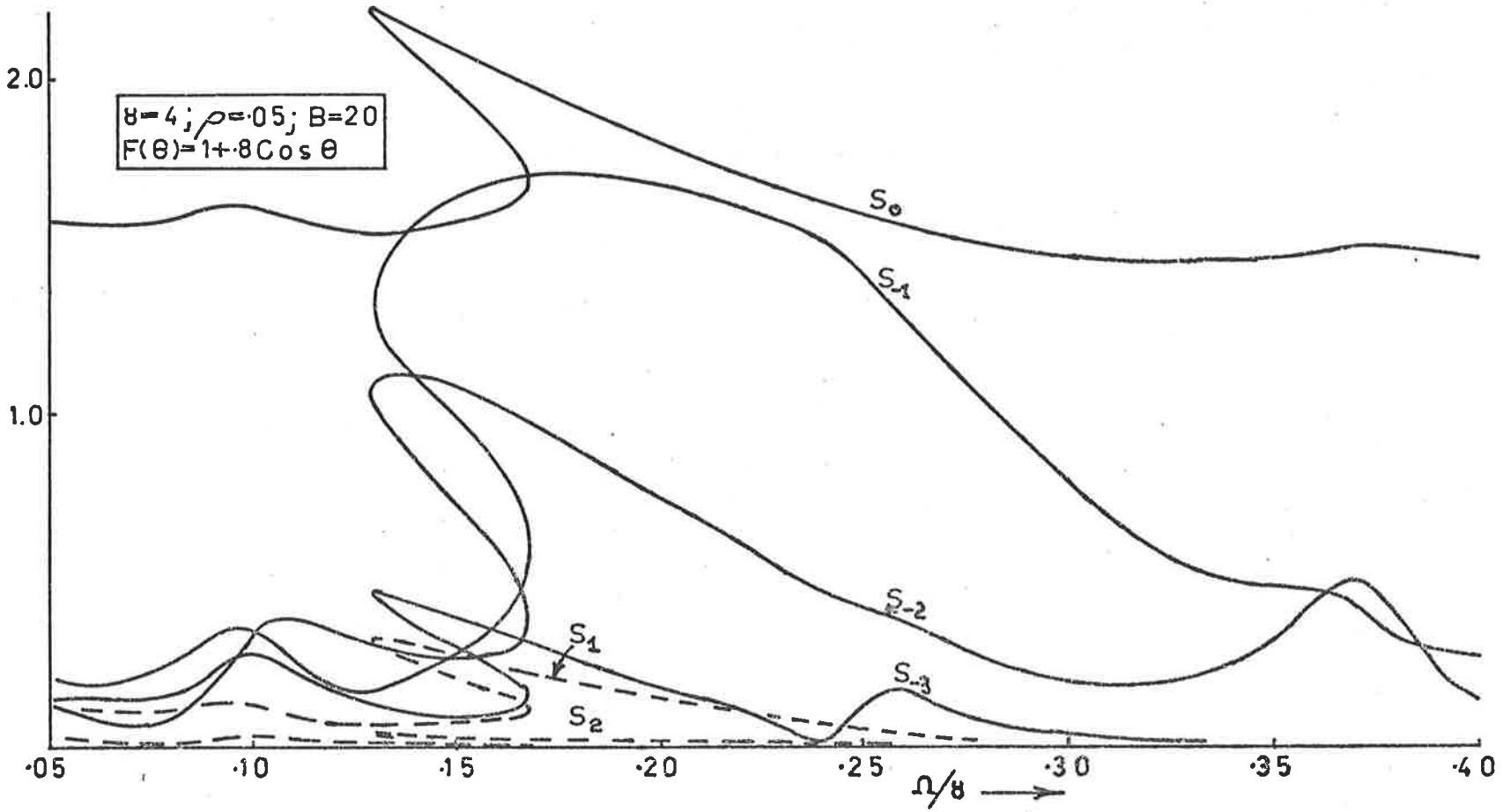

Solution obtained using 3 lower & 3 upper sidebands.

FIGURE 10.12 = SIDEBAND AMPLITUDES (cf. 10.10a)

more accurate the final results.

It is well to remember however that the analytical results obtained by the method discussed in this section apply to a system which effectively has infinite mechanical inertia, i.e. a constant speed and is therefore artificial.

In general, the author has found that the analytical solution gives the position of the right hand side of each of the resonant peaks of the torque speed curves with reasonable accuracy. That is, it agrees well with the position found from analogue and numerical solution and furthermore, the match improves as more lower side bands are included in the solution.

On the other hand, the position of the peak and of the left hand side of the resonant peak, as found by analysis, are both extremely sensitive to the number of lower side bands included in the solution. A similar sensitivity to small changes in any of the circuit parameters was most noticeable when using the analogue computer to obtain the results presented in Figures 5.11→5.16. Furthermore, as previously noted, results from the analogue computer in the vicinity of the peak were ambiguous and no satisfactory decision could be made within the period of time available before serious drift obscured the true results so that the most accurate answers are likely to come from numerical solution.

These in turn have proved to be ambiguous in the regions under discussion. They suggest that the final value of average speed at which the machine settles is strongly influenced by the mechanical inertia and to a lesser extent by the initial speed and position of the rotor. Such a

result is not surprising, as fluctuations in speed about the mean value must influence the amplitude of the various side bands in the flux waveform, and hence the value of the average torque produced at a particular average rotor speed.

In Figure 10.13, some transient speed time curves, obtained by numerical solution of the system equations, illustrate the dependence of the final speed on the initial speed and on the inertia. No systematic attempt has been made by the author to investigate the effects of different amounts of inertia on system performance.

It is of interest to note in this respect, that both methods of investigating system behaviour which take the rotor speed as an independent variable; viz. the phase amplitude investigation of Chapter 9 and the analysis of Chapter 10, lead to results which give re-entrant torque speed curves, suggesting that two different stable values of developed torque at one particular speed may be found for a limited range of speeds. However, when the system has finite inertia no such, clear cut multi valued torque speed curve has been found.

It is also appropriate to emphasise that while both the analogue computer and numerical solutions automatically include the effects of synchronous torques, the analytical results presented, represent average asynchronous torque only. Because of the pulsating nature of the asynchronous torque and the relatively small values of synchronous torque produced, these latter components only become significant when the inertia is sufficiently great that the perturbation about the rotor average position due to the former, are much less than the maximum effective synchronous torque angle of

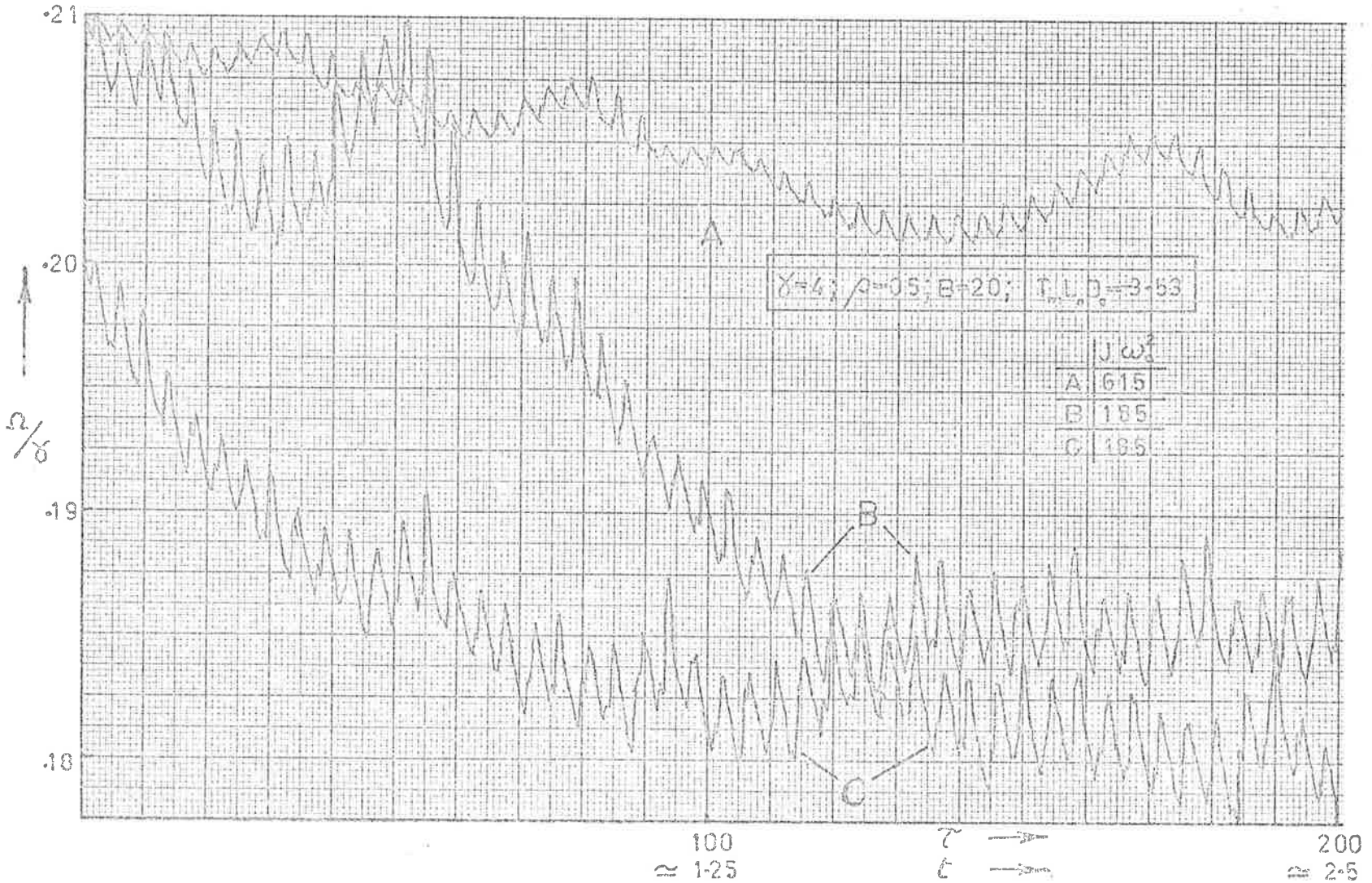

FIGURE 10.13: SPEED TIME CURVES FROM NUMERICAL SOLUTION

$\frac{p\Omega}{2m\gamma} \frac{\pi}{2}$ as derived in (10.58).

No synchronous torques have been calculated because it was felt that the amount of computing time required could not be justified.

10.7.2 Prototype machine

Appendix XII sets out the values of the various actual and normalised parameters of the prototype machine. A quintic approximation to the λ-i characteristics has been adopted and the cosine series for f(θ) has been truncated after six terms. Thus the exponent q in (10.1) becomes q = 5, while the upper bound, k = μ in (10.21) will be μ = 6.

Some analytical results are presented for the motoring region in Figure 10.14 for a number of different approximations as detailed in the figure caption. For purposes of comparison the measured results are also plotted.

In this case the precise formulation of (10.1) restricts the possible methods of representing iron losses to two, and Figures 10.14 and 10.15 each present results from both approaches. Figures 3.4 to 3.6 show the measured average iron losses as a function of speed for a particular applied voltage while Figures 4.10 and 4.11 are relevant to blocked rotor conditions.

Either an average value for ρ_2 (i.e. R_c) or an increased value for ρ_1 may be found from the experimental results shown in Figures 3.4 to 3.6. See Appendix XII. Thus curves A B & C of Figure 10.14 were obtained by putting $R_c = 525\Omega$ while curves D & E were obtained when $R_c \to \infty$ and an additional 5Ω series resistance was added to the circuit. The results represented by these five curves required seven hours of central

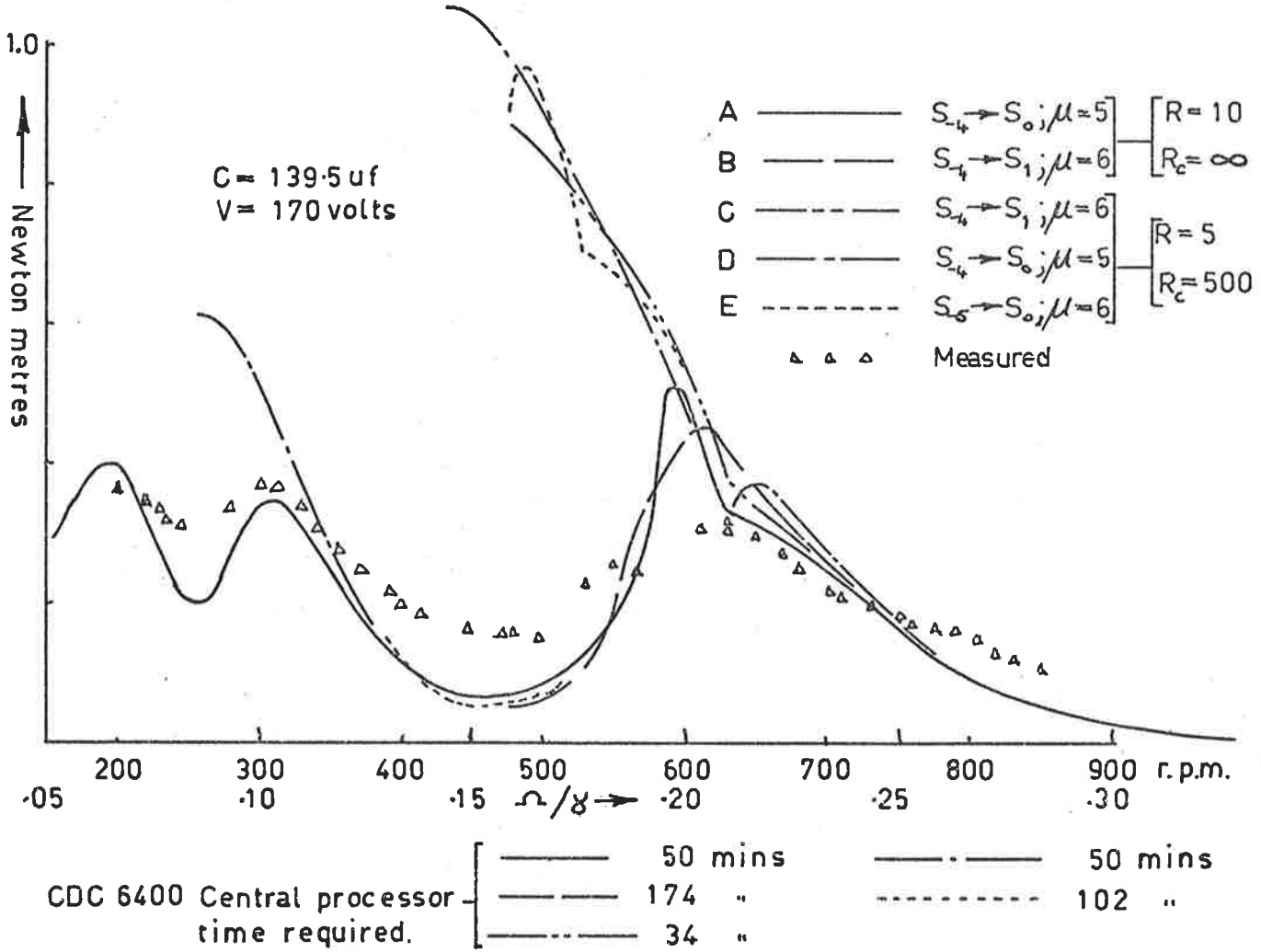

FIGURE 10.14 : ANALYTICAL SOLUTIONS : PROTOTYPE MACHINE

processor time on a CDC 6400 computer; so all solutions were pursued only until the general form was apparent, which explains the lack of completeness of the results.

It will be seen that the analytical results obtained when the iron losses are represented by a fixed shunt resistance, diverge markedly from the experimental results in certain definite regions. One major factor causing this to occur is the behaviour of the denominator of the function shown plotted in Figure 10.8. This particular term appears in (10.23) and (10.24) which are solved to give the various a_n; and also in (10.65) which gives the total average asynchronous torque.

Using the parameters of the particular machine under consideration it can be shown that this function (Figure 10.8) will pass through a maximum whenever the rotor speed is such that $\Omega/\gamma \simeq 0.2/n$ for upper sidebands or $-1.2/n$ for lower sidebands. The behaviour of the solution is such that it is imperative to include within the generating solution, any sideband which will cause such a divergence within the speed range of interest.

As discussed in earlier sections, the evidence suggests that the amplitude of the fundamental component of the flux waveform remains sensibly constant over the speed range of interest and that the form of the modulation envelope (or the trajectories in the phase plane) determined by the particular terminal conditions and rotor speed, is obtained by the build up of sidebands of appropriate order, magnitude and phase.

If, while attempting to find an analytical solution, a significant sideband is not included within the generating solution, then experience of many such attempts on the part of the author indicates that the fundamental amplitude and phase

changes significantly, which in turn influences the resultant amplitude and phase of all of those sidebands already included in the generating solution. The net result then often bears little resemblance to the true result obtained by including all significant sidebands within the generating solution.

Such an effect is indicated in Figures 10.10 and 10.12 and again in Figures 10.14 and 10.15. In the latter case it is clear that the first upper and sixth lower sideband will both result in a maximum for the function of Figure 10.8 in the vicinity of $\Omega/\gamma = 0.2$. These sidebands are therefore likely to be significant at this particular rotor speed and failure to include them will lead to erroneous results.

A study of Figure 10.14 shows that when the first upper sideband is included, an improved match results between theory and experiment in the vicinity of $\Omega/\gamma = 0.2$.

The better match obtained by adding additional series R rather than shunt R_c may be due to the fact that by doubling ρ_1 the magnitude of the function in Figure 10.8 is reduced to one quarter and so becomes much less significant. Hence the non-inclusion in the solution of the divergent sidebands is possibly not as critical.

An analytical solution involving four lower sidebands, the fundamental and one upper sideband was then sought for the whole speed range from standstill up to what would be the normal synchronous speed for a two pole machine i.e. 3000 r.p.m.

Experimental and analytical results are both plotted for comparison in Figure 10.16. Considering the approximations involved in representing the iron losses, the rotor geometry and the B-H characteristics, the assumption of infinite inertia, and the truncated sideband series necessitated by having to set a limit on computational time, the agreement is

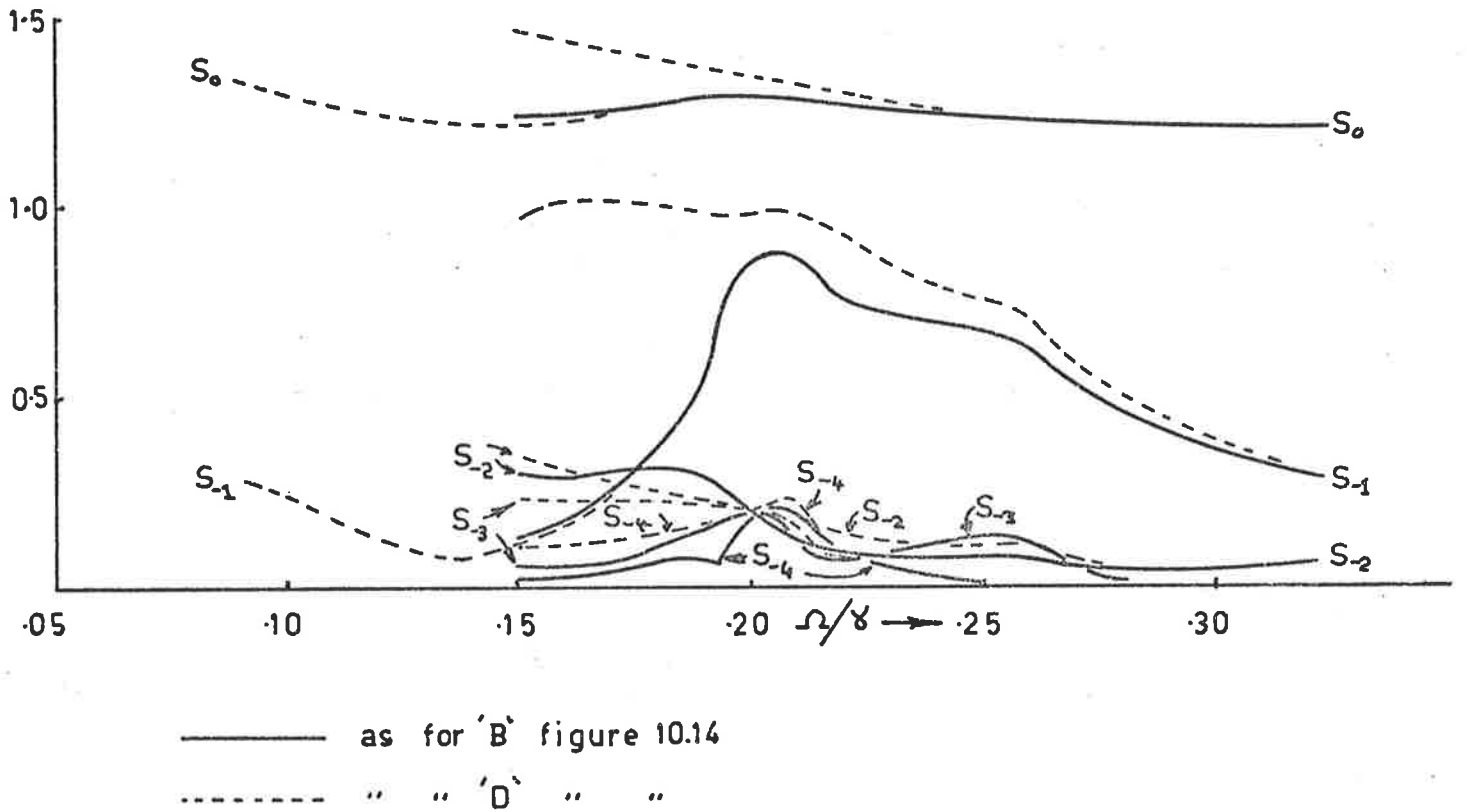

FIGURE 10.15: SIDEBAND AMPLITUDES: PROTOTYPE MACHINE

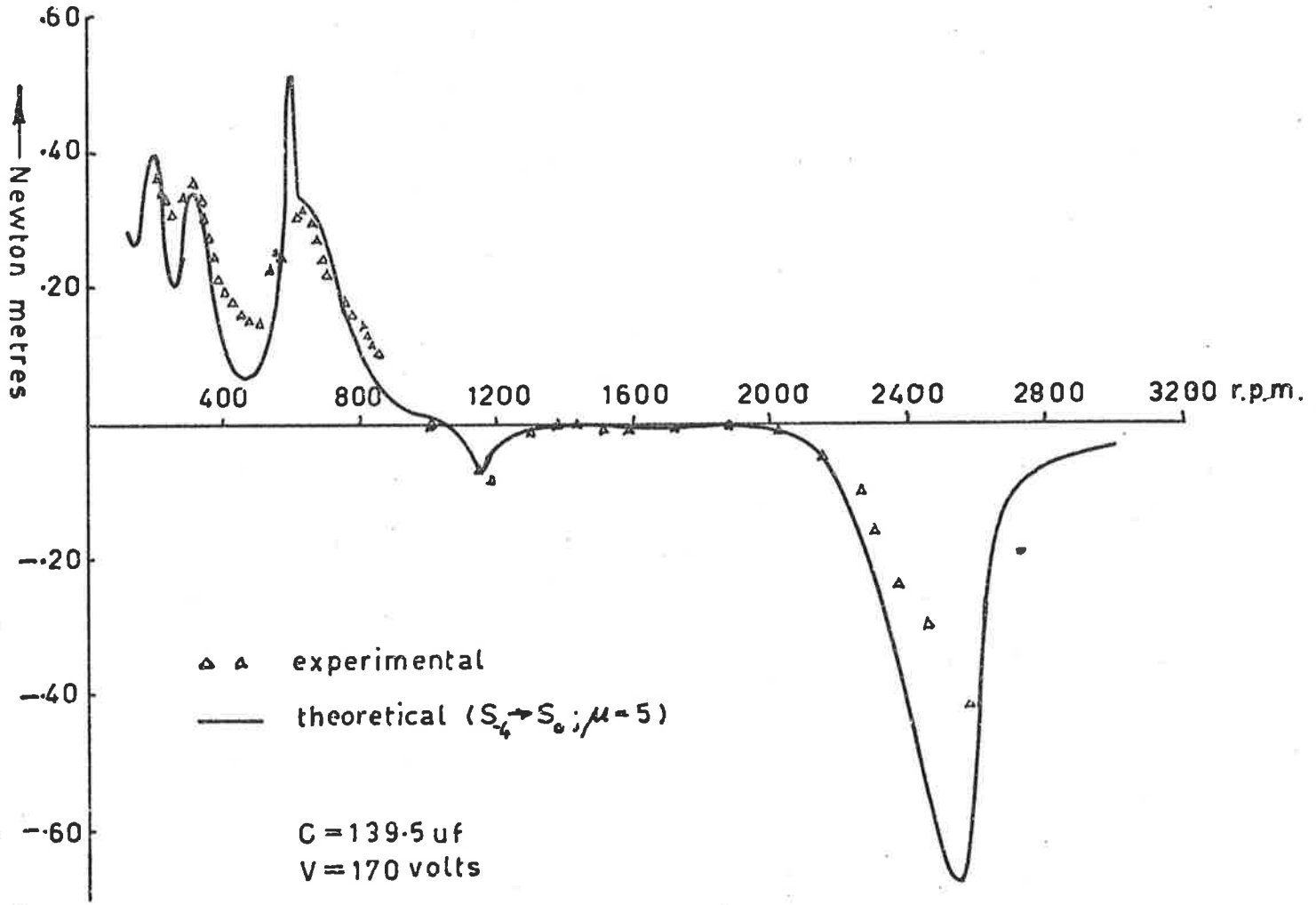

FIGURE 10.16: TORQUE SPEED CHARACTERISTIC FOR PROTOTYPE

satisfactory.

It seems reasonable to conclude that the theory developed in this section covers the major effects within such machines.

Figure 10.17 shows the contributions to the total torque by individual sidebands.

In addition to the normalised rotor speed scale Ω/γ, each sideband scale is also shown. These results illustrate what appears to be a fairly general approximation which may be applied to the behaviour of these devices. That is, that the peak torque contribution due to the n^{th} sideband occurs when $S_n \equiv \gamma+np\Omega \simeq \pm 2$

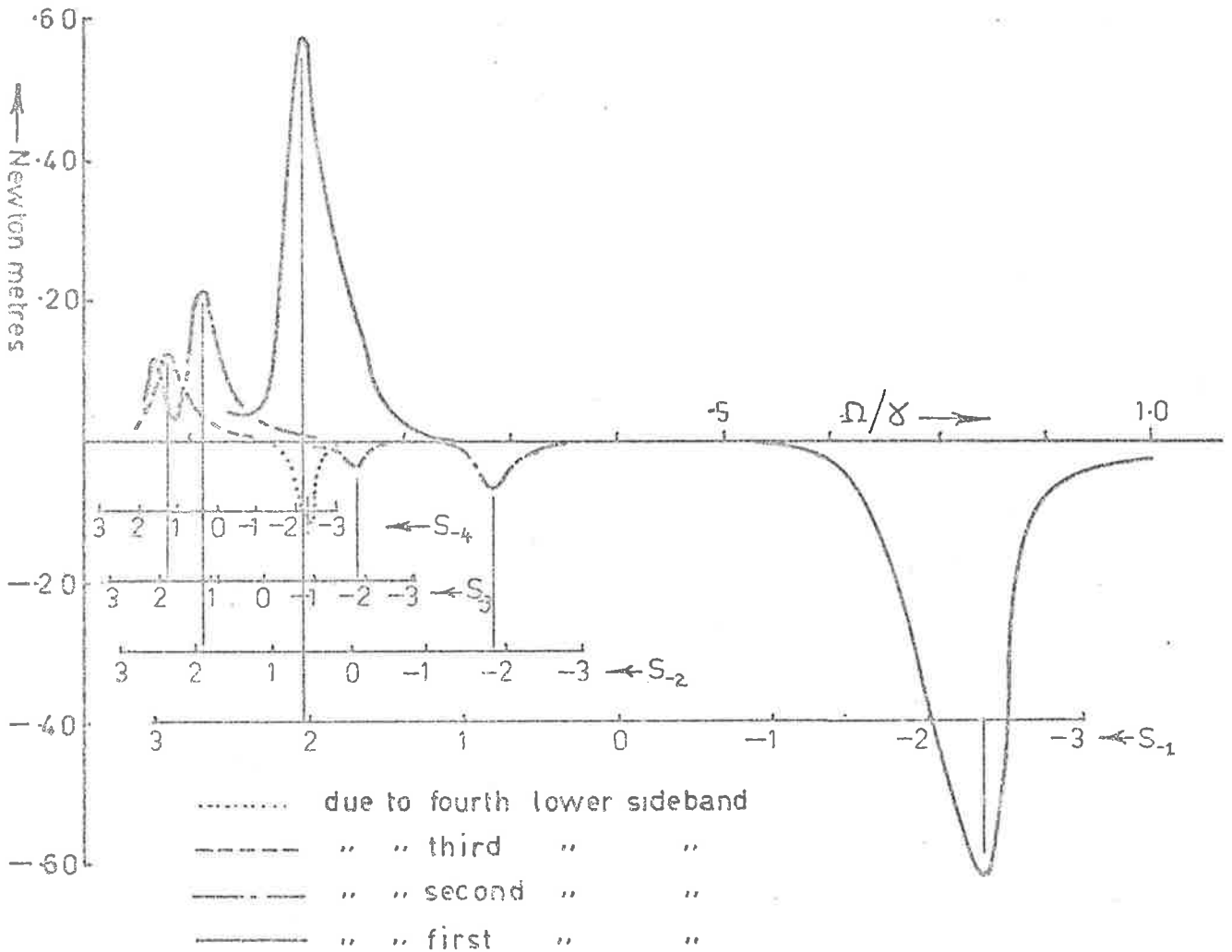

FIGURE 10.17 CONTRIBUTION TO TORQUE BY INDIVIDUAL SIDEBANDS

CHAPTER 11
Efficiency of Ferro-resonant Parametric Machines

The machines under discussion consist essentially of a saturating inductance subjected to an external forcing frequency ω_1 from the electrical circuit and an effective mechanical forcing frequency $\omega_2=p\omega_m$ resulting from the variation in rotor reluctance as the shaft carrying p poles rotates at ω_m. In general these two frequencies are incommensurate. Their interaction in the inductance produces a series of frequency components comprising integral multiples of ω_1 and ω_2, together with the sums and differences of these multiples.

That such a result is plausible may be seen by an examination of the physical nature of the machine. When the saturating stator windings are fed from a sinusoidal source of voltage at frequency ω_1 through a series capacitor and the winding resistance, periodic mmf's of frequencies $j\omega_1$ will be applied to across the reluctance of the stator and rotor iron. The latter is a periodic function of rotor position and may be represented by an expression similar to that in (4.22), except that it is also a function of flux density. The modulating effect of the moving rotor may therefore be represented by forward and backward moving Fourier series having components $np\omega_m$. Thus we may expect to find flux components in the stator windings having frequencies given by $j\omega_1+np\omega_m$ where $n=0,\pm1,\pm2,\pm3.....$ For the small values of damping which are relevant to the particular problem, the flux waveform though modulated, is essentially sinusoidal for a sinusoidal applied voltage which means that harmonics of ω_1 in the flux waveform may possibly be neglected. However, due

to the non linear λ-i relationship, it does not follow that the harmonics of ω_1 in the current waveform are negligible.

11.1 Power-frequency relationships

In a situation such as this where two or more different frequencies arising from incoherent sources are mixed in a non linear lossless reactance, certain relationships may be established among the power flows at certain frequencies, in terms of the relationships among these particular frequencies.

The situation is formally described by the Manley-Rowe equations [21], which for two frequencies take the form:-

$$\sum_{j,n} \frac{jP_{j,n}}{j\omega_1+n\omega_2} = 0 \qquad \text{.....(11.1)}$$

$$\sum_{j,n} \frac{nP_{j,n}}{j\omega_1+n\omega_2} = 0 \qquad \text{.....(11.2)}$$

where j and n are integers whose range depends upon the particular system under consideration and $P_{j,n}$ represents the input power associated with the component having a frequency $j\omega_1+n\omega_2$. For this particular problem, neglecting harmonics of the fundamental in the flux waveform, we may take:-

$$\left.\begin{aligned} j &= 0,1 \\ n &= 0,\pm1,\pm2,\pm\ldots\text{etc} \end{aligned}\right\} \qquad \text{.....(11.3)}$$

so that (11.1) and (11.2) become:-

$$\sum_{n=-r}^{+r} \left[\frac{P_{1,n}}{\omega_1+n\omega_2}\right] = 0 \qquad \text{.....(11.4)}$$

and

$$\sum_{n=-r}^{+r} \left[\frac{P_{o,n}}{\omega_2} + \frac{nP_{1,n}}{\omega_1+n\omega_2}\right] = 0 \qquad \text{.....(11.5)}$$

Now $P_{1,0}$ equals the power input to a lossless reactance at frequency ω_1; so that from (11.4) we have

$$P_1 \equiv P_{1,0} = \sum_{n=\pm 1,\ldots\pm r} \left[\frac{\omega_1 P_{1,n}}{\omega_{1,n}}\right] \qquad \ldots\ldots(11.6)$$

which for this particular problem does not include any losses in the stator winding resistance at frequency ω_1.

If we define

$$P_2 \equiv \sum_{n=-r}^{+r} [P_{o,n}] \qquad \ldots\ldots(11.7)$$

then

$$P_2 = -\sum_{n=-r}^{+r} \left[\frac{n\omega_2 P_{1,n}}{\omega_{1,n}}\right] \qquad \ldots\ldots(11.8)$$

where $\omega_{1,n} = \omega_1 + n\omega_2$

The essential nature of the relationship expressed by (11.6) and (11.8) may be brought out by examining the situation which occurs when only one particular side band is present. In which case (11.6) and (11.8) give:-

$$\frac{P_1}{\omega_1} = -\frac{P_{1,n}}{\omega_{1,n}} = \frac{P_2}{n\omega_2} \qquad \ldots\ldots(11.9)$$

where $\omega_{1,n} \equiv \omega_1 + n\omega_2$

and $P_1 + P_2 + P_{1,n} \equiv 0$, with the direction of positive power flow defined as into the lossless reactance.

11.2 Torque production

Each term of (11.9) has the dimensions of torque and since P_2 represents the power into the reactance from the shaft at frequency $\omega_2 = p\omega_m$ and hence also represents the power input at shaft frequency ω_m we can define a shaft torque in the direction of ω_m as

$$T = \frac{-P_2}{\omega_m} = \frac{-pP_2}{\omega_2} \qquad \ldots\ldots(11.10)$$

so that the contribution to the total output torque by the *nth* sideband becomes, from (11.10) and (11.9):-

$$T_n = \frac{npP_{1,n}}{\omega_{1,n}} \qquad \ldots\ldots(11.11)$$

Here, $P_{1,n}$ represents the power flow into the reactance at frequency $\omega_{1,n}$, but since the only source of voltage at this frequency is within the reactance itself, as discussed in Section 10.4, this power flow must in practice represent the

power dissipated in the circuit at frequency $\omega_{1,n}$, i.e. $P_{1,n}$ into the inductance must be negative.

Dropping the double subscript notation in (11.11), which can be done without danger of confusion, provided harmonics of frequency ω_1 are negligible, we may write

$$T_n = \frac{-npP_{sn}}{\omega_n} \qquad .....(11.12)$$

where P_{sn} represents the power dissipated in the circuit at the n^{th} sideband frequency $\omega_n \equiv \omega_1 + n\omega_2 \equiv \omega_1 + np\omega_m$.

Equation (11.12) has previously been presented as (10.59) in section 10.6.1.3, together with a discussion which covers a number of aspects of torque production in such parametric machines. The overall pattern of power flow and torque production as expressed by (11.6) and (11.8) may be illustrated by means of the mechanical analogy shown in Figure 11.1, where each differential represents the mechanical equivalent of (11.9) [30].

The original development of the Manley-Rowe relationships applied only to frequencies which were incommensurate [21], however it has since been shown that the relations remain valid provided the various frequencies involved, originate from incoherent sources even although their average values may be commensurate [1].

The former situation leads to a rather more useful result because in this case the various $\omega_{1,n}$ must be incommensurate both among themselves and with respect to ω_1 and ω_2, from which it follows that the various $P_{1,n}$ can represent energy dissipated in the circuit resistance at $\omega_{1,n}$ only, as previously discussed.

When the relationships are extended to include generators which are merely incoherent the possibility arises that some of the various $\omega_{1,n}$ may assume the same average value as ω_1, ω_2 or multiples thereof. (Here it is apposite to note that in practical machines the running integer j as used in equations (11.1) to (11.5) will not be restricted to 0,1. Higher values will be present so leading to a three dimensional stack of differentials similar to those of Figure 11.1. However, as has been stated a number of times already in this report, harmonics of ω_1 have been ignored in order to keep the discussion and analysis within bounds).

11.2.1 Synchronous torques

Thus at particular rotor speeds it will not be possible to assert that the only source of voltage at a particular frequency $\omega_{1,n}$, is within the non linear inductance, and hence it does not follow that the $P_{1,n}$ associated with it is represented entirely by power dissipated at $\omega_{1,n}$ in the circuit resistance. While equations (11.6) and (11.8) and the mechanical analogy of Figure 11.1 remain valid under these circumstances, they do not provide simple answers for the value of the resultant synchronous torques, and recourse must be made to the methods of Section 10.6.1.2.

11.3 Efficiency

The conversion efficiency in the lossless reactance, in this case the stator winding inductance, must be given by:-

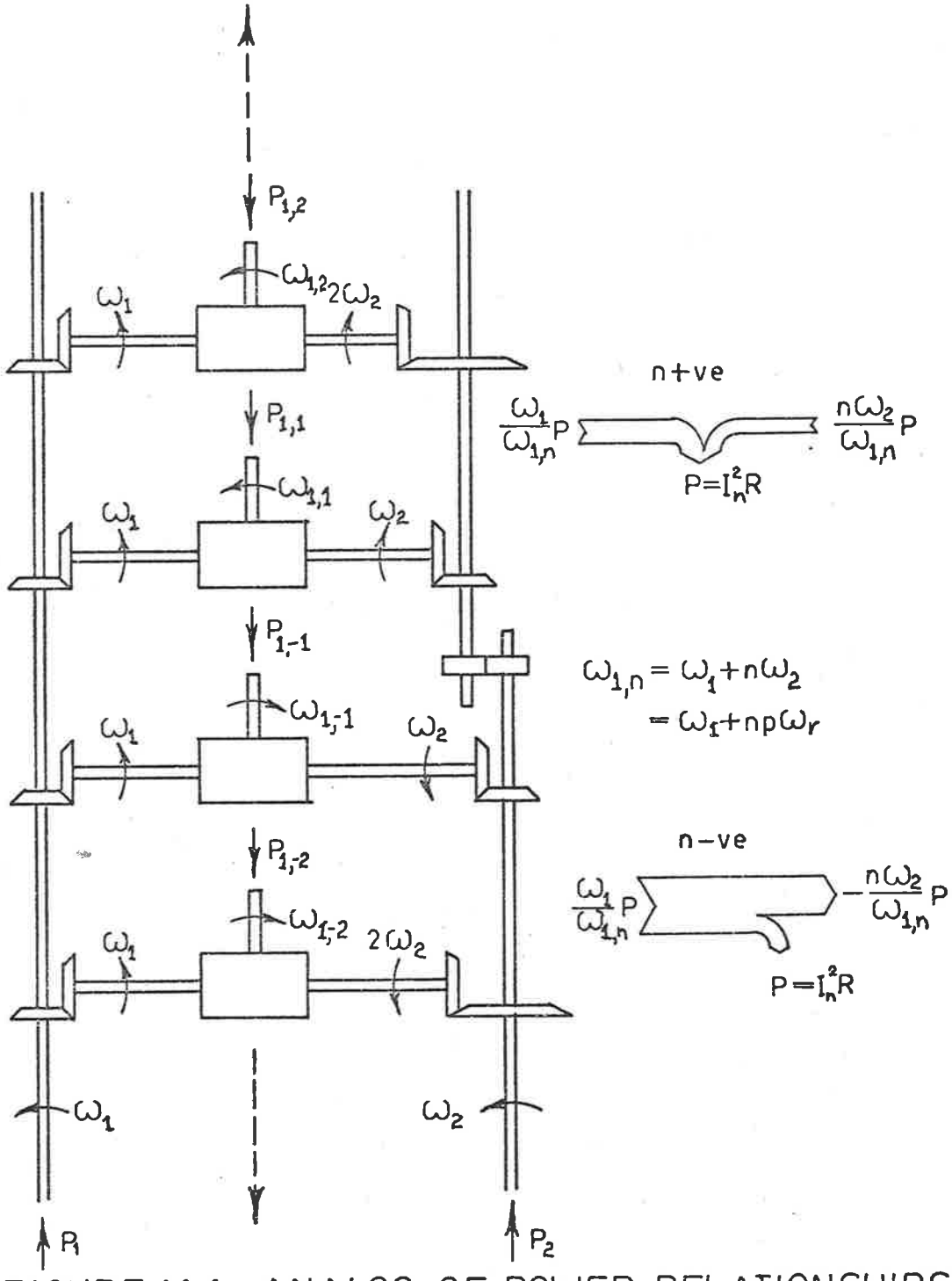

FIGURE 11.1 ANALOG OF POWER RELATIONSHIPS IN PARAMETRIC MACHINES

$$\eta = \frac{P_m}{P_1} = \frac{-P_2}{P_1} = -p\frac{\omega_m}{\omega_1}\frac{\Sigma[^n \frac{P_{1,n}}{\omega_{1,n}}]}{\Sigma[\frac{P_{1,n}}{\omega_{1,n}}]} \qquad \ldots\ldots(11.13)$$

from which it is clear that, whilst operating in the motor region, the presence of upper side bands for which n is positive, lowers the efficiency.

As the magnitude of any side band is related to the closeness of its frequency to the system natural frequency, the larger the value of γ, then the further from resonance will be all of the upper side band components and hence the smaller their magnitudes.

11.3.1 Operating efficiency

Overall efficiency of the machine is affected by losses at supply frequency in the stator resistance as well as by core losses.

Some estimate of the maximum practical overall efficiency may be made by taking into account the various practical factors which have emerged throughout the course of this report.

Thus the practical range for γ appears to be $3<\gamma<4$ so that the stator circuit impedance is relatively high for all upper side bands which may therefore be neglected. Hence the conversion efficiency becomes:-

$$\eta \simeq \frac{p\omega_m}{\omega_1}\frac{\frac{P_{1,-1}}{\omega_{1,-1}} + \frac{2P_{1,-2}}{\omega_{1,-2}} + \frac{3P_{1,-3}}{\omega_{1,-3}} + \ldots.}{\frac{P_{1,-1}}{\omega_{1,-1}} + \frac{P_{1,-2}}{\omega_{1,-2}} + \frac{P_{1,-3}}{\omega_{1,-3}} + \ldots..} \qquad \ldots\ldots(11.14)$$

The speed torque curves comprise a series of resonant peaks which occur as each lower side band in turn passes through the natural frequency, $\gamma_N \equiv \omega_N/\omega_o$, of the system under the combined effect of ω_1 and ω_m or γ and Ω, with the k*th* peak occurring when $P_{1,-k}/\omega_{1,-k}$ is a maximum.

Under practical operating conditions, ω_N lies in the vicinity of $2\omega_o$; so that resonance occurs very approximately when

$$\left.\begin{aligned} \omega_{1,-k} &= \omega_1 - kp\omega_m \simeq 2\omega_o \\ \text{i.e. when} \quad \omega_m &= \frac{\omega_1 - 2\omega_o}{kp} \\ \text{or when} \quad \frac{\Omega}{\gamma} &= \frac{1-\frac{2}{\gamma}}{kp} \end{aligned}\right\} \qquad \ldots\ldots(11.15)$$

The essential behaviour may be underlined by noting that at the k*th* torque peak, the k*th* lower side band predominates in the solution. In which case, we have from (11.14) and (11.15)

$$\eta \simeq \frac{kp\omega_m}{\omega_1} \simeq 1-\frac{2\omega_o}{\omega_1} = 1-\frac{2}{\gamma} \qquad \ldots\ldots(11.16)$$

which is independent of k and furthermore it increases with increasing γ. This represents an approximate expression for the efficiency of conversion of energy in the airgap inductance of the machine, at speeds in the vicinity of a torque peak. A further reduction in efficiency occurs due to the losses at ω_1 in the stator winding resistance. A very rough estimate of this can be made by noting that at the torque peaks under practically acceptable operating conditions, the amplitude of the sideband approximates that of the fundamental.

$$\text{i.e.} \quad \lambda_{sn} \simeq \lambda_1$$

$$\text{but} \quad \omega_{sn} \simeq 2\omega_o \text{ at resonance}$$

$$\text{so that} \quad \omega_{sn} \simeq \frac{2}{\gamma}\,\omega$$

$$\text{and} \quad V_{sn} \simeq \frac{2}{\gamma}\,V_L \simeq \frac{2}{\gamma}\,I_1\omega L$$

$$\text{Also} \quad I_{sn} = \frac{V_{sn}}{\sqrt{R^2+\frac{1}{\omega_{sn}^{\,2}\,C^2}}}$$

$$\simeq \omega_{sn} C V_{sn}$$

$$\simeq \frac{2}{\gamma}\,I_1\,\omega\omega_{sn}LC$$

$$\therefore \quad \frac{I_1}{I_{sn}} \simeq \frac{\gamma}{2\omega\omega_{sn}LC}$$

$$\simeq \frac{\gamma^2}{4}\,\frac{\omega_o^{\,2}}{\omega^2}$$

$$\simeq \frac{1}{4}$$

and $\frac{I_1^2 R}{I_{sn}^2 R} \simeq \frac{1}{16}$

This very rough estimate shows that the power lost in the stator resistance at fundamental frequency is of the order of 6% of that dissipated at the sideband resonant frequency. Thus the overall efficiency will be given approximately by

$$\eta \simeq \frac{1-\frac{2}{\gamma}}{1+\frac{1}{8\gamma}} = \frac{\gamma-2}{\gamma+1/8} \qquad \ldots\ldots(11.17)$$

Thus for this class of machine it seems likely that the upper bound to efficiency corresponding to γ in the range $3<\gamma<4$ will be $0.32<\eta<0.48$.

When the effect of coreloss is included actual operating efficiency will be lower still.

It is of interest to compare the rotor conversion efficiency of parametric machines with the rotor efficiency of a squirrel cage induction machine, which is also a brushless asynchronous device.

The rotor efficiency of a p-pole polyphase induction motor or a single phase induction motor in which the backward component of mmf is neglected (which corresponds to neglecting the upper sidebands in parametric machines) is given by:

$$\eta_R = 1-S = \frac{p}{2}\frac{\omega_m}{\omega_1} = \frac{p}{2}\frac{\Omega}{\gamma} \qquad .....(11.18)$$

which is shown plotted in Figure 11.2 as a function of $\frac{\Omega}{\gamma}$.

On the other hand we see from (11.16) that the parametric machine tends to behave as a machine having a variable number of poles and which, as the k*th* side band passes through resonance and dominates the solution, behaves as a 2kp pole machine, by which is meant, that the conversion efficiency associated with the k*th* lower side band at a particular rotor speed is k times that for a p-pole parametric machine and 2k times that for a p-pole induction machine. Thus the inevitable fall off with decreasing speed, in rotor conversion efficiency associated with a particular side band, as implied by (11.9), is offset by the increasing values of k in (11.16). Upper bounds to the rotor conversion efficiency are shown in Figure 11.2 for a number of lower side bands on the assumption that only one is present in the solution at any particular rotor speed. These suggest that parametric machines might be more efficient than conventional induction machines having the same number of poles, only at very low speeds, where normally the latter are not expected to operate.

The discussion in this section has centred about some gross simplifications, which have been invoked only to bring out the essential behaviour of the machine, consequently it must be taken as qualitative only.

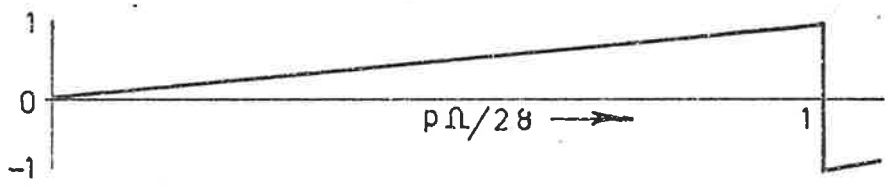

Conventional p-pole induction machine

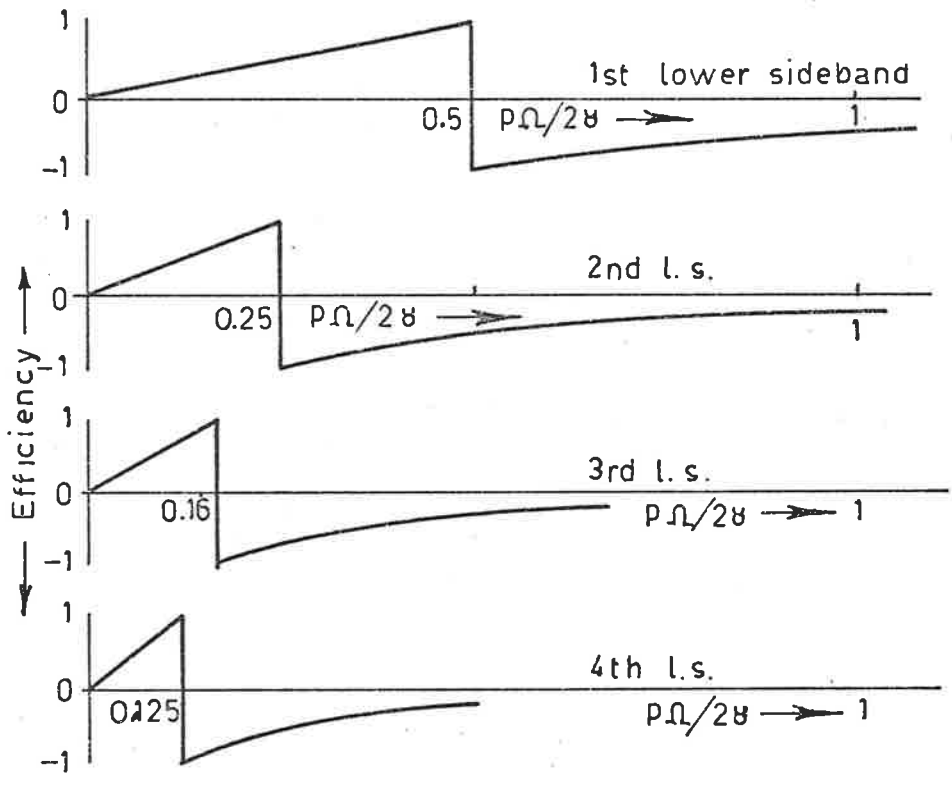

Parametric machine
(generating conditions shown negative)

FIGURE 11.2 AIRGAP CONVERSION EFFICIENCY

CHAPTER 12

Stability

It has been shown in previous sections that the behaviour of a particular machine of the type under discussion in this report, may be represented with reasonable accuracy by the pair of non-linear equations (4.38) and (4.39) reproduced here for convenience as (12.1) and (12.2) respectively.

$$\frac{T_m}{J\omega_o^2} = \ddot{\theta} + \frac{G}{J\omega_o}\dot{\theta} + \frac{F'(\theta)\psi^{(q+1)}}{(q+1)L_o J\omega_o^2 D_o^{\frac{2}{q-1}}} \qquad \ldots\ldots(12.1)$$

$$-B\sin\overline{\gamma\tau+\beta} = 2\rho_2\ell\dddot{\psi}+(1+4\rho_1\rho_2)\ddot{\psi} + 2(\rho_1+\rho_2)\dot{\psi}+\psi + (1+2\rho_1\frac{d}{d\tau} + \ell\frac{d^2}{d\tau^2})F(\theta)\psi^q \qquad \ldots\ldots(12.2)$$

OR:-

$$-B\sin\overline{\gamma\tau+\beta} = \ddot{\psi} + (1+2\rho\frac{d}{d\tau})(\psi+F(\theta)\psi^q) \qquad \ldots\ldots(12.3)$$

if iron losses can be neglected and the leakage inductance incorporated with the variable inductance.

If so desired for purposes of analysis these may be reduced to a set of first order non-linear equations, thus:-

$$
\left.
\begin{aligned}
\dot{x}_1 &= x_2 \\
x_2 &= \frac{T_m}{J\omega_o^2} - \frac{G}{J\omega_o} x_2 - \frac{F'(x_1)x_3^{q+1}}{(q+1)L_o J\omega_o^2 D_o^{\frac{2}{q-1}}} \\
\dot{x}_3 &= x_4 \\
\dot{x}_4 &= x_5 \\
2\rho_2 \ell \dot{x}_5 &= -B\sin\overline{\gamma x_6+\beta} - (1+4\rho_1\rho_2)x_5 - 2(\rho_1+\rho_2)x_4 - x_3 \\
&\quad -(1+2\rho_1\frac{d}{d\tau} + \ell\frac{d^2}{d\tau^2})F(x_1)x_3^q \\
\dot{x}_6 &= 1
\end{aligned}
\right\} \quad \ldots(12.4)
$$

where $x_1 = \theta$; $x_2 = \Omega$; $x_3 = \psi$; and $x_6 = \tau$

When ρ_2 can be neglected then

$$
\left.
\begin{aligned}
\dot{x}_4 &= -B\sin\overline{\gamma x_5+\beta} - (1+2\rho\frac{d}{d\tau})(x_3+F(x_1)x_3^q \\
\dot{x}_5 &= 1
\end{aligned}
\right\} \quad \ldots(12.5)
$$

In this case $x_5 = \tau$

Previous sections have been concerned with the problem of finding, by analogue, numerical or analytical methods, solutions ψ_o and $\Omega_o(=\dot{\theta}_o)$ which satisfy (12.1) and (12.2) or (12.3) for a given set of input conditions and system parameters. The discussion in this section of the report is concerned with the

stability of the solutions thus found. Analytical methods available for this purpose are far from straight forward in the case of non-linear, non-autonomous differential equations. Thus before an analytical approach is made, it is helpful to look at the expected physical behaviour of the machine under certain limiting conditions.

12.1 Steady state solutions with relatively large load inertia

When the total load inertia is sufficiently large that fluctuations in the rotor speed about the average value $\overline{\Omega}_o$, become insignificant, then the solution to (12.1) becomes almost trivial, because $\ddot{\theta} \to 0$ and $\dot{\theta}$ settles at that values for which the average electromagnetic torque just balances the mechanical torque applied to the machine from all sources.

A typical situation is depicted in Figure 12.1, in which curve 1 shows the value of the total mechanical torque from all sources opposing the direction of motion, while the hypothetical curve 2 shows the total electromagnetic torque developed by the machine, plotted as a function of speed for a given set of input conditions. This latter characteristic includes both asynchronous and synchronous torque components.

It is clear that stable operation as a result of asynchronous torque alone can occur at speeds corresponding to points A and D, whereas B represents an unstable position, because any small displacement in speed away from B results in a nett torque which tends to increase the initial displacement. Stable operation is possible at speeds corresponding to points C and E where both asynchronous and synchronous torques combine to provide the total required electromagnetic torque. At E the

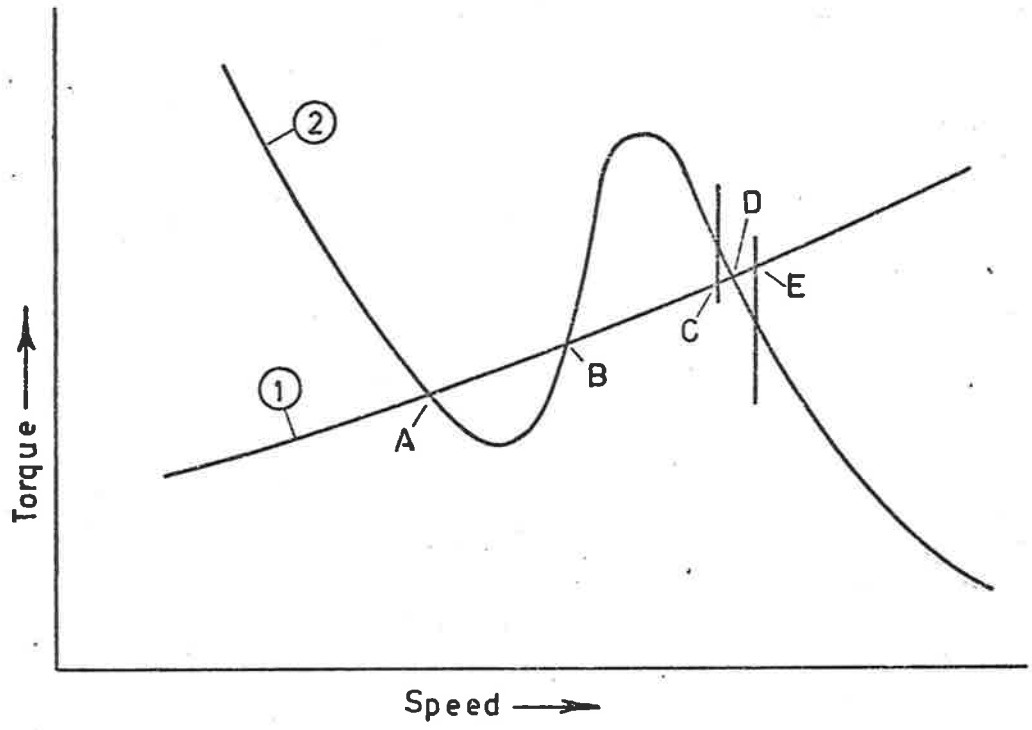

FIGURE 12.1

synchronous torque is positive i.e. it is directed in the direction of rotation.

Any small disturbance which tends to slow the rotor will thus result in an increased positive synchronous torque, so tending to restore the rotor position as discussed in Section 10.6.1.2. Too great a disturbance however will result in a loss of synchronism and the speed would fall to that corresponding to point D. Similarly any disturbance tending to advance the rotor position will, if sufficiently large, shift the operating point from C to D. Clearly, initial conditions will determine which of the four possible stable operating points is assumed.

One further possibility arises if curve 2 is obtained by the solution of (12.2) or (12.3) on the assumption that $\dot{\theta}$ is an independent variable. That is, that the solution so obtained may not be a stable solution in the sense that it may not exist in practice. Such a possibility should be investigated.

12.2 Solutions when the load has finite inertia

In practice, the alternate trains of positive and negative electromagnetic torque pulses do cause significant fluctuations in rotor speed about the mean value $\overline{\Omega}_o$. The magnitude of these fluctuations will be dependent upon the slope at the operating point of curve 1 in Figure 12.1. Thus the solution ψ_o will be influenced by both the system inertia and the mechanical torque-speed characteristic so that curve 2 will not be unique for a particular set of electrical circuit parameters. Furthermore, stable operation in the synchronous mode may be impossible at certain speeds because the natural hunting

frequency in this mode may bear a simple harmonic relationship to the frequency of the asynchronous torque pulses.

Instances of the fact that different load inertias may lead to the machine assuming different steady state operating speeds for similar mechanical load conditions are shown in Figures 10.9 and 10.13. The latter shows two speed time trajectories, both starting from the same initial state of the system but corresponding to two different total inertias leading to the two different settling points marked on Figure 10.9.

It is clear that any analytical approach designed to investigate the behaviour of the system in the vicinity of its operating points must encompass all of the above phenomena. Such an analysis is likely to be tedious, and also in view of the limitations on efficiency of these devices and the approximate nature of analytical solutions to the system equations, rather academic.

In the following sub-sections some possible approaches to the problem are presented.

12.3 Investigation of the stability of a solution

A number of different definitions of stability are possible [36] but in what follows it will be assumed that we are concerned to determine under what conditions the system will return to a previously existing state or limit cycle following a small disturbance. Both the nature and the extent of the disturbance will influence the result.

12.3.1 Linearising the system equations

Writing the set of equations (12.4) and (12.5) in the form

$$\dot{x} = f(x) \qquad \ldots\ldots(12.6)$$

where x is a vector, we see that there can be no solution $X = 0$ unless $B = 0$. It is convenient however for purposes of analysis to have the origin coincide with a solution. Thus if we allow the system to start from some initial state $[X]_o + [\xi]_o$ displaced by the small amount $[\xi]_o$ from the solution of interest then the subsequent behaviour expressed as $X+\xi$ must satisify the equations (12.4) and (12.5) as the case may be. Taking the latter set, with $q \equiv 3$ for simplicity, we find that:-

$$\left.\begin{aligned}
\dot{\xi}_1 &= \xi_2 \\
\dot{\xi}_2 &= -\frac{G}{J\omega_o}\xi_2 - \frac{F''(X_1)\xi_1 X_3^4 + 4F'(X_1)X_3^3\xi_3}{4L_o J\omega_o^2 D_o} \\
\dot{\xi}_3 &= \xi_4 \\
\dot{\xi}_4 &= -(1+2\rho\frac{d}{d\tau})[F'(X_1)X_3^3\xi_1 + (1+3F(X_1)X_3^2)\xi_3] \\
\dot{\xi}_5 &= 0
\end{aligned}\right\} \ldots(12.7)$$

which represents a set of first order linear equations with time dependent coefficients.

Unfortunately the time dependent coefficients are not periodic but only almost periodic so that the usual methods, based on Floquet's Theory, do not apply [41]. The problem is discussed but not resolved in references 4,5 and 26.

It is possible that a suitable Liapunov function might be found [36] but when it is recalled that ψ_o contains a series of top and bottom side bands and that Ω_o comprises an average value $\overline{\Omega}_o$ plus periodic oscillation about the average at frequencies $np\overline{\Omega}_o$ it will be realised that the total solution has a large number of degrees of freedom. Thus any Liapunov Function would need to take this into account if result of any significance are to be expected.

In the case where Ω is an independent variable, i.e. the system inertia is very large, the set of equations 12.7 reduce to

$$\dot{\xi}_3 = \xi_4$$

$$\dot{\xi}_4 = -(1+2\rho\frac{d}{d\tau})(1+3F(\theta)\psi_o^2)\xi_3$$

i.e. $$\ddot{\xi} + 2\rho(1+3F(\theta)\psi_o^2)\dot{\xi}+\xi(1+2\rho\frac{d}{d\tau})(1+3F(\theta)\psi_o^2) = 0 \qquad .....(12.8)$$

which may be written as:-

$$\ddot{\xi} + p(t)\dot{\xi} + q(t)\xi = 0 \qquad .....(12.9)$$

This may be tested for stability by Liapunov's Direct method by putting:-

$$\dot{\xi}_3 = \xi_4$$

and $$\dot{\xi}_4 = -q(t)\xi_3 - p(t)\xi_2$$

and using the function [15]:-

$$V = \xi_3^2 + \frac{1}{q(t)}\,\xi_4^2$$

provided $0 < q_1 \leqslant q(t) < q_2$ .....(12.10)

After differentiation and some simplification we find that:

$$\dot{V} = -\left(\frac{\dot{q}(t)+2p(t)q(t)}{q^2(t)}\right)\xi_4^2 \qquad .....(12.11)$$

Then if $\frac{\dot{q}+2pq}{q^2} \geqslant \varepsilon > 0$; $\dot{V}$ is negative semi-definite.

If we represent $(1+3F(\theta)\psi_o^2)$ as x, then

$$q(t) = x+2\rho\dot{x} \quad \text{and} \quad p(t) = 2\rho x.$$

Thus provided the inequality (12.10) holds and that $\dot{q}+2pq>0$ the solution will be stable i.e. it will be stable if:-

$$x+2\rho\dot{x} > 0$$

and $$\ddot{x}+(4\rho x+\frac{1}{2\rho})\dot{x}+2x^2 > 0 \qquad .....(12.12)$$

Inequalities (12.12) do not appear to lend themselves to general statements about x which indicate stability or otherwise.

An alternative approach may be taken when dealing with (12.9) by making the substitution [4,26]

$$\xi = \varepsilon e^{-\frac{1}{2}\int_o^t p(t)dt} \qquad \text{.....(12.13)}$$

so that (12.9) becomes:-

$$\left.\begin{aligned} &\ddot{\varepsilon} + (q(t) - \tfrac{1}{2}\dot{p}(t) - \tfrac{1}{4}p^2 t)\varepsilon = 0 \\ \text{or} \quad &\ddot{\varepsilon} + (x + \rho\ddot{x} - \rho^2 x^2)\varepsilon = 0 \end{aligned}\right\} \qquad \text{.....(12.14)}$$

where $x \equiv 1 + 3F(\theta)\psi_o^{\,2}$

Equation (12.14) is now in the standard form of a Hill's equation but, as mentioned above the coefficient of ε is not, in general, periodic. If the solution ψ_o is represented by the side band series in Appendix VIIIa and the rotor geometry is represented by the series (VIII.5) in Appendix VIIIb it is a relatively simple matter to show that the value of $x \equiv 1 + 3F(\theta)\psi_o^{\,2}$ will be given by:-

$$1 + \frac{3}{4}\sum_{K=-r}^{+r}\sum_{\ell=-r}^{+r}\sum_{m=0}^{\mu} a_K a_\ell d_m \Big[\cos\overline{(K-\ell-m)2\Omega\tau + \eta_K - \eta_\ell + \delta_m} + \cos\overline{(K-\ell-m)2\Omega\tau + \eta_K - \eta_\ell - \delta_m} + \cos\overline{2(\gamma + \Omega(K+\ell+m))\tau + \eta_K + \eta_\ell + \delta_m} + \cos\overline{2(\gamma + \Omega(K+\ell-m))\tau + \eta_K + \eta_\ell - \delta_m} \Big] \qquad \text{.....(12.15)}$$

Only when γ and Ω bear an integral relationship, will the function be periodic. If this is so then the standard method of analysis using Floquet's theory may be applied and the stability ascertained.

12.3.2 Investigating the transient behaviour of a solution

The methods discussed in the previous section suggest that any investigation of the stability is likely to be both difficult and tedious and furthermore will require a knowledge of the solution. An alternative approach, similar to that used in Section 8 for the blocked rotor transient behaviour may be adopted. In order to illustrate the method a solution to (12.3) will be sought on the assumption that the speed is an independent variable.

The solution will be assumed to take the form

$$S = \sum_{n=-r}^{r} (a_n \cos S_n \tau - b_n \sin S_n \tau) \qquad \ldots\ldots(12.16)$$

where a_n and b_n are both slowly varying functions of time. Application of the method used in Section 10 or use of the principle of harmonic balance leads to the following set of first order equations, after assumptions similar to those in Section 8 are made:-

$$2S_n \dot{a}_n = B_n \cos\beta_n - b_n(1-S_n^2) - 2\rho S_n a_n + \frac{3}{8} \sum_{K=0}^{\mu} d_K \Delta_n \left[\begin{array}{l} A_{K+n} \sin\overline{\delta_K - \varepsilon_n} - A_{-K+n} \sin\overline{\delta_K + \varepsilon_n} \\ -B_{K+n} \cos\overline{\delta_K - \varepsilon_n} - B_{-K+n} \cos\overline{\delta_K + \varepsilon_n} \end{array} \right]$$

$\ldots\ldots(12.17)$

$$2S_n\dot{b}_n = B_n\sin\beta_n - 2\rho S_n b_n + a_n(1-S_n^2)$$
$$+ \frac{3}{8}\sum_{K=0}^{\mu} d_K\Delta_n\left[\begin{array}{l} A_{K+n}\cos\overline{\delta_K-\varepsilon_n}+A_{-K+n}\cos\overline{\delta_K+\varepsilon_n} \\ +B_{K+n}\sin\overline{\delta_K-\varepsilon_n}-B_{-K+n}\sin\overline{\delta_K+\varepsilon_n}\end{array}\right]$$

.....(12.18)

where all $B_n = 0$ for $n \neq 0$;

$$\tan\varepsilon_n = 2\rho S_n$$

$$\Delta_n = \sqrt{1+4\rho^2 S_n^2}$$

and the A and B arise as coefficients of the fundamental cosine and sine terms respectively in S^3, where S is given by (12.16).

Equations (12.17) and (12.18) are essentially identical on the R.H.S. with (10.23) and (10.24) except that the latter pair include the effect of iron loss and are written in terms of amplitude and phase parameters rather than two amplitude components. Thus in (12.17) and (12.18), a_n and b_n correspond to $a_n\cos\eta_n$ and $a_n\sin\eta_n$ respectively in (10.23) and (10.24).

A solution to (12.17) and (12.18) will correspond to $\dot{a}_n = \dot{b}_n = 0$. We can examine the behaviour in the vicinity of such a steady state solution by studying the incremental equations as in the previous section. Thus if a particular set of values (a_{n_o}, b_{n_o}) comprise a solution to these equations, and we displace the system by an incremental amount, we may represent the subsequent solution by $a_{n_o}+\xi_n(t)$, $b_{n_o}+\varepsilon_n(t)$ so that we have:

$$2S_n\dot{\xi}_n = \sum^{n} \left[\frac{\partial(\text{RHSof12.17})}{\partial a_n}\,\xi_n + \frac{\partial(\text{RHSof12.17})}{\partial b_n}\,\epsilon_n\right] \quad \ldots.(12.19)$$

$$2S_n\dot{\epsilon}_n = \sum^{n} \left[\frac{\partial(\text{RHSof12.18})}{\partial a_n}\,\xi_n + \frac{\partial(\text{RHSof12.18})}{\partial b_n}\,\epsilon_n\right] \quad \ldots.(12.20)$$

Equations (12.19) and (12.20) now comprise a set of first order linear equations with constant coefficients; so that the standard methods of investigation appropriate to such equations, may be invoked.

The foregoing comments serve to indicate some possible approaches to the problem of determining the stability of solutions to the system equations. These approaches have not been followed up in this report however, for reasons suggested in Section 12.2.

CHAPTER 13

Further work

In the preceding sections of this report some of the inherent characteristics of a particular class of energy transducers have been investigated. The indications are that such devices are unlikely to be of commercial interest as certain disadvantages have emerged. It is the purpose of this Chapter to indicate very briefly, possible practical methods of improving the performance as well as to indicate further avenues of theoretical analysis and practical development.

13.1 Practical development

Some of the more serious disadvantages are:-

(i) more or less severe line current modulation, increasing with load
(ii) presence of higher harmonics in the line current
(iii) pulsating negative and positive torque pulses
(iv) unsatisfactory shape of torque-speed curve
(v) apparently have an inherently low efficiency
(vi) non self starting

Before discussing possible ways of either removing or improving these characteristics a rough analogy will be drawn between these machines and two-stroke internal combustion engines.

Each develops alternate positive and negative torque pulses, i.e. there is a compression and a firing stroke, with firing corresponding to the initiation of the jump. Increasing

supply voltage has an effect akin to advancing the spark, with both machines capable of going into an oscillatory mode instead of rotating, if this process in overdone.

With this analogy in mind it is not surprising that the remedies for some of the disadvantages ((i)-(vi)) above will be analogous to those employed for internal combustion engines.

Thus a "two cylinder" machine with rotors 180° out of phase, with the stators fed in parallel will reduce the total line current modulation and decrease the torque pulsations. However current harmonics will still be present; so a "six cylinder" machine connected as shown in Figure 13.1 will allow much of the harmonic current to circulate within the delta. Suitable adjustment of the relative rotor positions will reduce the torque pulsations still further.

Figure 13.2 shows galvanometer recordings of the instantaneous current waveform at three different positions in the circuit for different load conditions. It is clear that the modulation and harmonic content of the line current is significantly less than for individual stator windings.

Such a machine configuration also allows for the possibility of improving the shape of the torque speed curve by using different values of capacity with each stator winding. Figure 13.3 shows the result of adding two of the measured torque speed curves of the prototype machine.

Plate 13.1 shows a picture of an experimental "six cylinder" machine, which is essentially a linear machine having a "rotor" of the form of that shown in Figure 15 of Appendix I, but bent into a continuous circle for convenience. Five of the stator coils and associated magnetic circuits can be moved

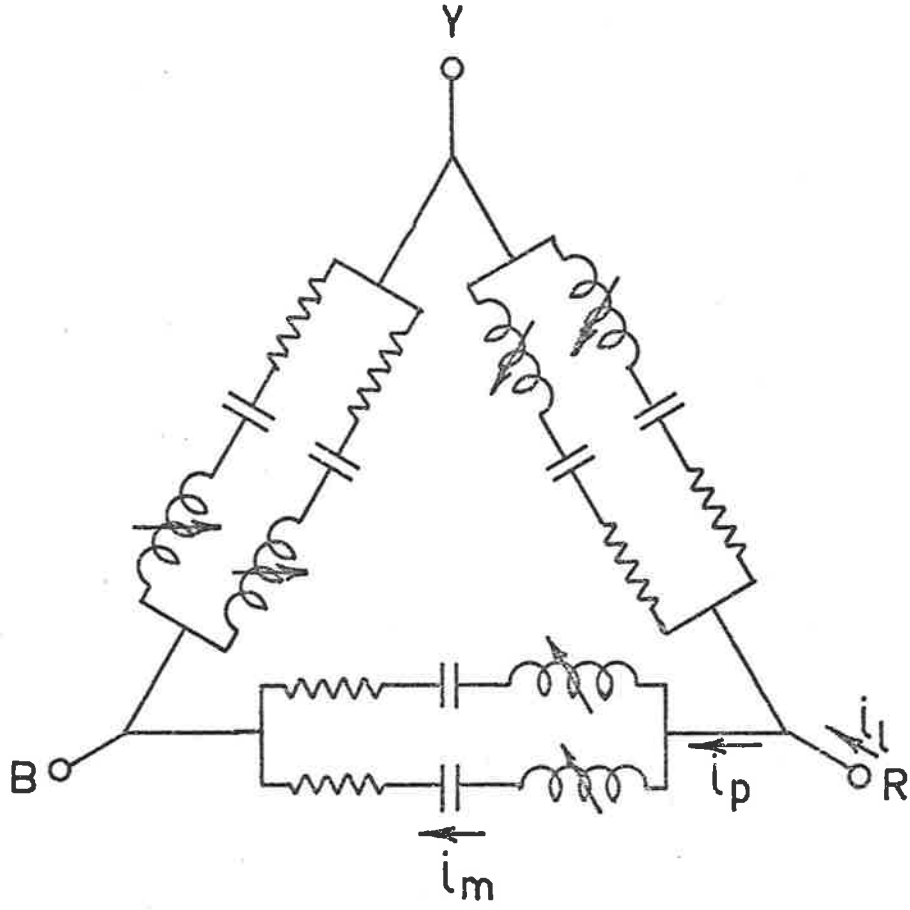

FIGURE 13.1: CONNECTIONS FOR 3 PHASE SIX 'CYLINDER' MACHINE

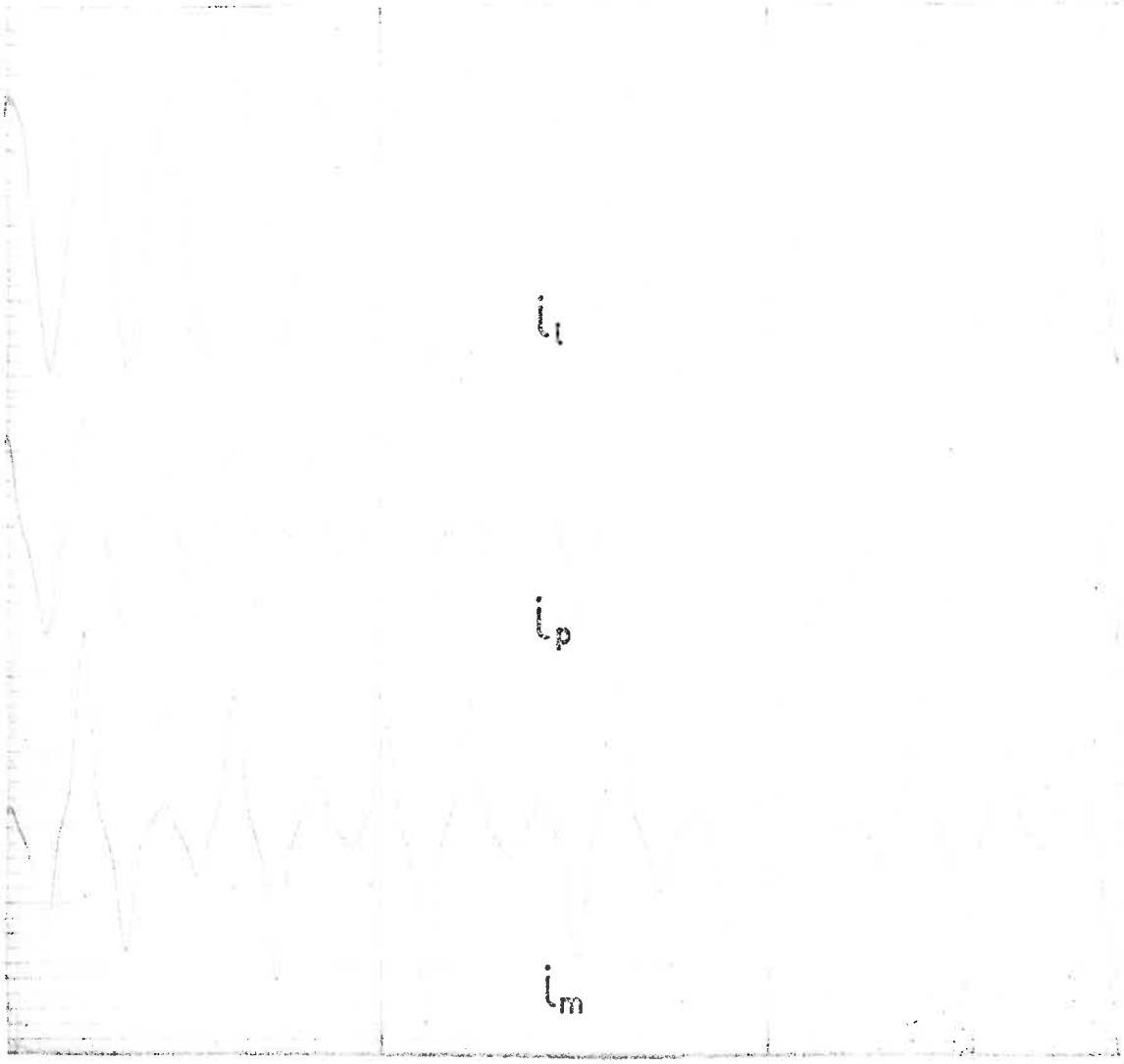

Currents i_l i_p & i_m in figure 13.1
Rotor speed ≃ 77 r p m

FIGURE 13.2a : CURRENT WAVEFORMS

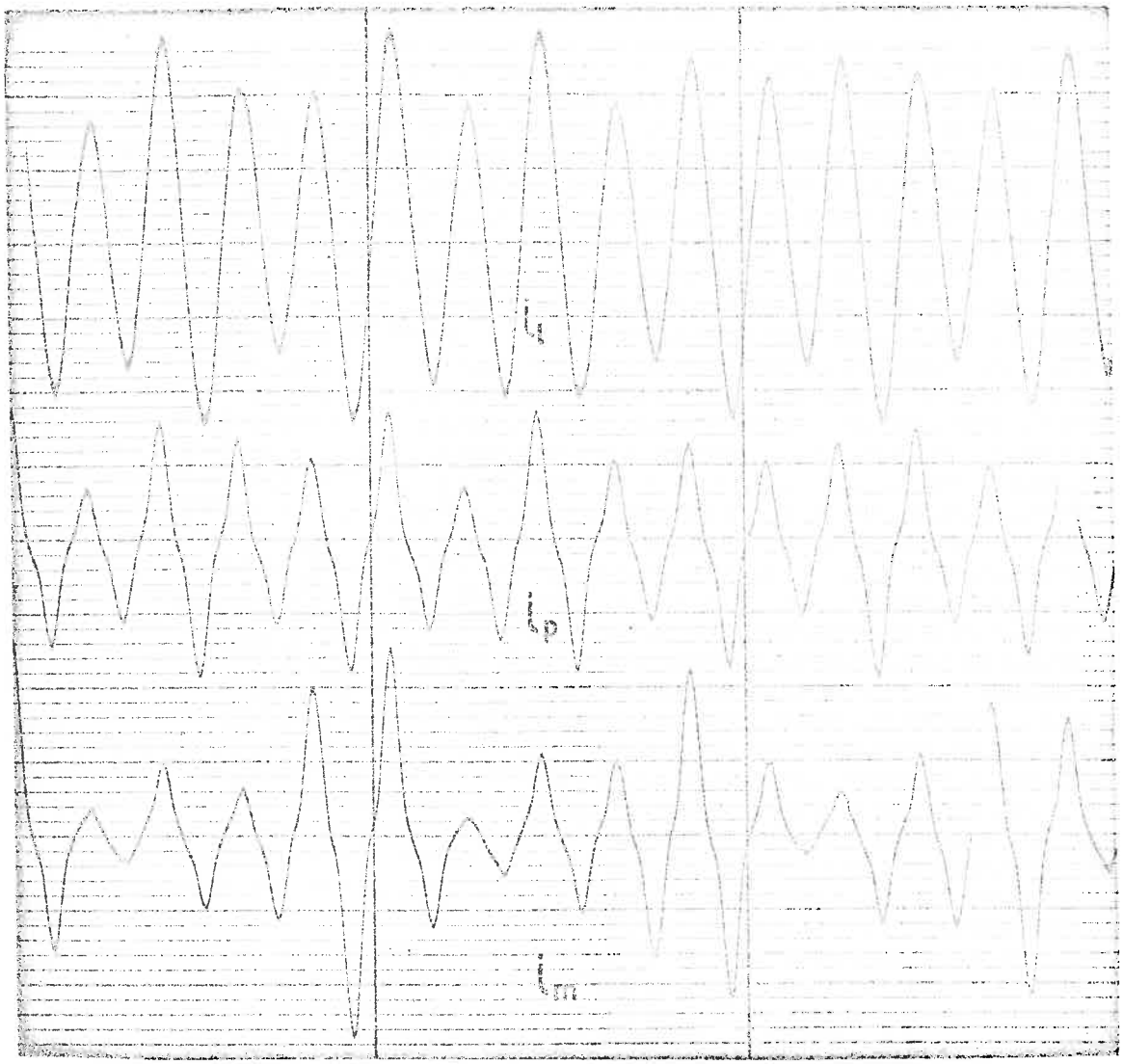

Currents i_l i_p & i_m in figure 13.1

Rotor speed ≃ 40 r p m

FIGURE 13.2b : CURRENT WAVEFORMS

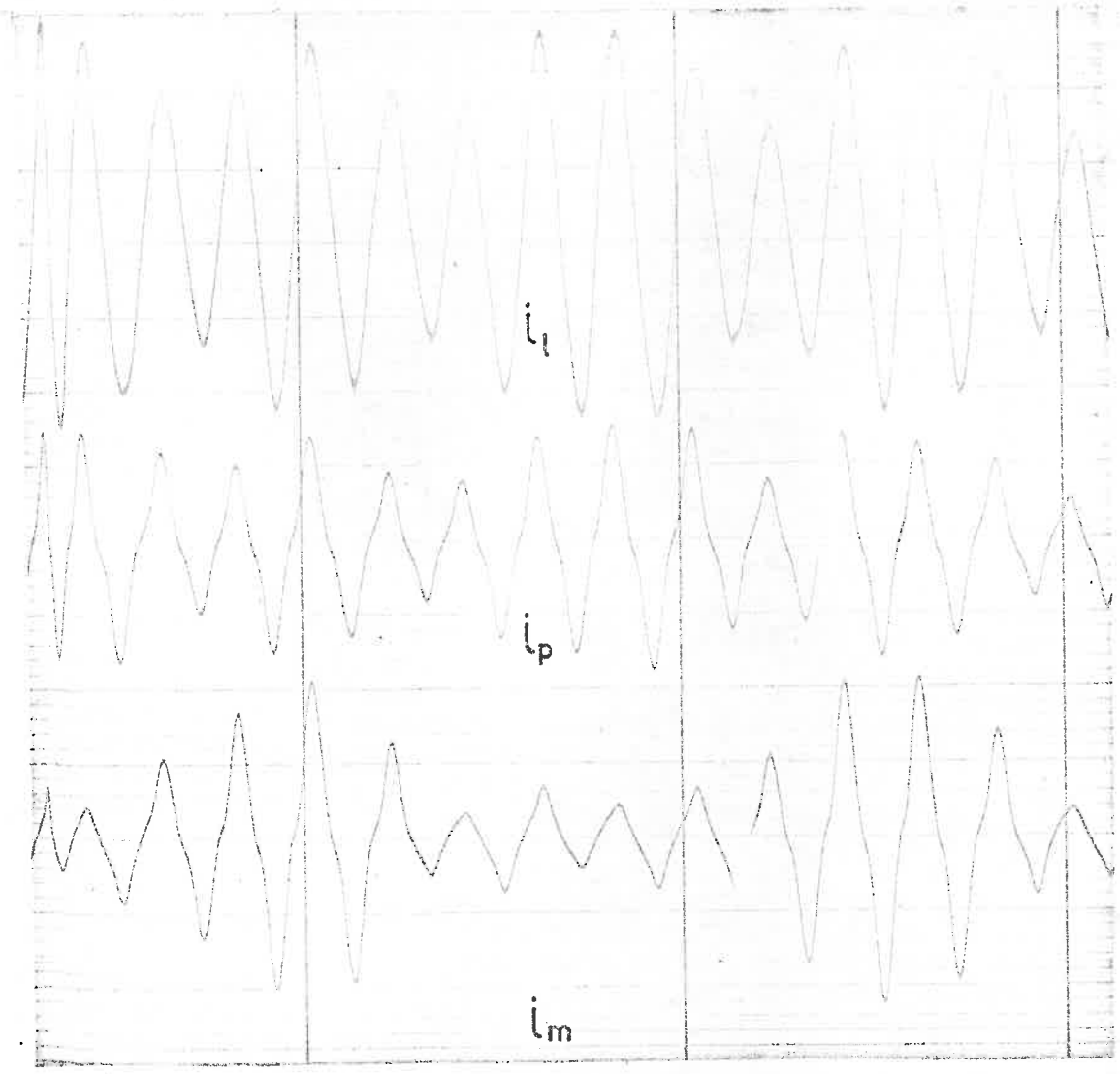

Currents i_l i_p & i_m in figure 13.1

Rotor speed $\simeq$ 22 r p m

FIGURE 13.2c: CURRENT WAVEFORMS

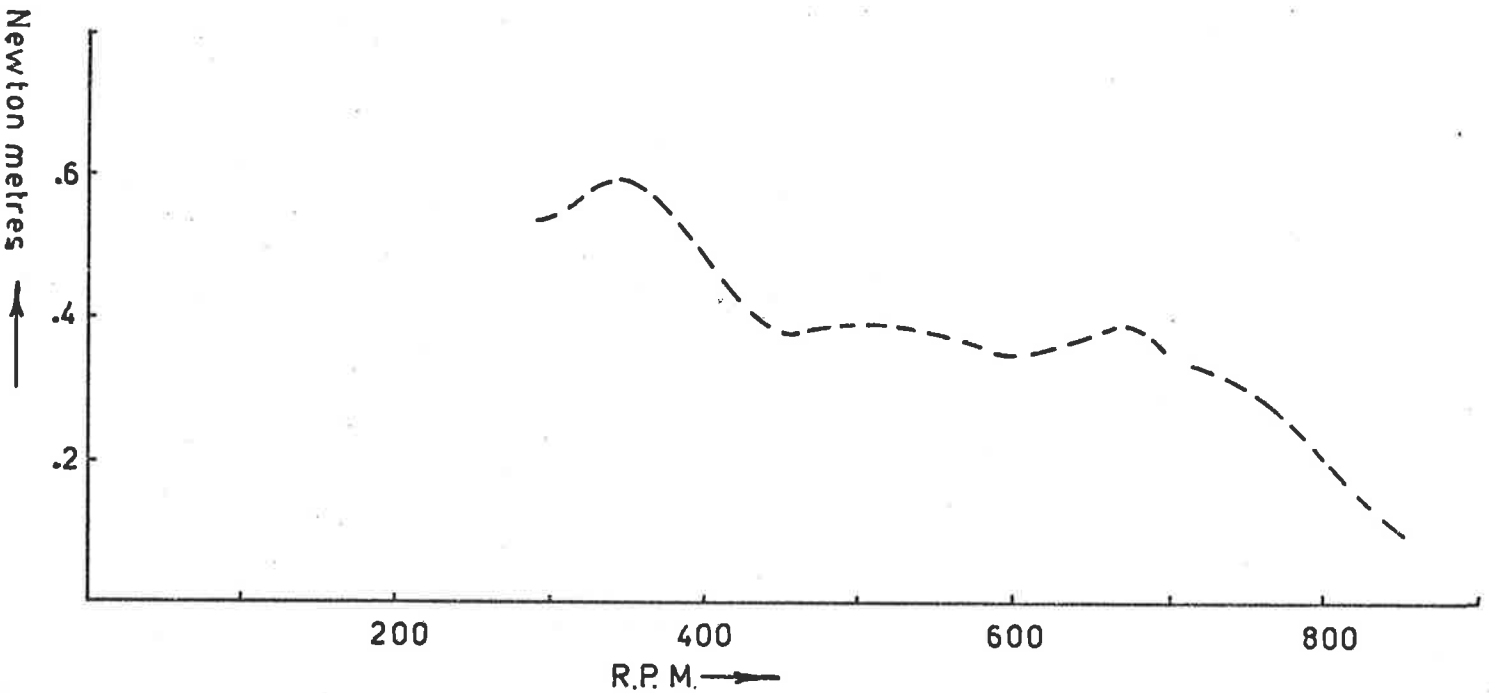

Summation of measured torque speed curves for: C = 104.5 μf, C = 139.5 μf] V = 160 volts

FIGURE 13.3

PLATE 13.1

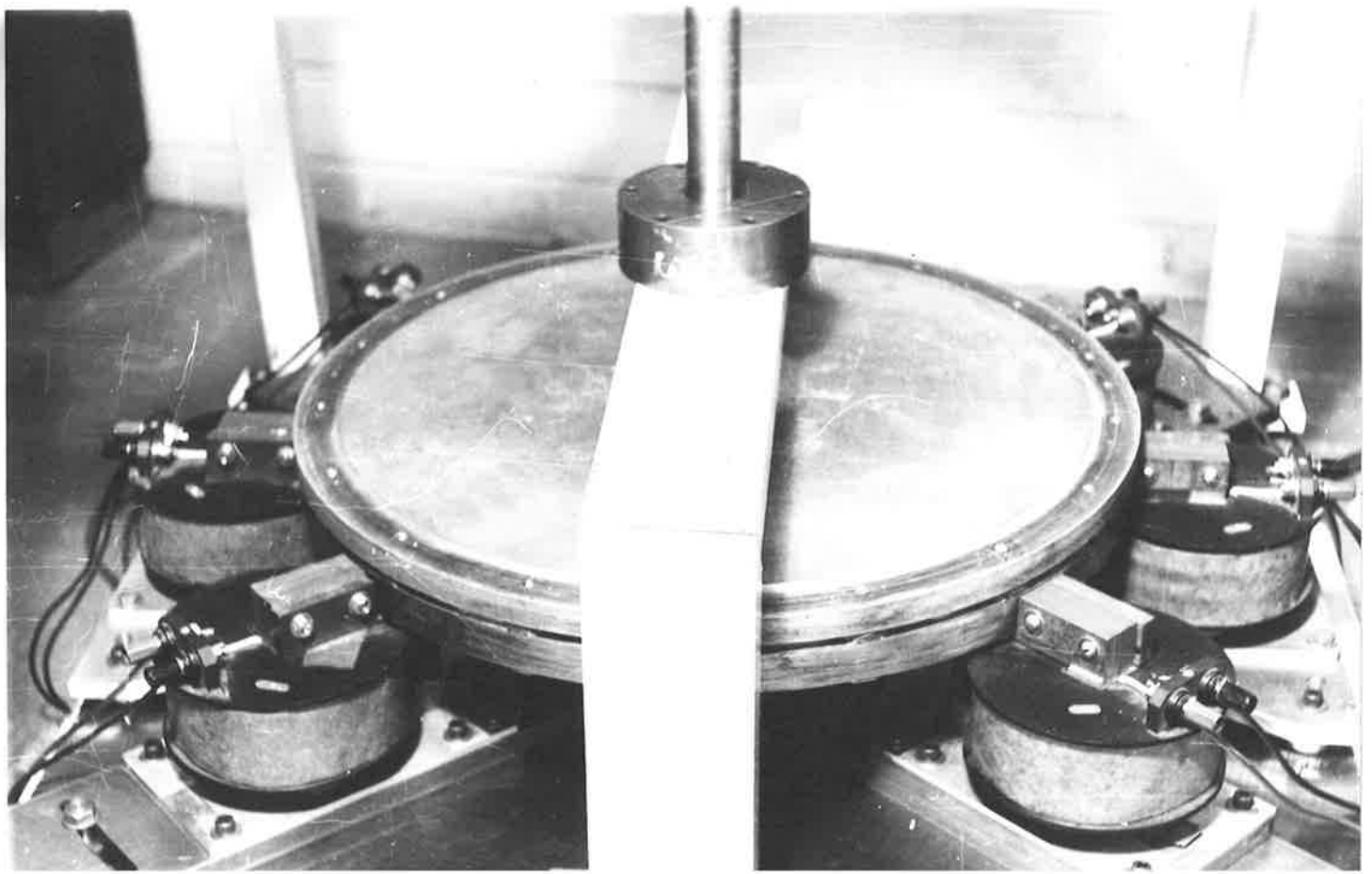

cir-cumferentially with respect to each other.

For this particular configuration, (vi) above requires an affirmative answer to the question: "Is it possible to so position the six stator coils that there is always a nett positive torque in one direction at standstill, for all armature positions?"

The use of sintered ferrite core material might solve the difficult problem of constructing compact "multicylinder" machines of laminated material while distributed polyphase stator windings offer further possibilities.

13.1.1 Power springs

Perhaps the most promising use for a machine utilising the principles under investigation is to provide a return spring mechanism which has a power gain. Such a device is shown schematically in Figure 2.2(d). The work done by the spring and armature as the spring expands, exceeds the work done in compressing the spring. A possible use would be in the weaving industry as a shuttle drive. However, all such linear devices suffer from the problem of alignment, because the transverse magnetic forces can very easily exceed the useful longitudional components.

Plate 2 shows a rotary version of a lossless spring, which uses a conventional $\frac{1}{4}$ horsepower induction motor frame and laminations, shaped as shown in Figure 2.2(b), as the armature to sustain repeated oscillations of 1 kgm over a vertical height of about 2 metres.

13.2 Theoretical development

The theoretical analysis presented in this report has been concerned with the most elementary form that such machines

PLATE 13.2

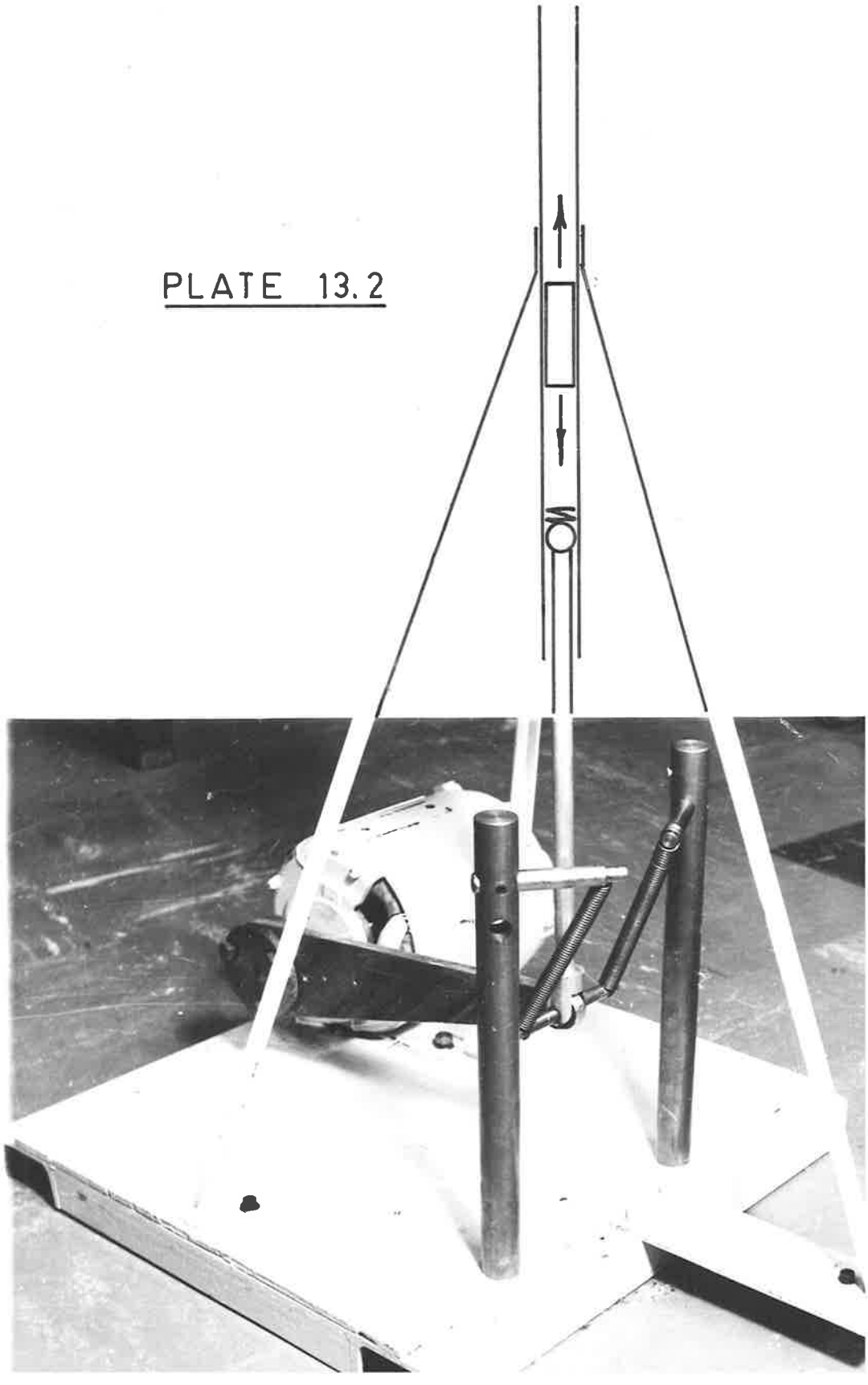

can assume. However, a number of interesting and perhaps fruitful possibilities exist for further development. Some are discussed briefly below.

13.2.1 Additional coupled circuits

The analysis so far presented has shown that a particular sideband component of the flux linkages associated with the circuit approaches resonance and hence tends to predominate in the solution, whenever the particular sideband frequency approaches the effective natural frequency of the circuit under these conditions of double excitation. The torque which results was shown to depend upon the energy dissipated at the particular sideband frequency; i.e. it depends upon the impedance of the circuit external to the time varying inductance Thus the two processes are to a certain extent independent; so that provision of additional coupled circuits of selected impedances may enable the relatively simple behaviour of the devices so far discussed, to be modified in a useful manner.

13.2.2 Three phase stator supply

The analytical problem involved would be difficult; so that it might best be investigated as a two phase supply (unbalanced four phase). It offers the possibility of starting torque.

13.2.3 Topology

Nothing has been said in this report about the optimum shape of such a machine for a given purpose nor about the assigning of a goodness factor [20]. It is a simple matter to show however, that for a given shape of machine, flux density and γ that:-

$$V \sqrt{\frac{C}{\text{Volume}}} = \text{constant} \qquad \ldots\ldots(13.1)$$

and furthermore that for a given saturation factor

$$D_o \propto \left(\frac{f}{V}\right)^2 \qquad \ldots(13.2)$$

Power available is proportional to the supply frequency, under the conditions of (13.1).

14. Conclusions

This report is concerned with the presentation and interpretation of some experimentally determined characteristics of one particular example of a class of electromechanical energy convertors, which depend for their action upon the behaviour of a series RLC circuit in which the inductance is both time and current dependent (in this case the stator winding inductance).

These results show that it is possible to construct a single phase machine, having neither electrical connections to, nor windings on the rotor, which is capable of operating over certain speed ranges as either a motor or a generator.

Furthermore, these experimental results indicate that such simple machines suffer from a number of practical disadvantages, the most significant of which are:-

(i) more or less severe line current modulation, increasing with load.
(ii) presence of a higher harmonies in the line current
(iii) pulsating negative and positive torque pulses
(iv) unsatisfactory shape of torque-speed curve
(v) apparently have an inherently low efficiency
(vi) not self starting

Discussion in Section 13 deals with possible methods of reducing disadvantages (i)-(iv) by suitable combinations of two or more elementary machines, while Section 11 presents an analysis and a discussion on the efficiency of such machines. This discussion indicates that an upper limit to the efficiency at any speed whilst operating as a motor is likely to be of the order of 50%.

Item (vi) above has not been resolved.

On the other hand such machines do possess characteristics which may be desirable under certain conditions.

For example:

(i) simpler construction than a squirrel cage induction machine

(ii) may operate over a range of speeds (determined by the intersection of the load and machine torque/speed characteristic)

(iii) whilst the maximum efficiency at any speed is unlikely to exceed 50% as discussed in Section 11, it is also shown that while these machines are still subject to the principle that conversion efficiency equals 1-slip, their effective pole number increases with decreasing speed; so tending to maintain conversion efficiency as the speed falls.

(iv) operating speed may be influenced by the supply voltage, series capacity or series resistance.

Perhaps the most remarkable feature of the experimental results is the shape of the torque speed curves, which resemble a series of skewed resonance curves; so the majority of this report is concerned with presenting both a physical explanation and an approximate analysis of the essential behaviour of this class of machines.

Thus, a mathematical model of the machine has been proposed and used to simulate the prototype machine on an analogue computer. Comparison of the results from the latter with the experimental data shows that the model behaves qualitatively as the original but that there are certain

quantitative discrepancies. Discussion in Section 5 attributes these discrepancies to inadequate representation of the iron losses and to analogue computer limitations. Nevertheless the agreement is such that use of the mathematical model as a means of representing the essential features of such machines appears justified.

As this model comprises a pair of non linear differential equations having periodic coefficients, results obtained from one set of input and system parameters cannot be extrapolated to another, while an explicit analytic solution is unlikely to exist.

This report has deliberately avoided the problem of finding an adequate model for the core losses as this alone would be a major problem, but has concentrated on the effects of periodic variation of a saturating inductance. Therefore, some results for somewhat idealised machines having no iron losses were obtained by analogue computer (Section 5) and by numerical methods (Section 6). Comparison of these results with those obtained by an approximate analytical solution for a system having a sufficiently large inertia that the speed may be regarded as an independent variable, shows that agreement between all three approaches is good in certain regions but less so in others for possible reasons discussed below.

Conclusions to be drawn concerning the physical behaviour of the system from Sections 7-9, in conjunction with the results from analogue, numerical and analytical solutions, may be summarised as follows:-

(i) The combination within the saturating stator inductance of the effects of the external stator supply at frequency ω_1 and the effective mechanical forcing frequency $p\omega_m \equiv \omega_2$,

due to the p-pole rotor turning at ω_m, results in the generation of a series of frequency components comprising integral multiples of ω_1 and ω_2 together with the sums and differences of these multiples.

(ii) In general the electrical circuit has three energy storage elements, one capacitive and two inductive with the two latter partially isolated by the effect of iron losses. Thus resonant response of a particular component of the solution (flux linkage or current) will occur whenever the rotor speed is such that the particular sideband frequency in question approaches a system natural frequency.

(iii) The natural frequencies of the system involving the capacitive element and the non linear inductive element, under conditions of external and internal forcing are dependent upon, and tend to increase with the amplitude of response which in turn is dependent upon the amplitude and frequency of both forcing functions.

(iv) The relative amplitude of the various sidebands in the solution will be related closely to the nearness or otherwise of their frequency to a natural resonant frequency. It is shown that because the external supply frequency is always greater than the small signal natural frequency, upper sidebands based on ω_1 never approach the main system resonance and except under certain conditions discussed in 10.1, will play a small role in the solution and hence may be neglected as a first approximation.

(v) Thus the approximate solution comprises a fundamental ω_1 plus a series of lower sidebands $\omega_1 - k\omega_2 \equiv \omega_1 - kp\omega_m \equiv \omega_{s_k}$ which

over an appropriate range of rotor speeds ω_m, will pass through resonance in turn. The Manley-Rowe relationships may be invoked to demonstrate the power-frequency relationships among the various sidebands and it is shown that the average asynchronous torque developed may be related to the amount of energy dissipated by the various sidebands in any lossy elements coupled to the circuit, provided that ω_1 and ω_2 are incommensurable. Hence the speed torque curve comprises a series of resonant responses, skewed in the direction of increasing ω_s (decreasing rotor speed for +ve ω_s).

(vi) Synchronous torques are developed at rotor speeds which are integral fractions of synchronous speed. As the two sources of frequency are still incoherent (but not incommensurable) at these speeds, the Manley-Rowe relationships still apply and may be used to evaluate asynchronous, but not synchronous torque. In general, under conditions of finite inertia the latter are too small to be of any practical significance.

(vii) The alternating positive and negative torque pulses result in a rotor speed which fluctuates about an average value with the amplitude of the fluctuations inversely related to the system inertia.

(viii) At rotor speeds such that $\omega_1 - kp\omega_m \equiv \omega_s$ becomes negative, induction generator action results which means that average torque due to the particular sideband is negative and mechanical energy is converted to electrical energy at ω_s into a sink and at ω_1 back to the supply.

The analytical solution takes the form of a set of simultaneous non linear algebraic equations which must be solved to give the various sideband amplitudes and phases. In general

it appears that the more sidebands incorporated within the solution the nearer the final result approaches that obtained from analogue or numerical methods except for certain regions where the system inertia is critical.

The analytical solution merely represents a possible solution to the system equations when the inertia is sufficientl great that the speed may be regarded as an independent variable. It also fails to represent adequately the iron losses. Nevertheless good agreement results on the negative slope portio of the speed torque curves both for the prototype machine and for the idealised machines. On the other hand much uncertainty exists concerning the position of the positive slope portion of these curves and of the peaks. It is clear from the results tha these are sensitive to system inertia but no systematic investigation was undertaken on this point because:-

(a) the results in these regions were unobtainable within the limit of reasonable analogue computer accuracy because of the long settling time. i.e. limit cycles were themselves subjected to limit cycles.

(b) the unsatisfactoriness of the numerical method without a graphics terminal

(c) the analytical solution would have been quite unwieldy if speed fluctuations had been allowed. Even with this restrictior computational time is prohibitive.

The agreement between the various methods of solution and between the analytical and experimental results for the prototype suggests that the mathematical model and the associated analyses of the characteristics of this model do represent substantially the essential behaviour of such

machines and may be used as a basis for establishing design criteria.

15 REFERENCES

1. Anderson, B.D.O., "When do the Manley-Rowe relations really hold?"; Proc.IEE, Vol 113, No.4, 1966

2. Bekey, G.A., and Karplus, W.J.; "Hybrid Computation"; (Wiley, 1968).

3. Bloch, A.; "Power relations in non-linear reactors"; Proc.IEE,Vol.115, No.1, 1968

4. Bellman, R.; "Perturbation Techniques in Mathematics, Physics and Engineering" (Holt,Rinehart and Winston, 1964).

5. Bellman, R.; "Stability Theory of Differential Equations" (McGraw-Hill, 1953)

6. British Patent Application 6738/31

7. British Patent Specification 10043/49

8. British Patent Specification 769/67

9. Cunningham, W.J.; "Introduction to non-linear analysis", (McGraw-Hill, 1958)

10. Fitzgerald, A.E. and Kingsley, C.; "Electric Machinery" (McGraw-Hill, 1961, 2nd edition).

11. Fischer, J.and Moser, H.; "The Representation of the Magnetization Curve by Simple Algebraic and Transcendental Functions"; Arch,Electrotech. 1956, 42 pp.286-299.

12. Hahn, W.; "Theory and Application of Liapunov's Direct Method"; (Prentice-Hall, 1963)

13. Hayashi, C.; "Non-linear Oscillations in Physical Systems"; (McGraw-Hill, 1964)

14. Hayward, J.; "The Development of Adders and Integrators for an Electronic Differential Analyzer"; M.E. Thesis, University of Adelaide, 1953.

15. Hsu, J.C. and Meyer, A.U.; "Modern Control Principles and Applications"; (McGraw-Hill, 1968).

16. Jayawant, B.V., and Rea, D.P.; "Multimodal and transitional behaviour in second-order nonlinear systems"; Proc.IEE, Vol.115, No.6, 1968.

17. Korn, G.A. and Korn, T.M.; "Electronic Analogue and Hybrid Computers"; (McGraw-Hill, 1964)

18. Ku, Y.H., Wolf, A.A., and Dietz, J.H.; "Taylor-Cauchy transforms for analysis of varying parameter systems"; Proc.IRE, June, 1961.

20. Laithwaite, E.R.; "Induction Machines for Special Purposes"; (Newnes, 1966).

21. Manley, J.M. and Rowe, H.E.; "Some general properties of nonlinear elements"; Proc.Inst.Rad.Engrs., Vol.44, 1956, P.904.

22. McLachlan, N.W.; "Ordinary Non-linear Differential Equations"; Oxford, 1965, 2nd ed.

23. Nicholson, A.F.; "Periodic solutions of van der Pol and Duffing equations"; IEEE Trans. on Circuit Theory, Vol.CT-12, No.4, 1965.

24. Pipes, L.A.; "Operational Methods in Nonlinear Mechanics" (Dover, 1965).

25. Pollard, J.; "Numerical Computing", (Science Press, Sydney, 1967).

26. Porter, B.; "Stability Criteria for Linear Dynamical Systems"; (Oliver and Boyd, 1967)

27. Possingham, M.L.; "The Selection and Development of a Multiplier for use with an Electronic Differential Analyzer"; M.E. Thesis, University of Adelaide 1955.

28. Powell, M.J.D.; "A Fortran Subroutine for Solving Systems of Nonlinear Algebraic Equations"; AERE-R.5947, Nov-1968.

29. Rudenberg, R.; "Transient Performance of Electric Power Systems"; (McGraw-Hill, 1950)

30. Seidel, H.; "Viewpoints on Parametric Interactions: The Frequency Relations"; (Bell Telephone Laboratories, Report)

31. Smith, B.H.; "Asynchronous Reluctance Motor Using Ferroresonance"; Proc.IEE, Vol.114, No.11, November, 1967.

32. Smith, B.H.; "A Simple Bilateral Variable-Ratio d.c. Pulse Converter"; IEEE Trans. on Industrial Electronics, and Control Instrumentation, Vol.IECI-15, No.1, 1968.

33. Smith, B.H.; "Commutation in a Bilateral Variable-Ratio d.c. Pulse Converter"; IEEE Trans. on Ind. Elec. and Control Inst., Vol.IECI-15, No.1, 1968.

34. Sokolnikoff, I.S. and E.S.; "Higher Mathematics for Engineers and Physicists"; (McGraw-Hill, 1941).

35. Teodorescu, D.; "Ferroresonant Servomotor"; Proc.IEE, 1968; Vol.115,No.6, pp842-846.

36. Tomovic, R.; "Introduction to Nonlinear Automatic Control Systems"; (Wiley 1966).

37. Trutt, F.C., Erdelyi, E.A.and Hopkins, R.E.; "Representatio of the Magnetization Characteristic of d.c. Machines for Computer Use"; Proc.IEEE; Winter Power Meeting, New York, 1967, Paper 31, pp.67-77.

38. Vowels, R.E.; "Laplace transform solution of linear differential equations with variable coefficients" AIEE Trans.on Communications and Electronics, Nov. 1963.

39. West, J.C. and Jayawant, B.V.; "A New Linear Oscillating Motor"; Proc.IEE, 1962, 109A, pp 292-300.

40. West, J.C., Jayawant,B.V., and Rea, D.P.; "Transition Characteristics of the jump phenomenon in non line resonant circuits"; Proc. IEE, Vol.114, No.3, 1967.

41. Whittaker, E.T. and Watson, G.N.; "Modern Analysis"; (Cambridge, 1915, 2nd edition).

II(a) Some details and specifications of the analogue computer

The elements available comprise:-

28 Buffers
16 Integrators
4 Adders
1 Diode Function Generator
10 Servo-multipliers
4 Electronic multipliers.

Signal amplitude is restricted to the range ±100 volts, and the basic amplifiers used in all elements have an output noise level of < 5mVp-p.

Integrater gain may be varied in decade steps from 1 to 1000. [14].

Multigang potentiometers are available for the servo-multipliers, the phase lag of which becomes >.08 degrees above 1.0 cycle per second [27].

The electronic multipliers had been built originally as a student project to a design supplied by the Weapons Research Establishment, Salsbury, South Australia. However, the design is such that is is extremely difficult to maintain them within the specified limits of ±.01% over all four quadrants [27]; so that the servo multipliers were used for preference whenever the time scale permitted.

II(b) Generation of $f'(\theta)$ and $f(\theta)$

Implementation of equations (5.1) to (5.4) on an analogue computer requires the formulation of both $f(\theta)$ and $f'(\theta) \equiv d(f(\theta))/d\theta$. The former can be developed from the latter by integration as follows:-

$$\int f'(\theta)d(\theta) = \int [\frac{df(\theta)}{d\theta} \frac{d\theta}{dt}]dt = \int df(\theta) = f(\theta) \quad .....(II.1)$$

Since $d\theta/dt \equiv \dot{\theta}$ is available in the problem set up, it is only necessary to multiply $f'(\theta)$ by $\dot{\theta}$ and integrate with respect to time, whilst making provision for the correct initial condition. Now θ is a dependent variable representing the angular position of the rotor, is continuous and increases indefinitely with time, but must be represented by a voltage which must not exceed 100. The problem can be overcome by reversing $\dot{\theta}$ after every one half pole pitch as suggested in Figure 5.4, to give a periodic function of θ which may then be applied to a diode function generator representation of $f'(\theta)$ over one half of one pole pitch. By reversing the sign of the output from the function generator, simultaneously with the reversal of $\dot{\theta}$, the correct form of $f'(\theta)$ results. By this means, θ can be kept within bounds and furthermore due to the symmetry of $f(\theta)$, the number of break-points available to form the approximation to $f'(\theta)$ is effectively doubled.

Details of the block diagram, electronic switch and compensating circuit are shown in Figure A.II.1. The latter circuit which maintains the average value of $f(\theta)$ constant at all operating speeds, is required because of the effect finite operating time of the change over relay.

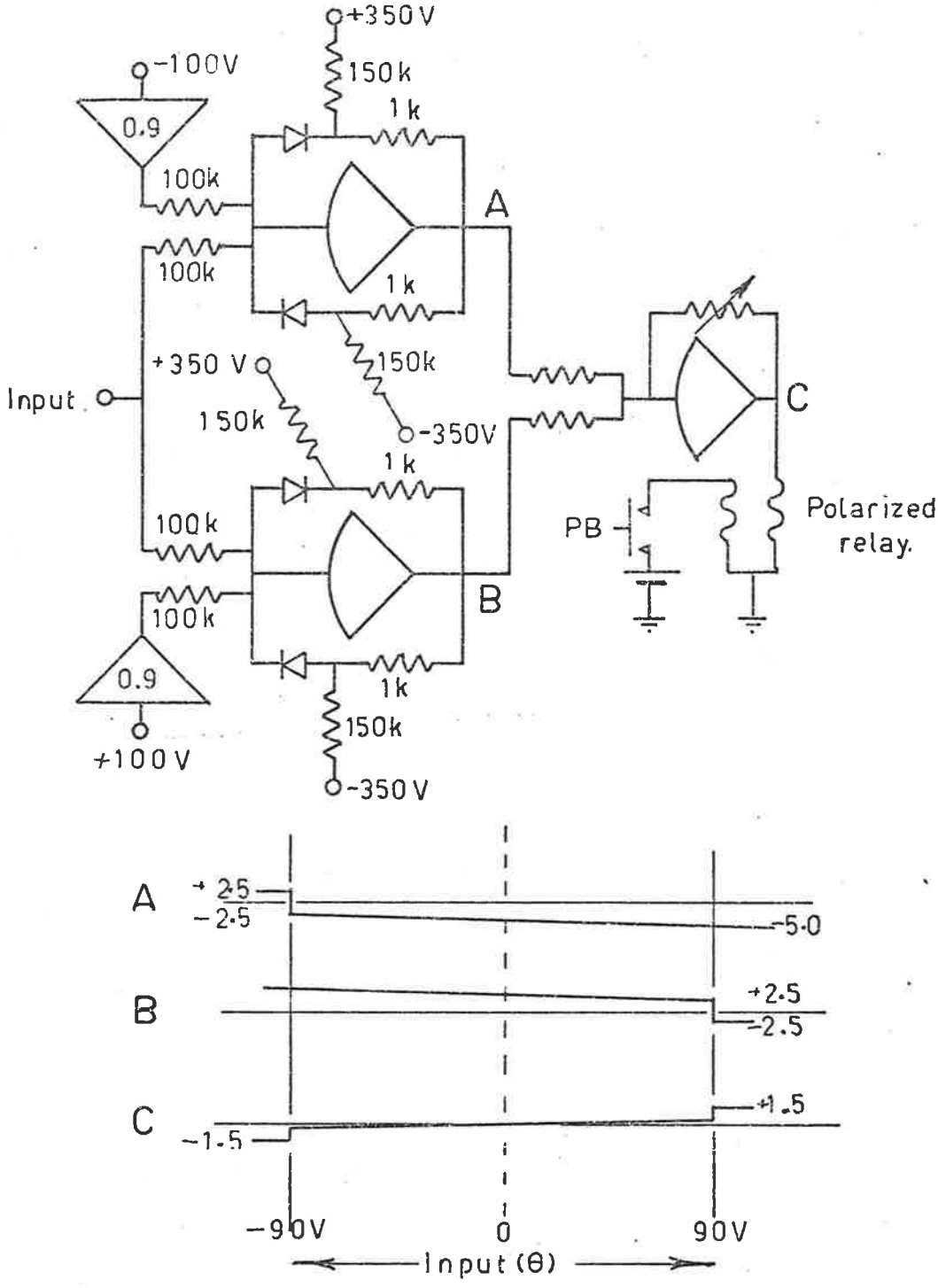

FIGURE AII.1a: ELECTRONIC SWITCH

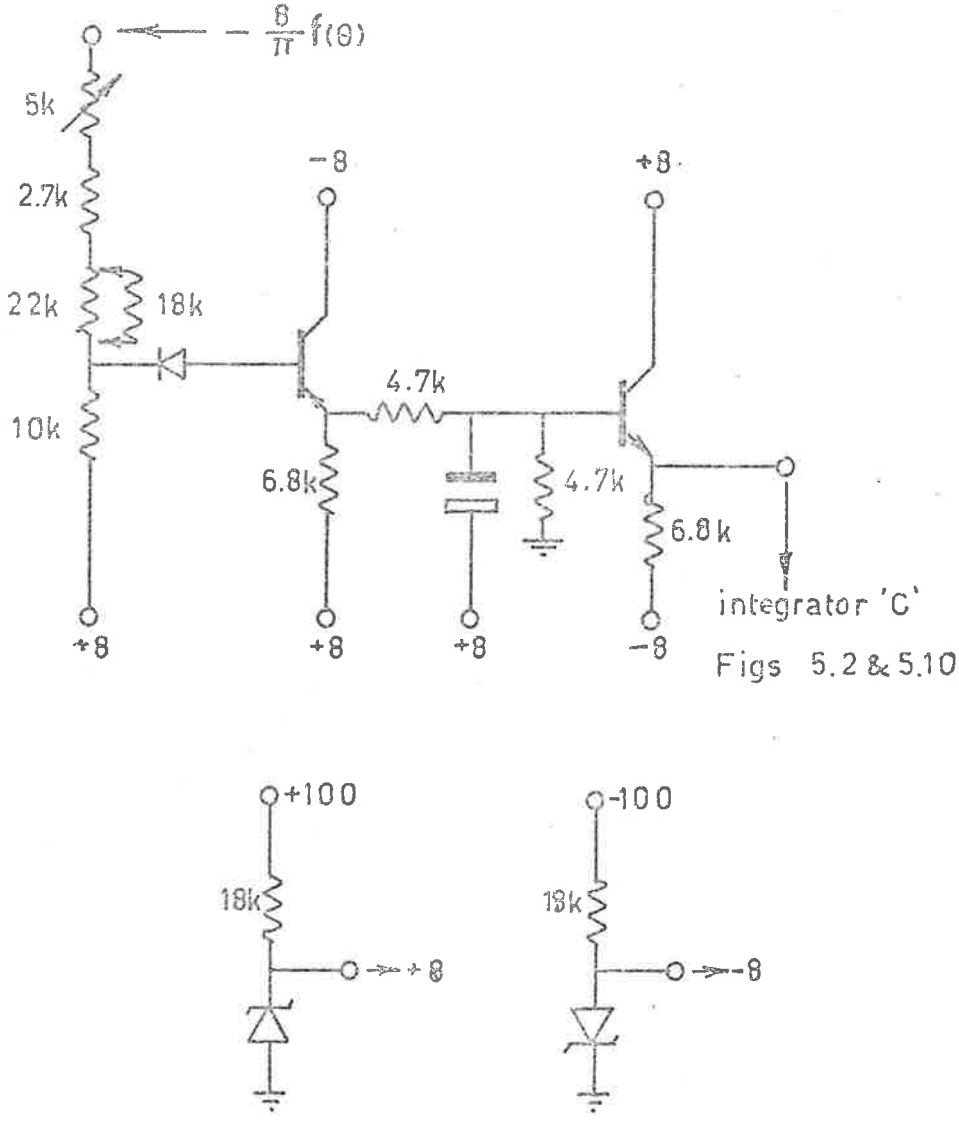

FIGURE AII.1b: STABILIZING CIRCUIT FOR F(θ)

II(c) Analogue computer scaling factors

In general, the amplitude scaling factors used in different portions of the analogue circuit were changed as circuit parameters were changed. The aim at all times being to keep the peak signal at any point in the network as close to ± 100 volts as possible. Tabulation of these scale factors for the numerous circuits and conditions serves no useful purpose.

Time scale factors were determined by the servo multiplier response. In the circuits of Figures 5.1 and 5.2 the wiper arms had to follow λ, whereas in the circuits of 5.9 and 5.10 they had to follow the rather more slowly varying $f(\theta)$. At 750 r.p.m., for a two pole machine, the second harmonic component of $f(\theta)$ has the same frequency as the supply voltage and hence the same as the fundamental component of λ.

Time scale factors of 100 and 20, respectively, were used in the two different simulations.

Typical values for the variables in Figures 5.9 and 5.10 were:-

$$3i;\quad 50\lambda,\ \frac{80}{\pi}\dot{\theta},\ \text{and}\ 800\ddot{\theta}$$

so leading to the following equations

$$(50\lambda) = 2.5\int v\,d\tau - \frac{5R}{6}\int (3i)\,d\tau - \frac{1}{24C}\iint (3i)\,d\tau \qquad .....(II.2)$$

$$(3i) = \frac{3}{50L_o}\left((50\lambda) + \frac{(50\lambda)^3}{2500} f(\theta)\right) \qquad .....(II.3)$$

$$\text{and } (800\ \ddot{\theta}) = -\frac{F}{J}\frac{\pi}{2}\left(\frac{80}{\pi}\dot{\theta}\right) - \frac{(50\lambda)^4\ f'(\theta)}{25JL_o x10^6} \qquad \text{.....(II.4)}$$

which in turn lead to the block diagrams shown in Figures 5.9 and 5.10.

III(a) Average torque under sine flux conditions

Calculation of the average torque under blocked rotor and sine-flux conditions requires the evaluation of:-

$$T_{ave} = -\frac{1}{\pi}\int_0^{\pi} \sum_{n=0}^{h} \frac{f'_n(\theta)\Lambda^{(2n+2)}}{(2n+2)L_o} \sin^{(2n+2)}(\omega t)\, d(\omega t)$$

In particular, the evaluation is required of:-

$$y_{(2n+2)} = \int_0^{\pi} \sin^{(2n+2)}(\alpha)\, d\alpha$$

$$= \int_0^{\pi} \sin\alpha \sin^{(2n+1)}\alpha\, d\alpha$$

$$= \left| -\cos\alpha \sin^{(2n+1)}\alpha \right|_0^{\pi} + \int_0^{\pi} (2n+1)\sin^{2n}\cos^2\alpha\, d\alpha$$

$$= (2n+1)\int_0^{\pi} (\sin^{2n}\alpha - \sin^{(2n+2)}\alpha)\, d\alpha$$

i.e. $$y_{(2n+2)} = \frac{2n+1}{2n+2}\, y_{2n}$$

or $$y_N = \frac{N-1}{N}\, y_{N-2} = \frac{N-1}{N}\cdot\frac{N-3}{N-2}\, y_{N-4} \quad \ldots\text{etc.}$$

In this case N is even; so that

$$y_N = \frac{N-1}{N}\cdot\frac{N-3}{N-2}\cdots\cdots\frac{3}{4}\cdot\frac{1}{2}\int_0^{\pi} d\alpha$$

$$= \frac{N-1}{N}\cdot\frac{N-3}{N-2}\cdots\cdots\frac{3}{4}\cdot\frac{1}{2}\cdot\pi$$

and

$$T_{ave} = -\sum_{n=o}^{h} \frac{f'_n(\theta)\Lambda^{(2n+2)}}{(2n+2)L_o} \cdot \frac{2n+1}{2n+2} \cdot \frac{2n-1}{2n} \cdot \cdots \cdot \frac{3}{4} \cdot \frac{1}{2}$$

i.e.

$$T_{ave} = -\sum_{n=0}^{h} \frac{f'_n(\theta)\Lambda^{(2n+2)}}{L_o} \quad \frac{(2n+1)!}{2^{2(n+1)}((n+1)!)^2} \qquad \ldots\ldots(III.I)$$

III(b) Fundamental component of current under sine-flux conditions.

When $i = \sum_{n=o}^{h} \frac{f_n(\theta)\lambda^{(2n+1)}}{L_o}$

and $\lambda = \Lambda \sin \omega t$

then the rms value of the fundamental component of the current must be given by:-

$$I_f = \frac{2}{\sqrt{2}\pi L_o} \int_{on=o}^{\pi} \sum^{h} f_n(\theta)\lambda^{(2n+1)} \sin \omega t d(\omega t)$$

$$= \frac{\sqrt{2}}{\pi L_o} \int_{on=o}^{\pi} \sum^{h} f_n(\theta)\Lambda^{(2n+1)} \sin^{(2n+2)} \omega t d(\omega t)$$

which, from the development in III(a) becomes

$$I_f = \sum_{n=o}^{h} \frac{\sqrt{2} f_n(\theta)\Lambda^{(2n+1)}}{L_o} \quad \frac{(2n+2)!}{2^{2(n+1)}((n+1)!)^2} \qquad \ldots\ldots(III.2)$$

III(c) RMS component of current under sine-flux conditions

The mean square value of the current must be given by:-

$$\frac{1}{\pi}\int_{o}^{\pi}\left[\sum_{n=o}^{h}\frac{f_n(\theta)\lambda^{(2n+1)}}{L_o}\right]^2 d(\omega t)$$

Now if we represent the power series:-

$$(1+a_1x+a_2x^2+a_3x^3.....)^2$$

by $1+A_1x+A_2x^2+A_3x^3.....$

with $a_n \equiv f_n(\theta)$ then:-

$$A_n = 2f_n(\theta) + \sum_{j=1}^{n-1} f_j(\theta)f_{n-j}(\theta)$$

so that i^2 becomes:-

$$\frac{\lambda^2}{L_o}^2\left[f_o^2(\theta) + \sum_{n=1}^{2h}(2f_o(\theta)f_n(\theta) + \sum_{j=1}^{n-1} f_j(\theta).f_{n-j}(\theta))\lambda^{2n}\right]$$

which, for $\lambda = \Lambda\sin\omega t$ gives:-

$$I_R^2 = \frac{\Lambda^2}{\pi L_o}^2\int_{o}^{\pi}\left[f_o^2(\theta)\sin^2\omega t + \sum_{n=1}^{2h}(2f_o(\theta)f_n(\theta) + \sum_{j=1}^{n-1} f_j(\theta)f_{n-j}(\theta))\right.$$

$$\left.\Lambda^{2n}\sin^{2n+2}(\omega t)\right]d(\omega t)$$

$$= \frac{\Lambda^2}{L_o^2}\left[\frac{f_o^{\,2}(\theta)}{2} + \sum_{n=1}^{2h}\left(2f_o(\theta)f_n(\theta) + \sum_{j=1}^{h-1} f_j(\theta)f_{n-j}(\theta)\right)\right.$$

$$\left.\Lambda^{2n}\frac{(2n+2)!}{2^{2(n+1)}((n+1)!)^2}\right] \qquad \text{.....(III.3)}$$

III(d) Equivalent linear inductance

When dealing with currents which are periodic functions of time, in a circuit element which has a known but non-linear λ-i relationship, an equivalent linear inductance may be defined from the following relationship:-

$$\tfrac{1}{2}L_f I_f^2 = \frac{1}{2\pi}\int_o^{\pi} \lambda i \, d(\omega t)$$

Thus when

$$i = \sum_{n=o}^{h} \frac{f_n(\theta)\lambda^{(2n+1)}}{L_o}$$

and

$$\lambda = \Lambda \sin\omega t$$

$$\tfrac{1}{2}L_f I_f^2 = \frac{1}{2\pi}\int_o^{\pi} \sum_{n=o}^{h} \frac{f_n(\theta)\lambda^{(2n+2)}}{L_o} \, d(\omega t)$$

$$= \frac{1}{2\pi}\int_o^{\pi} \sum_{n=o}^{h} \frac{f_n(\theta)\Lambda^{(2n+2)}}{L_o} \sin^{(2n+2)}\omega t . d(\omega t)$$

which, from III(a), becomes:-

$$\tfrac{1}{2}L_f I_f^2 = \sum_{n=o}^{h} \frac{f_n(\theta)\Lambda^{(2n+2)}(2n+2)!}{2L_o \; 2^{(2n+2)}((n+1)!)^2}$$

Substituting for I_f^2 from (III.2) gives

$$L_f = \frac{L_o}{\sum_{n=o}^{h} \frac{f_n(\theta)\Lambda^{(2n+2)}(2n+2)!}{2^{(2n+1)}((n+1)!)}} \qquad \text{.....(III.4)}$$

$$\text{or} \qquad L_f = \frac{\Lambda}{\sqrt{2}I_f} \qquad \text{.....(III.5)}$$

$$\text{i.e.} \quad \omega L_f I_f = \frac{\omega\Lambda}{\sqrt{2}} = 4.44\Lambda f \qquad \text{.....(III.6)}$$

as would be expected for a sinusoidal flux linkage relationship.

An alternative definition leading to an equivalent linear inductance has been expressed as [22]:-

$$\tfrac{1}{2}L_R I_R^2 = \frac{1}{2\pi}\int_o^{\pi} \lambda i d(\omega t)$$

from which it follows that:-

$$L_R = L_o \frac{\sum_{n=o}^{h} \Lambda^{2n} f_n(\theta) \frac{(2n+2)!}{2^{(2n+1)}((n+1)!)^2}}{f_o^2(\theta) + \sum_{n=1}^{2h}\left(2f_o(\theta)f_n(\theta) + \sum_{j=1}^{n-1} f_j(\theta) f_{n-j}(\theta)\right)\frac{\Lambda^{2n}(2n+2)!}{2^{2n+1}((n+1)!)^2}}$$

.....(III.7)

Relationships between $\omega L_f I_f / I_f$ calculated from (III.5) and (III.2) or (III.4) using the value of $f(\theta)$ found for the prototype machine, are plotted for comparison with the experimentally found characteristics in Figure A.III.1. As might be expected the degree of agreement is similar to that shown in Figures 4.5 and 4.6.

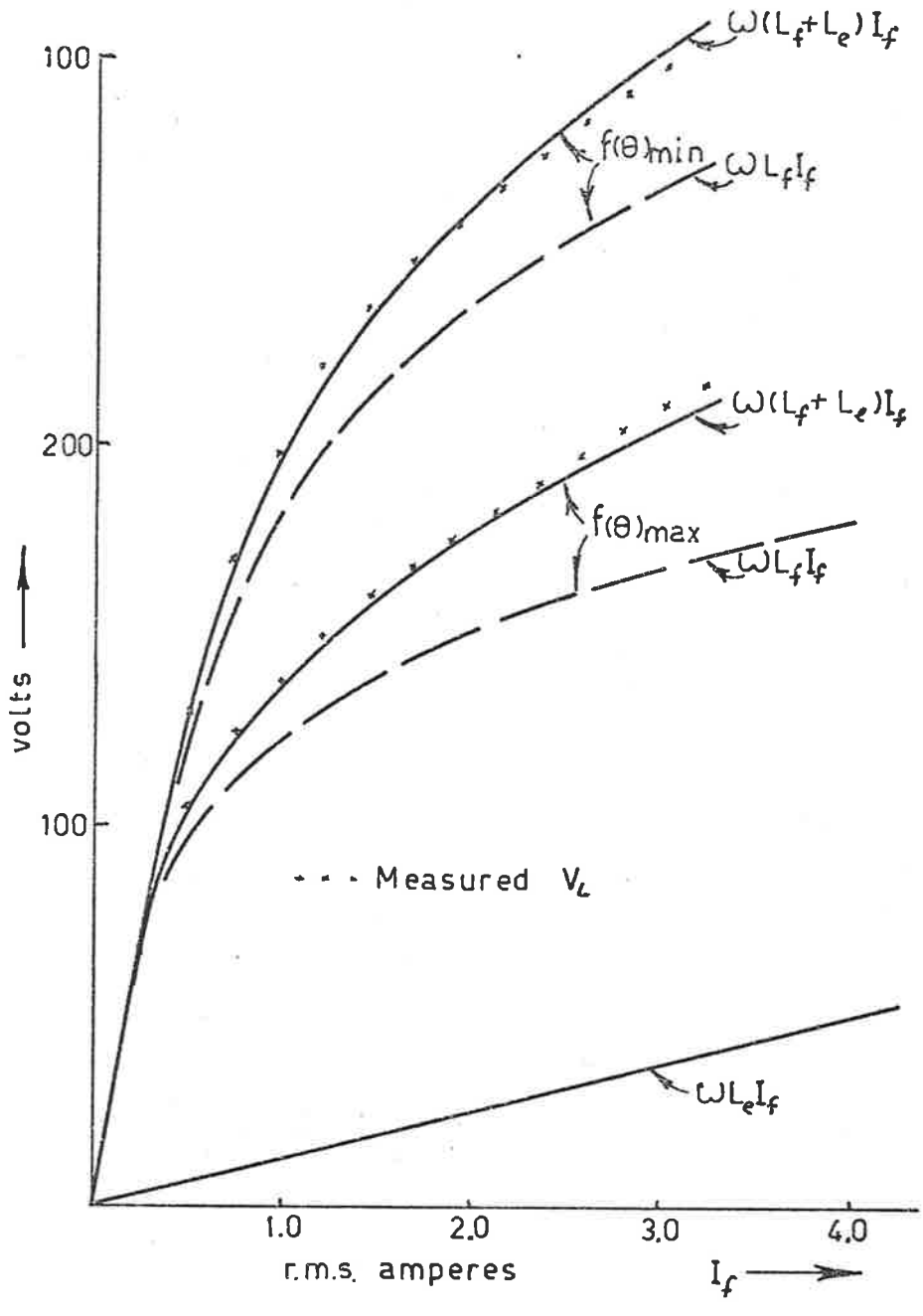

FIGURE AIII.1: COMPARISON OF THEORETICAL AND MEASURED INDUCTANCE VOLTAGE

III(e) Plots of V_L-I_R versus plots of V_L-I_f

It is shown in Section 7 that the approximate operating conditions for a particular machine may be established very simply and conveniently by plotting the measured coil voltage against the fundamental component of current, i.e. by plotting $\omega L_f I_f$ against I_f, for two rotor positions corresponding to the extremes of rotor reluctance. In practice it is more convenient to measure rms or rectified average values, rather than fundamental components. While the voltage across the inductance remains essentially sinusoidal, the current wave form may contain significant harmonic components. Thus it is of interest to know what error results if the rms value of the current is used rather than the fundamental component.

In III(d) above expressions were developed for two different'equivalent linear inductances'.

Because $\frac{1}{2}L_f I_f^2 \equiv \frac{1}{2}L_R I_R^2$

it follows that $$\frac{\omega L_r I_r}{\omega L_f I_f} = \frac{I_f}{I_R} \qquad \text{.....(III.8)}$$

The term $\omega L_f I_f$ represents not only the rms value of the fundamental component, but also the overall rms value of the voltage across the winding inductance because for the values of series resistance encountered in practical devices of this nature, the flux waveform is virtually sinusoidal,

thus the term $\omega L_r I_r$ appears to have neither physical significance nor relevance to this problem.

The quantities easily measurable in practice are $V_f \equiv \omega L_f I_f$ and I_r, and because $I_r > I_f$ a plot of V_f versus I_r will be displaced with respect to a plot of V_f versus I_f. An indication of the magnitude of error involved is given by plotting $I_{R/}I_f$ as a function of the peak value of the saturation factor for a simple quintic approximation

When $\lambda = \Lambda \sin \omega t$

then $i_{peak} \equiv i_p = \frac{\Lambda}{L_o} k_{sp}$

where k_{sp} is the peak value of the saturation factor. From equations (III.2) and (III.3) we find for a simple quintic approximation that:-

$$\frac{I_R}{I_f} = \frac{(63k_{sp}^2+34k_{sp}+31)^{\frac{1}{2}}}{\sqrt{2}(5k_{sp}+3)} \qquad \ldots\ldots(III.9)$$

which is shown plotted in Figure A.III.2.

Some elementary geometry shows that for a quintic approximation

$$\frac{\Delta V_f}{\Delta_f} / \frac{\Delta I_f}{\Delta_f} = \frac{5k_{sp}+3}{25k_{sp}-17} \qquad \ldots\ldots(III.10)$$

Putting $\Delta I_{f/}I_f$ in (III.10) $\equiv (I_R-I_f)_{/}I_f$ from (III.9) shows that plotting measured V_f against I_R rather than

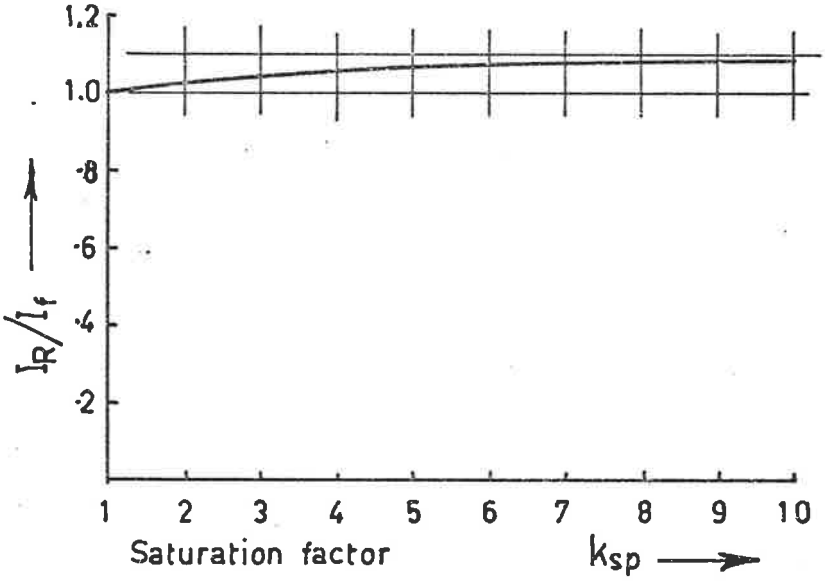

$$\frac{I_R}{I_f} = \frac{(63k_{sp}+34k_{sp}+31)^{1/2}}{\sqrt{2}\,(5k_{sp}+3)}$$

FIGURE A.III.2 : RATIO OF TOTAL RMS TO FUNDAMENTAL RMS CURRENT

against I_f, results in a characteristic having apparent errors in ordinate values of not more than 2% for $k_{sp} \leqslant 10$.

These results suggest that for purposes of estimating the voltage, capacity and resistance appropriate for a particular machine, as discussed in Section 7.3, measured $V_{f/}I_R$ characteristics are adequate.

IV Domains in the frequency damping plane in which ferro-resonant jumps can occur

When iron losses and leakage inductance are both present, the electrical circuit equation in normalised form becomes:-

$$-B\sin(\gamma\tau+\beta) = 2\rho_2\ell\dddot{\psi}+(1+4\rho_1\rho_2)\ddot{\psi}+2(\rho_1+\rho_2)\dot{\psi}+\psi$$

$$+(1+2\rho_1\frac{d}{d\tau}+\ell\frac{d^2}{d\tau^2})(\sum_{n=o}^{h} f_n(\theta)\psi^{2n+1}) \qquad .....IV.1$$

As discussed in Section 7, the steady state solution under blocked rotor conditions with $f_n(\theta)\equiv F_n$ takes the form:-

$$\psi = a_o \sin(\gamma\tau+\eta_o)$$

$$= x\sin\gamma\tau+y\cos\gamma\tau \qquad .....IV.2$$

provided that neither the amplitude of the driving function B, nor the circuit damping are excessive.

Substituting (IV.2) into (IV.1) and equating coefficients of the sine and cosine terms respectively gives:-

$$B\cos\beta = [2\rho_2(1-\ell\gamma^2)+2\rho_1 A]\gamma y + [(1-\ell+4\rho_1\rho_2)\gamma^2 - A(1-\ell\gamma^2)]x \qquad .....(IV.3)$$

$$B\sin\beta = [(1-\ell+4\rho_1\rho_2)\gamma^2-A(1-\ell\gamma^2)]y - [2\rho_2(1-\ell\gamma^2)+2\rho_1 A]\gamma x \qquad .....(IV.4)$$

and hence

$$\frac{B^2}{a_o}_2 = 4\rho_1{}^2\gamma^2[\frac{\rho_2}{\rho_1}(1-\ell\gamma^2)+A]^2 + [(1-\ell+4\rho_1\rho_2)\gamma^2-A(1-\ell\gamma^2)]^2 \qquad .....(IV.5)$$

Using the methods of Appendix III it may be shown that the fundamental component of

$$\sum_{n=o}^{h} F_n(a_o\sin(\gamma\tau+\eta_o))^{2n+1}$$

may be written as $A(x\sin\gamma\tau+y\cos\gamma\tau)$,

where $A = \sum_{n=o}^{h} a_o{}^{2n}P_n$

and $P_n = F_n\frac{(2n+2)!}{2^{2n+1}((n+1)!)^2}$

Jumps are possible provided $\frac{dB^2}{da_o}_2=0$ at two real, positive values of $a_o{}^2$. After differentiation and some manipulation of (IV.5) we find that

$$\frac{dB^2}{da_o}_2 = C_1+C_2A(A+2a_o{}^2\frac{dA}{da_o}_2)+C_3(A+a_o{}^2\frac{dA}{da_o}_2) \qquad .....(IV.6)$$

where

$$\left.\begin{aligned} C_1 &\equiv 4\rho_2{}^2\gamma^2(1-\ell\gamma^2)^2+(1-\ell+4\rho_1\rho_2)^2\gamma^4 \\ C_2 &= 4\rho_1{}^2\gamma^2+(1-\ell\gamma^2)^2 \\ C_3 &= -2(1-\ell)(1-\ell\gamma^2)\gamma^2 \end{aligned}\right\} \qquad .....(IV.7)$$

IV.1 Cubic approximation (n=1)

This condition gives

$$A = 1+\frac{3}{4}a_o{}^2F_1 \quad \text{and} \quad \frac{dA}{da_o}{}^2 = \frac{3}{4}F_1$$

Then writing $r \equiv a_o{}^2F_1$, (IV.6) becomes, when $\frac{dB^2}{da_o}{}^2$ is equated to zero:

$$\frac{9}{16}C_2r^2+(C_2+\frac{C_3}{2})r+\frac{C_1+C_2+C_3}{3} = 0 \qquad \text{.....(IV.8)}$$

the roots of which are (provided $C_2 \neq 0$)

$$r = -\frac{8}{9}(1+\frac{C_3}{2C_2})(1\pm\sqrt{1-\frac{3(C_1+C_2+C_3)C_2}{(2C_2+C_3)^2}}) \qquad \text{.....(IV.9)}$$

These roots are real if

$$1 - \frac{3(C_1+C_2+C_3)C_2}{(2C_2+C_3)^2} \geq 0 \qquad \text{.....(IV.10)}$$

and positive if the two inequalities:-

$$1 + \frac{C_3}{2C_2} < 0 \qquad \text{.....(IV.11)}$$

and $(C_1+C_2+C_3) > 0$ .....(IV.12)

are satisfied. Using (IV.7) it is a simple matter to show that (IV.12) is always satisfied; so that the necessary and sufficient conditions for jumps to be able to take place, are given by (IV.10) and (IV.11). Substitution of (IV.7) into (IV.10) and (IV.11) shows that the two roots are real provided:-

$$[4\rho_1{}^2\gamma^2+(1-\ell\gamma^2)(1-\gamma^2)]^2$$

$$-12[\rho_2\gamma\{4\rho_1{}^2\gamma^2+(1-\ell\gamma^2)^2\}+\rho_1\gamma^3(1-\ell)]^2 \geqslant 0 \quad \ldots\ldots(IV.13)$$

and are both positive, provided

$$\rho_1{}^2 < \frac{(\gamma^2-1)(1-\ell\gamma^2)}{4\gamma^2} \quad \ldots\ldots(IV.14)$$

IV.2 Quintic approximation (n=2)

In this case $A = 1+\frac{5}{8}a_o{}^4F_2$

and $\frac{dA}{da_o{}^2} = \frac{5}{4}a_o{}^2F_2$

Then writing $r \equiv a_o{}^4F_2$, (IV.6) becomes, when $dB^2/da_o{}^2$ is equated to zero:-

$$\frac{125}{64}C_2r^2+\frac{15}{4}(C_2+\frac{C_3}{2})r + C_1+C_2+C_3 = 0 \quad \ldots\ldots(IV.15)$$

the roots of which are (provided $C_2 \neq 0$)

$$r = -\frac{24}{25}(1+\frac{C_3}{2C_2})(1\pm\sqrt{1 - \frac{20}{9}\frac{(C_1+C_2+C_3)C_2}{(2C_2+C_3)^2}}) \quad \ldots\ldots(IV.16)$$

These roots are real if

$$1 - \frac{20}{9}\frac{(C_1+C_2+C_3)C_2}{(2C_2+C_3)^2} \geqslant 0 \quad \ldots\ldots(IV.17)$$

and positive if the two inequalities:-

$$1 + \frac{C_3}{2C_2} < 0 \qquad \text{.....(IV.18)}$$

and $$C_1+C_2+C_3 > 0 \qquad \text{.....(IV.19)}$$

are satisfied. Expressions (IV.18) and (IV.19) are identical with (IV.11) and (IV.12); so that after substitution of (IV.7) into (IV.17) we find that the two roots are real provided

$$[4\rho_1{}^2\gamma^2+(1-\ell\gamma^2)(1-\gamma^2)]^2$$

$$-5[\rho_2\gamma(4\rho_1{}^2\gamma^2+(1-\ell\gamma^2)^2)+\rho_1\gamma^3(1-\ell)]^2 \geqslant 0 \qquad \text{.....(IV.20)}$$

and are both positive, provided

$$\rho_1{}^2 < \frac{(\gamma^2-1)(1-\ell\gamma^2)}{4\gamma^2} \qquad \text{.....(IV.21)}$$

IV.3 Discussion

Inequalities (IV.13), (IV.20) and (IV.14) or (IV.21) enable boundaries to be defined for domains in the frequency-damping plane within which it is possible for ferro-resonant jumps to occur. It is a straight forward problem to extend this analysis to include both higher values and a range of values of 'n' if required.

These boundaries may be found by writing the above inequalities as equations and solving for ρ_1 as a function of γ over a range of values for ρ_2 and ℓ.

Typical results are shown plotted in Figures 7.5(a) and (b) for n=1 and 2 respectively. In each case the area within which jumps are possible is that bounded by the

particular curve and the frequency axis ($\rho_1=0$). It is clear that satisfaction of (IV.13) or (IV.20) as the case may be, is sufficient [as the areas so defined lie wholly within the areas defined by (IV.14) or (IV.21)] provided $\gamma > 1$.

V Nature of the singular points and stability.

The parameters appearing in equation (8.7) are defined as follows [9]:-

$$a = \frac{\partial X}{\partial x}\Big]_{x_o, y_o}$$

$$b = \frac{\partial X}{\partial y}\Big]_{x_o, y_o}$$

$$c = \frac{\partial Y}{\partial x}\Big]_{x_o, y_o}$$

$$d = \frac{\partial Y}{\partial y}\Big]_{x_o, y_o}$$

where $X \equiv \frac{dx}{d\tau}$ and $Y \equiv \frac{dy}{d\tau}$ are given by equations (8.2) and (8.3) respectively.

For the case of a cubic non linearity, i.e. n = 1, these parameters take the following values

$$\left.\begin{aligned} a &= -2\rho\gamma\left(1+\tfrac{3}{4}\,Fr_o^{\,2}+\tfrac{3}{2}Fx_o^{\,2}\right) - \tfrac{3}{2}Fx_o y_o \\ b &= -\left(1-\gamma^2+\tfrac{3}{4}Fr_o^{\,2}+\tfrac{3}{2}Fy_o^{\,2}\right) - 2\rho\gamma\tfrac{3}{2}Fx_o y_o \\ c &= 1-\gamma^2+\tfrac{3}{4}Fr_o^{\,2}+\tfrac{3}{2}Fx_o^{\,2} - 2\rho\gamma\tfrac{3}{2}Fx_o y_o \\ d &= -2\rho\gamma\left(1+\tfrac{3}{4}Fr_o^{\,2}+\tfrac{3}{2}Fy_o^{\,2}\right) + \tfrac{3}{2}Fx_o y_o \end{aligned}\right\} \quad \ldots\ldots(V.1)$$

The pair of equations (8.7) thus represent a pair of first order linear differential equation in the incremental variables u and v; so that the characteristic equation of

the perturbed system becomes

$$\begin{vmatrix} a-\lambda & b \\ c & d-\lambda \end{vmatrix} = 0$$

or $\lambda^2-(a+d)\lambda+ad-bc = 0$ .....(V.2)

The nature of the roots of this equation determines the behaviour of the system in the vicinity of the particular steady state solution of (7.1) or the nature of the corresponding singularity of (8.4) [9].

Thus if

(i) $(a-d)^2+4bc > 0$

and $ad-bc < 0$

the singularity is a saddle point

(ii) $(a-d)^2+4bc > 0$

and $ad-bc > 0$

the singularity is a node which is stable if $a+d < 0$ and unstable if $a+d > 0$

(iii) if $(a-d)^2+4bc < 0$

the singularity may be either a stable focus, a centre or an unstable focus depending upon whether $(a+d)$ is less than, equal to or greater than zero.

V.I Boundaries between different singularities in the B^2/r^2 plane

These may be found by substituting the expressions (V.I) into the criteria listed in (i) to (iii) above, followed by the use of (7.8) in order to eliminate terms containing ρ.

It is of interest to note that in this problem

$$a+d = -4\rho\gamma(1+\frac{3}{2}\,Fr_o^{\,2}) < 0$$

so that any nodes or foci must be stable

V.I.I. Boundaries between nodes and foci

This contour is given by

$$(a-d)^2+4bc = 0$$

which after substitution and reduction shows that foci exist whenever

$$B^2F < \frac{(1+\frac{3}{2}Fr_o^{\,2}-\gamma^2)^2(1+\frac{3}{4}\,Fr_o^{\,2})^2}{\frac{9}{16}Fr_o^{\,2}} - \gamma^2(2+\frac{3}{2}Fr_o^{\,2}-\gamma^2) \quad \ldots.(V.3)$$

Some typical results are shown plotted on Figures 7.1 to 7.3.

V.I.2 Boundaries between nodes and saddles

Saddles exist when

$$(a-d)^2+4bc > 0$$

and

$$ad-bc < 0$$

The former is satisfied whenever (V.3) is not satisfied, while substitution and reduction shows that the second inequality is satisfied whenever:-

$$B^2F < \frac{\frac{3}{2}F^2r_o^4\gamma^2}{1+\frac{9}{4}Fr_o^2}(\gamma^2-1-\frac{3}{4}Fr_o^2) \qquad .....(V.4)$$

The boundary obtained by writing (V.4) as an equation coincides with the locus of points of inflection of the r^2F/B^2F curves obtained from (7.8) for a range of values for ρ. This shows quite clearly the unstable nature of solutions which occur on the negative slope portion of the r^2F/B^2F curves.

VI Analogue computer determination of phase-amplitude relations.

For a cubic approximation, equations (9.1) and (9.2) become:-

$$2\gamma\dot{x} = B\cos\beta - 2\rho\gamma Kx - (K-\gamma^2)y - \frac{3}{4}r^2 2\rho\Omega F'(\theta)y \qquad .....(VI.1)$$

$$2\gamma\dot{y} = B\sin\beta - 2\rho\gamma Ky + (K-\gamma^2)x + \frac{3}{4}r^2 2\rho\Omega F'(\theta)x \qquad .....(VI.2)$$

where $K \equiv 1+\frac{3}{4}r^2F(\theta)$

These equations are already in a normalised form with an independent variable τ. It is convenient to operate in real time t on the computer such that $t = \tau/2$ and to allow for maximum values of x and y of the order of five. Thus (VI.1) and (VI.2) may be rearranged to give:-

$$20\frac{dx}{dt} = \frac{2}{5\gamma}.10(5B\cos\beta - 10\rho\gamma Kx - 5(K-\gamma^2)y - 7.5r^2\rho\Omega F'(\theta)y)$$

.....(VI.3)

$$20\frac{dy}{dt} = \frac{2}{5\gamma}.10(5B\sin\beta - 10\rho\gamma Ky + 5(K-\gamma^2)x + 7.5r^2\rho\Omega F'(\theta)x)$$

.....(VI.4)

$F(\theta)$ may be generated from $F'(\theta)$ by means of a diode function generator and saw tooth oscillator in a manner similar to that described in Appendix II(b); so leading to the block diagrams shown in Figures 9.1 and 9.2. Speed changes are accomplished by resetting the oscillator period and the gains of buffers B1 and B2 in Figure 9.1.

An expression for the average torque in terms of the amplitude of the solution, under sine flux conditions, was developed in Appendix III(a). When the amplitude is a slowly varying function of time an approximate value for the average torque may be found by finding the average value of T_{ave} as given by (III.1).

Thus in this case, if the analogue computer is used to produce

$$\int \left(\frac{3}{32} \frac{F'(\theta) r^4}{D_o L_o} - V_{offset}\right) dt = V_{out} \qquad \ldots\ldots (VI.5)$$

as shown in Figure A.VI.1, and V_{offset} is adjusted until $V_{out} = 0$ on the average, then the value of V_{offset} gives the average value of T_{ave}, which may be plotted as a function of speed as in Figures 9.8→9.11.

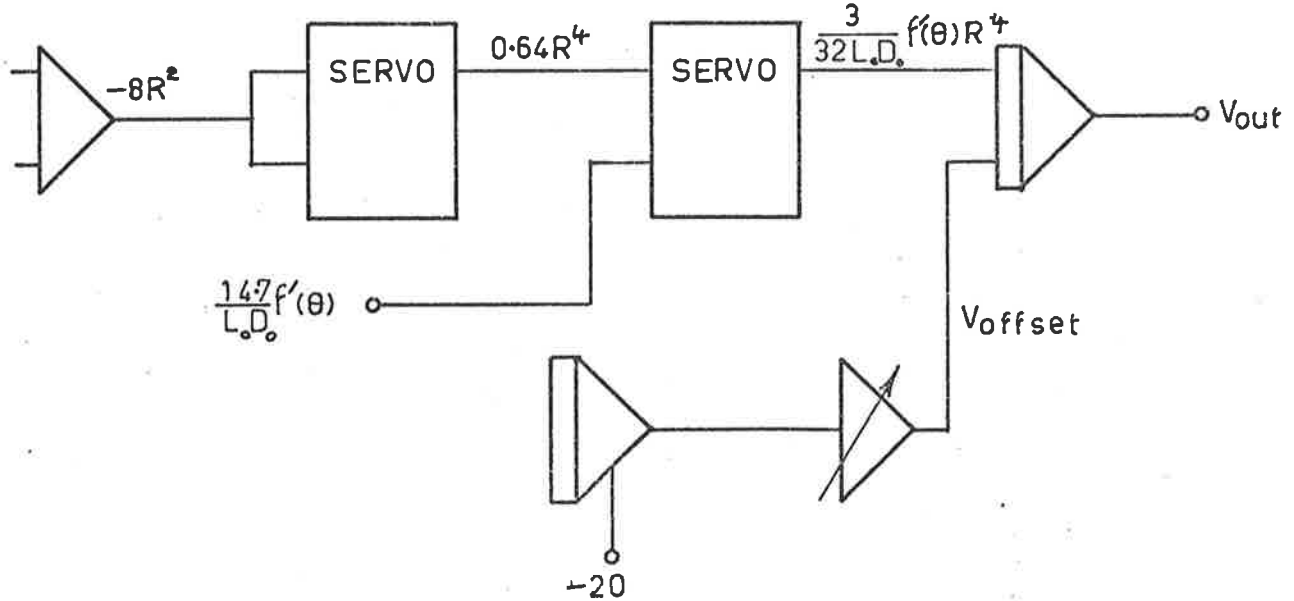

FIGURE AVI.1: DETERMINATION OF Tave.

VII Further details of the Perturbation Method

It is assumed for the purposes of the method [23] that the non linear equation, after having been expressed in the form

$$G\ (\dddot{\psi}, \ddot{\psi}, \dot{\psi}, \psi) = 0 \qquad \ldots\ldots (VII.1)$$

may be expressed in a power series of an amplitude parameter μ, as follows:-

$$G = G_{\mu=o} + \mu\left(\frac{dG}{d\mu}\right)_{\mu=o} + \frac{\mu^2}{2!}\left(\frac{d^2G}{d\mu^2}\right)_{\mu=o} \qquad \ldots\ldots (VII.2)$$

$$\equiv H_o + \mu H_1 + \frac{\mu^2}{2!} H_2 + \ldots\ldots \qquad \ldots\ldots (VII.3)$$

where the $H_i = \left.\frac{d^i G}{d\mu^i}\right|_{\mu=0}$ $\qquad \ldots\ldots (VII.4)$

and that the solution similarly may be expressed as:-

$$\psi = \mu g_1(\tau) + \frac{\mu^2}{2!} g_2(\tau) + \frac{\mu^3}{3!} g_3(\tau) \qquad \ldots\ldots (VII.5)$$

Thus $H_1 = \left.\frac{dG}{d\mu}\right|_{\mu=o}$

$$= \left[\frac{\partial G}{\partial \dddot{\psi}} \frac{\partial \dddot{\psi}}{\partial \mu} + \frac{\partial G}{\partial \ddot{\psi}} \frac{\partial \ddot{\psi}}{\partial \mu} + \frac{\partial G}{\partial \dot{\psi}} \frac{\partial \dot{\psi}}{\partial \mu} + \frac{\partial G}{\partial \psi} \frac{\partial \psi}{\partial \mu}\right]_{\mu=o}$$

$$= \left[\frac{\partial G}{\partial \dddot{\psi}}(\dddot{g}_1 + \mu \dddot{g}_2 + \ldots) + \frac{\partial G}{\partial \ddot{\psi}}(\ddot{g}_1 + \mu \ddot{g}_2 + \ldots)\right.$$

$$\left. + \frac{\partial F}{\partial \dot{\psi}}(\dot{g}_1 + \mu \dot{g}_2 + \ldots) + \frac{\partial G}{\partial \psi}(g_1 + \mu g_2 + \ldots)\right]_{\mu=o}$$

$$= \left(\frac{\partial G}{\partial \dddot{\psi}}\right)_{\mu=o} \dddot{g}_1 + \left(\frac{\partial G}{\partial \ddot{\psi}}\right)_{\mu=o} \ddot{g}_1 + \left(\frac{\partial G}{\partial \dot{\psi}}\right)_{\mu=o} \dot{g}_1 + \left(\frac{\partial G}{\partial \psi}\right)_{\mu=o} g_1 \ldots$$

$$\equiv L_1(g_1) \qquad \ldots\ldots (VII.6)$$

Similarly

$$H_2 = \left.\frac{d^2G}{d\mu^2}\right|_{\mu=o} = \left.\frac{d}{d\mu}\frac{dG}{d\mu}\right|_{\mu=o} = \frac{d}{d\mu}[\quad]_{\mu=o}$$

$$= \frac{\partial}{\partial\ddot{\psi}}[\quad]\frac{\partial\dddot{\psi}}{\partial\mu} + \frac{\partial}{\partial\dddot{\psi}}[\quad]\frac{\partial\ddot{\psi}}{\partial\mu} + \frac{\partial}{\partial\dot{\psi}}[\quad]\frac{\partial\dot{\psi}}{\partial\mu} + \frac{\partial}{\partial\psi}[\quad]\frac{\partial\psi}{\partial\mu} + \frac{\partial}{\partial\mu}[\quad]$$

all at $\mu=0$ .....(VII.7)

Where the symbol [ ] represents the expression in square brackets in (VII.6).

Nicholson defines the first four terms of (VII.7) as $L_2(g_1,g_1)$

where $L_2(g_1,g_1) = \Sigma\Sigma\frac{\partial^2 G}{\partial\psi^{(i)}\partial\psi^{(j)}}\, g_1^{(i)} g_1^{(j)}$

The final term of (VII.7) may be recognised as $L_1(g_2)$. Nicholson provides general expressions for the various $L_m(g_1,g_2\cdots g_m)$ and for the various H_i in terms of these L_m, however a simple rule for generating H_{k+1} from H_k follows from inspection of what happens when each successive full derivative is taken.

Thus the general term $L_j(g_{i_1},g_{i_2}\cdots g_{i_j})$ where $i_1+i_2+\ldots i_j = k$ becomes

① $\frac{\partial}{\partial\mu} \rightarrow L_j(g_{i_1+1},g_{i_2},\cdots g_{i_j}$

$+ L_j(g_{i_1},g_{i_2+1},\cdots g_{i_j})$

$+ L_j(g_{i_1},g_{i_2},\cdots g_{i_j+2})$

② The operation

$$\frac{\partial}{\partial \ddot{\psi}} \frac{\partial \ddot{\psi}^{*}}{\partial \mu} + \frac{\partial}{\partial \ddot{\psi}} \frac{\partial \ddot{\psi}}{\partial \mu} + \frac{\partial}{\partial \dot{\psi}} \frac{\partial \dot{\psi}}{\partial \mu} + \frac{\partial}{\partial \psi} \frac{\partial \psi}{\partial \mu}$$

leads to

$$L_{j+1}(g_{i_1}, g_{i_2}, \ldots . g_{i_j}, g_1)$$

Thus we have

$$H_1 = L_1(g_1)$$

$$H_2 = L_1(g_2) + L_2(g_1, g_1)$$

$$H_3 = L_1(g_3) + L_2(g_2, g_1) + L_2(g_2, g_1) + L_2(g_1, g_2) + L_3(g_1, g_1, g_1)$$

$$= L_1(g_3) + 3L_2(g_1, g_2) + L_3(g_1, g_1, g_1)$$

$$H_4 = L_1(g_4) + L_2(g_3, g_1) + 3L_2(g_2, g_2) + 3L_2(g_1, g_3) + 3L_3(g_1, g_2, g_1)$$

$$+ L_3(g_2, g_1, g_1) + L_3(g_1, g_2, g_1) + L_3(g_1, g_1, g_2) + L_4(g_1, g_1, g_1, g_1)$$

$$= L_1(g_4) + 4L_2(g_1, g_3) + 3L_2(g_2, g_2) + 6L_3(g_1, g_1, g_2) + L_4(g_1, g_1, g_1, g_1)$$

Similarly

$$H_5 = L_1(g_5) + 5L_2(g_1, g_4) + 10L_2(g_2, g_3) + 10L_3(g_1, g_1, g_3)$$

$$+ 15L_3(g_1, g_2, g_2) + 10L_4(g_1, g_1, g_1, g_2) + L_5(g_1, g_1, g_1, g_1, g_1)$$

$$\ldots\ldots\ldots\ldots \text{etc} \qquad \ldots\ldots (VII.8)$$

Returning now to the equation for which a solution is sought, we have

$$G = B\sin(\gamma\tau+\beta) + 2\rho_2\ell\dddot{\psi}+(1+4\rho_1\rho_2)\ddot{\psi}+2(\rho_1+\rho_2)\dot{\psi}+\psi$$
$$+(1+2\rho_1\frac{d}{d\tau}+\ell\frac{d^2}{d\tau^2})F(\theta)\psi^q \qquad \text{.....(VII.9)}$$

$$\text{Thus } H_o = G\Big|_{\mu=o} = G\Big|_{\dddot{\psi},\ddot{\psi},\dot{\psi},\psi=o}$$
$$= B\sin(\gamma\tau+\beta) \qquad \text{.....(VII.10)}$$

In order to find expressions for the following H_i, expressions for the various L_m must be found. These in turn require expressions for the various partial derivatives of G.

Thus from (VII.9), <u>when μ=0</u>:-

$$\left.\begin{aligned}\frac{\partial G}{\partial \dddot{\psi}} &= 2\rho_2\ell \\ \frac{\partial G}{\partial \ddot{\psi}} &= 1+4\rho_1\rho_2 \\ \frac{\partial G}{\partial \dot{\psi}} &= 2(\rho_1+\rho_2) \\ \frac{\partial G}{\partial \psi} &= 1\end{aligned}\right\} \qquad \text{.....(VII.11)}$$

For odd non linearities all even partial derivatives are zero.

For Cubic non-linearity:-

$$\left.\begin{aligned}
\frac{\partial^3 G}{\partial \psi^3} &= 6\left(1+2\rho_1\frac{d}{d\tau}+\ell\frac{d^2}{d\tau^2}\right)F(\theta)\\
\frac{\partial^3 G}{\partial \psi^2 \partial \dot{\psi}} &= 12\left(\rho_1+\ell\frac{d}{d\tau}\right)F(\theta)\\
\frac{\partial^3 G}{\partial \psi \partial \dot{\psi}^2} &= 12\ell F(\theta)\\
\frac{\partial^3 G}{\partial \psi^2 \partial \ddot{\psi}} &= 6\ell F(\theta)
\end{aligned}\right\} \quad \ldots\ldots(VII.12)$$

All higher partial derivatives are zero.

For Quintic non-linearity

All third order partial derivatives are zero.

$$\left.\begin{aligned}
\frac{\partial^5 G}{\partial \psi^5} &= 120\left(1+2\rho_1\frac{d}{d\tau}+\ell\frac{d^2}{d\tau^2}\right)F(\theta)\\
\frac{\partial^5 G}{\partial \psi^4 \partial \dot{\psi}} &= 240\left(\rho_1+\ell\frac{d}{d\tau}\right)F(\theta)\\
\frac{\partial^5 G}{\partial \psi^3 \partial \dot{\psi}^2} &= 240\ell F(\theta)\\
\frac{\partial^5 G}{\partial \psi^4 \partial \ddot{\psi}} &= 120\ell F(\theta)
\end{aligned}\right\} \quad \ldots\ldots(VII.13)$$

All higher partial derivatives are zero.

Then from (VII.11)

$$L_1(g) = \frac{\partial G}{\partial \dddot{\psi}} \dddot{g} + \frac{\partial G}{\partial \ddot{\psi}} \ddot{g} + \frac{\partial G}{\partial \dot{\psi}} \dot{g} + \frac{\partial G}{\partial \psi} g$$

$$= 2\rho_2 \ell \dddot{g} + (1+4\rho_1\rho_2)\ddot{g} + 2(\rho_1+\rho_2)\dot{g} + g \qquad \text{.....(VII.14)}$$

From (VII.12)

$$L_3(fgh)$$

$$= (fgh)6(1+2\rho_1\frac{d}{d\tau}+\ell\frac{d^2}{d\tau^2})F(\theta)$$

$$+ (\dot{f}gh+f\dot{g}h+fg\dot{h})12(\rho_1+\ell\frac{d}{d\tau})F(\theta)$$

$$+ (\dot{f}\dot{g}h+f\dot{g}\dot{h}+\dot{f}g\dot{h})12\ell F(\theta)$$

$$+ (\dddot{f}gh+f\ddot{g}h+fg\ddot{h})6\ell F(\theta) \qquad \text{.....(VII.15)}$$

and $L_3(g,g,g)$

$$= 6g^3(1+2\rho_1\frac{d}{d\tau}+\ell\frac{d^2}{d\tau^2})F(\theta)$$

$$+ 36g^2\dot{g}(\rho_1+\frac{\ell d}{d\tau})F(\theta)$$

$$+ 36\dot{g}^2 g\ell F(\theta)$$

$$+ 18\ddot{g}g^2\ell F(\theta)$$

$$= 3!(1+2\rho_1\frac{d}{d\tau}+\frac{d}{d\tau^2})(F(\theta)g^3) \qquad \text{.....(VII.16)}$$

Similarly

$$L_5(g,g,g,g,g)$$

$$= 5!(1+2\rho_1\frac{d}{d\tau}+\frac{d^2}{d\tau^2})(F(\theta)g^5) \qquad \text{.....(VII.17)}$$

VIII(a) Expansion of sideband series raised to some power.

Consider the series:-

$$S \equiv \sum_{k=-r}^{r} a_k \cos\left(\overline{\gamma+k2\Omega)\tau+\eta_k}\right.$$

Then

$$S^2 = \sum_{k=-r}^{r}\sum_{\ell=-r}^{r} a_k a_\ell \cos\left(\overline{\gamma+k2\Omega)\tau+\eta_k}\right. \cos\left(\overline{\gamma+\ell2\Omega)\tau+\eta_\ell}\right.$$

$$= \tfrac{1}{2}\sum_{k=-r}^{r}\sum_{\ell=-r}^{r} a_k a_\ell \left[\cos\left(\overline{2k\Omega\tau-2\ell\Omega\tau+\eta_k-\eta_\ell}\right.\right.+\cos\left.\left(\overline{2(\gamma+k\Omega+\ell\Omega)\tau+\eta_k+\eta_\ell}\right.\right]$$

Similarly:-

$$S^3 = \tfrac{1}{4}\sum_{k=-r}^{r}\sum_{\ell=-r}^{r}\sum_{m=-r}^{r} a_k a_\ell a_m \left[\begin{array}{l} 3\cos\left(\overline{\gamma+2(m+k-\ell)\Omega)\tau+\eta_m+\eta_k-\eta_\ell}\right. \\ +\cos\left(\overline{3\gamma+2(m+k+\ell)\Omega)\tau+\eta_m+\eta_k+\eta_\ell}\right. \end{array}\right]$$

$$S^4 = \frac{1}{8}\sum_{k}\sum_{\ell}\sum_{m}\sum_{n} a_k a_\ell a_m a_n \left[\begin{array}{l} 3\cos\left(\overline{2(m+k-\ell-n)\Omega\tau+\eta_m+\eta_k-\eta_\ell-\eta_n}\right. \\ +4\cos\left(\overline{2\gamma+2(m+k+n-\ell)\Omega)\tau+\eta_m+\eta_k+\eta_n-\eta_\ell}\right. \\ +\cos\left(\overline{4\gamma+2(m+k+n+\ell)\Omega)\tau+\eta_m+\eta_k+\eta_n+\eta_\ell}\right. \end{array}\right]$$

and

$$S^5 = \frac{1}{16} \sum\sum\sum\sum\sum_{k\ell mnp} a_k a_\ell a_m a_n a_p \begin{bmatrix} 10\cos(\overline{\gamma+2(m+k+\ell-n-p)\Omega)\tau+\eta_m+\eta_k+\eta_\ell-\eta_n-\eta_p} \\ +5\cos(\overline{3\gamma+2(m+k+\ell+n-p)\Omega)\tau+\eta_m+\eta_k+\eta_\ell+\eta_n-\eta_p} \\ +\cos(\overline{5\gamma+2)(m+k+\ell+n+p)\Omega)\tau+\eta_m+\eta_k+\eta_\ell+\eta_n+\eta_p} \end{bmatrix}$$

etc ....

.....(VII.1)

Such expansions may be written down very simply by noting the following characteristics of the expansion of S^n:-

(i) The coefficients of γ within the various cosine terms will be n,(n-2),(n-4) ...etc.

(ii) The excess of +ve signs over -ve signs of the phase angles η and the integral coefficents of Ω will equal the coefficient of γ in any term of the expansion.

(iii) The external coefficients of the various cosine terms are readily obtained from the inverse Chebychev series. e.g. Chebychev Polynomials may be generated from the recursive formula [25]

$$T_n(x) = 2xT_{n-1}(x) - T_{n-2}(x)$$

giving

$$\left.\begin{aligned} T_o &= 1 \\ T_1 &= x \\ T_2 &= 2x^2-1 \\ T_3 &= 4x^3-3x \\ T_4 &= 8x^4-8x^2+1 \\ T_5 &= 16x^5-20x^3+5x \quad \text{etc} \end{aligned}\right\} \quad .....(VIII.2)$$

from which it follows:-

$$\left.\begin{aligned} 1 &= T_o \\ x &= T_1 \\ x^2 &= \tfrac{1}{2}(T_2+T_o) \\ x^3 &= \tfrac{1}{4}(T_3+3T_1) \\ x^4 &= \tfrac{1}{8}(T_4+4T_2+3T_o) \\ x^5 &= \tfrac{1}{16}(T_5+5T_3+10T_1) \quad \text{etc} \end{aligned}\right\} \qquad \ldots\ldots(\text{VIII.3})$$

It is clear that there is a one to one correspondence between the T_k terms in x^n as given by (VIII.3) and the cos $(k\gamma+\ldots)$ terms in S^n as given by (VIII.1), both as regards the number of such terms and the magnitude of their coefficients.

Because the circuit is highly non-linear, third harmonics of the fundamental will be present in the current waveform and to a lesser extent in the flux waveform. As a result a more accurate representation of the flux or current waveform would be given by

$$S = \sum_{k=-r}^{r} a_k \cos(\overline{\gamma+2k\Omega)\tau+\eta_k} + \sum_{h=-3r}^{3r} b_h \cos(\overline{3\gamma+2h\Omega)\tau+\varepsilon_h} \qquad \ldots\ldots(\text{VIII.4})$$

from which we can find for the case of a cubic:-

$$S^3 = \tfrac{1}{4}\sum_{j=-r}^{r}\sum_{k=-r}^{r}\sum_{\ell=-r}^{r} a_j a_k a_\ell \left[\begin{aligned} &3\cos(\overline{\gamma+2(j+k-\ell)\Omega)\tau+\eta_k+\eta_j-\eta_\ell} \\ &+\cos(\overline{3\gamma+2(j+k+\ell)\Omega)\tau+\eta_k+\eta_j+\eta_\ell} \end{aligned}\right]$$

$$+\frac{3}{4}\sum_{k=-r}^{r}\sum_{j=-r}^{r}\sum_{n=-3r}^{r} a_k a_j b_n \left[\begin{array}{l} \cos\left(\overline{\gamma+2(n-j-k)\Omega}\right)\tau+\varepsilon_n-\eta_j-\eta_k \\ +2\cos\left(\overline{3\gamma+2(n+j-k)\Omega}\right)\tau+\varepsilon_n+\eta_j-\eta_k \\ +\cos\left(\overline{5\gamma+2(n+j+k)\Omega}\right)\tau+\varepsilon_n+\eta_j+\eta_k \end{array}\right]$$

$$+\frac{3}{4}\sum_{k=-r}^{r}\sum_{m=-3r}^{3r}\sum_{n=-3r}^{3r} a_k b_m b_n \left[\begin{array}{l} 2\cos\left(\overline{\gamma+2(k+m-n)\Omega}\right)\tau+\eta_k+\varepsilon_m-\varepsilon_n \\ +\cos\left(\overline{5\gamma+2(m+n-k)\Omega}\right)\tau+\varepsilon_m+\varepsilon_n-\eta_k \\ +\cos\left(\overline{7\gamma+2(m+n+k)\Omega}\right)\tau+\varepsilon_m+\varepsilon_n+\eta_k \end{array}\right]$$

$$+\frac{1}{4}\sum_{m=-3r}^{3r}\sum_{n=-3r}^{3r}\sum_{q=-3r}^{3r} b_m b_n b_q \left[\begin{array}{l} 3\cos\left(\overline{3\gamma+2(m+n-q)\Omega}\right)\tau+\varepsilon_m+\varepsilon_n-\varepsilon_q \\ +\cos\left(\overline{9\gamma+2(m+n+q)\Omega}\right)\tau+\varepsilon_m+\varepsilon_n+\varepsilon_q \end{array}\right]$$

.....(VIII.5)

VIII(b) Interaction of rotor and sidebands

Expansion of $F(\theta)g_1^q$

The rotor geometry is defined by:-

$$F(\theta) = 1+d_1\cos\overline{p\Omega\tau+\delta_1}+d_2\cos\overline{2p\Omega\tau+\delta_2}+\ldots d_\mu\cos\overline{\mu p\Omega\tau+\delta\mu}$$

$$= \sum_{k=o}^{\mu} d_k\cos\overline{kp\Omega\tau+\delta_k} \qquad \ldots\ldots(VIII.5)$$

where $d_o\cos\delta_o \equiv 1$ and p equals the number of poles.

From (VIII.1) it is clear that the expansion of:-

$$g_1^q = \left(\sum_{n=-r}^{r} a_n\cos(\gamma+2np\Omega)\tau+\eta_n\right)^q$$

may be written (when q is odd) as:-

$$\sum_{n=-qr}^{qr}\left[A_n\cos\overline{(\gamma+np\Omega)\tau+\alpha_n}+\right.$$

$$+B_n\cos\overline{(3r+np\Omega)\tau+p_n}$$

$$\left.+H_n\cos\overline{(q\gamma+np\Omega)\tau+\xi_n}\right]$$

and in particular, when q = 3, as:-

$$g_1^3 = \sum_{n=-3r}^{3r}\left[\begin{array}{l}\frac{3}{4}A_n\cos\overline{(\gamma+np\Omega)\tau+\alpha_n} \\ \\ +\frac{1}{4}B_n\cos\overline{(3\gamma+np\Omega)\tau+\xi_n}\end{array}\right] \qquad \ldots\ldots(VIII.6)$$

so that the fundamental terms in $F(\theta)g_1^3$ are as follows:-

$$\frac{3}{4}\frac{d_o}{2}(A_o\cos\overline{\gamma\tau+\alpha_o-\delta_o} + A_o\cos\overline{\gamma\tau+\alpha_o+\delta_o})$$

$$+\frac{3}{4}\frac{d_1}{2}(A_1\cos\overline{\gamma\tau+\alpha_1-\delta_1} + A_{-1}\cos\overline{\gamma\tau+\alpha_{-1}+\delta_1})$$

$$+\frac{3}{4}\frac{d_2}{2}(A_2\cos\overline{\gamma\tau+\alpha_2-\delta_2} + A_{-2}\cos\overline{\gamma\tau+\alpha_{-2}+\delta_2})$$

$$+ \ldots\ldots\ldots\ldots\ldots$$

$$= \frac{3}{4}\sum_{k=o}^{\mu}\frac{dk}{2}(A_k\cos\overline{\gamma\tau+\alpha_k-\delta_k} + A_{-k}\cos\overline{\gamma\tau+\alpha_{-k}+\delta_k}) \quad \ldots\ldots(VIII.7)$$

First upper side band term in $F(\theta)g_1^3$ are as follows:-

$$\frac{3}{4}\frac{d_o}{2}(A_1\cos(\overline{\gamma+2\Omega)\tau+\alpha_1-\delta_o} + A_1\cos(\overline{\gamma+2\Omega)\tau+\alpha_1+\delta_o})$$

$$+\frac{3}{4}\frac{d_1}{2}(A_2\cos(\overline{\gamma+2\Omega)\tau+\alpha_2-\delta_1} + A_o\cos(\overline{\gamma+2\Omega)\tau+\alpha_o+\delta_1})$$

$$+\frac{3}{4}\frac{d_2}{2}(A_3\cos(\overline{\gamma+2\Omega)\tau+\alpha_3-\delta_2} + A_{-1}\cos(\overline{\gamma+2\Omega)\tau+\alpha_{-1}+\delta_2}$$

$$+ \ldots\ldots\ldots$$

$$= \frac{3}{4}\sum_{k=o}^{\mu}\frac{d_k}{2}(A_{k+1}\cos(\overline{\gamma+2\Omega)\tau+\alpha_{k+1}-\delta_k} + A_{-k+1}\cos(\overline{\gamma+2\Omega)\tau+\alpha_{-k+1}+\delta_k})$$

$$\ldots\ldots(VIII.8)$$

And in general the n*th* side band terms will be given by:-

$$\frac{3}{4}\sum_{k=o}^{\mu}\frac{d_k}{2}\left(A_{k+n}\cos\left(\overline{\gamma+2n\Omega)\tau+\alpha_{k+n}}-\delta_k\right.\right.$$

$$\left.\left.+A_{-k+n}\cos\left(\overline{\gamma+2n\Omega)\tau+\alpha_{-k+n}}+\delta_k\right)\right) \qquad \text{.....(VIII.9)}$$

In addition to these side bands based on the fundamental there will be one or more series based on harmonics of the fundamental. In the case of a cubic non linearity the n*th* side band of the third harmonics of the fundamental will be given by

$$\frac{1}{4}\sum_{k=o}^{\mu}\frac{d_k}{2}\left(B_{k+n}\cos\left(\overline{3\gamma+2n\Omega)\tau+\xi_{k+n}}-\delta_k\right.\right.$$

$$\left.\left.+B_{-k+n}\cos\left(\overline{3\gamma+2n\Omega)\tau+\xi_{-k+n}}+\delta_k\right)\right) \qquad \text{.....(VIII.10)}$$

Thus $L_3(g_1,g_1,g_1) = 6(1+2\rho_1\frac{d}{d\tau}+\ell\frac{d^2}{d\tau^2})(F(\theta)g_1^{\,3})$

which, if we define $S_n \equiv \gamma+2n\Omega$ and $S_{3n} \equiv 3\gamma+2n\Omega$, becomes:-

$$6(1+2\rho_1\frac{d}{d\tau}+\ell\frac{d^2}{d\tau^2})\sum_{n=-r}^{r}\sum_{k=o}^{\mu}\left[\frac{3}{4}\frac{d_k}{2}\left(A_{k+n}\cos\overline{S_n\tau+\alpha_{k+n}}-\delta_k\right.\right.$$

$$\left.\left.+A_{-k+n}\cos\overline{S_n\tau+\alpha_{-k+n}}+\delta_k\right)\right.$$

$$+\frac{1}{4}\frac{d_k}{2}\left(B_{k+n}\cos\overline{S_{3n}\tau+\xi_{k+n}}-\delta_k\right.$$

$$\left.\left.+B_{-k+n}\cos\overline{S_{3n}\tau+\xi_{-k+n}}+\delta_k\right)\right]$$

.....(VIII.11)

From which it follows that the coefficient of cos $S_n\tau$ must be:-

$$\sum_{k=o}^{\mu} \frac{9}{4} d_k [A_{k+n}((1-S_n{}^2\ell)\cos\overline{\alpha_{k+n}-\delta_k}-2\rho_1 S_n \sin\overline{\alpha_{k+n}-\delta_k}) + A_{-k+n}((1-S_n{}^2\ell)\cos\overline{\alpha_{-k+n}+\delta_k}-2\rho_1 S_n \sin\overline{\alpha_{-k+n}+\delta_k})]$$

$$= \sum_{k=o}^{\mu} \frac{9}{4} d_k \Delta_n [A_{k+n}\cos\overline{\alpha_{k+n}-\delta_k+\varepsilon_n}+A_{-k+n}\cos\overline{\alpha_{-k+n}+\delta_k+\varepsilon_n}] \quad \ldots\ldots(VIII.12)$$

where $\Delta_n = \sqrt{(1-S_n{}^2\ell)^2+4\rho_1{}^2 S_n{}^2}$ and $\tan\varepsilon_n = \frac{2\rho_1 S_n}{1-S_n{}^2\ell}$

Similarly the coefficients of Sin $S_n\tau$ must be:-

$$-\sum_{k=o}^{\mu} \frac{9}{4} d_k \Delta_n [A_{k+n}\sin\overline{\alpha_{k+n}-\delta_k+\varepsilon_n}+A_{-k+n}\sin\overline{\alpha_{-k+n}+\delta_k+\varepsilon_n}] \quad \ldots\ldots(VIII.13)$$

The coefficient of cos $S_{3n}\tau$ is then given by

$$\sum_{k=o}^{\mu} \frac{3}{4} d_k \Delta_{3n} [B_{k+n}\cos\overline{\xi_{k+n}-\delta_k+\varepsilon_{3n}}+B_{-k+n}\cos\overline{\xi_{-k+n}+\delta_k+\varepsilon_{3n}}] \quad \ldots\ldots(VIII.14)$$

and that of sin $S_{3n}\tau$ by:-

$$-\sum_{k=o}^{\mu} \frac{3}{4} d_k \Delta_{3n} [B_{k+n}\sin\overline{\xi_{k+n}-\delta_k+\varepsilon_{3n}}+B_{-k+n}\sin\overline{\xi_{-k+n}+\delta_k+\varepsilon_{3n}}] \quad \ldots\ldots(VIII.15)$$

where $\Delta_{3n} = \sqrt{(1-S^2_{3n}\ell)^2+4\rho_1{}^2S^2_{3n}}$ and $\tan \varepsilon_{3n} = \dfrac{2\rho_1 S_{3n}}{1-S^2_{3n}\ell}$

The coefficients of the cosine and sine terms in H_3 will then be given by (VIII.12) and (VIII.13) respectively, while the cos $S_{3n}\tau$ and sin $S_{3n}\tau$ terms having coefficients given by (VIII.14) and (VIII.15) respectively comprise the "remainder terms" of 10.17. i.e. they are forcing terms applied to $-L_1(g_3)$, and so enable g_3 to be determined in terms of the various a_n and η_n.

At certain rotor speeds, a lower side band based on an harmonic of the fundamental, may tend to diverge. In this case such harmonic side bands must be included in $g_1(\tau)$.

For example when third harmonics are included, the solution will be of the form given by (VIII.4); so leading to an expression for $g_1{}^3$ similar to that of (VIII.5), from which $F(\theta)g_1{}^3$ may be evaluated.

In this case H_3 will comprise all of those terms which have fundamental frequency of γ or 3γ, whilst the "remainder terms" of (10.17) will comprise those having fundamental frequencies of 5γ, 7γ and 9γ. The solution will proceed as before.

IX Current associated with a particular sideband.

If:-

$$i = \frac{\lambda}{L_o}(1+f(\theta)\lambda^{2N})$$

i.e. $$i = \frac{\psi}{D_o^{\frac{1}{2N}} L_o}(1+F(\theta)\psi^{2N}) \qquad \ldots\ldots(IX.1)$$

where D_o and $F(\theta)$ are defined in (4.22), and ψ can be represented by a series of side bands as in (10.13), then it is clear from Appendices VIII(a) and (b) that the current will consist of a series of side bands based on the fundamental.

In particular (VIII.9) shows that for a cubic non-linearity the coefficient of the cosine component of current in the *nth* side band based on the fundamental must be proportional to:-

$$X_n = a_n \cos\eta_n + \frac{3}{4}\sum_{k=o}^{\mu} \frac{d_k}{2}(A_{n+k}\cos\overline{\alpha_{n+k}-\delta_k}+A_{n-k}\cos\overline{\alpha_{n-k}+\delta_k}) \qquad \ldots\ldots(IX.2)$$

and the sine component must be proportional to:-

$$Y_n = -a_n \sin\eta_n - \frac{3}{4}\sum_{k=o}^{\mu} \frac{d_k}{2}(A_{n+k}\sin\overline{\alpha_{n+k}-\delta_k}+A_{n-k}\sin\overline{\alpha_{n-k}+\delta_k}) \qquad \ldots\ldots(IX.3)$$

The r.m.s. value of any particular side band component of the current will then be

$$I_n = \frac{\sqrt{X_n^2+Y_n^2}}{\sqrt{2}D_o^{\frac{1}{2}}L_o} \qquad \ldots\ldots(IX.4)$$

This may be evaluated with the help of the truncated series (10.23) and (10.24) which may be written, for $n \neq 0$, as:-

$$\frac{(1+4\rho_1\rho_2-\ell)S_n^2 a_n \cos\eta_n + 2\rho_2 S_n(1-\ell S_n^2)a_n \sin\eta_n}{\Delta_n}$$

$$= a_n \cos\overline{\eta_n+\varepsilon_n} + \frac{3}{4}\sum_{k=o}^{\mu}\frac{d_k}{2}\left(A_{n+k}\cos\overline{\alpha_{n+k}-\delta_k+\varepsilon_n} + A_{n-k}\cos\overline{\alpha_{n-k}+\delta_k+\varepsilon_n}\right)$$

$\ldots\ldots(IX.5)$

and

$$\frac{(1+4\rho_1\rho_2-\ell)S_n^2 a_n \sin\eta_n - 2\rho_2 S_n(1-\ell S_n^2)a_n \cos\eta_n}{\Delta_n}$$

$$= a_n \sin\overline{\eta_n+\varepsilon_n} + \frac{3}{4}\sum_{k=o}^{\mu}\frac{d_k}{2}\left(A_{n+k}\sin\overline{\alpha_{n+k}-\delta_k+\varepsilon_n} + A_{n-k}\sin\overline{\alpha_{n-k}+\delta_k+\varepsilon_n}\right)$$

$\ldots\ldots(IX.6)$

Comparison of (IX.2 and 3) with (IX.5 and 6) respectively shows that the components of the latter are simply those of the former shifted in phase by ε_n; so that some elementary trigonometry shows that $X_n^2+Y_n^2$ = sum of the squares of the L.H.S. of (IX.5) and (IX.6) respectively.

$$\text{i.e. } 2I_n^2 D_o L_o^2 = \frac{a_n^2}{\Delta_n^2}[(1+4\rho_1\rho_2\ell)^2 S_n^4 + 4\rho_2^2 S_n^2 (1-\ell S_n^2)^2] \qquad .....(IX.7)$$

where $\Delta_n^2(1-\ell S_n^2)^2+4\rho_1^2 S_n^2$

When leakage reactance and iron loss are absent or neglected, (IX.7) becomes

$$I_n^2 = \frac{a_n^2 S_n^4}{2D_o L_o^2 (1+4\rho_1^2 S_n^2)} \qquad .....(IX.8)$$

which after converting to actual physical parameters becomes:-

$$I_n^2 = \frac{\Lambda_n^2 \omega_n^2}{R^2 + \frac{1}{\omega_n^2 C^2}} \qquad .....(IX.9)$$

Similarly (IX.7) becomes

$$I_n^2 = \frac{\Lambda_n^2 \omega_n^2}{R_c^2 (R^2 + (\omega_n L_\ell - \frac{1}{\omega_n C})^2)}[(R_c+R)^2 + (L_\ell \omega_n - \frac{1}{\omega_n C})^2] \qquad .....(IX.10)$$

The above argument, although carried out using a single cubic non linearity, is perfectly general and applies what ever the complexity or degree of the λ-i relationship.

X Solution when one sideband only is present

If the solution to (10.1) comprises the fundamental and one sideband only it may be expressed as:-

$$\psi = a_o \cos\overline{\gamma\tau+\eta_o} + a_n \cos S_n\tau+\eta_n \qquad \ldots\ldots(X.1)$$

In the case of a cubic nonlinearity, the values of a_o, η_o, a_n and η_n are obtained from the simultaneous solution of the equations (10.23) and (10.24)

When iron loss can be neglected and the leakage inductance has been included within $f(\theta)$, these equations become:-

$$0 = B\sin\beta + (1-\gamma^2)a_o\cos\eta_o - 2\rho\gamma a_o \sin\eta_o + \frac{3}{4}\Delta_o\left[A_o\cos\overline{\eta_o+\varepsilon_o} + \frac{d_n}{2}\left(A_n\cos\overline{\eta_n-\delta_n+\varepsilon_o} + A_{-n}\cos\overline{2\eta_o-\eta_n+\delta_n+\varepsilon_o}\right)\right] \qquad \ldots\ldots(X.2)$$

$$0 = B\cos\beta - 2\rho\gamma a_o\cos\eta_o - (1-\gamma^2)a_o\sin\eta_o - \frac{3}{4}\Delta_o\left[A_o\sin\overline{\eta_o+\varepsilon_o} + \frac{d_n}{2}\left(A_n\sin\overline{\eta_n-\delta_n+\varepsilon_o} + A_{-n}\sin\overline{2\eta_o-\eta_n+\delta_n+\varepsilon_o}\right)\right] \qquad \ldots\ldots(X.3)$$

$$0 = (1-S_n^2)a_n\cos\eta_n - 2\rho S_n a_n\sin\eta_n + \frac{3}{4}\Delta_n\left[A_n\cos\overline{\eta_n+\varepsilon_n} + \frac{d_n}{2}\left(A_o\cos\overline{\eta_o+\delta_n+\varepsilon_n} + A_{2n}\cos\overline{2\eta_n-\eta_o-\delta_n+\varepsilon_n}\right)\right] \qquad \ldots\ldots(X.4)$$

$$0 = -2\rho S_n a_n\cos\eta_n - (1-S_n^2)a_n\sin\eta_n - \frac{3}{4}\Delta_n\left[A_n\sin\overline{\eta_n+\varepsilon_n} + \frac{d_n}{2}\left(A_o\sin\overline{\eta_o+\delta_n+\varepsilon_n} + A_{2n}\sin\overline{2\eta_n-\eta_o-\delta_n+\varepsilon_n}\right)\right] \qquad \ldots\ldots(X.5)$$

where the various A are the coefficients of terms in the expansion of ψ^3, as given in Appendix VIII(a), and take the following values

$$A_o = a_o(a_o^2+2a_n^2)$$
$$A_n = a_n(2a_o^2+a_n^2)$$
$$A_{2n} = a_n^2 a_o$$
$$A_{-n} = a_o^2 a_n$$

$\tan \varepsilon_n = 2\rho S_n$ and d_n is the coefficient of the n*th* harmonic in $f(\theta)$.

Equations (X.4) and (X.5) may be rearranged to give:

$$(\gamma_N^2-S_n^2)\, a_n\cos\eta_n - 2\rho S_n \gamma_N^2 a_n \sin\eta_n$$
$$= -\frac{3}{8}\Delta_n d_n (A_o \cos\overline{\eta_o+\delta_n+\varepsilon_n} + A_{2n}\cos\overline{2\eta_n-\eta_o-\delta_n+\varepsilon_n}) \quad \ldots\ldots(X.6)$$

and

$$2\rho S_n \gamma_N^2 a_n\cos\eta_n + (\gamma_N^2-S_n^2) a_n \sin\eta_n$$
$$= -\frac{3}{8}\Delta_n d_n (A_o \sin\overline{\eta_o+\delta_n+\varepsilon_n} + A_{2n}\sin\overline{2\eta_n-\eta_o-\delta_n+\varepsilon_n}) \quad \ldots\ldots(X.7)$$

where $\gamma_N^2 \equiv 1+\frac{3}{4}\frac{A_n}{a_n} = 1+\frac{3}{4}(2a_o^2+a_n^2)$

Then (X.6) x $\cos\eta_n$ + (X.7) x $\sin\eta_n$

and (X.6) x $\sin\eta_n$ - (X.7) x $\cos\eta_n$

after some manipulation yields:-

$$\sin\overline{\eta_n-\eta_o-\delta_n} = \frac{8a_n.2\rho S_n^{\,3}}{3d_n a_o(a_o^{\,2}+a_n^{\,2})\Delta_n^{\,2}} \qquad .....(X.8)$$

$$\cos\overline{\eta_n-\eta_o-\delta_n} = -\frac{8a_n(\gamma_N^{\,2}-S_n^{\,2}+4\rho^2 S_n^{\,2}\gamma_N^{\,2})}{3d_n a_o(a_o^{\,2}+3a_n^{\,2})\Delta_n^{\,2}} \qquad .....(X.9)$$

These last two equations yield

$$\frac{9}{64}\frac{\Delta_n^{\,4}a_o^{\,2}d_n^{\,2}}{a_n^{\,2}} = \frac{4\rho^2 S_n^{\,6}}{(a_o^{\,2}+a_n^{\,2})^2} + \frac{(\gamma_N^{\,2}-S_n^{\,2}+4\rho^2 S_n^{\,2}\gamma_N^{\,2})^2}{(a_o^{\,2}+3a_n^{\,2})^2}$$

.....(X.10)

which may be rearranged to give (10.36)

Then (X.2) x $\cos\eta_o$ - (X.3) x $\sin\eta_o$

and (X.2) x $\sin\eta_o$ + (X.3) x $\cos\eta_o$

followed by some manipulation yields:

$$\sin\overline{\eta_n-\eta_o-\delta_n} = \frac{\Delta_o B\cos\overline{\eta_o-\beta+\varepsilon_o}-2\rho\gamma^3 a_o}{\frac{3}{8}d_n\Delta_o^{\,2}a_n(a_n^{\,2}+a_o^{\,2})} \qquad .....(X.11)$$

$$\cos\overline{\eta_n-\eta_o-\delta_n} = \frac{\Delta_o B\sin\overline{\eta_o-\beta+\varepsilon_o}-(\gamma_n^{\,2}-\gamma^2+4\rho^2\gamma^2\gamma_n^{\,2})a_o}{\frac{3}{8}d_n\Delta_o^{\,2}a_n(3a_o^{\,2}+a_n^{\,2})} \qquad ....(X.12)$$

After substitution of (X.8) and (X.9) into the L.H.S., (X.11) and (X.12) yield

$$\left[\frac{a_o^2 B^2}{\Delta_o^2} = \frac{2\rho\gamma^3 a_o^2}{\Delta_o^2} + \frac{2\rho S_n^3 a_n^2}{\Delta_n^2}\right]^2$$

$$+ \left[\frac{(\gamma_n^2-\gamma^2+4\rho^2\gamma^2\gamma_n^2)a_o^2}{\Delta_o^2} + \frac{(\gamma_N^2-S_n^2+4\rho^2 S_n^2\gamma_N 2)}{\Delta_n^2}\frac{(3a_o^2+a_n^2)a_n^2}{(a_o^2+3a_n^2)}\right]^2$$

.....(X.13)

where $\gamma_n = 1+\frac{3}{4}\frac{A_o}{a_o} = 1+\frac{3}{4}a_o^2$

Inspection of (X.13) shows that as $a_n \to 0$ this relationship reverts to that in (7.8) for a stationary rotor.

XI Asynchronous torque when leakage reactance and iron losses are present

Equation (10.59) shows that the contribution to the total torque by the *nth* sideband is proportional to the total power dissipated at that frequency. Thus when iron loss is present the torque will be sum of the component given by (10.64) plus

$$\frac{-np}{\omega_o S_n} \cdot \frac{(\omega_n \Lambda_n)^2}{R_c} \qquad \text{(from (10.34))}$$

$$= \frac{-npa_n^2 S_n}{L_o D_o \overline{q-1}^2} \rho_2 \qquad \text{(from (4.37))}$$

i.e.

$$T_n = \frac{-npa_n^2 S_n}{L_o D_o \overline{q-1}^2} \left[\rho_2 + \rho_1 (1-\ell) \frac{S_n^2}{\Delta_n^2}\right] \qquad \ldots\ldots (XI.1)$$

Thus the total torque becomes

$$T = \sum_{n=-r}^{+r} \frac{-npa_n^2 S_n}{L_o D_o \overline{q-1}^2} \left[\rho_2 + \rho_1 (1-\ell) \frac{S_n^2}{\Delta_n^2}\right] \qquad \ldots\ldots (XI.2)$$

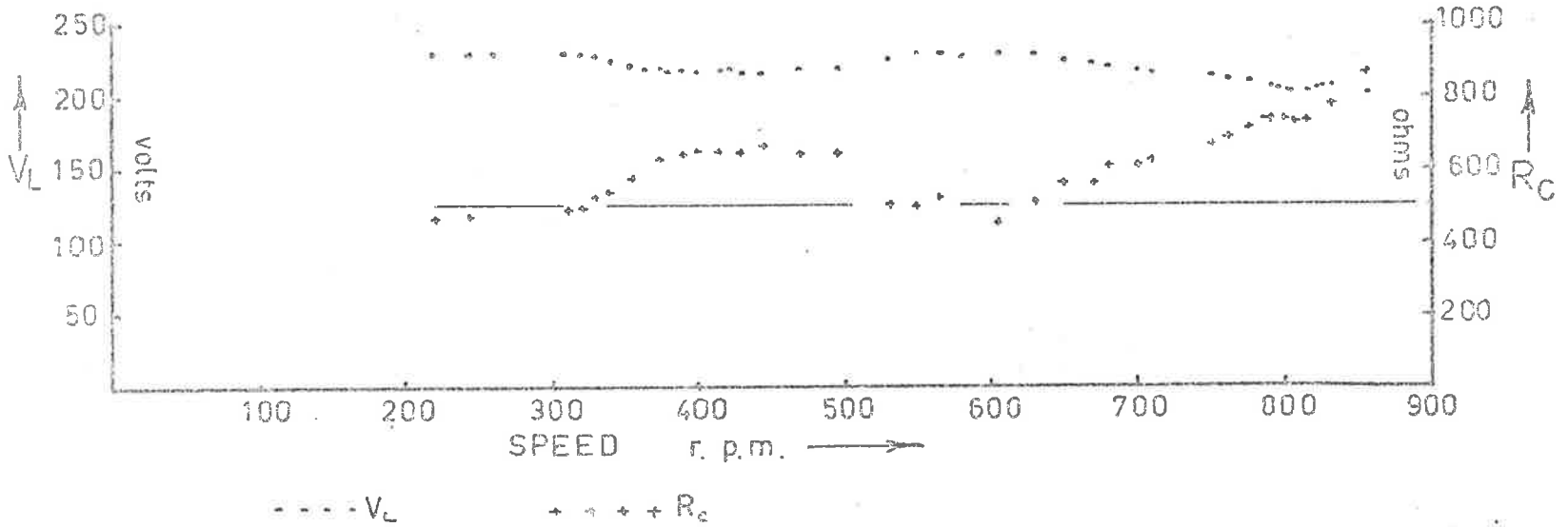

FIGURE A.XII.1

X11 Parameters of prototype machine

Under running conditions, due to the modulation on the amplitude of the line current, the responses of the meters indicating RMS line current, input power and RMS voltage across the stator windings are pulsating; so that the data presented in Figures 3.4 to 3.6 and A.XII.1 are the result of estimating the average readings given by these instruments and tend to be the mean value between the limits of fluctuation rather than a true average.

An estimate of the iron losses in the machine may be obtained from

$$P_c = P_{in} - (P_m + P_f + P_r) \qquad \ldots\ldots(XII.1)$$

where P_{in} is given by average reading of the wattmeter,

$P_m = T_{ave} \times \omega_{ave}$ = average mechanical output power,

P_f = Friction and windage power,

and $P_r = (I_{r_{ave}})^2 R$ = average copper loss

Iron loss data presented in Figures 3.4-3.6 were obtained by this method. By similar methods an estimate of the average value of the RMS voltage (V_L) across the stator winding inductance can be calculated from the measured average value of the voltage across the stator windings, the average current and the winding resistance. Typical results are shown in Figure A.XII.1. Hence an estimate may be found of the value of the shunt resistance required to represent the average value of the iron losses at a particular speed and applied

voltage from

$$R_c = \frac{V_L^2}{P_C} \qquad \ldots\ldots(XII.2)$$

Using this approach, the set of values for R_c shown in Figure A.XII.1 were obtained for a particular set of input conditions for the prototype machine. These data merely give the result of the above calculations and do not necessarily give a useful representation of circuit damping in the machine under running conditions.

For stationary rotor conditions, a similar approach leads to the rather more valid and useful results given in Figures 4.10 and 4.11. It is interesting to note that if the values of V_L in Figure A.XII.1 are applied to the curve representing the mean value of $f(\theta)$ ($\simeq 145°$) in Figure 4.11, values of R_c result which are not significantly different to those in A.XII.1.

The remaining parameters of the prototype have been discussed in previous sections but are summarized below for convenience.

(a) The rotor geometry is described by the function of rotor position θ, as described in section 4.3.1 and Figure 4.4. Fourier analysis of the function represented by the dashed line in the latter figure leads to the following expression:-

$$f(\theta) = 4.74 + 5.78\cos 2\theta + 3.75\cos 4\theta + 1.96\cos 6\theta + 0.92\cos 8\theta + 0.4\cos 10\theta + 0.2\cos 12\theta \qquad \ldots\ldots(XII.3)$$

(b) Series resistance of the windings = 5.0Ω

(c) Small signal inductance of stator windings = 0.832 henries.

(d) Leakage reactance of the stator windings = 0.04 henries

(e) Series capacitance variable - but for results presented in section 10.7.2 a value of 139.5μF was used

(f) value of R_c for purposes of calculation taken as 525Ω.

Thus:-

D_o	d_o	d_1	d_2	d_3	d_4	d_5	d_6
4.74	1.0	1.22	.791	.414	.194	.084	.042

$R = 5.0\Omega$

$L_o = 0.832$ henries

$L_\ell = 0.04$ henries

When C = 139.5μF; V = 170 volts and $R_c \simeq 525$ ohms

then

$\omega_o = 1/\sqrt{(L_o+L_\ell)C}$ 90.7 rad/sec

$\gamma = \omega/\omega_o$ 3.46

$\rho_1 = R/2\omega_o(L_o+L_\ell)$ = 0.0317

$\rho_2 = \omega_o L_o/2R_c$ = 0.072

$\ell = L_\ell/(L_o+L_\ell)$ = 0.459

$B = \sqrt{2}\, V(1-\ell)\gamma^2 D_o^{\frac{1}{q-1}}/\omega$ = 12.83

XIII Analytical Programme SBAND5

This makes use of a programme NS01A[28] for solving a set of non-linear algebraic equations which are the end product, in this case, of attempting to find a solution for:-

$$-B\sin\overline{\gamma\tau+\beta} = 2\rho_2\ell\dddot{\psi}+(1+4\rho_1\rho_2)\ddot{\psi}+2(\rho_1+\rho_2)\dot{\psi}+\psi$$

$$+(1+2\rho_1\frac{d}{d\tau}+\ell\frac{d^2}{d\tau^2})F(\theta)\psi^q \qquad \text{.....(A.XIII.1}$$

where the required solution is of the form

$$\psi = \sum_{n=-R_L}^{+R_u} a_n\cos(\overline{\gamma+2n\Omega)\tau+\eta_n} \qquad \text{.....(A.XIII.2}$$

and $$F(\theta) = \sum_{k=0}^{\mu} d_k\cos\overline{kp\Omega\tau+\delta_k} \qquad \text{.....(A.XIII.3}$$

where $d_o \equiv 1$ and $\delta_o \equiv 0$

and the equations for the n*th* sideband become:-

$$0 = B_n\sin\beta_n+(1-(1+4\rho_1\rho_2)S_n^2)a_n\cos\eta_n$$

$$-2[(\rho_1+\rho_2)S_n-\rho_2\ell S_n^3]a_n\sin\eta_n$$

$$+\frac{5}{8}\Delta_n\sum_{k=0}^{\mu}\frac{d_k}{2}[A_{n+k}\cos\overline{\alpha_{n+k}-\delta_k+\varepsilon_n}+A_{n-k}\cos\overline{\alpha_{n-k}+\delta_k+\varepsilon_n}]$$

.....(A.XIII.4

$$0 = B_n\cos\beta_n-(1-(1+4\rho_1\rho_2)S_n^2)a_n\sin\eta_n$$

$$-2[(\rho_1+\rho_2)S_n-\rho_2\ell S_n^3]a_n\cos\eta_n$$

$$-\frac{5}{8}\Delta_n\sum_{k=0}^{\mu}\frac{d_k}{2}[A_{n+k}\sin\overline{\alpha_{n+k}-\delta_k+\varepsilon_n}+A_{n-k}\sin\overline{\alpha_{n-k}+\delta_k+\varepsilon_n}]$$

.....(A.XIII.5

where all $B_n]_{n\neq 0} = 0$; $\tan\varepsilon_n = 2\rho_1 S_n/(1-\ell S_n^2)$

and $\Delta_n = \sqrt{(1-\ell S_n^2)^2+4\rho_1^2 S_n^2}$, $S_n = \gamma+2n\Omega$

A_{k+n}, α_{k+n}, A_{k-n}, α_{k-n} come from the expansion of

$$\left[\sum_{n=-R_L}^{Ru} a_n \cos(\gamma+2n\Omega)\tau+\eta_n\right]^5$$

$$= \sum_{-3R_L-2Ru}^{3Ru+2R_L} A_n \cos(\overline{\gamma+2n\Omega)\tau+\alpha_n} + \text{higher harmonics}$$

In the programme, indices run from 1 to R_1+R_u+1 for the total number of sidebands. Thus the fundamental corresponds to R_L+1. When a summation running from 1 to R_L+R_u+1 is raised to the fifth power the indices run from $-(2R_u+2R_L-1)$ to $3R_u+3R_L+1$. Therefore it is convenient to add a second pedestal; so that indices run from 5 to $5R_u+5R_L+5$. The fundamental occurs now at $2R_u+3R_L+5$.

Indices for the coefficients and phase angles in $F(\theta)$ run from $1\rightarrow(\mu+1 = Q)$ and the programme is valid provided

$$Q \leqslant P \quad \text{where} \quad P = R_L+R_u+1$$

Constant C(47) is common to both SBAND5 and SUBROUTINE CALFUN, and represents the current value of rotor speed as an independent variable.

With two equations for each sideband the total number of equations to be solved will be $2 \times (R_L+R_u+1) = 2P$

The variables x of NSO1A are related to the a_n and η_n as follows:-

$$a_n \Big]_{-R_L}^{R_u} \rightarrow a_j \Big]_{1}^{R_L+R_u+1}$$

in the programme and similarly for the η_n

Then $x_{2j} = a_j$ and $x_{2j-1} = \eta_j$

The programme is written for a maximum value of P = 11; so that N, the number of equations to solve = 22.

When P < 11 the appropriate dimensions must be set in the DIMENSION declaration for X, F, AJINV, W and in the CALL NSO1A, and CALL MATRIX statements.

See reference 28 for details of constants associated with NSO1A.

A set of initial values for the various x_n is required. In the absence of further information these may be set equal to zero except for $X(2R_L+2)$ and $X(2R_L+1)$ corresponding to a_o and η_o respectively. The former can be estimated from the value of B, while the latter $\simeq -\frac{\pi}{2}$.

Once an acceptable solution is obtained, print out occurs the speed is incremented and the cycle repeats.

Input data required

This is punched on six cards

(i) DATA (C(I), I = 1,3)/R_L, R_u, Q/

R_L = number of lower sidebands required in the solution

R_u = number of upper sidebands required

Q = μ+1 = number of harmonics +1 in $F(\theta)$

(ii) DATA (C(I), I=4,8)/B, ρ_1,ρ_2,ℓ,γ/

(iii) DATA (C(I), I=9,16)/1,d_1,d_2...d_8/

Rotor geometry coefficients

(iv) DATA (C(I), I=17,24)/0,δ_1,δ_2...δ_8/

Rotor geometry phase angles

(v) DATA (C(I), I=25,46)/22 x 0/

Values of B_n and β_n initially set to zero

(vi) DATA (X(I), I=1,2P)/...../

Sets initial values of a_n and η_n
where P = C(1)+C(2)+1 = R_L+R_u+1

```
                PROGRAM SBAND5(INPUT,OUTPUT)
000003          DIMENSION X(12),F(12),AJINV(12,12),W(360)
000003          DIMENSION S(11),DF(11),DT(11),A(11),TOR(11)
000003          INTEGER P,DUM
000003          COMMON/PARAM/C(47)
000003          DATA(C(I),I=1,3)/4.1,1.1,6.1/
000003          DATA(C(I),I=4,8)/12.83,.0634,0.,.0459,3.46/
000003          DATA(C(I),I=9,16)/1.,1.22,.79,.413,.194,.084,.042,0./
000003          DATA(C(I),I=17,24)/8*0./
000003          DATA(C(I),I=25,46)/22*0./
000003          DATA(X(I),I=1,12)/-1.,.08,-5.,.13,-3.4,.34,-.11,.5,-1.4,1.28,-.02,
                I.04/                          Estimated initial values of an analog
000003          P=C(1)+C(2)+1
000007          DUM=C(1)+1
000012          C(24+DUM)=C(4)                 Sets value of Bo in appropriate place.
000014       40 FORMAT((1H8,10E11.3/) )
000014          PRINT 40,(C(I),I=1,46)
000026          N=2*P
000030          STEP=.001
000031          ACC=.000001
000033          MAXFUN=2000
000034          DMAX=40
000035          DO 90 M=1,34                   Sets the speed range
000037          K=74-M
000041          C(47)=.0025*K*C(8)             Sets the actual speed
000044          CALL NS01A(12,X,F,AJINV,STEP,DMAX,ACC,MAXFUN,0,W)
000055          TORT=0.
```

```
000056          DO 55 J=1,P
000060          S(J)=C(8)+2*(J-DUM)*C(47)
000067          DF(J)=2*C(5)*S(J)
000073          DT(J)=(1.-C(7)*S(J) *S(J))**2+DF(J)*DF(J)
000101          A(J)=X(2*J)
000103          TOR(J)=-(J-DUM)*A(J)*A(J)*(2*C(6)*S(J)+DF(J)*(1.-C(7))*S(J)*S(J)/
               IDT(J))
000121          TORT=TORT+TOR(J)
000123       55 CONTINUE
000125          PRINT 60,K,(X(I),I=1,N),(TOR(I),I=1,P),TORT
000151       60 FORMAT(//(1H ,I2,10E12.3/3X,10E12.3/3X,10E12.3))
000151       90 CONTINUE
000153          STOP
000155          END
```

$S_n = s + 2n\Omega$

$2\rho s_n$

$4\rho^2 s_n^2 + (1-\ell s_n^2)^2$

Torque components

Torque

```
                SUBROUTINE CALFUN(N,X,F)
000006          DIMENSION X(1),F(1),A(11),ET(11),AC(55),AS(55),AA(55),AL(55),
               IS(11),DF(11),DD(11),DT(11),DL(11),DM(11),EP(11)
000006          COMMON/PARAM/C(47)
000006          INTEGER Q,P,PP,DUM,PED
000006          Q=C(3)
000007          P=C(1)+C(2)+1
000013          PP=5*P
000015          PED=2*P+2
000017          DUM=C(1)+1
000022          DO 5 I=1,P
000024          A(I)=X(2*I)
000027          ET(I)=X(2*I-1)
000032        5 CONTINUE
000034          DO 10 I=1,PP
000036          AC(I)=0.
000040          AS(I)=0.
000041       10 CONTINUE
000043          DO 50 I=1,P
000045          DO 50 J=1,P
000046          DO 50 K=1,P
000047          DO 50 L=1,P
000050          DO 50 M=1,P
000051          AC(I+J+K-L-M+PED)=AC(I+J+K-L-M+PED)+A(I)*A(J)*A(K)*A(L)*A(M)*COS
               I(ET(I)+ET(J)+ET(K)-ET(L)-ET(M))
000111          AS(I+J+K-L-M+PED)=AS(I+J+K-L-M+PED)+A(I)*A(J )*A(K)*A(L)*A(M)*SIN
               I(ET(I)+ET(J)+ET(K)-ET(L)-ET(M))
000152       50 CONTINUE
000167          DO 60 I=5,PP
000170          AA(I)=SQRT(AC(I)*AC(I)+AS(I)*AS(I))   Calculating R_k
000201          IF(AA(I) )54,54,55
```

```
000205       54 AL(I)=0.
000207          GO TO 60
000210       55 AL(I)=ATAN2(AS(I),AC(I))
000217       60 CONTINUE
000224          DO 100 K=1,P
000225          S(K)=C(8)+2*(K-DOM)*C(47)
000234          DF(K )=2*C(5)*S(K)
000241          DD(K)=1.-C(7)*S(K)*S(K)
000246          DT(K)=SQRT(DD(K)*Dn(K)+DF(K)*DF(K))
000257          EP(K)=ATAN2(DF(K),DD(K))
000265          DL(K)=1.-(1.+4*C(5)*C(6))*S(K)*S(K)
000275          DM(K)=DF(K)+2*C(6)*S(K)*DD(K)
000305          F(2*K-1)=0.
000311          F(2*K)=0.
000313          DO 90 I=1,Q
000314          F(2*K-1)=F(2*K-1)+.3125*C(I+8)*DT(K)*(AA(K+PED+I-1)*COS(AL(K+PED+
               II-1)+EP(K)-C(I+16))+AA(K+PED-I+1)*COS(AL(K+PED-I+1)+EP(K)+C(I+16)
               U))
000362          F(2*K)=F(2*K)+.3125*C(I+8)*DT(K)*(AA(K+PED+I-1)*SIN(AL(K+PED+I-1)+
               IEP(K)-C(I+16))+AA(K+PED-I+1)*SIN(AL(K+PED-I+1)+C(I+16)+EP(K)))
000430       90 CONTINUE
000432          F(2*K-1)=F(2*K-1)+C(K+24)*SIN(C(K+35))+A(K)*(DL(K)*COS(ET(K))-
               IDM(K)*SIN(ET(K)))
000464          F(2*K)=-F(2*K)+C(K+24)*COS(C(K+35))-A(K)*(DL(K)*SIN(ET(K))+DM(K)*
               ICOS(ET(K)))
000516      100 CONTINUE
```

Calculating α_k

S_m

$2\rho_1 S_m$

$1-\ell S_m^2$

Δ_m

ℓ_m

$1-(1+4\rho_2)S_m^2$

$2\rho_1 S_m + 2\rho_2 S_m(1-\ell S_m^2)$

Smith, B. H. (1967). Asynchronous reluctance motor using ferroresonance. *Proceedings of the Institution of Electrical Engineers*, *114*(11), 1707-1716.

Smith, B. H. (1968). A simple bilateral variable-ratio dc pulse converter. *IEEE Transactions on Industrial Electronics and Control Instrumentation, 15*(1), 1-5.

Smith, B. H. (1968). Commutation in a bilateral variable-ratio dc pulse converter. *IEEE Transactions on Industrial Electronics and Control Instrumentation, 15*(1), 6-11.